The Chemistry of Phenalenyl: Elucidating the Mechanism of Dimerization and Decomposition of Phenalenyl

フェナレニルの化学：

フェナレニルが示す二量化反応および分解反応の機構解明

Kazuyuki Uchida

2016

Department of Chemistry, Graduate School of Science,

Osaka University

Contents

-Chapter 1-
General Introduction

1.1 Theme of the Thesis

Organic free radicals have attracted much interest of fundamental chemists as important intermediates on the organic reactions. In general, organic free radicals are known to be short-lived species, which show a facile decomposition through a dimerization as well as hydrogen abstraction, oxidation, and dispropotionation. In 1900, a first preparation of a persistent hydrocarbon radical was reported by Gomberg,[1] which explored a recent chemistry of organic stable radicals. Triphenylmethy (**1.1**) exists as an equilibrium mixture with its dimer in solution state, whereas **1.1** is stable in inert atmosphere enough to be characterized. The dimerization mode of **1.1** had been long discussed and the unique head-to-tail structure was confidently identified by NMR spectroscopy[2] and X-ray crystallographic analysis.[3] On the basis of this discovery, various stable hydrocarbon radicals were designed and synthesized.

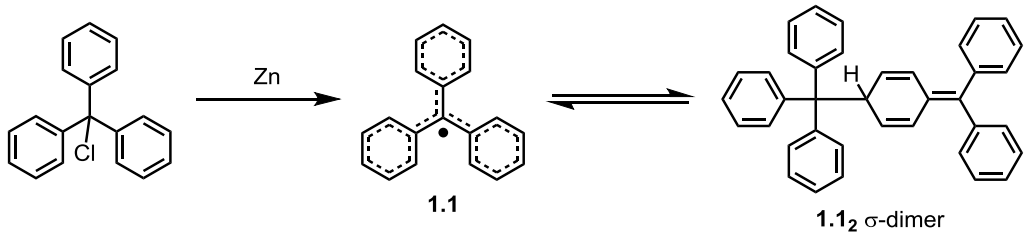

Figure 1.1.1. σ-Dimerization of **1.1**.

Although the σ-bond formation (σ-dimerization) has been considered as an essential dimerization mode of hydrocarbon radicals, the view was changed by the observation of a π-dimerization demonstrated by the radical anion of tetracyanoethylene (TCNE, **1.2**). **1.2**$^{\bullet-}$ forms a diamagnetic dimer in a face-to-face arrangement with an extraordinarily short π–π separation distance of about 2.9 Å, owing to a covalent bonding interaction between two unpaired electrons on each **1.2**$^{\bullet-}$ unit through four carbon centers (2e/4c multicenter bonding). The unique dimerization mode was observed in various radical ions (see chapter 1.2), and detailed investigations of the unique dimerization mode have been performed on the basis of experimental and theoretical approaches. The unique multicenter bonding has played a key role in the material chemistry, and the multicenter bonded dimers have attracted attention as significant building blocks of the molecular-based metals, magnets, and superconductive materials.

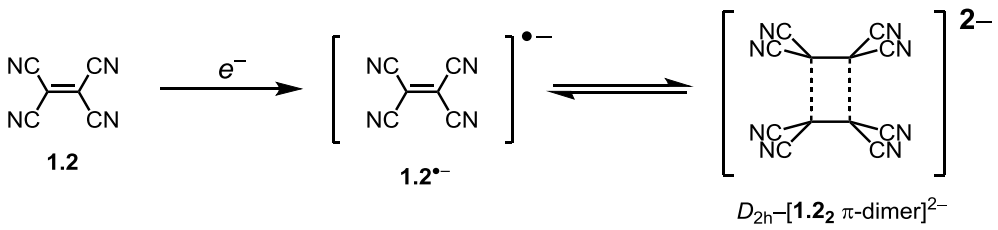

Figure 1.1.2. π-Dimerization of **1.2**$^{\bullet-}$.

Phenalenyl, which is a neutral hydrocarbon radical having a thermodynamically stabilized nature due to the delocalization of its unpaired electron over six α carbon atoms, has played an important role in the fundamental and material chemistry owing to the strong multicenter bonding that works effectively between two phenalenyl units. In 1999, first isolation of phenalenyl derivative, 2,5,8-tri-*tert*-butylphenalenyl (**1.4**), was reported by Nakasuji *et. al.*[4] **1.4** was isolated as a π-dimer with a considerably shorter π–π separation distance (3.2–3.3 Å) than the sum of van der Waals radius (3.4 Å). The nature of 2e/12c multicenter bonding demonstrated by **1.4** was well studied on the basis of experimental and theoretical approaches. In contrast, some phenalenyl derivatives including parent phenalenyl (**1.3**) is expected to demonstrate a σ-bond formation to give corresponding σ-dimers, and the essential dimerization behavior of phenalenyl derivatives has been in question for the past a half century. Hence, the fundamental understanding of the essential dimerization of phenalenyl is required for the molecular designs of a novel phenalenyl-based materials.

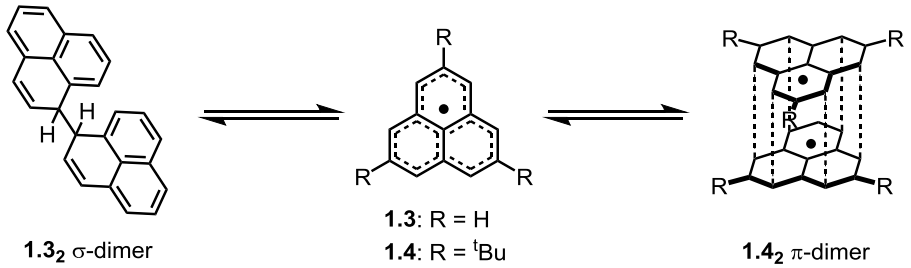

Figure 1.1.3. Bimodal dimerization of phenalenyls.

This thesis describes the systematic studies on the essential dimerization behavior of phenalenyl derivatives with various substituted groups at 2,5,8-positions. Introduction of substituted groups at 2,5,8-positions bearing little spin densities does not affect significantly the spin nature of phenalenyl, which enabled the detailed investigation of the essential dimerization of phenalenyl. In chapter 2 and 3, dimerization behaviors of novel phenalenyl derivatives (**2.1a**, **2.1b**, and **3.1** in Figure 1.1.4) was fully investigated in solution and solid state.

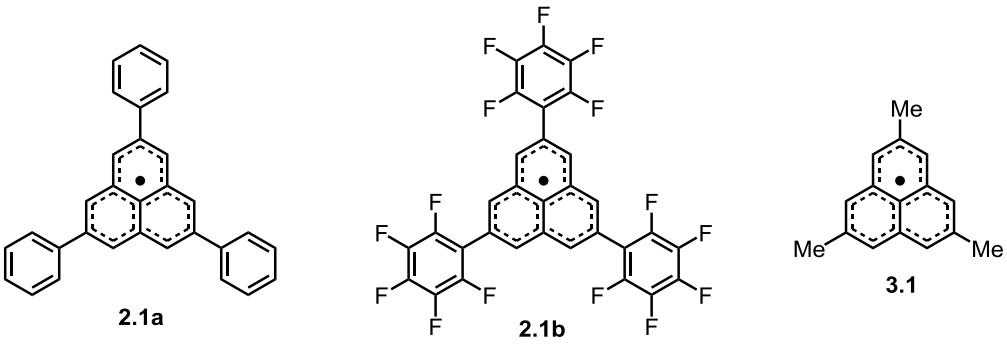

Figure 1.1.4. Novel phenalenyl derivatives.

2.1a and **2.1b** adopted selectively π-dimer and σ-dimer, respectively, which was unambiguously confirmed by X-ray crystallographic analysis and NMR spectroscopy. The substantial dependence of the dimerization modes suggests strongly the σ and π dimerization modes are energetically competitive, and the preference of the dimerization can be controlled readily with the substituted groups. Actually, another association mode of **2.1b** was successfully obtained

by the crystallization in high temperature gas phase. **2.1b** constructed one-dimensional chains through the continuous multicenter bonding between **2.1b**s, and the solid state properties were fully investigated experimentally.

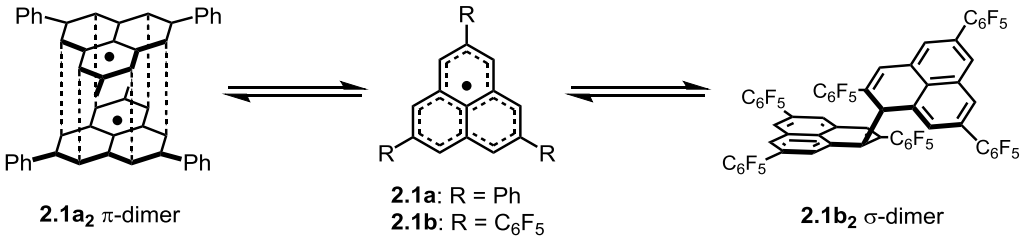

Figure 1.1.5. Dimerization modes of **2.1a** and **2.1b**.

3.1 with the smallest perturbations demonstrated a bimodal dimerization in solution and solid state. Molecular geometries of **3.1** dimers were undoubtedly confirmed by X-ray crystallographic analysis. Furthermore, **3.1** formed three dimerization modes; that is $\mathbf{3.1}_2$ σ-dimer *RR*/*SS* form, $\mathbf{3.1}_2$ σ-dimer *RS* form, and $\mathbf{3.1}_2$ π-dimer. The energetic preference of the dimerization modes was determined experimentally on the basis of NMR studies. In addition, first observation of the σ-bond fluxionality of phenalenyl σ-dimer was accomplished, and the mechanism was fairly investigated by EXSY measurements and theoretical calculations.

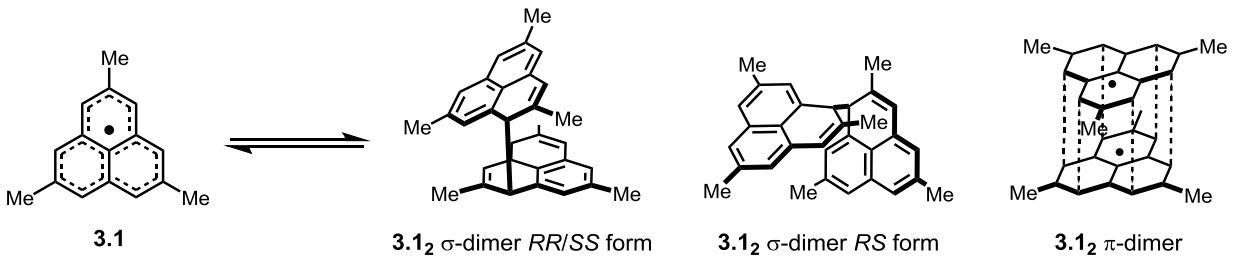

Figure 1.1.6. Dimerization modes of **3.1**.

In chapter 4, the decomposition mechanism of parent phenalenyl (**1.3**) into peropyrene (**4.3**) (Figure 1.1.7) was experimentally elucidated by the direct synthesis of biphenalenylidenes (*E*-**4.1** and *Z*-**4.1**), which are long unidentified reactive intermediates, using a clean photochemical reaction of dihydroperopyrene (**4.2**). The facile decomposition process includes two unusual reactions; that is, 1) a rapid *E*–*Z* isomerization between *E*-**4.1** and *Z*-**4.1**, and 2) conrotatory ring-closure of *Z*-**4.1** not conforming to the Woodward-Hoffmann rule. The unusual reactivities of *E*, *Z*-**4.1** were fully investigated by spectroscopic analyses as well as computational studies, which corroborates that the ground states of *E*, *Z*-**4.1** destabilized by the singlet biradical nature contribute significantly to the unique reactions.

In chapter 5, a novel synthetic method of peropyrene derivatives having substituted groups at 2,9-positions was explored. Detailed investigation of a decomposition of biphenalenylidenes **4.1** into peropyrene (**4.3**), as mentioned in chapter 4, enabled a successful preparation of new peropyrene derivatives (**5.1a–c**). Introduction of substituted groups at 2.9-positions resulted in a negligible change in the electronic structure of peropyrene in single-molecule level, whereas the molecular alignments in crystalline states depends significantly on the effects of substituted groups.

To elucidate the feasibility of **5.1a–c** for the investigation of singlet fission process, photophysical properties in crystalline state was well studied by spectroscopic analyses.

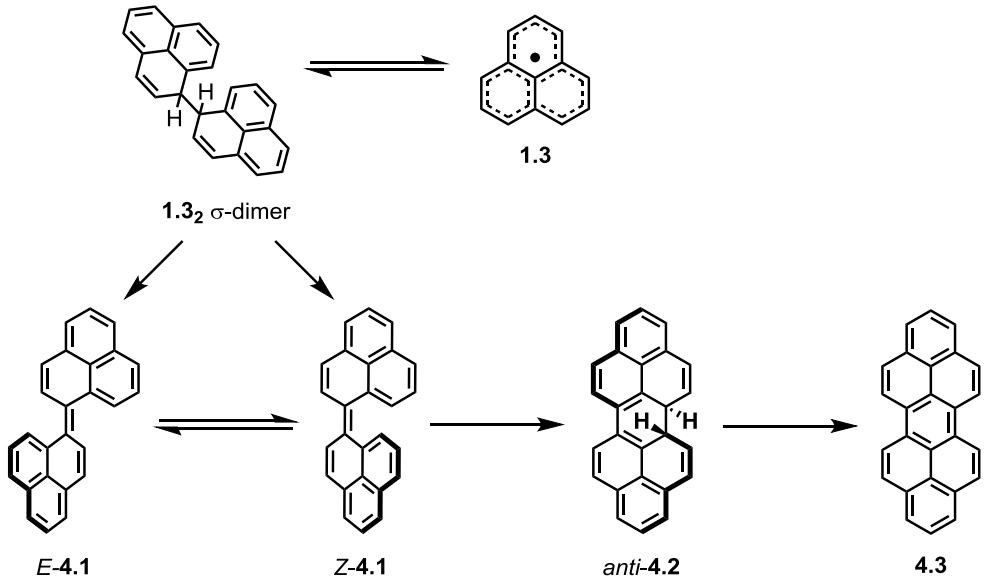

Figure 1.1.7. Decomposition pathway of parent phenalenyl **1.3**.

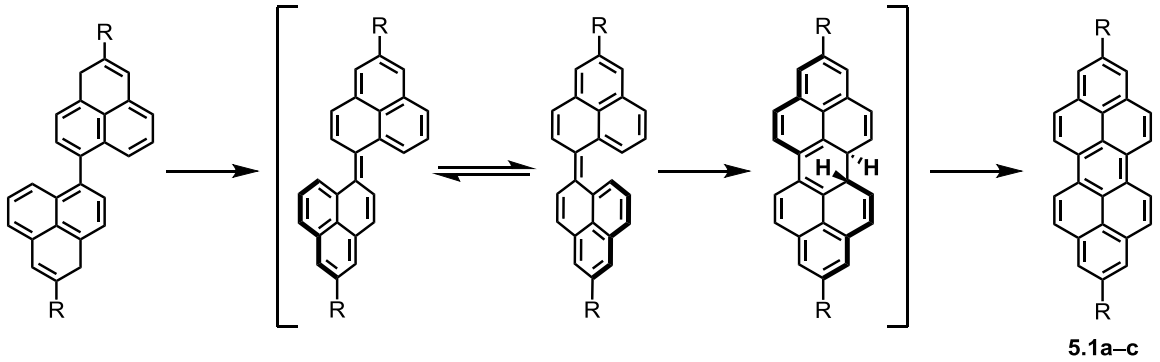

Figure 1.1.8. New synthetic approach to the peropyrene derivatives

1.2 Multicenter bonding of radical ions

Organic electron donors and acceptors give persistent radical ions, which have long played an important role in the material chemistry as building blocks of the molecular-based materials. The radical ions give the self-assembled dimers owing to the strong intermolecular interactions arising from the multicenter bonding.

Tetracyanoethylene (TCNE, **1.2**) is one of the most studied electron acceptors, and the radical anion, **1.2**$^{\bullet-}$, was isolated in crystalline states as electron transfer salts with various counter cations.[5–7] After the first characterization of **1.2**$^{\bullet-}$ in crystalline state,[8] three dimerization modes have been found to date; that is, a σ-dimer octacyanobutanediide ([**1.2**$_2$ σ-dimer]$^{2-}$)[9] and two π-dimers (D_{2h}–[**1.2**$_2$ π-dimer]$^{2-}$ and C_2–[**1.2**$_2$ π-dimer]$^{2-}$)[5–7,10,11] as shown in Figure 1.2.1. Particularly, D_{2h}–[**1.2**$_2$ π-dimer]$^{2-}$ with short π–π separation distance of about 2.9 Å is a dominant dimerization mode of **1.2**$^{\bullet-}$. The considerably shorter distance than the sum of van der Waals radius (3.4 Å)

indicates the presence of strong attractive forces between two **1.2**$^{\bullet-}$ moieties. In addition, The C–CN bonds of D_{2h}–[**1.2**$_2$ π-dimer]$^{2-}$ bend away from nominal planes of **1.2**$^{\bullet-}$ by 5.3°, which infers the admixture of sp^3 hybridization into the sp^2 carbon atoms. These structural features invoked the term of multicenter bonding, and the unique nature of two electron–four center (2e/4c) bonding has been studied experimentally and theoretically.

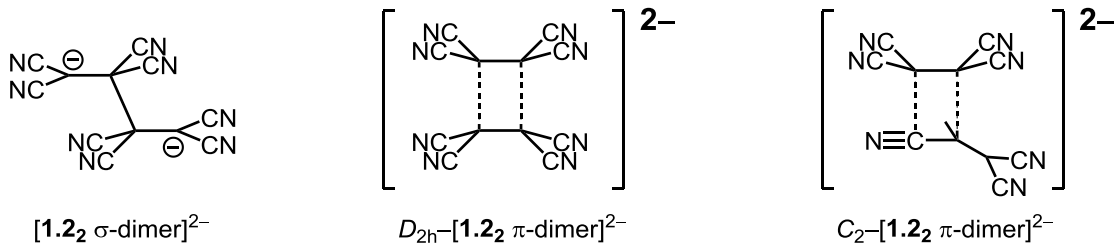

Figure 1.2.1. Dimerization modes of **1.2**$^{\bullet-}$.

Theoretical calculations[5–7,12,13] predicted that the HOMO and LUMO of D_{2h}–[**1.2**$_2$ π-dimer]$^{2-}$ should be formed from the bonding and antibonding combination of two SOMOs of **1.2**$^{\bullet-}$ (Figure 1.2.2), accompanied by a formation of multicenter bonding. Thus, the presence of the 2e/4c bonding can be corroborated by spectroscopic analyses. D_{2h}–[**1.2**$_2$ π-dimer]$^{2-}$ showed a characteristic absorption band that was not observed in monomeric **1.2**$^{\bullet-}$.[5–7,12,14] The absorption band can be ascribed to the HOMO–LUMO transition of D_{2h}–[**1.2**$_2$ π-dimer]$^{2-}$, indicating the presence of the multicenter bonding between **1.2**$^{\bullet-}$s. Further evidences were obtained by IR spectra,[5–7,12] FT-Raman spectra,[15] ESR spectra,[14] magnetic data,[5,6] and ^{13}C magic angle spinning (MAS) NMR spectroscopy,[16] which confirmed that **1.2**$^{\bullet-}$ forms D_{2h}–[**1.2**$_2$ π-dimer]$^{2-}$ with the singlet ground state in solution and solid state through the strong multicenter 2e/4c bonding.

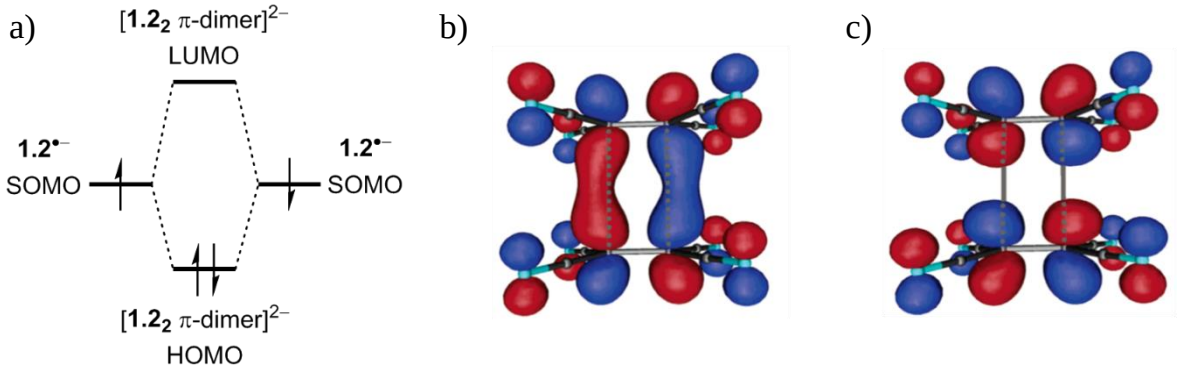

Figure 1.2.2. a) Molecular orbital diagram of D_{2h}–[**1.2**$_2$ π-dimer]$^{2-}$. b) HOMO and c) LUMO of D_{2h}–[**1.2**$_2$ π-dimer]$^{2-}$. Reprinted with permission from ref. 7. Copyright 2007, American Chemical Society.

Computational studies suggested that [**1.2**$_2$ dimer]$^{2-}$ has two local minima on the calculated potential energy surface, which are corresponding to [**1.2**$_2$ σ-dimer]$^{2-}$ and D_{2h}–[**1.2**$_2$ π-dimer]$^{2-}$, whereas the interaction energy of D_{2h}–[**1.2**$_2$ π-dimer]$^{2-}$ is always repulsive due to the large coulomb repulsion between **1.2**$^{\bullet-}$s.[5–7,12] The unique multicenter bonding observed experimentally was reproduced by taking the presence of counter cations into considerations.[13,17] Actually, the structures of **1.2**$^{\bullet-}$ dimers depend significantly on the counter cations. In contrast, the geometries and

bond dissociation energies of D_{2h}–[**1.2**$_2$ π-dimer]$^{2-}$ are almost independent of the counter cations,[14] and the further detailed investigation has been conducted on the basis of experimental and computational methods.

Analogy to **1.2**, multicenter bonded dimers of other electron acceptors were also observed in solution and solid states. The radical anion of 7,7,8,8-tetracyano-*p*-quinodimethane (TCNQ, **1.5**) is known to form not only a σ-dimer[18,19] but a π-dimer with slightly shorter π–π separation distance of 3.1–3.3 Å than the sum of van der Waals radius (3.4 Å).[20,21] In contrast to the eclipsed π-dimer of **1.2**$^{\bullet-}$, most **1.5**$^{\bullet-}$ derivatives adopt a slipped stacking π-dimer to avoid the exchange repulsion. Tetrafluorinated analogue of TCNQ, (F_4TCNQ, **1.6**), also gives a slipped stacking π-dimer with a short separation distance of about 3.2 Å.[22] In addition, *p*-benzoquinone derivatives, 2,3-dichloro-5,6-dicyano-*p*-benzoquinone (DDQ, **1.7**) and 2,3,5,6-tetrachloro-*p*-benzoquinone (*p*-chloranil, **1.8**), also give persistent radical anions, which form corresponding π-dimers with short interplanar distances of 2.9–3.0 Å.[14,23,24] The features of multicenter bonded π-dimers were well studied by spectroscopic techniques, and formation of multicenter bonding was experimentally confirmed.[14]

Tetrathiafulvalene (TTF, **1.9**), which is a strong electron donor, is known to give a persistent radical cation, and the self-association has been investigated for the application in material chemistry. The crystal structure of radical cation of **1.9** (**1.9**$^{\bullet+}$) was observed in bromide[25] and perchlorate[26] salt as shown in Figure 1.2.3. **1.9**$^{\bullet+}$ adopted a face-to-face π-dimer with extremely shorter π–π separation distances of 3.3–3.5 Å between the sulfur atoms than the sum of van der Waals contacts of sulfur atoms (3.7 Å). The shorter separation distance suggests strongly the presence of multicenter bonding between two **1.9**$^{\bullet+}$ units. Computational studies supports this idea, and formation of new molecular orbitals (HOMO and LUMO shown in Figure 1.2.4) was predicted as observed in [**1.2**$_2$ π-dimer]$^{2-}$.[27]

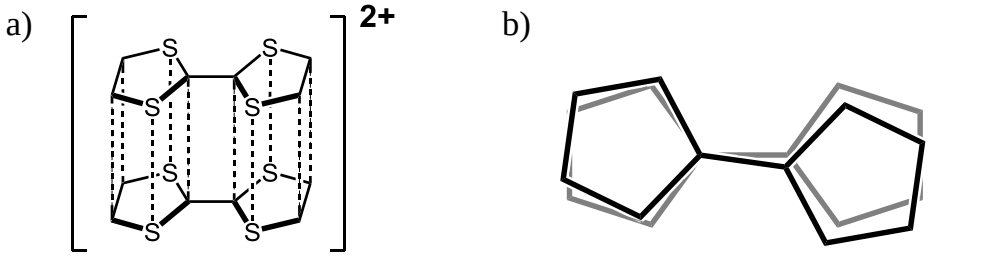

Figure 1.2.3. a) Multicenter bonded π-dimer of **1.9**$^{\bullet+}$. b) Face-to-face alignment of [**1.9**$_2$ π-dimer]$^{2+}$.

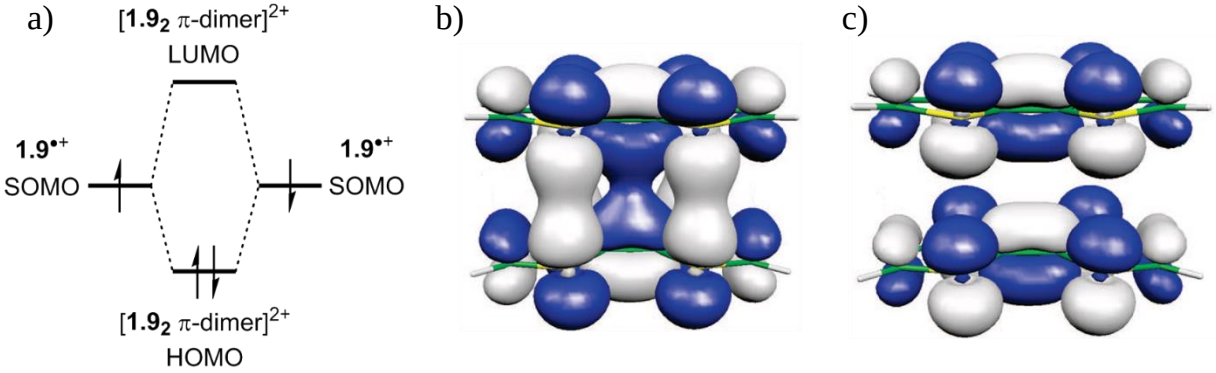

Figure 1.2.4. a) Molecular orbital diagram of [**1.9**$_2$ π-dimer]$^{2+}$. b) HOMO and c) LUMO of [**1.9**$_2$ π-dimer]$^{2+}$. Counter anions were omitted for clarity. Adapted with permission from ref. 27. Copyright 2009, American Chemical Society.

Presence of the multicenter bonding was confirmed by spectroscopic analyses as performed in [**1.2**$_2$ π-dimer]$^{2-}$. The electronic absorption measurements showed a characteristic band of the HOMO–LUMO transition of [**1.9**$_2$ π-dimer]$^{2+}$, which indicates the formation of multicenter bonding.[28] The bond dissociation energy of [**1.9**$_2$ π-dimer]$^{2+}$ was estimated by variable temperature ESR measurements to be 3.8 kcal mol^{-1} in dichloromethane, and the noticeable dependence of the bond dissociation energy on the solvent polarity was observed. In contrast, the spectral feature observed in electronic absorption spectra recorded in solvents with various polarities showed negligible difference, which suggests the nature of multicenter bonding is independent of the solvent polarity.[28]

Multicenter bonding of other radical cations, such as octamethylbiphenylene (OMB, **1.10**), has also been investigated.[29] **1.10**$^{\bullet+}$ adopts a slipped stacking π-dimer with short π–π separation distance of about 3.2 Å. The concave-concave motif of [**1.10**$_2$ π-dimer]$^{2+}$ dimer inferred the presence of strong attractive force between two radical cations. The diamagnetic nature of multicenter bonding was well characterized by spectroscopic techniques.

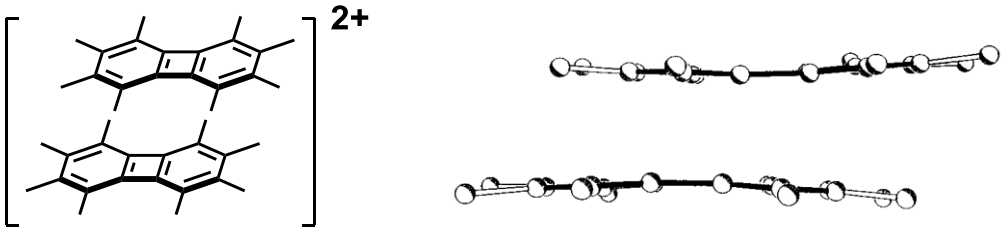

Figure 1.2.5. Molecular geometry of [**1.10**$_2$ π-dimer]$^{2+}$. Reprinted with permission from ref. 29. Copyright 2000, American Chemical Society.

1.3 Phenalenyl

Phenalenyl (**1.3**) is an odd-alternant hydrocarbon radical having a thermodynamically stabilized nature due to the delocalization of its unpaired electron over six α carbon atoms, as illustrated in Scheme 1.3.1 and Figure 1.3.1. Most hydrocarbon radicals require the steric protections for the isolation to improve their persistency, whereas **1.3** with a remarkable thermodynamic stability can be isolated with a limited steric protection, leading to the self-association to give a multicenter bonded π-dimer as observed in tri-*tert*-butyl derivative **1.4** (see chapter 1.3.2).[4,30] Recently, the assemblies of phenalenyls based on the strong multicenter bonding have been attracted much interest as promising building blocks for molecular-based materials due to their high electron conductivity[31,32] and non-linear optical properties,[33] and numerous phenalenyl-based compounds have been synthesized to date.

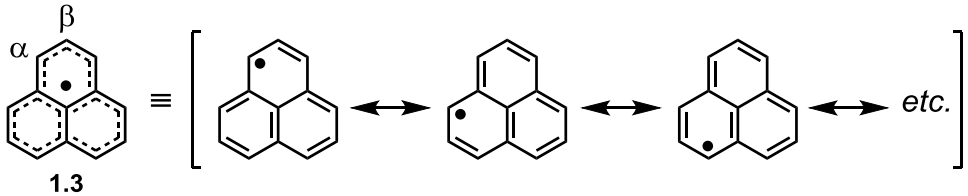

1.3

1,3,4,6,7,9-: α positions
2,5,8-: β positions

Scheme 1.3.1. Resonance structures of **1.3**.

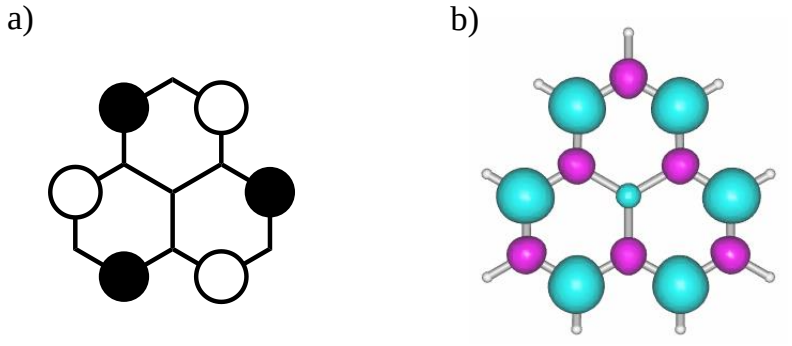

Figure 1.3.1. a) SOMO and b) spin density distribution map of **1.3**.

1.3.1 Parent phenalenyl

Numerous efforts have been devoted to synthesize and isolate parent phenalenyl **1.3** in 1950s according to the synthetic procedures shown in Scheme 1.3.2.[34–36] Successful observation of **1.3** was accomplished by the ESR measurements,[37,38] which showed well-resolved hyperfine splittings. Nevertheless, the isolation of **1.3** in pure form has yet been unsuccessful due to the facile decomposition in the presence of oxidized reagents.

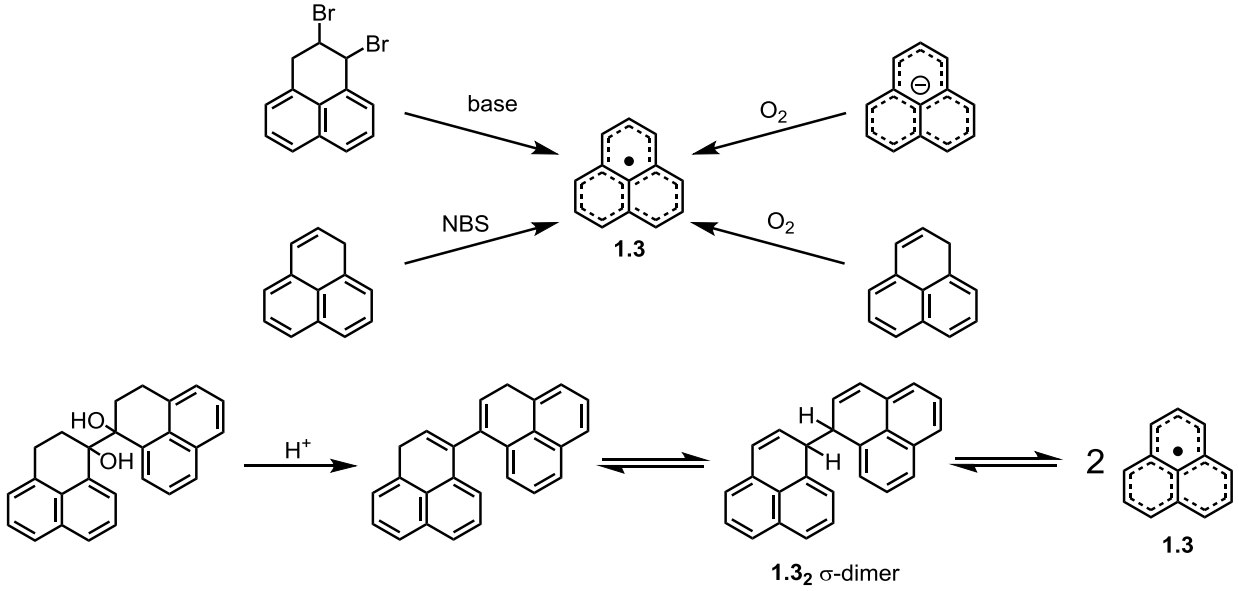

Scheme 1.3.2. Synthetic methods of **1.3**.

Formation of diamagnetic dimers (**1.3**$_2$) was observed by variable temperature ESR measurements,[39,40] whereas the dimerization mode of **1.3** has not been observed directly. The product analysis infers the formation of the σ-dimer of **1.3**. Peropyrene **4.3**, which is a close-shell hydrocarbon compound, was identified as a decomposed product.[34,36] Although the decomposition mechanism has not been clarified, the dehydrogenation of **1.3**$_2$ σ-dimer should lead to the decomposed product. The electronic absorption measurements conducted at low temperature supports this idea. No characteristic absorption band ascribed to π-dimer was observed, suggesting the formation of a colorless σ-dimer at low temperature.[39,40]

1.3.2 Isolation and characterization of phenalenyl π-dimer

In 1999, Nakasuji and co-workers reported the first isolation of a phenalenyl derivative by introducing sterically hindered *tert*-butyl groups at β positions.[4] 2,5,8-Tri-*tert*-butylphenalenyl (**1.4**) was prepared from a hydro-precursor, phenalene, by the treatment with *p*-chloranil in a degassed solvent (see Scheme 1.3.3). Steric protection with bulky *tert*-butyl groups prevented a σ-dimerization, leading to the formation of multicenter bonded π-dimer. The molecular geometry of **1.4**$_2$ π-dimer was unambiguously confirmed by X-ray crystallographic analysis (Figure 1.3.2).[4,41] **1.4** adopted a staggered stacking π-dimer with a shorter π–π separation distance of 3.201(8)–3.323(6) Å than the sum of van der Waals radius (3.4 Å), which indicates the presence of the strong covalent bonding interaction between two phenalenyl moieties in π-dimerization mode.

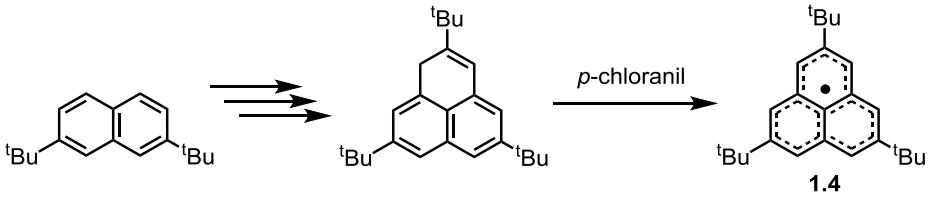

Scheme 1.3.3. Synthetic procedure of **1.4**.[4]

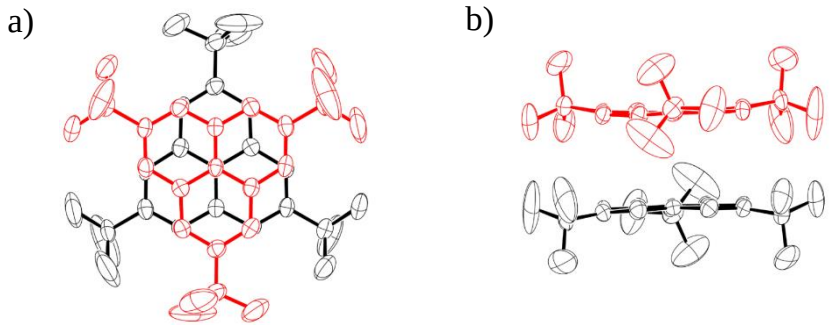

Figure 1.3.2. Molecular geometry of **1.4**$_2$ π-dimer. a) Top view and b) side view. Reprinted with permission from ref. 41. Copyright 2014, The Chemical Society of Japan & Wiley-VCH Verlag GmbH & Co. KGaA.

The covalent bonding interaction between two phenalenyl units was estimated quantitatively by the SQUID measurement.[42] SQUID measurements conducted with a polycrystalline sample of **1.4**$_2$ π-dimer suggested the singlet ground state of **1.4**$_2$ π-dimer and the covalent bonding interaction, $2J/k_B$, was determined to be −2000 K. The strong covalent bonding interaction was also corroborated with the electronic absorption measurements recorded in a dispersed KBr pellet. **1.4**$_2$ π-dimer showed an intense absorption band centered at 612 nm, which is corresponding to the HOMO–LUMO transition of **1.4**$_2$ π-dimer. The HOMO and LUMO of phenalenyl π-dimer is formed from the bonding and antibonding combinations of SOMOs of **1.4**s; thus, the wide HOMO–LUMO splitting reflects the strong covalent bonding interaction between two **1.4**s.

NMR spectroscopy and the electronic absorption measurements are the powerful tools to elucidate the essential dimerization mode of phenalenyls adopted in solution state. Monomeric **1.4** showed no signal in NMR spectra,

whereas broad peaks were observed at lower temperature, which are ascribed to a diamagnetic **1.4$_2$** π-dimer.[30] In addition, a characteristic absorption band at 595 nm was observed in the electronic absorption spectrum recorded at low temperature.[43] The absorption band was assigned to the HOMO–LUMO transition of **1.4$_2$** π-dimer as observed in the spectrum measured in KBr pellet.

1.3.3 Steric effect on the dimerization modes of phenalenyl

Steric effect on the dimerization modes of phenalenyl was investigated experimentally by Kochi *et al*. with phenalenyl derivatives having alkyl substituted groups at α and β carbon atoms (**1.11**–**1.14**, shown in Figure 1.3.3).[39,40] ESR measurements suggested that the introduction of alkyl groups should not affect the spin structure of phenalenyl. **1.11**–**1.13** showed an irreversible change in VT ESR measurements due to a gradual decomposition, whereas **1.14** demonstrated a reversible dimerization. Although the dimerization mode was not observed directly, VT electronic absorption measurements suggested the **1.14** forms solely the σ-dimer.

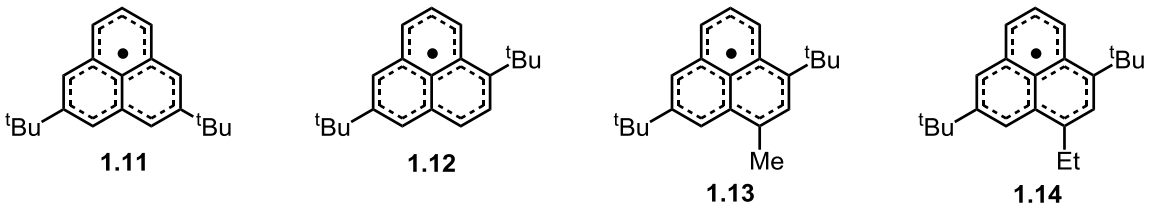

Figure 1.3.3. Phenalenyl derivatives with alkyl substituted groups.

1.3.4 Phenalenyl derivatives with electronic perturbations

In 1975, Haddon suggested that phenalenyl should be a remarkable building block for the molecular conductor owing to the strong multicenter bonding between neighboring molecules.[44] However, substantial tunings to decrease the on-site coulomb repulsion should be required to construct the molecular-based metals. Introduction of hetero atoms at α positions is an effective way to change the electronic structure of phenaleyl. On the basis of this molecular design, various phenalenyl analogues with hetero atoms at α positions were synthesized and characterized in solution and solid state.

Perchlorophenalenyl (**1.15**) was synthesized and characterized by Haddon *et al.* (Scheme 1.3.4).[45–47] Introduction of chlorine atoms at α positions of phenalenyl resulted in the delocalization of an unpaired electron over chlorine atoms, which was confirmed by the *g*-value of 2.0058 estimated by ESR measurements.[45]

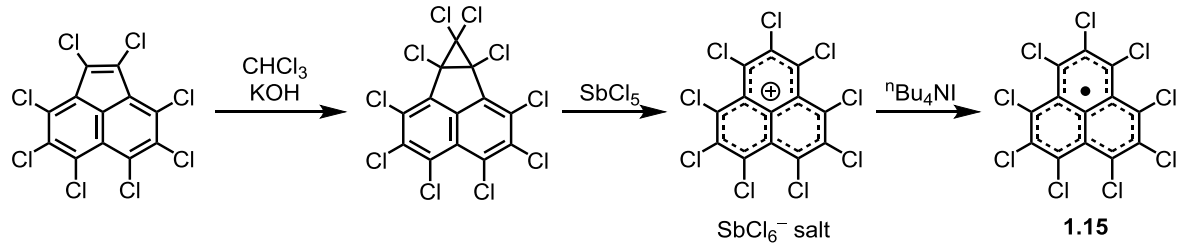

Scheme 1.3.4. Synthetic procedure for **1.15**.

Steric effect of chlorine atoms at α carbon atoms affected the molecular geometry of **1.15**.[46,47] **1.15** has a nonplanar geometry due to the steric repulsion between chlorine atoms, which was corroborated by X-ray crystallographic analysis. Whereas **1.4** adopted a π dimerization mode with a staggered stacking motif, **1.15** constructed one-dimensional columns that incorporates both staggered and eclipsed stacking motives due to the twisted geometry of **1.15** and the lattice frustrations. The π–π separation distance between neighboring **1.15**s in the columns is significantly longer (3.78 Å) than that of $\mathbf{1.4}_2$ π-dimer (3.2–3.3 Å). The larger π–π separation distance was reflected on the solid state properties of **1.15**. One-dimensional chains of **1.15** showed the Curie paramagnetism within the temperature range from 380 K to 100 K, and a weak antiferromagnetic behavior was observed below 100 K. The electroconductivity of **1.15** column was also estimated to be 10^{-10} S cm^{-1} at room temperature, which suggests that the weak multicenter bonding interaction between **1.15**s leads to the Mott–Hubbard insulator.

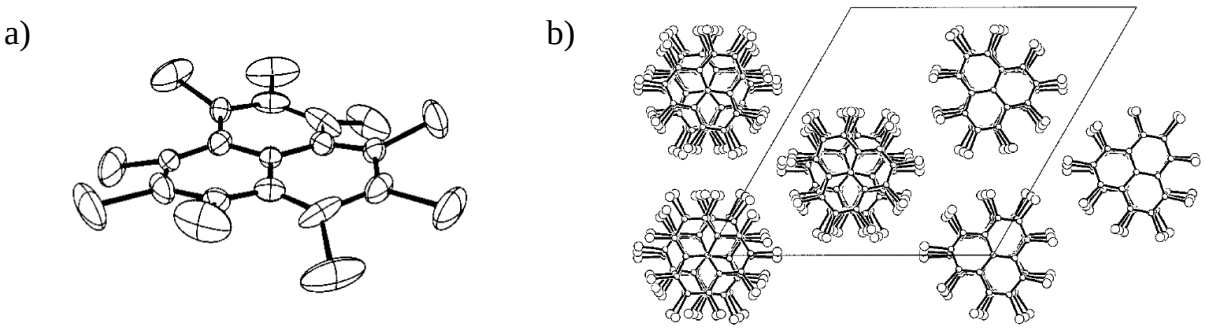

Figure 1.3.4. a) Molecular geometry and b) packing diagram of **1.15**. Reprinted with permission from ref. 47. Copyright 2001, American Chemical Society.

Phenalenyl analogues with sulfur atoms at α positions were also synthesized by Haddon *et al.* (**1.16**–**1.18**, in Figure 1.3.5).[48–51] Introduction of sulfur atoms resulted in the delocalization of its unpaired electron over the hetero atoms, leading to the decrease of spin density on α carbon atoms. The substantial change in the spin density was reflected on the hyperfine coupling constants (HFCCs) estimated by ESR measurements. HFCCs of **1.16** at α carbon atoms were estimated to be 0.540 and 0.507 mT,[48] which is significantly smaller than that of parent phenalenyl **1.3** (0.630 mT).[37,38] Introduction of additional sulfur atoms decreased the spin density on α carbon atoms. HFCC of **1.17** was determined to be 0.485 mT,[50] suggesting the decrease of the spin density on α carbon atoms.

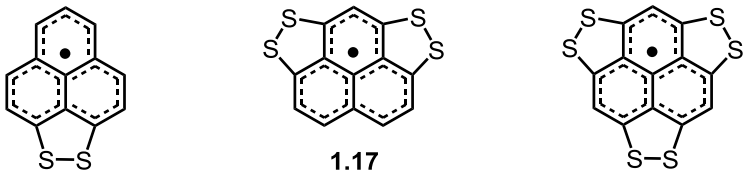

1.16 **1.17** **1.18**

Figure 1.3.5. Phenalenyl derivatives having sulfur atoms.

Dithiophenalenyl **1.16** was isolated as a π-dimerization mode with a staggered stacking motif, which was confirmed by X-ray crystallographic analysis.[49] π–π separation distance between **1.16**s in the π-dimer was 3.13–3.22 Å at 100 K, which is significantly shorter than that observed in the π-dimer of **1.4**. In addition, relatively short contacts were observed between sulfur atoms (3.555 Å), which is considerably shorter than the sum of van der Waals radius (3.7 Å). The conductivity at room temperature was determined to be 10^{-6} S cm^{-1}, which suggests the assembly of **1.16** should be a Mott-Hubbard insulator.

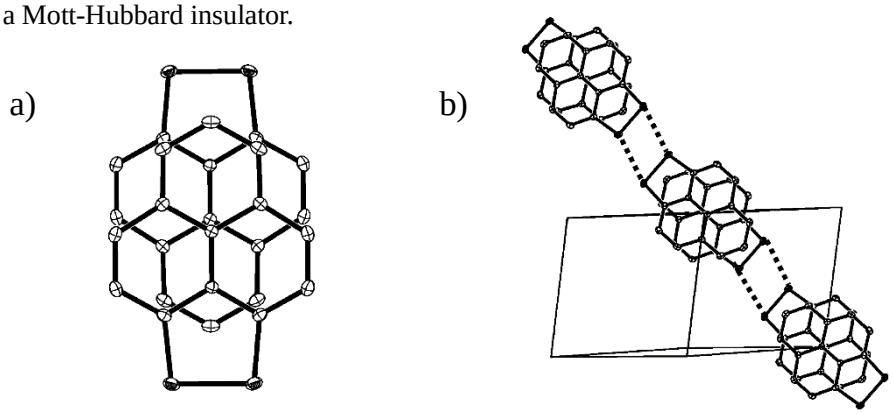

Figure 1.3.6. a) Molecular geometry and b) packing diagram of **1.16**. Reprinted with permission from ref. 49. Copyright 2007, American Chemical Society.

In contrast to the π-dimerization of **1.16**, tetrathiophenalenyl **1.17** adopted a unique σ-dimerization mode with a disulfide bond.[50] Bond dissociation energy of the disulfide bond of **1.17** was estimated by a computational calculation to be 11.9–12.9 kcal mol^{-1}, which is considerably larger than that of the disulfide bond formed by **1.16** (5.7 kcal mol^{-1}). It should be noted that the bond dissociation energy of the disulfide bond formed by hexatiophenalenyl **1.18** is estimated to be 19.9 kcal mol^{-1}. Whereas **1.18** has not yet been isolated, it would adopt the σ-dimerization mode with a strong disulfide bond.

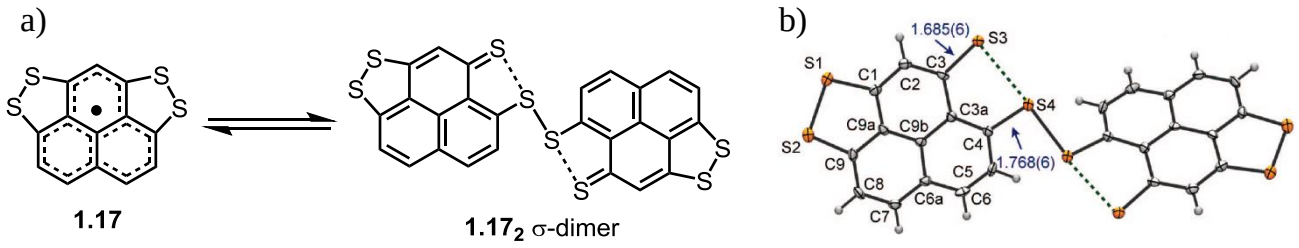

Figure 1.3.7. a) σ-dimerization of **1.17**. b) Molecular geometry of **1.17**$_2$ σ-dimer. Reprinted with permission from ref. 50. Copyright 2008, American Chemical Society.

Oxygen substituted phenalenyls, **1.19**–**1.21**, were also prepared by Haddon *et al*. and Morita *et al*.[49,52] Introduction of oxygen atoms also decreased the spin density on α carbon atoms due to the delocalization of an unpaired electron, which was supported by ESR measurements.

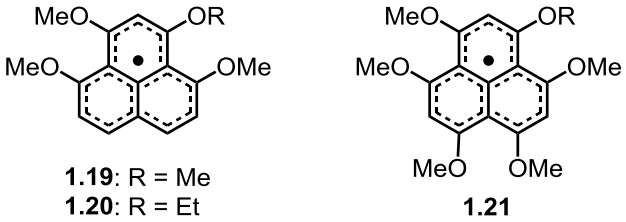

Figure 1.3.8. Oxygen substituted phenalenyl derivatives.

Unlike other derivatives, dimerization modes of **1.19**–**1.21** have not been observed directly. **1.20** demonstrated a facile decomposition to give peropyrene derivative **1.22**. As predicted in the case of parent phenalneyl **1.3**, dehydrogenation of the σ-dimer of **1.20** would be a key step for the decomposition, whereas the dimer was not detected experimentally.

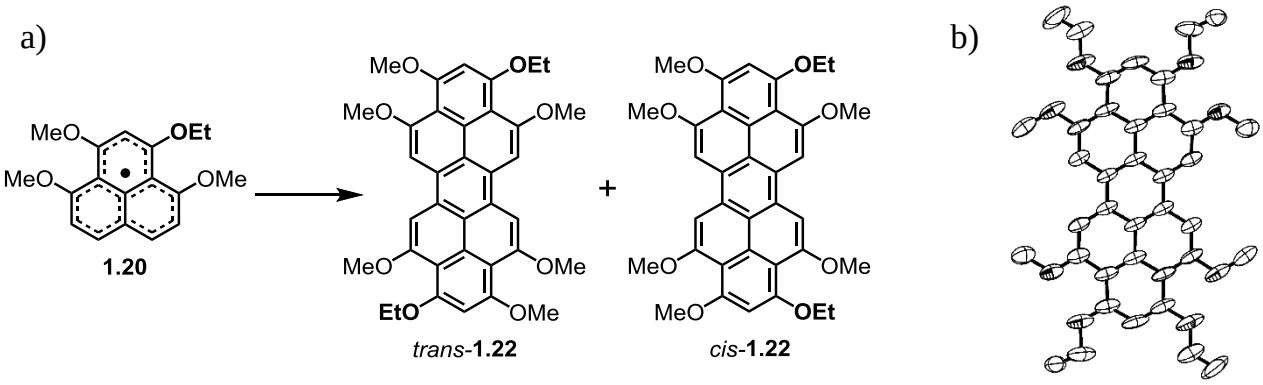

Figure 1.3.9. a) Decomposition of **1.20**. b) Molecular geometry of **1.22**. The crystal of **1.22** contains *trans*- and *cis*-isomers in 1:1 ratio, resulting in the disordered alignment in the crystal. Reprinted with permission from ref. 49. Copyright 2007, American Chemical Society.

1.4 References

(1) Gomberg, M. *J. Am. Chem. Soc.* **1900**, *22* (11), 752.

(2) Lankamp, H.; Nauta, W. T.; Mac Lean, C. *Tetrahedron Lett.* **1968**, *9* (2), 249.

(3) Allemand, J.; Gerdil, R. *Acta Crystallogr. Sect. B Struct. Crystallogr. Cryst. Chem.* **1978**, *34* (7), 2214.

(4) Goto, K.; Kubo, T.; Yamamoto, K.; Nakasuji, K.; Sato, K.; Shiomi, D.; Takui, T.; Kubota, M.; Kobayashi, T.; Yakusi, K.; Ouyang, J. *J. Am. Chem. Soc.* **1999**, *121* (7), 1619.

(5) Novoa, J. J.; Lafuente, P.; Sesto, R. E. Del; Miller, J. S. *Angew. Chem. Int. Ed.* **2001**, *40*(13), 2540.

(6) Sesto, R. E. Del; Miller, J. S.; Lafuente, P.; Novoa, J. J. *Chem. Eur. J.* **2002**, *8* (21), 4894.

(7) Miller, J. S.; Novoa, J. J. *Acc. Chem. Res.* **2007**, *40* (3), 189.

(8) Lemervovskii, D. A.; Stukan, R. A.; Tarasevich, B. N.; Slovokhotov, T. L.; Antipin, T. U.; Kalinin, A. E.; Struchov, Y. T. *Struct, Khim.* **1981**, *7*, 240.

(9) Zhang, J.; Sesto, R. E. Del.; Gordon, D. C.; Miller, J. S.; Zhang, J.; Liable-Sands, L. M.; Rheingold, A. L.; Burkhart, B. M. *Chem. Commun.* **1998**, *4* (13), 1385.

(10) Novoa, J. N.; Ribas-Ariño, J.; Shum, W. W.; Miller, J. S. *Inorg. Chem.* **2007**, *46* (1), 103.

(11) Graham, A. G.; Mota, F.; Shurdha, E.; Rheingold, A. L.; Novoa, J. J.; Miller, J. S. *Chem. Eur. J.* **2015**, *21* (38), 13240.

(12) Novoa, J. J.; Lafuente, P.; Del Sesto, R. E.; Miller, J. S. *CrystEngComm* **2002**, *4* (65), 373.

(13) Cui, Z.; Lischka, H.; Mueller, T.; Plasser, F.; Kertesz, M. *ChemPhysChem* **2014**, *15* (1), 165.

(14) Lü, J.-M.; Rosokha, S. V; Kochi, J. K. *J. Am. Chem. Soc.* **2003**, *125* (40), 12161.

(15) Casado, J.; Burrezo, P. M.; Ramírez, F. J.; Navarrete, J. T. L.; Lapidus, S. H.; Stephens, P. W.; Vo, H.-L.; Miller, J. S.; Mota, F.; Novoa, J. J. *Angew. Chemie Int. Ed.* **2013**, *52* (25), 6421.

(16) Strohmeier, M.; Barich, D. H.; Grant, D. M.; Miller, J. S.; Pugmire, R. J.; Simons, J. *J. Phys. Chem. A* **2006**, *110* (25), 7962.

(17) Jung, Y.; Head-Gordon, M. *Phys. Chem. Chem. Phys.* **2004**, *6* (9), 2008.

(18) Hoffmann, S. K.; Corvan, P. J.; Singh, P.; Sethulekshmi, C. N.; Metzger, R. M.; Hatfield, W. E. *J. Am. Chem. Soc* **1983**, *105* (14), 4608.

(19) Zhao, H.; Heintz, R. A.; Dunbar, K. R.; Rogers, R. D. *J. Am. Chem. Soc.* **1996**, *118* (50), 12844.

(20) Miller, J. S.; Zhang, J. H.; Reiff, W. M.; Dixon, D. A.; Preston, L. D.; Reis, A. H.; Gebert, E.; Extine, M.; Troup, J.; Epstein, A. J.; Ward, M. D. *J. Phys. Chem.* **1987**, *91* (16), 4344.

(21) Garcia-Yoldi, I.; Miller, J. S.; Novoa, J. J. *J. Phys. Chem. A* **2009**, *113* (25), 7124.

(22) Metzger, R. M.; Heimer, N. E.; Gundel, D.; Sixl, H.; Harms, R. H.; Keller, H. J.; Nöthe, D.; Wehe, D. *J. Chem. Phys.* **1982**, *77* (12), 6203.

(23) Marzotto, A.; Clemente, D. A.; Pasimeni, L. *J. Crystallogr. Spectrosc. Res.* **1988**, *18* (5), 545.

(24) Yan, Y.-K.; Mingos, D. M. P.; Müller, T. E.; Williams, D. J.; Kurmoo, M. *J. Chem. Soc. Daltn Trans.* **1995**, 2509.

(25) Scott, B. A.; La Placa, S. J.; Torrance, J. B.; Silverman, B. D.; Welber, B. *J. Am. Chem. Soc.* **1977**, *99* (20), 6631.

(26) Yakushi, K.; Nishimura, S.; Sugano, T.; Kuroda, H.; Ikemoto, I. *Acta Crystallogr. Sect. B Struct. Crystallogr. Cryst. Chem.* **1980**, *36* (2), 358.

(27) Garcia-Yoldi, I.; Miller, J. S.; Novoa, J. J. *J. Phys. Chem. A* **2009**, *113* (2), 484.

(28) Rosokha, S. V.; Kochi, J. K. *J. Am. Chem. Soc.* **2007**, *129* (4), 828.

(29) Kochi, J. K.; Rathore, R.; Maguères, P. Le. *J. Org. Chem.* **2000**, *65* (21), 6826.

(30) Suzuki, S.; Morita, Y.; Fukui, K.; Sato, K.; Shiomi, D.; Takui, T.; Nakasuji, K. *J. Am. Chem. Soc.* **2006**, *128* (8), 2530.

(31) Chi, X.; Itkis, M. E.; Patrick, B. O.; Barclay, T. M.; Reed, R. W.; Oakley, R. T.; Cordes, A. W.; Haddon, R. C. *J. Am. Chem. Soc.* **1999**, *121* (44), 10395.

(32) Pal, S. K.; Itkis, M. E.; Tham, F. S.; Reed, R. W.; Oakley, R. T.; Haddon, R. C. *Science* **2005**, *309* (5732), 281.

(33) Yoneda, K.; Nakano, M.; Fukuda, K.; Matsui, H.; Takamuku, S.; Hirosaki, Y.; Kubo, T.; Kamada, K.; Champagne, B. *Chem. Eur. J.* **2014**, *20* (35), 11129.

(34) Reid, D. H. *Q. Rev. Chem. Soc.* **1965**, *19* (3), 274.

(35) Boekelheide, V.; Larrabee, C. E. *J. Am. Chem. Soc.* **1950**, *72* (3), 1245.

(36) Reid, D. H. *Tetrahedron* **1958**, *3* (3), 339.

(37) Bennett, J. E. *Nature* **1960**, *188* (4749), 485.

(38) Gerson, F. *Helv. Chim. Acta* **1966**, *49* (5), 1463.

(39) Small, D.; Rosokha, S. V.; Kochi, J. K.; Head-Gordon, M. *J. Phys. Chem. A* **2005**, *109* (49), 11261.

(40) Zaitsev, V.; Rosokha, S. V.; Head-Gordon, M.; Kochi, J. K. *J. Org. Chem.* **2006**, *71* (2), 520.

(41) Kubo, T. *Chem. Rec.* **2015**, *15* (1), 218.

(42) Fukui, K.; Sato, K.; Shiomi, D.; Takui, T.; Itoh, K.; Gotoh, K.; Kubo, T.; Yamamoto, K.; Nakasuji, K.; Naito, A. *Synth. Met.* **1999**, *103* (1-3), 2257.

(43) Small, D.; Zaitsev, V.; Jung, Y.; Rosokha, S. V.; Head-Gordon, M.; Kochi, J. K. *J. Am. Chem. Soc.* **2004**, *126* (42), 13850.

(44) Haddon, R. C. *Nature* **1975**, *256* (5516), 394.

(45) Haddon, R. C.; Chichester, S. V.; Stein, S. M.; Marshall, J. H.; Mujsce, A. M. *J. Org. Chem.* **1987**, *52* (4), 711.

(46) Koutentis, P. A.; Haddon, R. C.; Oakley, R. T.; Cordes, A. W.; Brock, C. P. *Acta Crystallogr. Sect. B Struct. Sci.* **2001**, *57* (5), 680.

(47) Koutentis, P. A; Chen, Y.; Cao, Y.; Best, T. P.; Itkis, M. E.; Beer, L.; Oakley, R. T.; Cordes, A. W.; Brock, C. P.; Haddon, R. C. *J. Am. Chem. Soc.* **2001**, *123* (17), 3864.

(48) Haddon, R. C.; Wudl, F.; Kaplan, M. L.; Marshall, J. H.; Cais, R. E.; Bramwell, F. B. *J. Am. Chem. Soc.* **1978**, *100* (24), 7629.

(49) Beer, L.; Mandal, S. K.; Reed, R. W.; Oakley, R. T.; Tham, F. S.; Donnadieu, B.; Haddon, R. C. *Cryst. Growth Des.* **2007**, *7* (4), 802.

(50) Beer, L.; Reed, R. W.; Robertson, C. M.; Oakley, R. T.; Tham, F. S.; Haddon, R. C. *Org. Lett.* **2008**, *10* (14), 3121.

(51) Bag, P.; Tham, F. S.; Donnadieu, B.; Haddon, R. C. *Org. Lett.* **2013**, *15* (6), 1198.

(52) Ueda, A.; Suzuki, S.; Yoshida, K.; Fukui, K.; Sato, K.; Takui, T.; Nakasuji, K.; Morita, Y. *Angew. Chem. Int. Ed. Engl.* **2013**, *52* (18), 4795.

-Chapter 2-
2,5,8-Triarylphenalenyl:
Elucidating the Effects of Substituted Groups on the Dimerization Mode of Phenalenyl

2.1 Introduction

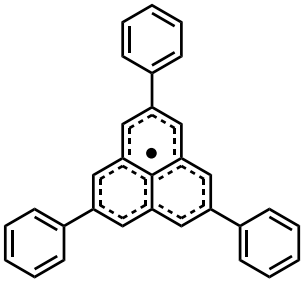

TPPLY **2.1a**

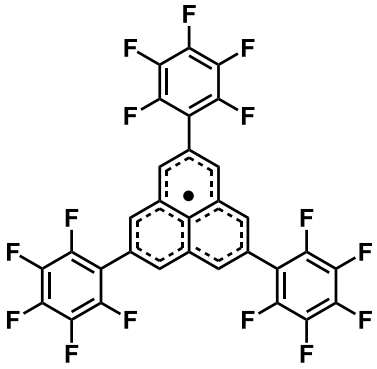

TPFPPLY **2.1b**

Numerous efforts have been devoted to understand the dimerization behavior of phenalenyl on the basis of theoretical[1–3] and experimental[4–8] approaches. According to the previous reports, introduction of substituted groups at α positions affects significantly the dimerization behavior of phenalenyl due to the steric and electronic perturbations; thus, phenalenyl derivatives having three substituted groups on the β carbon atoms are ideal candidates for studying the effect of substituted groups on the natural dimerization behavior.

In chapter 2, the essential dimerization modes of 2,5,8-triphenylphenalenyl (TPPLY, **2.1a**)[9] and 2,5,8-tris(pentafluorophenyl)phenalenyl (TPFPPLY, **2.1b**)[10], which are phenalenyl derivatives designed and synthesized by our group, were discussed. Computational calculations were conducted to estimate molecular geometries and electronic structures of **2.1a** and **2.1b** with a UB3LYP/6-31G** method. Twisted angles between a phenalenyl plane and substituted groups are determined to be 39.2° for **2.1a** and 41.3° for **2.1b**, respectively, and the steric hindrance is enough small for **2.1a** and **2.1b** to adopt both σ and π-dimerization modes. With focused on the spin density distributions calculated with a UBLYP/6-31G**//UB3LYP/6-31G** method, the unpaired electrons are localized on phenalenyl moieties as parent phenalenyl. In contrast, considerable difference was observed between electrostatic potential maps of **2.1a** and **2.1b**. The electron withdrawing effect of pentafluorophenyl groups decreased the electron density on a phenalenyl moiety of **2.1b**, leading to the significant difference in the dimerization behavior and reactivity.

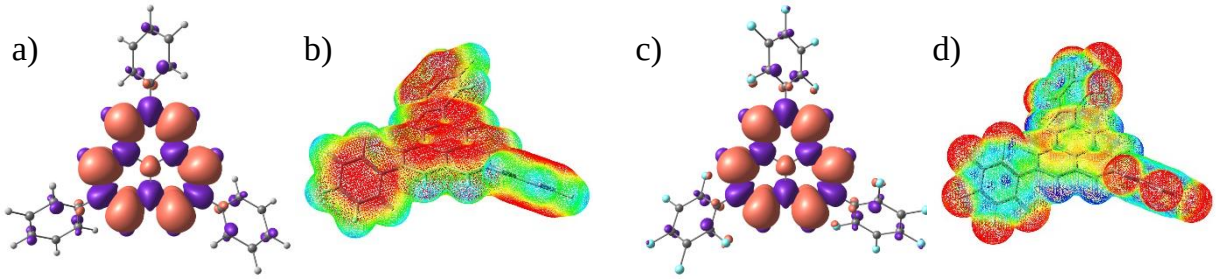

Figure 2.1.1. a) Spin density map and b) electrostatic potential map of **2.1a**. c) Spin density map and d) electrostatic potential map of **2.1b**. Figure 2.1.1d was reprinted with permission from ref. 10. Copyright 2014, Wiley-VCH Verlag GmbH & Co. KGaA.

2.2 Synthesis of TPPLY and TPFPPLY

The synthetic procedures for TPPLY **2.1a** and TPFPPLY **2.1b** are displayed in Scheme 2.2.1 and Scheme 2.2.2, respectively. **2.1a** was synthesized in 8 steps from 2,7-diphenylnaphthalene (**2.3**) which was prepared by the Suzuki-Miyaura coupling of 2,7-dibromonaphthalene (**2.2**) with phenylboronic acid. The monobrominated compound (**2.4**) was obtained by the selective lithiation of the dibrominated derivative prepared from **2.3** by the treatment with excess amount of bromine. **2.4** was converted readily into **2.5** by the Heck reaction, and following reduction and hydrolysis gave **2.7**. Although the intramolecular Friedel-Crafts cyclization of the acyl chloride derivative prepared from **2.7** gave a non-negligible amount of a byproduct containing a five-membered ring, the phenalanone derivative **2.8** was obtained in pure form after a silica gel column chromatography. Phenalene derivative (**2.10**), which is the key precursor for **2a**, was prepared by reduction and dehydration. Dehydrogenation of the phenalene derivative **2.10** with an equimolar *p*-chloranil in a degassed sealed tube gave rise to dark violet cubic crystals of **2.1a**.

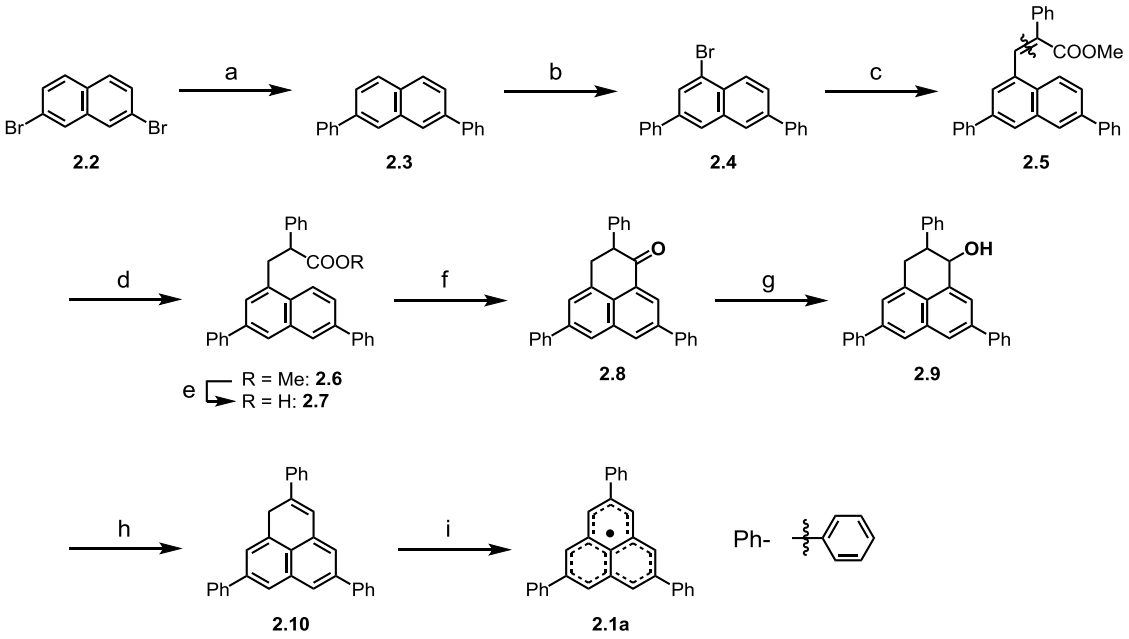

Scheme 2.2.1. Synthetic procedure for **2.1a**. Reagent and condition: a) $PhB(OH)_2$, $Pd(PPh_3)_4$, K_2CO_3, toluene/EtOH/H_2O (4/1/1), 70 °C, 91% yield; b) (i) bromine, acetic acid, 110 °C, (ii) ^nBuLi, ether, −78 °C, 52% yield; c) methyl 2-phenylacrylate, $Pd(OAc)_2$, PPh_3, K_2CO_3, $^nBu_4NBr$, DMF, 80 °C, 48% yield; d) $NiCl_2$, $NaBH_4$, DCM/MeOH (1/1), RT; e) 10% NaOHaq., EtOH, 90 °C, 54% yield (2 steps); f) (i) $(COCl)_2$, 60 °C, (ii) $AlCl_3$, DCM, −78 to −30 °C, 27% yield; g) $NaBH_4$, DCM/EtOH (1/1), RT, h) *p*-$TsOH{\cdot}H_2O$, toluene, 120 °C, quantitative yield (2 steps); i) *p*-chloranil, toluene/hexane (11/9), 30 °C, 67% yield. *p*-chloranil = 2,3,5,6-tetrachloro-1,4-benzoquinone.

2.1b was also synthesized from 2,7-dibromonaphthalene (**2.2**) in 9 steps. The synthetic approach is basically similar to that for **2.1a**, whereas some optimizations of reaction conditions are required because the presence of nucleophiles results in the decomposition of pentafluorophenyl groups through a nucleophilic aromatic substitution. The formyl derivative (**2.12**), which was prepared from diarylnaphthalene (**2.11**), was converted quantitatively to the unsaturated ester (**2.13**), then hydrogenation and subsequent hydrolysis afforded carboxylic acid (**2.15**) in high yield. The intramolecular Friedel-Crafts cyclization of the acyl chloride derived from **2.15** gave diarylphenalanone (**2.16**), and additional pentafluorophenyl group was inserted by the nucleophilic aromatic substitution with hexafluorobenzene to afford triarylphenalanone (**2.17**). Phenalene derivative (**2.19**) was prepared by reduction followed by dehydration. Treatment of phenalene (**2.19**) with DDQ under nitrogen atmosphere gave **2.1b** as a white powder. Surprisingly, **2.1b** is stable enough to be purified by column chromatography in air.

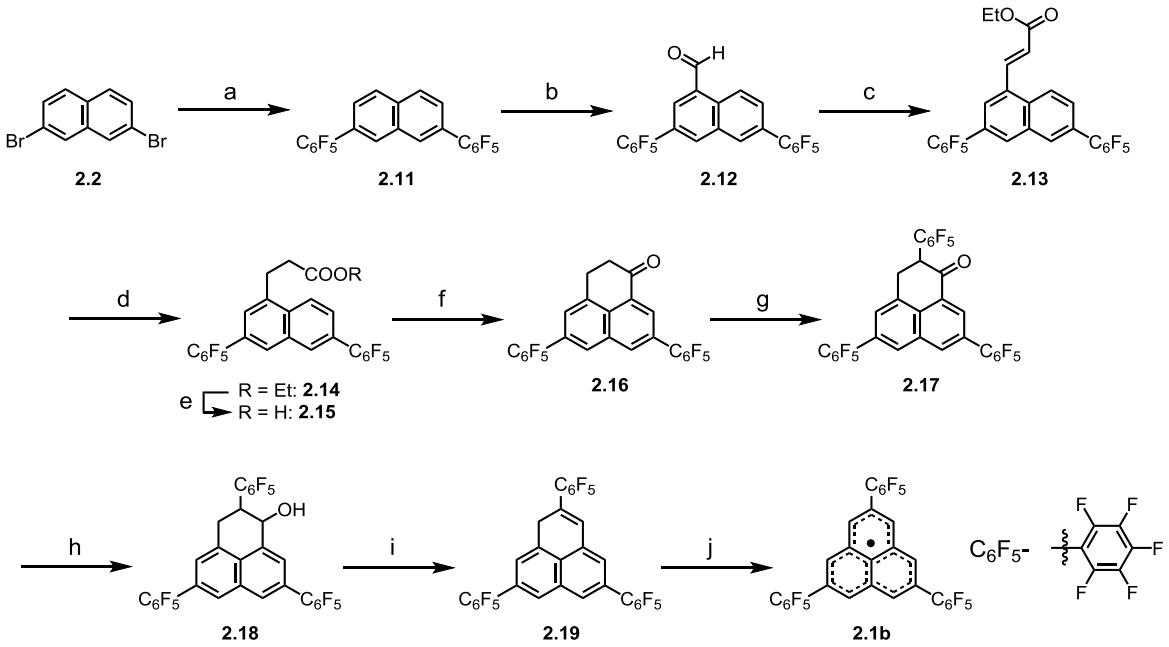

Scheme 2.2.2. Synthetic procedure for **2.1b**. Reagent and condition: a) $C_6F_5B(OH)_2$, $Pd_2(dba)_3$, P^tBu_3, CsF, Ag_2O, DMF, 100 °C, 52% yield; b) $CHCl_2OCH_3$, $AlCl_3$, DCM, −78 to −40 °C, 81% yield; c) NaH, triethyl phosphonoacetate, THF, RT, quantitative yield; d) H_2 (1 atm), 10% Pd-C, DCM/EtOH (1/10), RT, quantitative yield; e) 10% NaOHaq., THF, 60 °C, quantitative yield; f) (i) $(COCl)_2$, 60 °C, (ii) $AlCl_3$, DCM, −78 to −40 °C, 81% yield; g) NaH, C_6F_6, THF, 65 °C, 60% yield; h) $NaBH_4$, DCM/EtOH (1/1), RT, 81% yield; i) *p*-$TsOH{\cdot}H_2O$, toluene, 120 °C, 93% yield; j) DDQ, toluene, 80 °C, 90% yield. DDQ = 2,3-dichloro-5,6-dicyano-1,4-benzoquinone.

2.3 X-ray crystallography

2.3.1 Molecular geometry of TPPLY π-dimer

Recrystallization of **2.1a** from degassed toluene/hexane mixed solvent gave dark violet cubic crystals which are suitable for X-ray crystallographic analysis. Molecular geometry of **2.1a** was shown in Figure 2.3.1. **2.1a** forms a π-dimer with extraordinarily short contacts between α carbon atoms bearing large spin density ($D_{\alpha\alpha}$ = 3.067 Å at 300 K and 3.017 Å at 100 K). The distance between central carbon atoms, D_{cc}, with little spin density is slightly longer than $D_{\alpha\alpha}$ (D_{cc} = 3.145 Å at 300 K and 3.111 Å at 100 K), resulting in the concave-concave overlap of **2.1a**$_2$ π-dimer. This geometry is striking contrast to the convex-convex overlap of **1.4**$_2$ π-dimer ($D_{\alpha\alpha}$ = 3.306 Å on average, and D_{cc} = 3.201 Å at 300 K),[11] which indicates that the sterically less hindered phenyl groups lead to the shorter π–π separation distance between α carbon atoms.

The dihedral angle between phenalenyl backbone and phenyl groups is determined to be 35°, and phenyl groups adopt the edge-to-face configuration dominated by CH–π interactions. This conformation is well consistent with a geometry expected by a computational calculation at UM05-2X/6-31G** level. CH–π interactions between side phenyl groups can be estimated from the difference of interaction energy between **1.3**$_2$ π-dimer and **2.1a**$_2$ π-dimer, suggesting each six CH–π interactions contribute approximately 1.7 kcal mol^{-1} to the interaction energy.

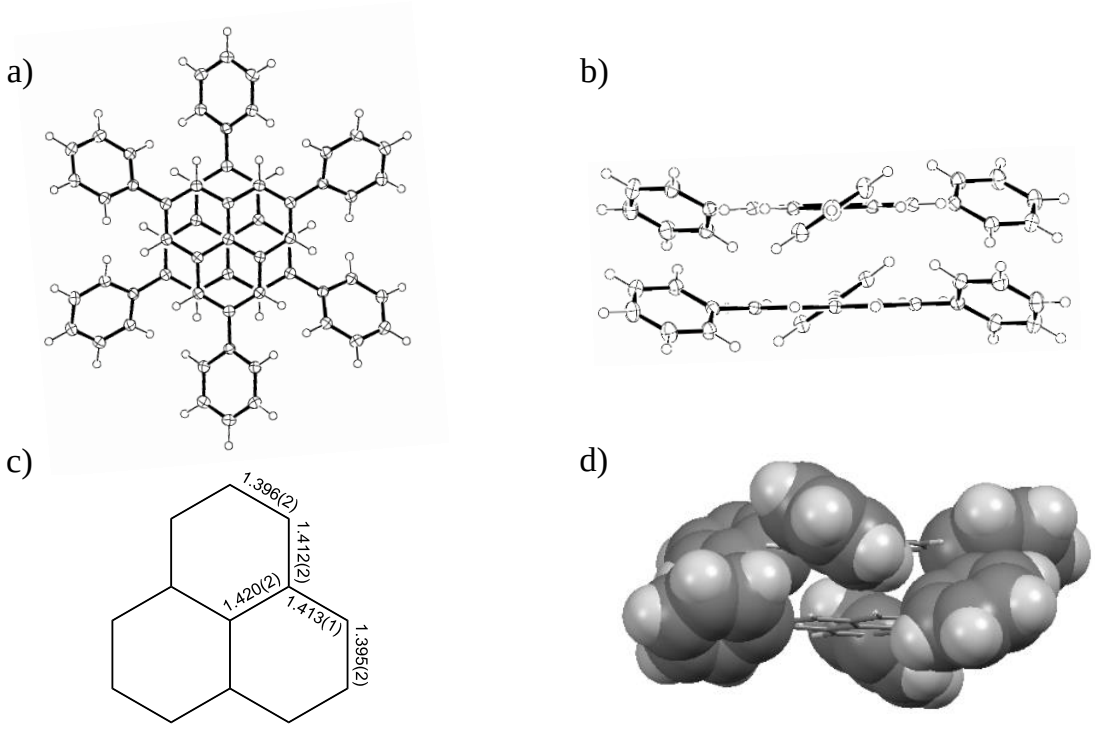

Figure 2.3.1. Ortep drawing of **2.1a**$_2$ π-dimer at the 50% probability level. a) Top view and b) side view. c) Bond lengths of phenalenyl unit in **2.1a**$_2$ π-dimer. d) Conformation of phenyl groups. a) b) Reprinted with permission from ref. 9. Copyright 2014, American Chemical Society.

Crystal System = cubic, a = 20.203(3) Å, V = 8245(1) Å^3, Space Group = $Ia\bar{3}$ (#206), Z = 16, μ(MoKα) = 0.72 cm^{-1}, T = 100 K, $R1$ [F^2>2σ(F^2)] = 0.041, $wR2$(all data) = 0.104, S = 1.09, Refl./param. = 1584/122.

2.3.2 Molecular geometry of TPFPPLY σ-dimer

Recrystallization of **2.1b** from acetonitrile gave greenish yellow plates suitable for X-ray crystallographic analysis. The crystal structure was displayed in Figure 2.3.2. **2.1b** adopts a σ-dimerization mode with a *RR*/*SS* configuration. The bond length of C(sp^3)–C(sp^3) single bond connecting two phenalenyl units is 1.636(6) Å, which is considerably longer than the general C(sp^3)–C(sp^3) σ-bond (1.54 Å). This result indicates the single bond between **2.1b**s is relatively weak, leading to another association mode in a high temperature phase (chapter 2.6.1). Furthermore, bond lengths in phenalenyl units suggested the electronic structure of **2.1b** is almost identical to that of phenalene.

The dihedral angles between phenalenyl ring and pentafluorophenyl groups are 36–62°, and two of six pentafluorophenyl groups lie on phenalenyl rings. The interaction between pentafluorophenyl groups and phenalenyl moieties is considered to be analogous to the electrostatic interaction between benzene and hexafluorobenzene,[12] giving an additional interaction energy between two **2.1b**s.

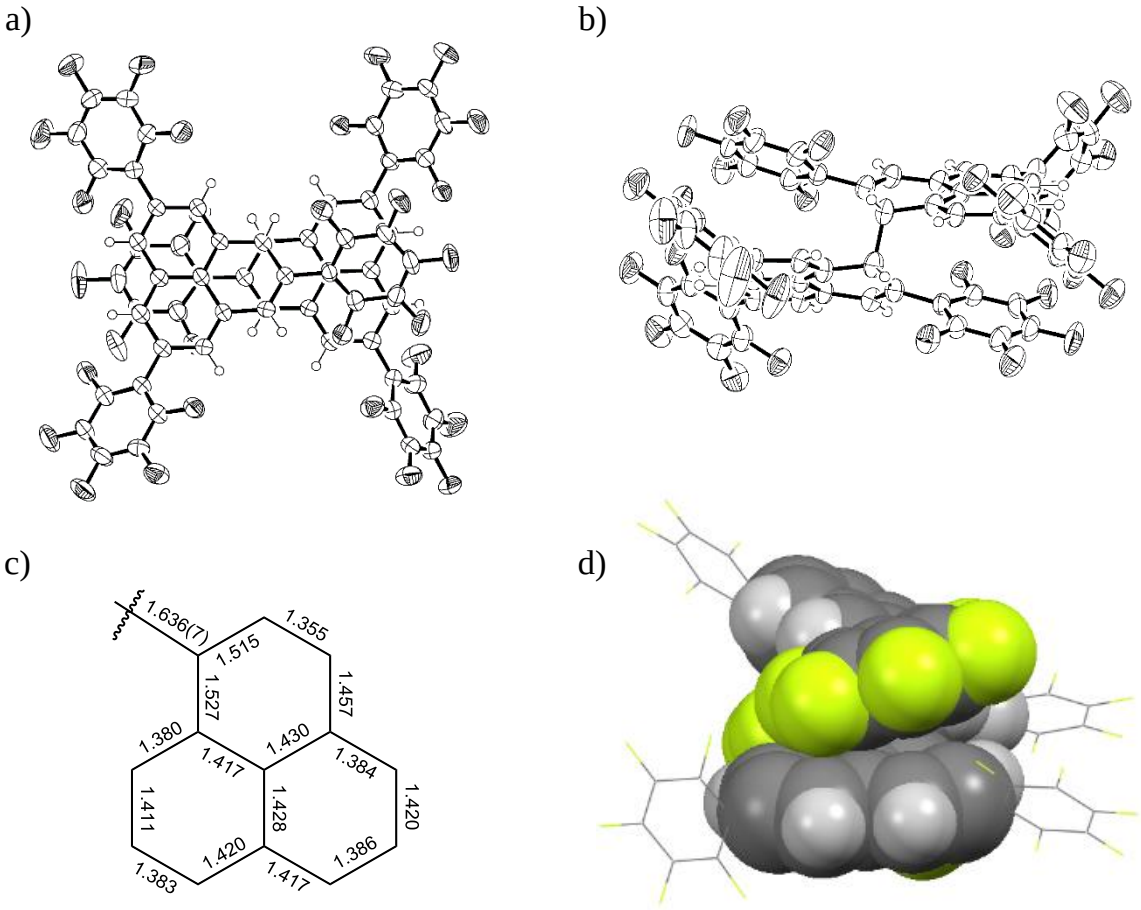

Figure 2.3.2. Ortep drawing of **2.1b**$_2$ σ-dimer at the 50% probability level. a) Top view and b) side view. c) Bond lengths of phenalenyl unit in **2.1b**$_2$ σ-dimer. d) Geometry of pentafluorophenyl groups and phenalenyl moiety. Crystal System = monoclinic, a = 23.685(7) Å, b = 7.479(2) Å, c = 27.734(8) Å, β = 94.140(4)°, V = 4900(2) Å^3, Space Group = $P2_1/c$ (#14), Z = 4, μ(MoKα) = 1.85 cm^{-1}, T = 200 K, $R1$ [$F^2>2\sigma(F^2)$] = 0.079, $wR2$(all data) = 0.237, S = 1.02, Refl./param. = 11059/829.

2.4 Solid state properties of TPPLY π-dimer and TPFPPLY σ-dimer

2.4.1 Electronic absorption spectra

Electronic absorption spectrum in solid state gave significant insights into the covalent bonding interaction contributing to the formation of multicenter bonding between two phenalenyl moieties. As shown in Figure 2.4.1, **2.1a** and **2.1b** demonstrated weak absorption bands (**2.1a**: 570 nm, ε = 186 cm^{-1} M^{-1}, **2.1b**: 570 nm, ε = 133 cm^{-1} M^{-1}) in dilute solutions, attributing to forbidden transitions of monomeric radicals as observed in **1.4** (540 nm, $\varepsilon \approx 10^2$ cm^{-1} M^{-1}).[5,11,13]

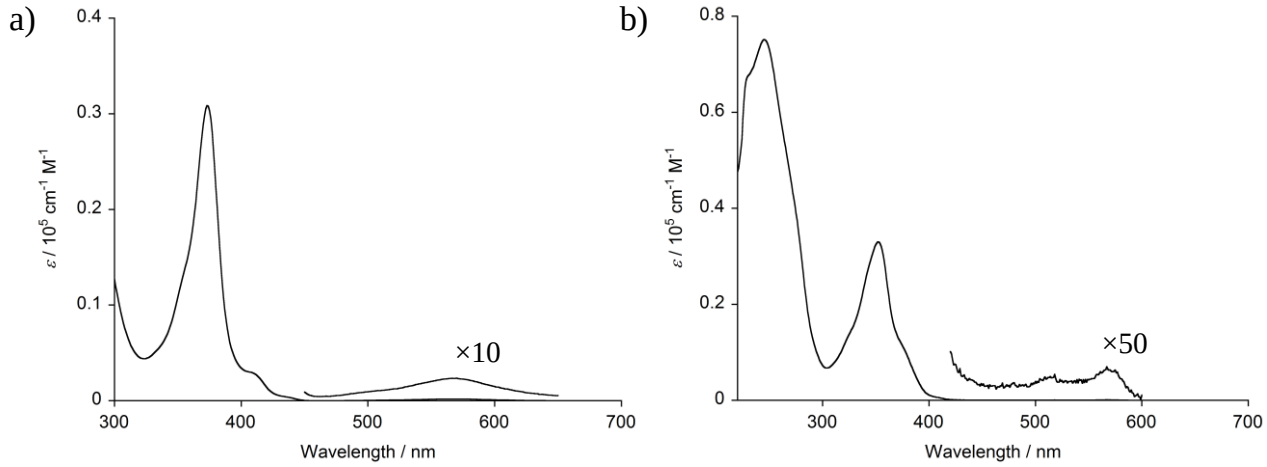

Figure 2.4.1. Electronic absorption spectra of a) **2.1a** in toluene and b) **2.1b** in DCM.

Unlike the electronic absorption spectrum in dilute solution, **2.1a**$_2$ π-dimer represented an intense absorption band centered at 574 nm (Figure 2.4.2) in KBr pellet, which can be assignable to the HOMO–LUMO transition of **2.1a**$_2$ π-dimer. HOMO and LUMO of phenalenyl π-dimer are formed from the bonding and antibonding combinations of two SOMOs; thus, the HOMO–LUMO splitting reflects directly the strength of covalent bonding interactions. Shorter π–π separation distance of **2.1a**$_2$ π-dimer resulted in a blue shift of HOMO–LUMO transition compared to **1.4**$_2$ π-dimer (612 nm).

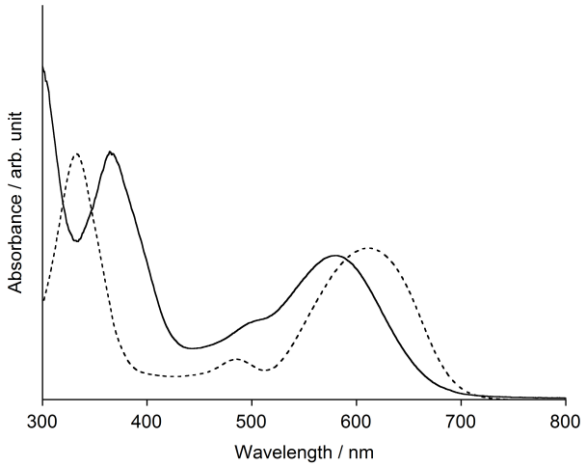

Figure 2.4.2. Electronic absorption spectra of **2.1a**$_2$ π-dimer (solid) and **1.4**$_2$ π-dimer (dashed) in KBr pellet.

In contrast to **2.1a$_2$** π-dimer, **2.1b$_2$** σ-dimer showed a featureless absorption spectrum in KBr pellet (Figure 2.4.3). This result fully supports the idea that the electronic structure of **2.1b$_2$** σ-dimer is similar to phenalene derivative as expected by the X-ray crystallographic analysis.

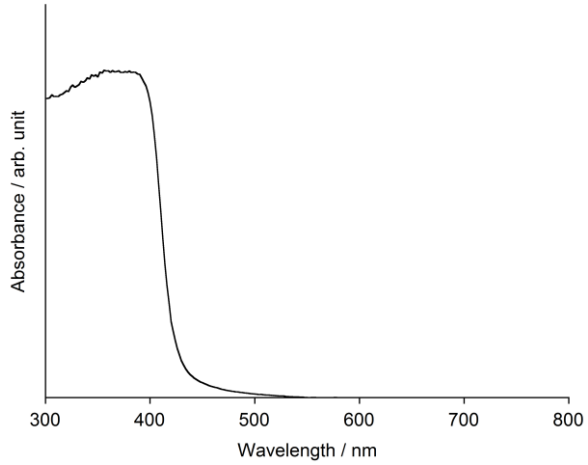

Figure 2.4.3. Electronic absorption spectrum of **2.1b$_2$** σ-dimer in KBr pellet.

2.4.2 Magnetic susceptibility measurement of TPPLY π-dimer

The covalent bonding interaction between two phenalenyl sites can be estimated quantitatively by the magnetic susceptibility measurement. Energy splitting of **1.4$_2$** π-dimer was estimated from an increasing susceptibility above 200 K to be 2000 K (4.0 kcal mol^{-1}) by SQUID measurements.[14] In contrast, a polycrystalline sample of **2.1a$_2$** π-dimer represented no susceptibility increase within the temperature range from 4 K to 380 K (Figure 2.4.4), indicating a prominent diamagnetic character of **2.1a$_2$** π-dimer. As observed in the electronic absorption spectrum in solid state, a shorter π–π separation distance of **2.1a$_2$** π-dimer enhances the strength of covalent bonding interaction between two phenalenyl sites, leading to a stronger diamagnetic behavior with respect to **1.4$_2$** π-dimer.

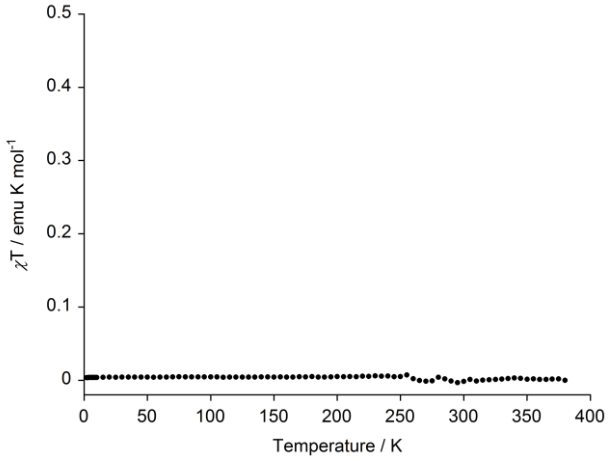

Figure 2.4.4. χT–T plot of the polycrystalline sample of **2.1a$_2$** π-dimer.

2.5 Dimerization behavior of TPPLY and TPFPPLY in solution state

2.5.1 Electron spin resonance spectrum

Electron spin resonance (ESR) spectra of TPPLY (**2.1a**) were measured in a degassed toluene solution. As shown in Figure 2.5.1a, a dilute solution of **2.1a**$_2$ π-dimer gave a well resolved multiline ESR spectrum (g = 2.003) assignable to monomeric **2.1a**. Hyperfine coupling constants (HFCCs) of protons on phenalenyl moiety and phenyl substituents were determined as depicted in Figure 2.5.1c, which is fully consistent with the values estimated with a UBLYP/6-31G**//UB3LYP/6-31G** method. HFCC of the phenalenyl α protons, a(H_α), is identical to those of nonsubstituted phenalenyl **1.3** (a(H_α) = 0.630 mT)[15,16] and a *tert*-butyl derivative **1.4** (a(H_α) = 0.620 mT)[11], suggesting an unpaired electron is localized on the phenalenyl site.

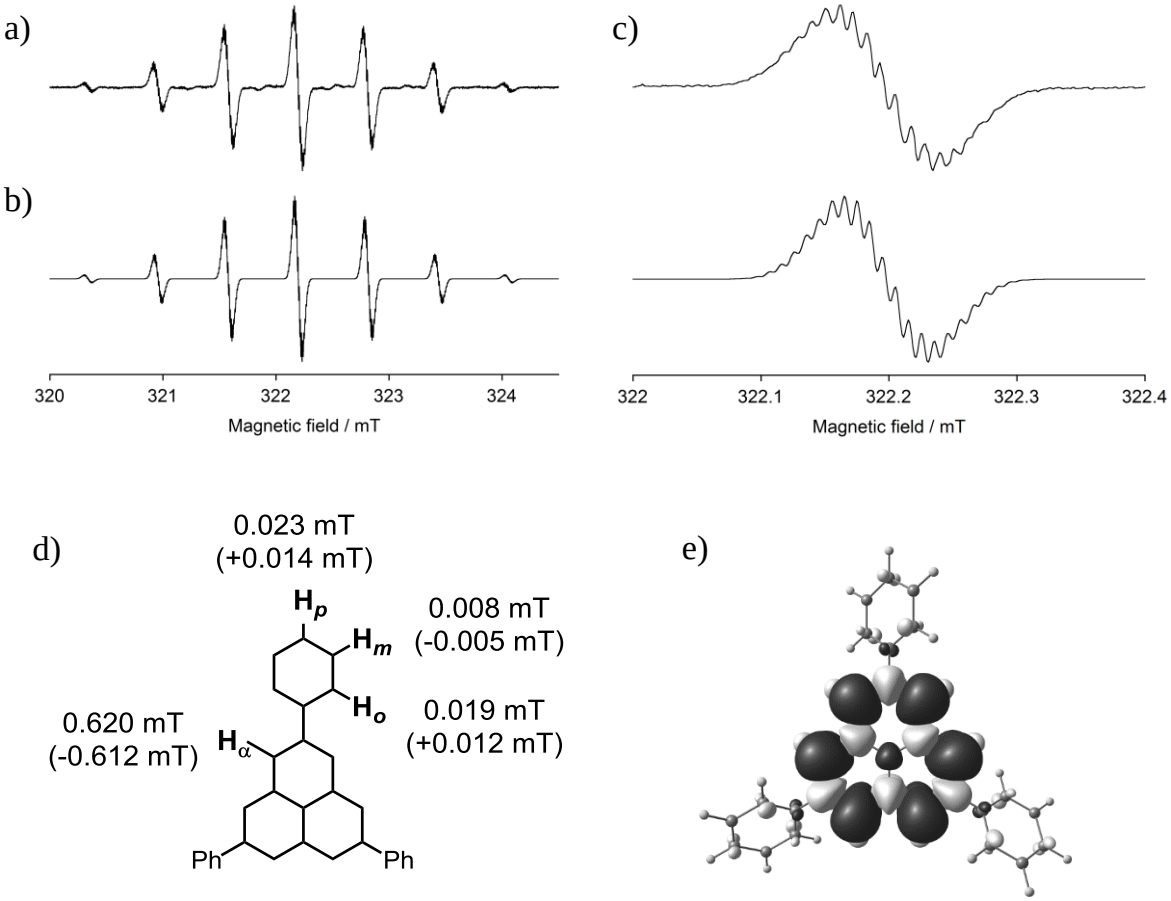

Figure 2.5.1. a) Observed (1×10^{-5} M, g = 2.003) and b) simulated ESR spectra of **2.1a** in toluene at 270 K. c) Magnified view of the centered peak. d) Experimentally determined HFCCs (in mT) of **2.1a**. In parentheses, HFCCs estimated by a UBLYP/6-31G**//UB3LYP/6-31G** method and the McConnell model. e) Spin density map calculated by a UBLYP/6-31G**//UB3LYP/6-31G** method. Black and gray surfaces represent α and β spin densities drawn at 0.0005 e/au^3 level, respectively. Reprinted with permission from ref. 9. Copyright 2014, American Chemical Society.

The ESR signal of **2.1a** decreased in the intensity upon decreasing temperature and disappeared at 170 K. This result indicates that the decrease of temperature resulted in the formation of the diamagnetic dimer of **2.1a** as observed in the cases of other phenalenyl derivatives. The intensity change can be expressed quantitatively along the thermodynamic equilibrium, and thermodynamic parameters for dimerization, ΔH and ΔS, were estimated by using the van't Hoff equation to be −9.6 kcal mol^{-1} and −18 cal K^{-1} mol^{-1}. The enthalpy change is almost identical to those for **1.3** (ΔH = −10.2 kcal mol^{-1}) and **1.4** (ΔH = −9.5 kcal mol^{-1}).[5,13]

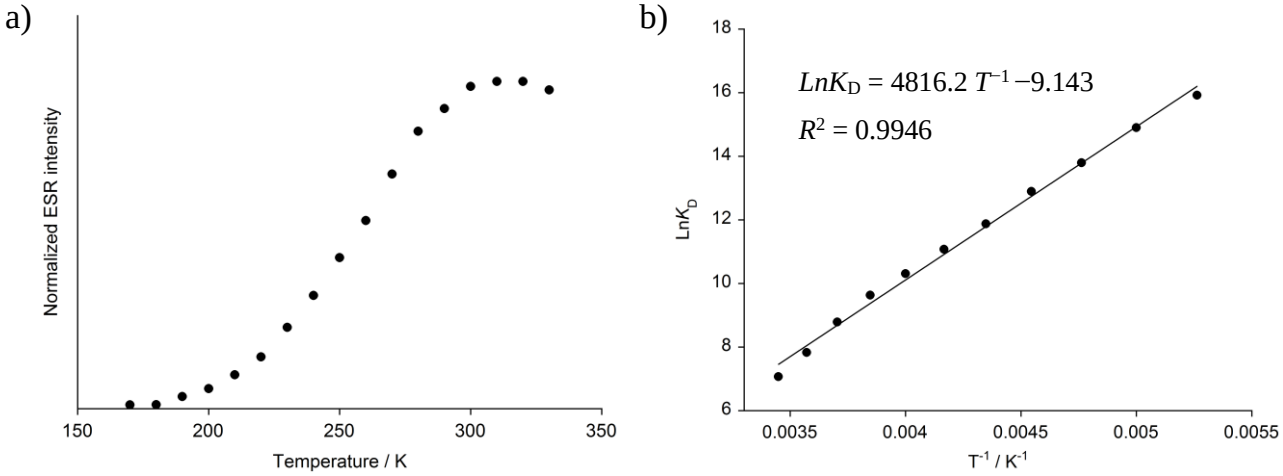

Figure 2.5.2. a) Temperature dependency of ESR signal intensity. b) Van't Hoff plot. Reprinted with permission from ref. 9. Copyright 2014, American Chemical Society.

TPFPPLY **2.1b**$_2$ σ-dimer also showed an unambiguous ESR spectrum corresponding to monomeric **2.1b** in a degassed toluene solution (Figure 2.5.3a). HFCCs determined by a spectral simulation are well correspondence with that estimated by theoretical calculations at UBLYP/6-31G**//UB3LYP/6-31G** level (Figure 2.5.3c). HFCC of phenalenyl α protons $a(H_\alpha)$ was estimated to be 0.622 mT, which is identical to those for **2.1a** and other phenalenyl derivatives. As shown in a spin density map (Figure 2.5.3d), an unpaired electron resides on the phenalenyl moiety.

The ESR signal of **2.1b** decreased in the intensity with decreasing temperature and disappeared at 230 K (Figure 2.5.4). Thermodynamic parameters for the dimerization of **2.1b** were determined from the intensity changes using the Van't Hoff plot to be ΔH = −15 kcal mol^{-1} and ΔS = −32 cal K^{-1} mol^{-1}. The enthalpy change was significantly larger than that for **2.1a** and other derivatives. Theoretical calculations support the results. Larger association energies are expected by the theoretical calculations for phenalenyl derivatives having electron withdrawing groups.[9] In addition, the electrostatic interaction between pentafluorophenyl groups and phenalenyl planes observed in crystalline phase by X-ray crystallography contributes to the prominent dimerization behavior.

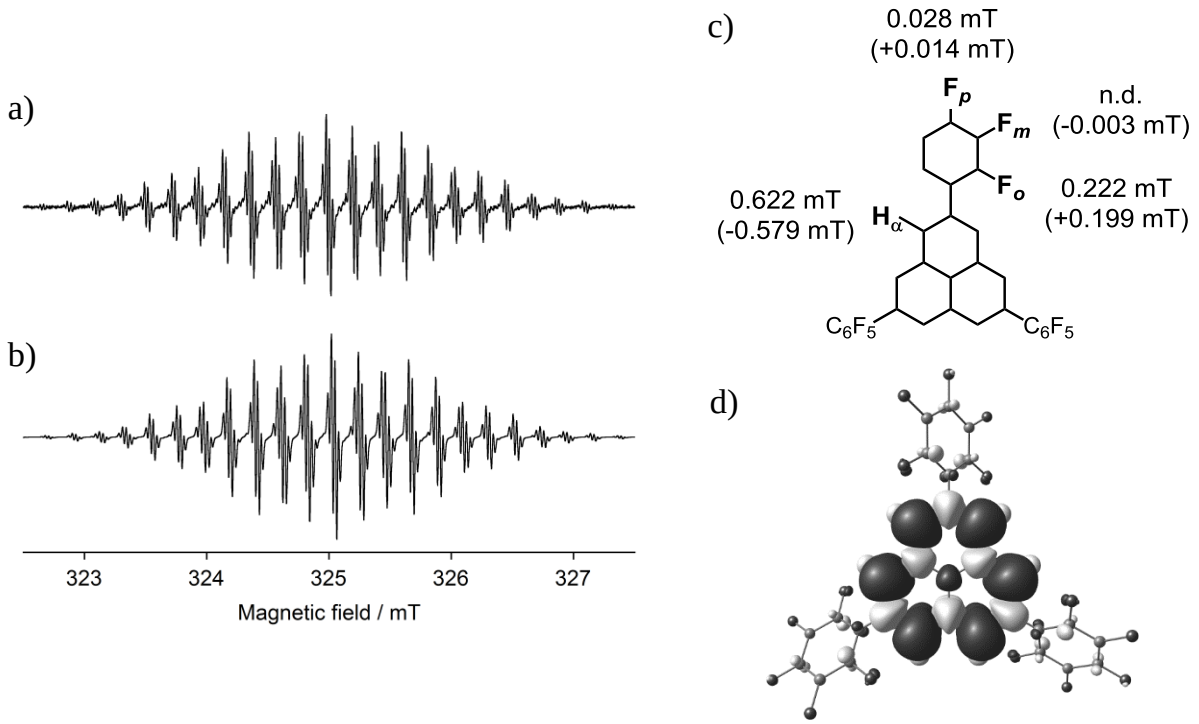

Figure 2.5.3. a) Observed (1.5×10^{-4} M, g = 2.003) and b) simulated ESR spectra of **2.1b** in toluene at RT. c) Experimentally determined HFCCs (in mT) of **2.1b**. In parentheses, HFCCs estimated by a UBLYP/6-31G**//UB3LYP/6-31G** method and the McConnell model. d) Spin density map calculated by a UBLYP/6-31G**//UB3LYP/6-31G** method. Black and gray surfaces represent α and β spin densities drawn at 0.0005 e/au^3 level, respectively. Reprinted with permission from ref. 10. Copyright 2014, Wiley-VCH Verlag GmbH & Co. KGaA.

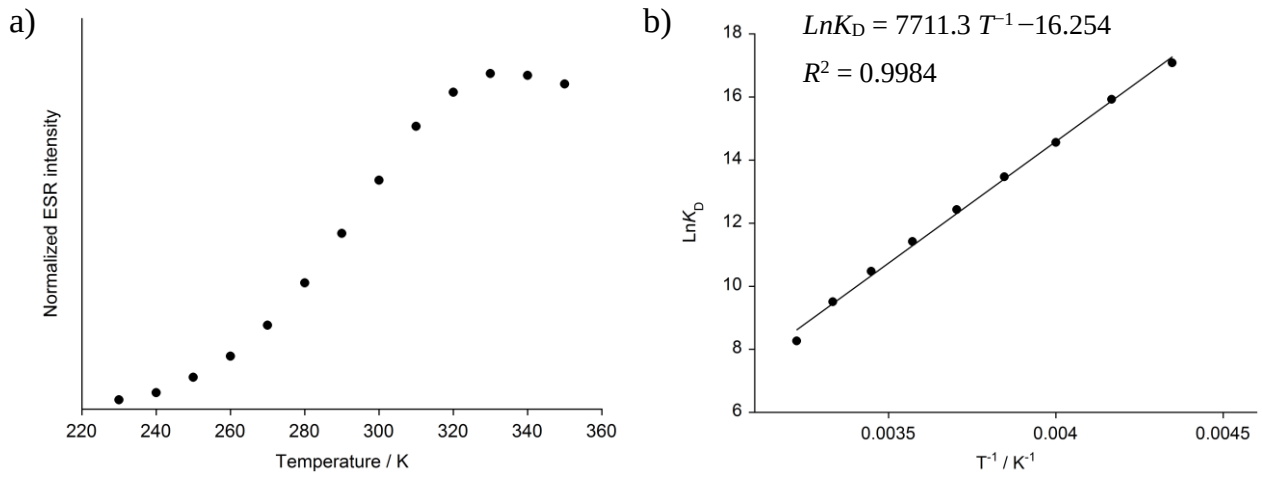

Figure 2.5.4. a) Temperature dependency of ESR signal intensity. b) Van't Hoff plot.

2.5.2 ^{1}H NMR spectroscopy of TPPLY and TPFPPLY

Structural characterizations of diamagnetic dimers of **2.1a** and **2.1b** in solution state were conducted by ^{1}H NMR spectroscopy at low temperature. ^{1}H NMR spectra of **2.1a** were recorded with generating it by a treatment of hydro-precursor phenalene **2.10** with *p*-chloranil in degassed dichloromethane-d_2, because of the extremely low solubility of **2.1a**$_2$ π-dimer. **2.1a** showed no signal in ^{1}H NMR spectrum at 273 K, whereas broaden signals appeared at 6.8 ppm and 7.5 ppm upon cooling the solution to 203 K (Figure 2.5.5). The characteristic signal at 6.8 ppm can be assigned to α protons of phenalenyl π-dimer as reported in the case of **1.4**$_2$ π-dimer (6.5 ppm),[17] and peaks around 7.5 ppm were attributed to side phenyl groups. This assignment is fully consistent with the computationally predicted chemical shifts with a GIAO-HF/6-311+G** method (H_o: 7.4 ppm, H_m; 7.1 ppm, H_p: 7.1 ppm, H_α: 6.3 ppm). It should be noted that no signal corresponding to **2.1a**$_2$ σ-dimer was detected, suggesting **2.1a** adopts a π-dimer solely as the most stable dimerization mode even in solution state. Theoretical calculations predicted that π-dimerization mode of **2.1a** is 2.8 kcal mol^{-1} less stable than the σ-dimerization mode,[9] whereas the energy difference is quite small to reverse the preference of dimerization mode by a calculation method and a solvent effect.

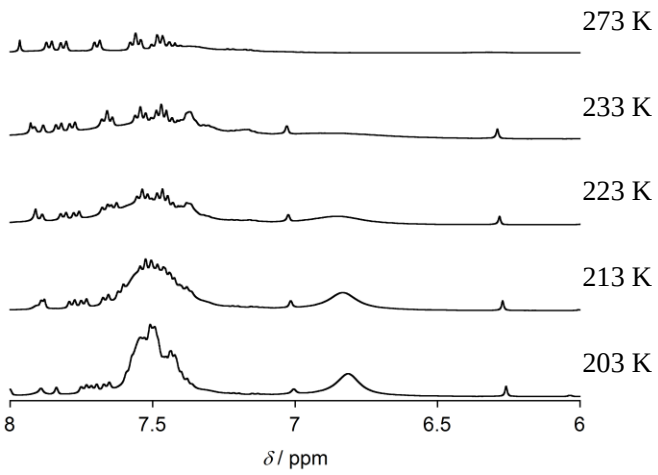

Figure 2.5.5. Variable temperature ^{1}H NMR spectra of **2.1a** in dichloromethane-d_2 (10 mM solution). Small peaks are arising from 2,5,8-triphenylphenalenone. Reprinted with permission from ref. 9. Copyright 2014, American Chemical Society.

The dimerization mode of **2.1b** in solution state was also characterized by ^{1}H NMR spectra in $CDCl_3$. Large association energy of **2.1b** resulted in the appearance of NMR signals arising from a diamagnetic dimer even at 298 K. The dimerization mode was identified to **2.1b**$_2$ σ-dimer on the basis of 2D-NMR techniques (^{1}H–^{1}H COSY and NOESY). Phenalenyl σ-dimer potentially has three stereoisomers originating from two asymmetric carbon centers (*RR*/*SS* chiral form and *RS meso* form), whereas only a diastereomer was observed in ^{1}H NMR spectrum. Considering from the X-ray structure, **2.1b** forms solely the σ-dimer *RR*/*SS* configuration in solution state. Subsequent cooling the solution to 233 K resulted in a progressive line sharpening and no evidence of π-dimerization was found. Experimental results are correspondence with the molecular geometry expected by theoretical calculations at M05-

2X/6-31G** level.[9] The most stable isomer among **2.1b** dimers is expected to be the σ-dimer *RR*/*SS* form as observed by ^{1}H NMR spectroscopy. The optimized structure of **2.1b$_2$** σ-dimer *RR*/*SS* form is almost identical to the X-ray structure, suggesting the existence of the electrostatic interaction between pentafluorophenyl groups and phenalenyl planes.

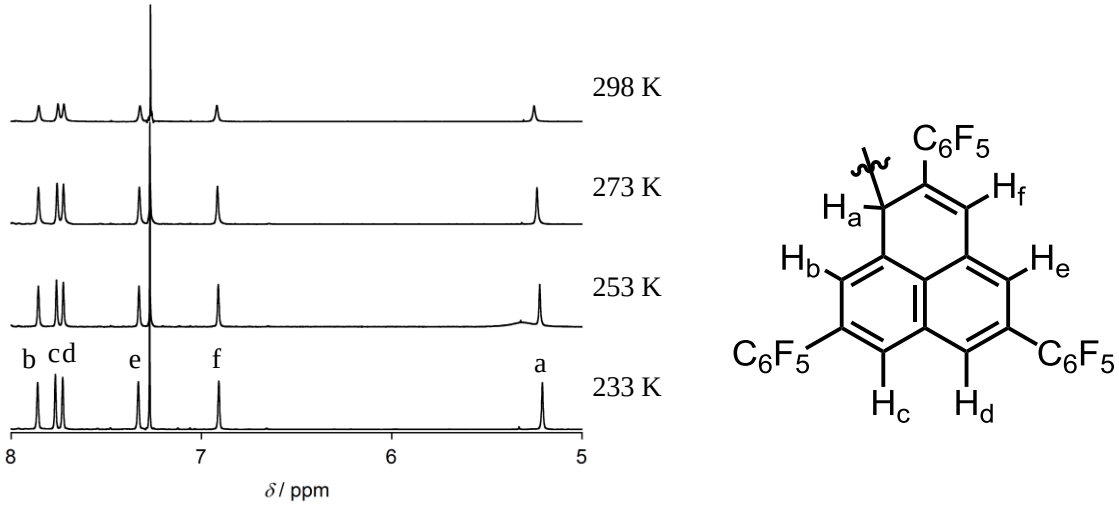

Figure 2.5.6. Variable temperature ^{1}H NMR of **2.1b** in $CDCl_3$ (5 mM solution).

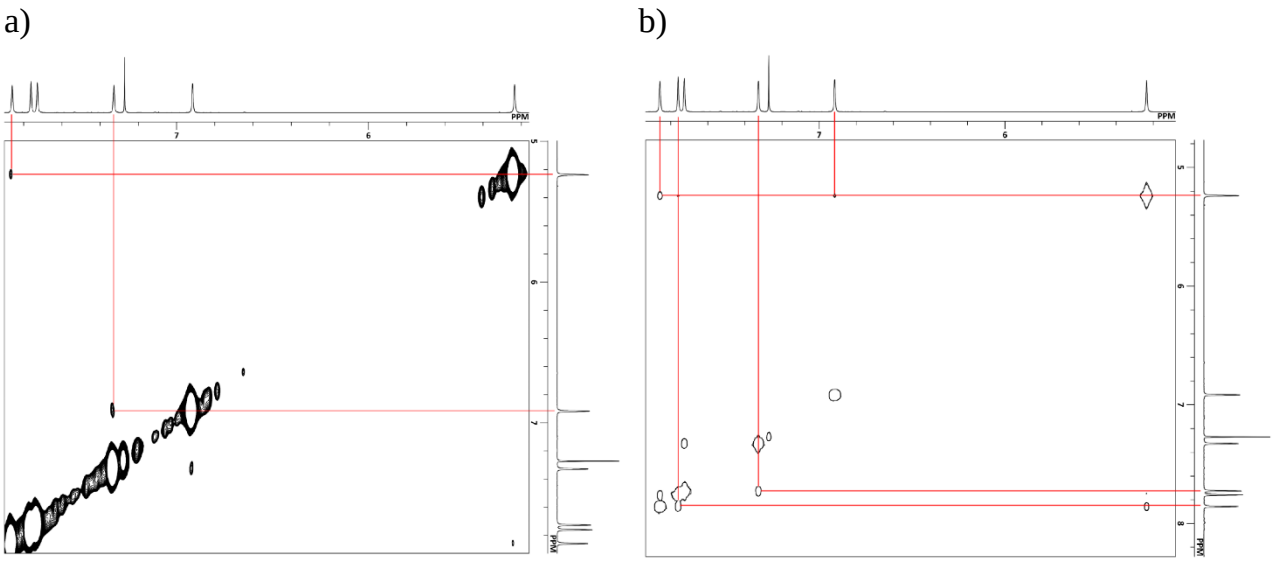

Figure 2.5.7. a) NOESY and b) ^{1}H–^{1}H COSY spectra of **2.1b$_2$** σ-dimer in $CDCl_3$.

2.5.3 Effect of substituted groups on phenalenyl dimerization modes

TPPLY (**2.1a**) and TPFPPLY (**2.1b**) demonstrated a strong propensity to dimerization both in solution and solid state, and the dimerization modes were characterized by ^{1}H NMR spectroscopy and X-ray crystallographic analysis. Introduction of substituted groups gave no effect on the spin nature of phenalenyl according to the result of ESR spectra, whereas the preference of dimerization mode is considerably affected. **2.1a** and **2.1b** form π-dimer and σ-dimer, respectively, which is striking contrast to the natural understanding that the preference of phenalenyl dimerization mode is controlled by the steric effect of substituted groups. The sterically less hindered phenyl groups lead **2.1a** to π-dimerization mode; in contrast, introduction of bulkier pentafluorophenyl groups resulted in the σ-dimerization of **2.1b**. This results can be rationalized by the differences in the electrostatic potential and the additional interaction energy arising from side substituted groups. As shown in Figure 2.1.1, significant difference was observed in the electrostatic potential between **2.1a** and **2.1b** calculated by a UB3LYP/6-31G** method. **2.1b** having electron withdrawing pentafluorophenyl groups has the electron deficient phenalenyl plane with respect to **2.1a** with phenyl groups. C(sp^3)–C(sp^3) σ-bond connecting electron deficient carbon atoms is known to have a large bond dissociation energy.[18] Actually, the association energy of **2.1b** determined by VT ESR measurements was considerably larger than that of other derivatives; thus, the σ-bond formation in **2.1b** is energetically favorable than π-dimerization due to the electron deficiency of the phenalenyl ring. Furthermore, additional interaction arising from substituted groups also affects the dimerization modes. As observed in X-ray structure, CH–π interactions between phenyl groups of **2.1a**$_2$ π-dimer contributes significantly to the association energy, and the electrostatic interaction between pentafluorophenyl groups and phenalenyl planes stabilizes σ-dimerization mode of **2.1b**. Although these additional interactions are substantially weak, the small energy difference between σ- and π-dimerization modes results in the inversion of the preference of dimerization mode. In order to estimate the intrinsic dimerization behavior of phenalenyl, additional studies of a phenalenyl derivative without electronic perturbations are required (see chapter 3).

2.6 Exploring another association modes of TPPLY and TPFPPLY

2.6.1 Construction of TPFPPLY 1D-chain

Metastable association modes which are slightly less stable in energy than stable ones can be isolable by changing the experimental conditions such as solvents and temperatures. TPFPPLY (**2.1b**) was isolated as a σ-dimerization mode having a long C–C single bond and demonstrated a facile dissociation into monomeric **2.1b** in solution state even at room temperature, which suggests the monomeric **2.1b** might give anther association modes by crystallizing at higher temperature phase.

Heating a powdered sample of **2.1b**$_2$ σ-dimer at 573 K in a degassed sealed tube resulted in melting accompanied by a dramatic color change from white to violet, and subsequent cooling to room temperature led to a formation of violet needles suitable for X-ray crystallographic analysis. X-ray structure of a new crystalline phase is shown in Figure 2.6.1.[10] In the violet crystals, **2.1b** formed not a σ-dimer but the one-dimensional chain with intermolecular distances of 3.6467 Å at 10 K. **2.1b** adopts an eclipsed stacking motif due to the electrostatic interaction between pentafluorophenyl groups,[19,20] in contrast to the staggered stacking motif of **2.1a**$_2$ π-dimer and **1.4**$_2$ π-dimer.[11] It should be noted that the equidistant 1D-structure is persistent even at 10 K, suggesting that a first order spin-Peierls transition is prominently suppressed by the structural effects of **2.1b**.

As observed in packing structure of perfluorinated aromatic rings, pentafluorophenyl groups adopted a slipped face-to-face configuration. Distances between side pentafluorophenyl groups were significantly short (av. 3.252 Å), and the twisted angles of pentafluorophenyl groups with respect to phenalenyl planes is 38.13° on average, which are dominated by the electrostatic interaction between fluorine atoms and aromatic ring of pentafluorophenyl groups. Furthermore, separation distances between phenalenyl sites are unambiguously determined by the geometry of pentafluorophenyl groups, resulting in the suppression of excessive contacts of phenalenyl sites.

Each phenalenyl 1D-chain is tied together with neighboring phenalenyl chains by the weak H–F hydrogen bond between phenalenyl unit and pentafluorophenyl groups. The 1D-chains are isolated by surrounding substituted groups bearing little spin density; thus, the magnetic interaction between 1D-chains is negligible.

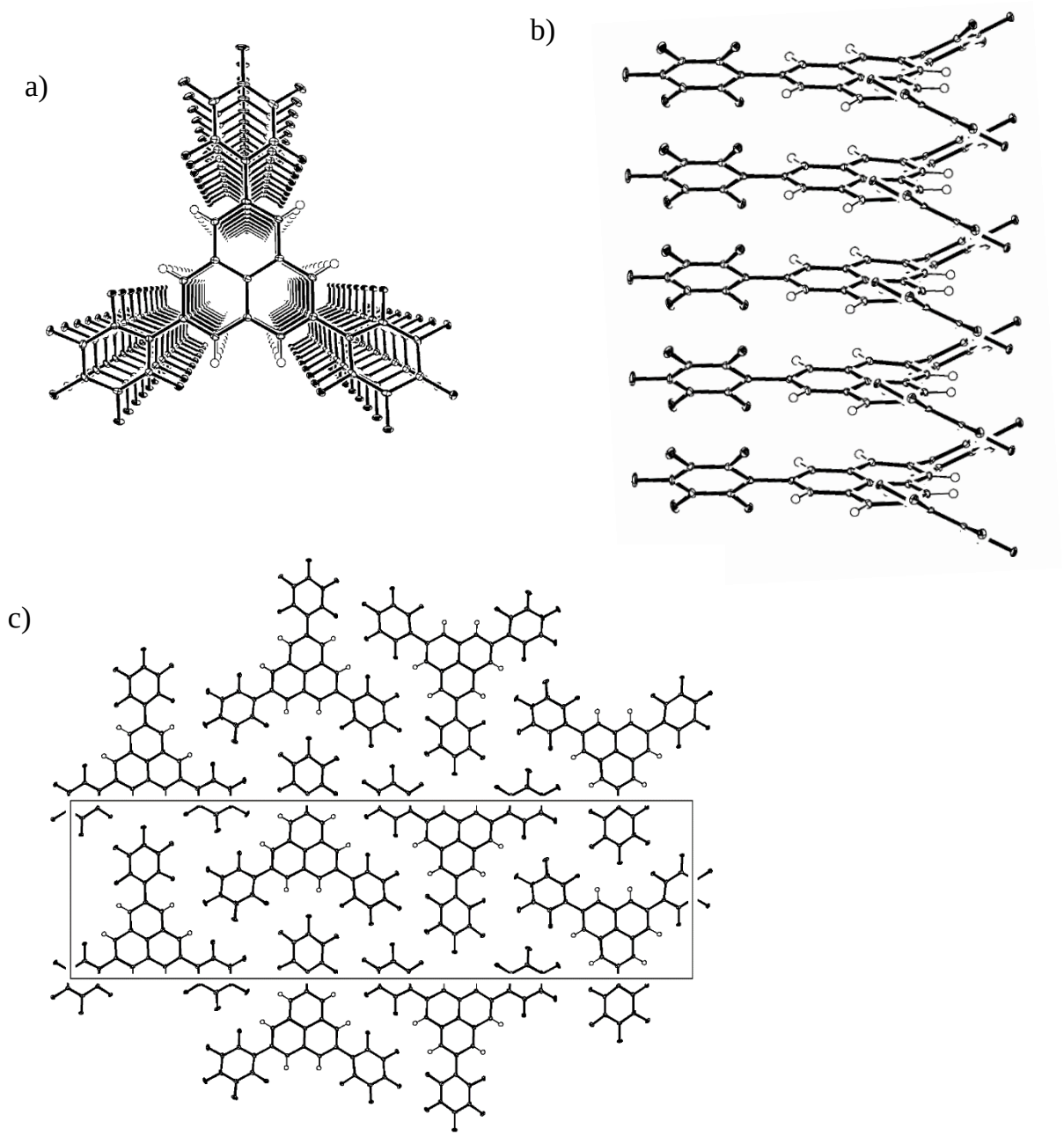

Figure 2.6.1. Ortep drawing of **2.1b** 1D-chain at the 50% probability level. a) Top view and b) side view of 1D-chain. c) Packing diagram in the (1 0 0) plane. Reprinted with permission from ref. 10. Copyright 2014, Wiley-VCH Verlag GmbH & Co. KGaA.

Crystal System = orthorhombic, a = 3.6467(4) Å, b = 13.3184(13) Å, c = 46.5175 Å, V = 2259.3(4) Å^3, Space Group = $P2_12_12_1$ (#19), Z = 4, μ(MoKα) = 2.03 cm^{-1}, T = 10 K, $R1$ [$F^2>2\sigma(F^2)$] = 0.0335, $wR2$(all data) = 0.0897, S = 1.044, Refl./param. = 5426/415.

2.6.2 Solid state properties of TPFPPLY 1D-chain

Significant overlap of SOMOs of **2.1b** in 1D-chain leads to the formation of continuous multicenter bonding. Indeed, the electronic absorption spectrum of powdered **2.1b** 1D-chain showed an intense absorption band centered at 798 nm arising from the delocalized electron, which was not observed in monomeric and σ-dimer of **2.1b** (Figure 2.6.2).

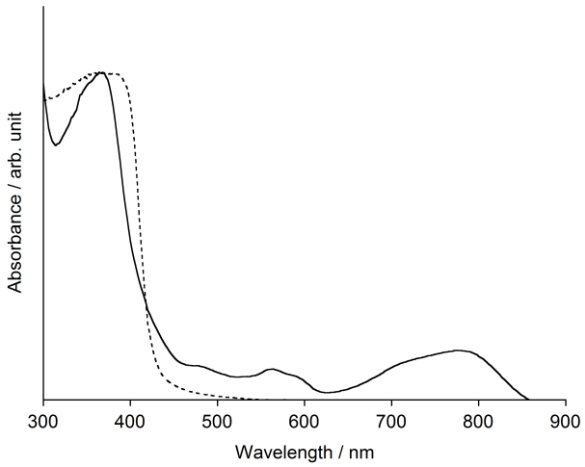

Figure 2.6.2. Electron absorption spectrum of **2.1b** 1D-chain (solid) and **2.1b**$_2$ σ-dimer (dashed) in KBr pellet.

To elucidate the magnetic interaction in **2.1b** 1D-chain, SQUID measurement was conducted within the temperature range from 2 K to 380 K (Figure 2.6.3). Magnetic susceptibility (χ) decreased continuously upon cooling then reached a minimum at 70 K, and subsequent cooling resulted in an increase of χ values by the effect of paramagnetic impurities or crystal defects.

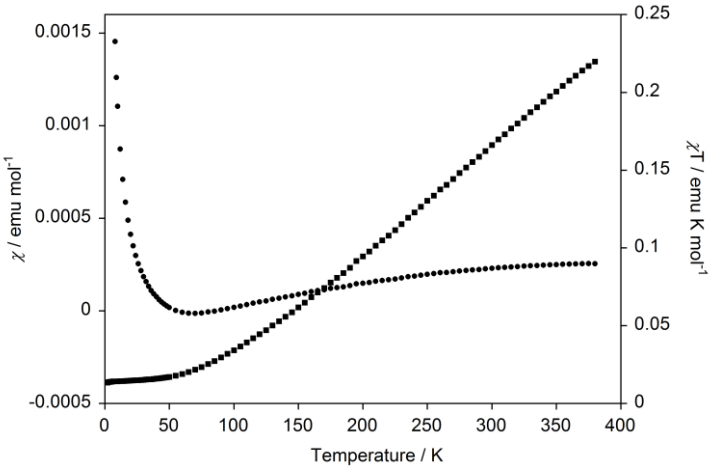

Figure 2.6.3. Temperature dependence of χ and χT for polycrystalline sample of **2.1b** 1D-chain at 1 T. Dots and squares denote the experimental χ and χT values, respectively.

The experimentally obtained χ curve was fitted to a uniform antiferromagnetic spin-1/2 Heisenberg chain model (namely, Bonner-Fisher model)[21] modified with inter-chain magnetic interaction (z*'J*) in the framework of a mean-field approximation reported by Hatfield *et al.*[22,23] and with a finite-chain model developed by Mila *et al.*[24] The best fitting was obtained with the following parameters: J/k_B = −279 K, zJ'/k_B = +908 K, N_0 (average length of finite chains), however, the magnetic interactions between neighboring chains are unrealistically large because the phenalenyl moieties in 1D-chains are fully isolated by pentafluorophenyl groups bearing little spin densities. The curve fitting was also conducted with an alternating antiferromagnetic spin-1/2 Heisenberg chain model. The parameters can be estimated to be $J_1 = -327$ K, $J_2 = -147$ K, and ρ (defect concentration) = 4%, whereas no evidence of dimerization was observed by the X-ray diffuse scattering patterns even at 10 K. It might be required to consider the second-order or higher-order phase transitions.

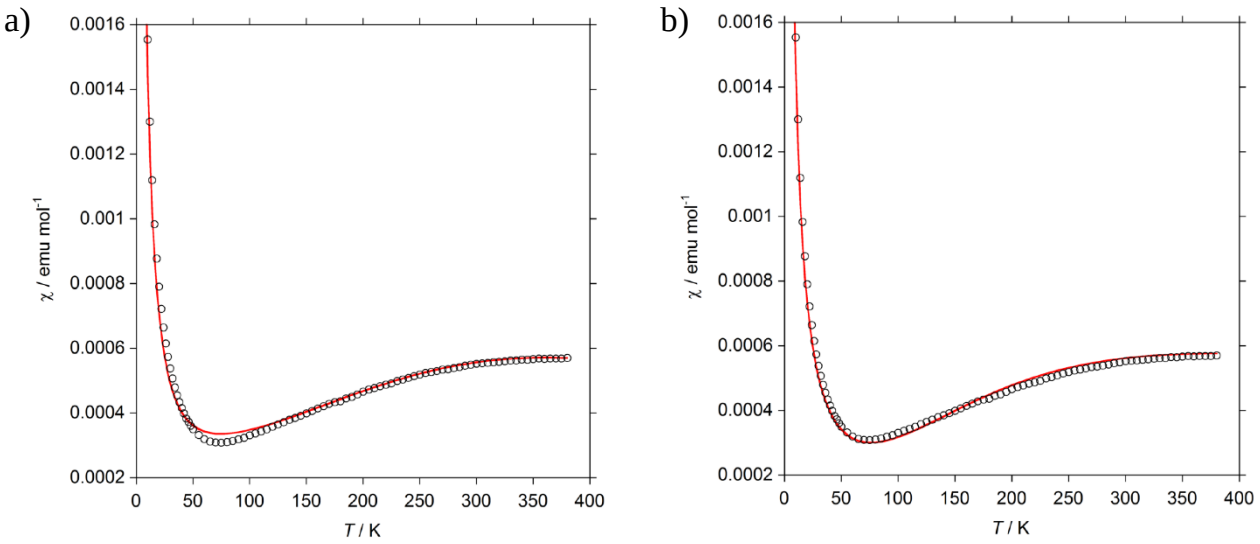

Figure 2.6.4. Curve fitting of χ vs. T plot based on a) the modified Bonner-Fisher model and b) the alternating antiferromagnetic spin-1/2 Heisenberg chain model.

1D-chains composed of organic radicals are promising candidates for the electoconductive materials.[25] EHMO calculations of **2.1b** 1D-chain expected the existence of a half-filled band with a relatively wide band width (0.29 eV) in the stacking direction, inferring that the 1D-chain would show the large electroconductivity. Elecroconductivity of a compressed pellet of **2.1b** 1D-chain was measured by the two probe method. However, the electroconductivity at room temperature was less than 1×10^{-10} S cm^{-1}; that is, **2.1b** 1D-chain behaves as an insulator. A widely accepted criterion for electroconductive behavior is described as U/W, where U is the on-site coulomb repulsion and W is the bandwidth. On-site coulomb repulsion can be estimated from CV measurement (chapter 2.7) to be 1.66 eV. The large U/W value leads **2.1b** 1D-chian to the Mott-Hubbard insulator.

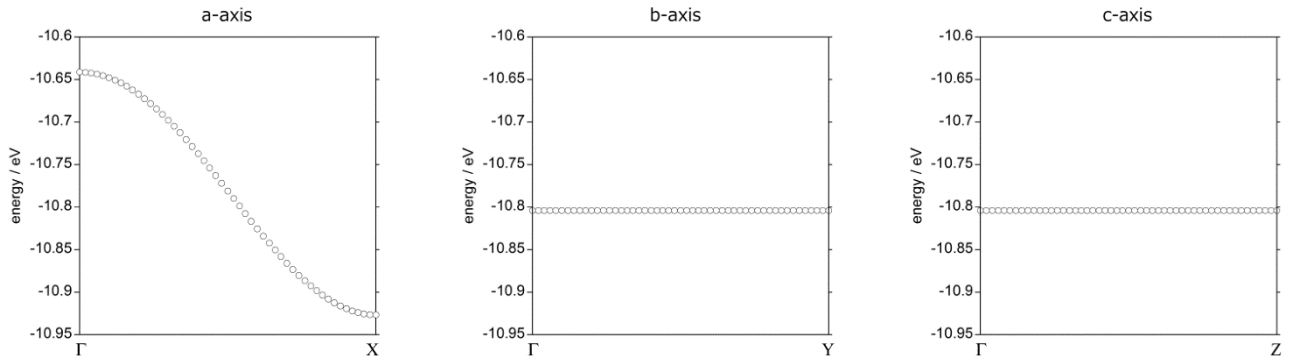

Figure 2.6.5. EHMO band structures of **2.1b** 1D-chain on the basis of X-ray structure determined at 10 K.

2.6.3 Construction of mixed 1D-chain composed of TPPLY and TPFPPLY

Heating the powdered samples of **2.1a** and **2.1b** in a degassed sealed tube at 573 K resulted in melting and subsequent cooling gave dark brown needles which are suitable for X-ray crystallographic analysis. **2.1a** and **2.1b** formed alternative stacking 1D-chains with the similar structure to the **2.1b** 1D-chain. π–π separation distance between neighboring phenalenyls in a 1D-column was 3.69 Å, which is almost identical to that for **2.1b** 1D-chain. In contrast, distances between phenyl and pentafluorophenyl groups were shorter than the sum of van der Waals radius (3.376 Å and 3.394 Å) by the effect of the electrostatic interaction as well as van der Waals interaction, leading the phenalenyl sites to an eclipsed stacking motif. With focused on the inter-chain alignments, **2.1a** interacted with neighboring **2.1a** through CH–π interactions, and **2.1b** formed H–F hydrogen bond between neighboring **2.1b**.

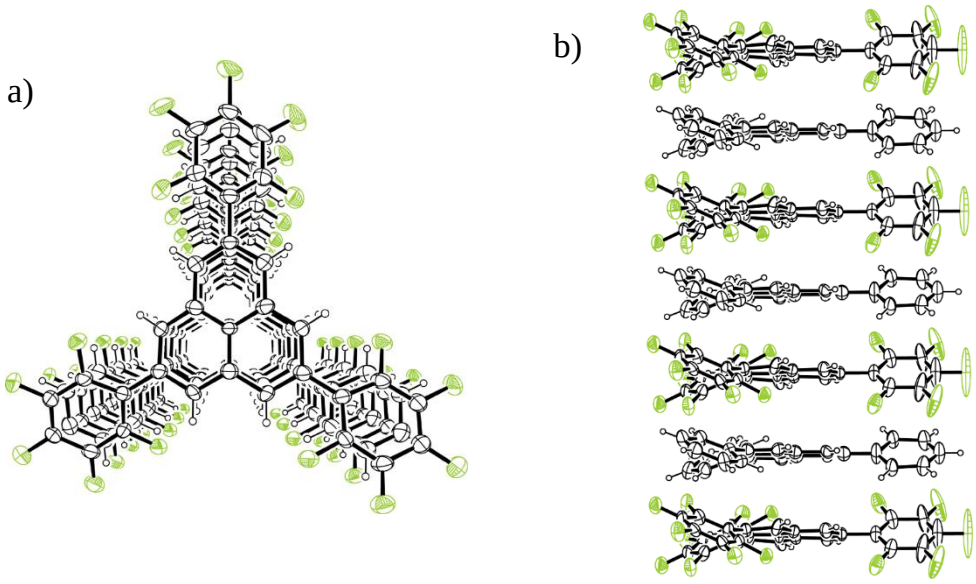

Figure 2.6.6. Ortep drawing of mixed 1D-chain of **2.1a** and **2.1b** at the 50% probability level. a) Top view and b) side view of 1D-chain. Crystal System = monoclinic, a = 7.3802(4) Å, b = 13.440(4) Å, c = 22.339(6) Å, β = 94.08(6)°, V = 2210.3(10) Å^3, Space Group = $P2/n$ (#13), Z = 2, μ(MoKα) = 1.36 cm^{-1}, T = 200 K, $R1$ [$F^2>2\sigma(F^2)$] = 0.1654, $wR2$(all data) = 0.5106, S = 1.395, Refl./param. = 5045/353.

The electronic structure of mixed 1D-chain was estimated by the electronic absorption spectrum in KBr pellet. The mixed 1D-chain showed a broad and intense absorption band centered at 834 nm, which showed a significant red shift with respect to **2.1b** 1D-chain. The spectral change was rationalized by a difference of SOMO energy levels between **2.1a** and **2.1b**. As observed by CV measurement (see chapter 2.7), SOMO level of **2.1b** having electron withdrawing pentafluorophenyl groups is lower in energy than that of **2.1a**, thus, the energy difference resulted in the decrease of covalent bonding interaction, leading to the red shift of the absorption band.

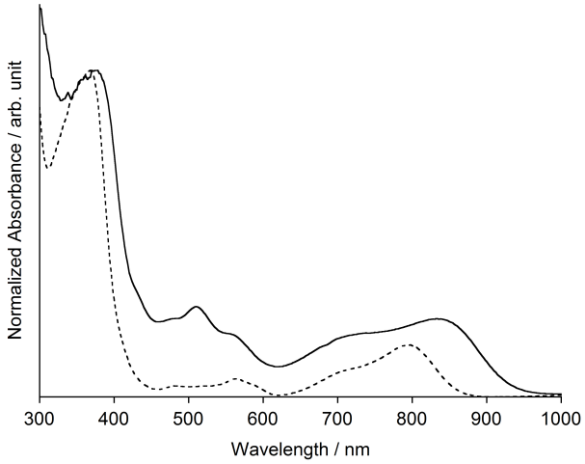

Figure 2.6.7. Electronic absorption spectra of the mixed 1D-chain (solid) and **2.1b** 1D-chain (dashed) measured in KBr pellet.

2.7 Stability of TPPLY and TPFPPLY

Nonsubstituted phenalenyl demonstrates a rapid decomposition through the oxidation by molecular oxygen to give phenalenone as a decomposed product.[26,27] In contrast, TPPLY (**2.1a**) and TPFPPLY (**2.1b**) showed a remarkable tolerance to these decomposition reactions even in air-saturated solution. Half-lives of **2.1a** and **2.1b** were determined experimentally from the decay of ESR signals, to be 3 hours and 4 days, respectively (Figure 2.7.1).

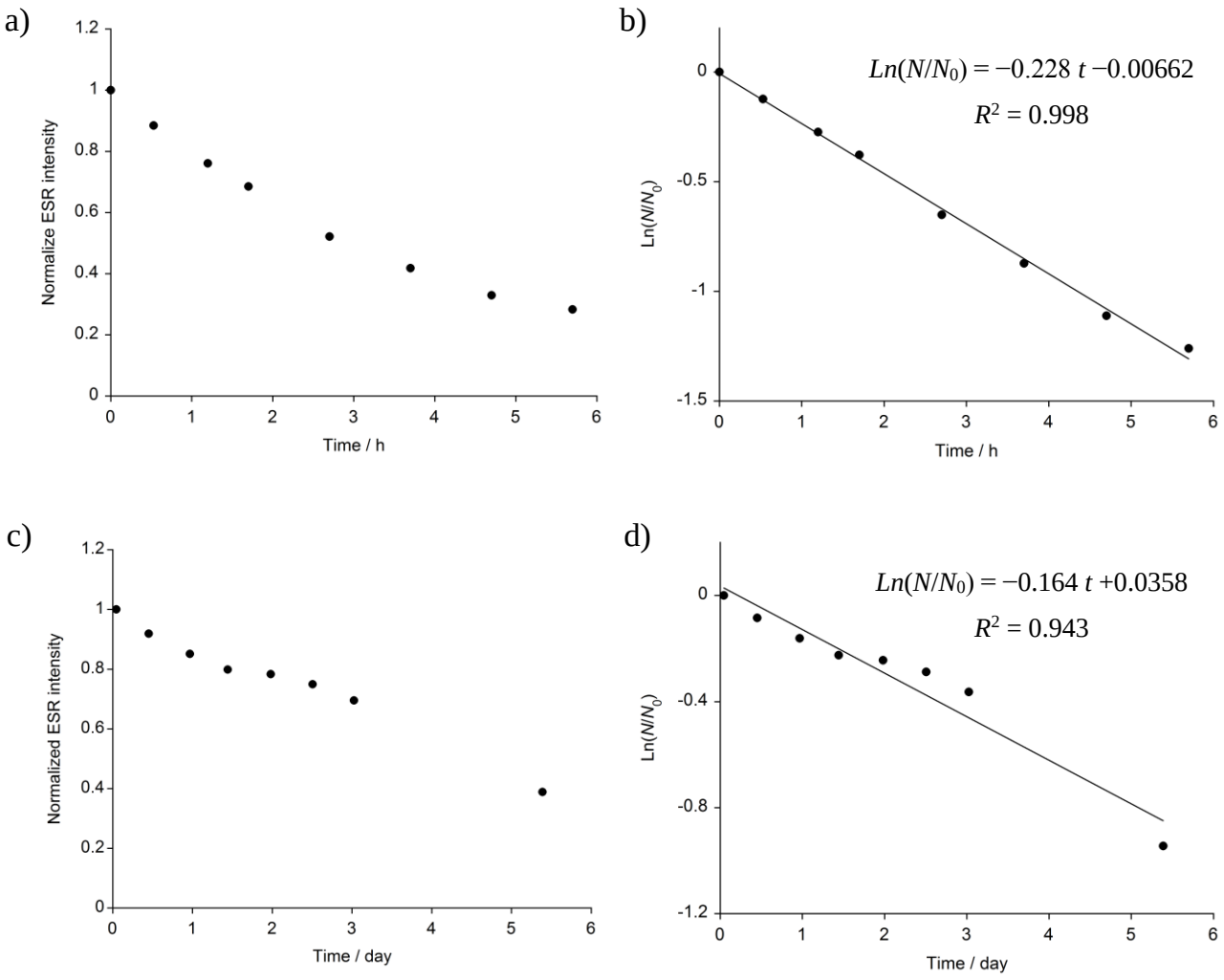

Figure 2.7.1. Time dependent ESR signal intensity of a) **2.1a** and c) **2.1b** in air saturated toluene solution. Half-lives of b) **2.1a** and d) **2.1b** were determined from the intensity changes.

2.1b demonstrated a remarkable stability to oxidation reaction compared to **2.1a**, leading to a significant difference of half-lives. The essential difference of stability was rationalized by the energy levels of SOMOs, which were estimated by cyclic voltammetry (CV). Electrochemical behavior of **2.1a** was observed by using **2.1a**$^+$ PF_6^- salts prepared from **2.10** and trityl hexafluorophosphate. **2.1a** showed a reversible oxidation wave (^{ox}E = 0.02 eV) and an

irreversible reduction wave (^{red}E = −1.57 eV). On the other hand, CV of **2b** was observed by using the sample of **2b** σ-dimer, and **2b** revealed two reversible redox waves; ^{ox}E = 0.36 eV, ^{red}E = −1.30 eV. From the comparison of redox potentials, the SOMO level of **2b** is considerably lower (~0.3 eV) than that of other derivatives, leading to the decrease of reactivity toward molecular oxygen.

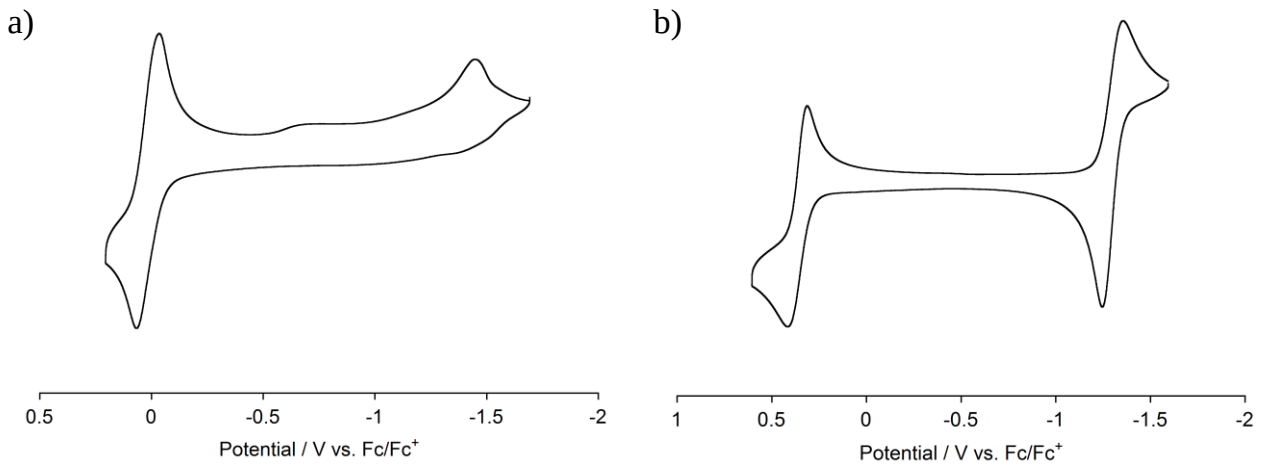

Figure 2.7.2. Cyclic voltammograms of a) **2.1a** (V vs. Fc/Fc$^+$, in 0.1 M ^{n}Bu$_4$NClO$_4$/DCM, scan rate = 100 mV s^{-1}, room temperature) and b) **2.1b** (V vs. Fc/Fc+, in 0.1 M ^{n}Bu$_4$NClO$_4$/DCM, scan rate = 50 mV s^{-1}, room temperature).

2.8 Conclusion

Previous studies on the dimerization mode of phenalenyl suggested that the preference of dimerization mode is dominated by the steric effect of substituted groups, whereas this systematic study on the dimerization mode of 2,5,8-triarylphenalenyl gave a different insight. The experimental assessment of dimerization modes of TPPLY (**2.1a**) and TPFPPLY (**2.1b**) suggested that sterically less hindered **2.1a** formed a π-dimerization mode and **2.1b** with bulkier pentafluorophenyl groups adopted a σ-dimerization mode, which was confirmed by X-ray crystallography and ^{1}H NMR, despite the spin structure of phenalenyl was not affected by the substituted groups. As results of experimental and theoretical analyses, the σ-dimer connected with a long C(sp^3)–C(sp^3) σ-bond and the π-dimer formed by a strong multicenter covalent bonding interaction are energetically degenerated; thus, the preference of the dimerization mode is easily inversed by additional interactions arising from substituted groups. Moreover, metastable association mode was also isolable in high temperature phase. Melting method led to 1D-chains based on continuous multicenter covalent bonding interaction. These results suggest the chemical modification lead to a novel association mode of phenalenyl.

2.9 Experimental

All experiments were conducted according to the literature reported by our group.[9,10]

2.10 References

(1) Tian, Y.-H.; Kertesz, M. *J. Am. Chem. Soc.* **2010**, *132* (31), 10648.

(2) Cui, Z. H.; Lischka, H.; Beneberu, H. Z.; Kertesz, M. *J. Am. Chem. Soc.* **2014**, *136* (15), 5539.

(3) Cui, Z.; Gupta, A.; Lischka, H.; Kertesz, M. *Phys. Chem. Chem. Phys.* **2015**.

(4) Koutentis, P. a; Chen, Y.; Cao, Y.; Best, T. P.; Itkis, M. E.; Beer, L.; Oakley, R. T.; Cordes, A. W.; Brock, C. P.; Haddon, R. C. *J. Am. Chem. Soc.* **2001**, *123* (17), 3864.

(5) Small, D.; Rosokha, S. V; Kochi, J. K.; Head-Gordon, M. *J. Phys. Chem. A* **2005**, *109* (49), 11261.

(6) Zaitsev, V.; Rosokha, S. V.; Head-Gordon, M.; Kochi, J. K. *J. Org. Chem.* **2006**, *71* (2), 520.

(7) Beer, L.; Mandal, S. K.; Reed, R. W.; Oakley, R. T.; Tham, F. S.; Donnadieu, B.; Haddon, R. C. *Cryst. Growth Des.* **2007**, *7* (4), 802.

(8) Beer, L.; Reed, R. W.; Robertson, C. M.; Oakley, R. T.; Tham, F. S.; Haddon, R. C. *Org. Lett.* **2008**, *10* (14), 3121.

(9) Mou, Z.; Uchida, K.; Kubo, T.; Kertesz, M. *J. Am. Chem. Soc.* **2014**, *136* (52), 18009.

(10) Uchida, K.; Hirao, Y.; Kurata, H.; Kubo, T.; Hatano, S.; Inoue, K. *Chem. - An Asian J.* **2014**, *9* (7), 1823.

(11) Goto, K.; Kubo, T.; Yamamoto, K.; Nakasuji, K.; Sato, K.; Shiomi, D.; Takui, T.; Kubota, M.; Kobayashi, T.; Yakusi, K.; Ouyang, J. *J. Am. Chem. Soc.* **1999**, *121* (7), 1619.

(12) Tiekink, E. R. T.; Zukerman-Schpector, J. *The Importance of Pi-Interactions in Crystal Engineering*, WILEY, **2012**.

(13) Small, D.; Zaitsev, V.; Jung, Y.; Rosokha, S. V.; Head-Gordon, M.; Kochi, J. K. *J. Am. Chem. Soc.* **2004**, *126* (42), 13850.

(14) Fukui, K.; Sato, K.; Shiomi, D.; Takui, T.; Itoh, K.; Gotoh, K.; Kubo, T.; Yamamoto, K.; Nakasuji, K.; Naito, A. *Synth. Met.* **1999**, *103* (1-3), 2257.

(15) Bennett, J. E. *Nature* **1960**, *188* (4749), 485.

(16) Gerson, F. *Helv. Chim. Acta* **1966**, *49* (5), 1463.

(17) Suzuki, S.; Morita, Y.; Fukui, K.; Sato, K.; Shiomi, D.; Takui, T.; Nakasuji, K. *J. Am. Chem. Soc.* **2006**, *128* (8), 2530.

(18) McMillen, D. F.; Golden, D. M. *Ann, Rev. Phys. Chem* **1982**, *33*, 493.

(19) Blanchard, M. D.; Hughes, R. P.; Concolino, T. E.; Rheingold, A. L. *Chem. Mater.* **2000**, *12* (6), 1604.

(20) Ehrlich, S.; Moellmann, J.; Grimme, S. *Acc. Chem. Res.* **2013**, *46* (4), 916.

(21) Bonner, J. C.; Fisher, M. E. *Phys. Rev.* **1964**, *135* (3A), A640.

(22) Estes, W. E.; Gavel, D. P.; Hatfield, W. E.; Hodgson, D. J. *Inorg. Chem.* **1978**, *17* (6), 1415.

(23) Hatfield, W. E.; Weller, R. R.; Hall, J. W. *Inorg. Chem.* **1980**, *19* (12), 3825.

(24) Mila, F.; Millet, P.; Bonvoisin, J. *Phys. Rev. B* **1996**, *54* (17), 925.

(25) Haddon, R. C. *Nature* **1975**, *256* (5516), 394.

(26) Reid, D. H. *Tetrahedron* **1958**, *3* (3), 339.

(27) Reid, D. H. *Q. Rev. Chem. Soc.* **1965**, *19* (3), 274.

-Chapter 3-
Direct Evidence for the σ-Bond Fluxionality of Phenalenyl σ-Dimer: Six-Fold σ-Bond Shift Demonstrated by 2,5,8-Trimethylphenalenyl

3.1 Introduction

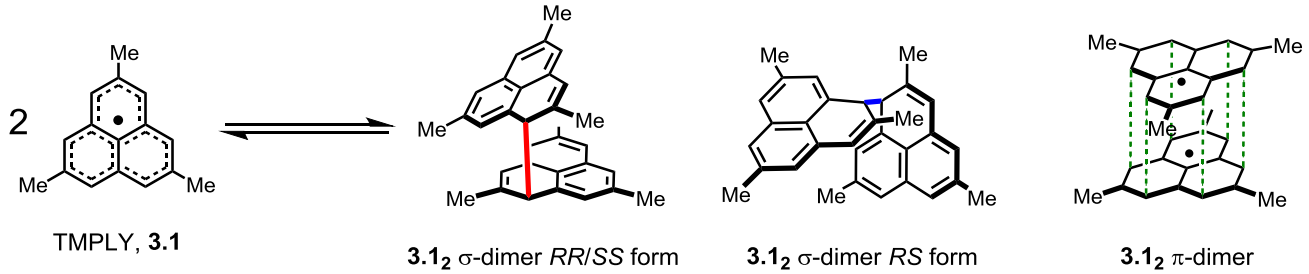

As mentioned in chapter 2, detailed investigations of the dimerization modes of phenalenyl were performed by synthesizing phenalenyl derivatives having three aryl groups at β positions, which are sterically less hindered substituted groups than *tert*-butyl groups. Isolation and characterization of dimerization modes of TPPLY **2.1a** and TPFPPLY **2.1b** in both solution and solid states gave qualitative insights into the preference of the dimerization mode.[1,2] **2.1a** having three phenyl groups adopts the π-dimerization mode with an extraordinarily small π–π separation distance owing to the energetic support of CH–π interactions between side phenyl groups. In contrast, **2.1b** with electron withdrawing pentafluorophenyl groups prefers the σ-dimerization mode despite of the larger steric hindrance of substituted groups than phenyl groups. The electron deficiency of phenalenyl sites in **2.1b** facilitates the σ-bond formation. This systematic studies on the dimerization mode of phenalenyl derivatives with various substituted groups suggested that the two dimerization modes are close in energy and the additional factors of substituted groups significantly affect the preference of dimerization mode. Thus, further investigations with a phenalenyl derivative having smaller steric and electronic perturbations are required for deeper understanding of the essential dimerization of phenalenyl.

This chapter 3 describes the dimerization modes and solution state dynamics demonstrated by 2,5,8-trimethylphenalenyl (TMPLY, **3.1**). Methyl group is expected to be a suitable substituted group for the detailed investigation of dimerization mode due to its small steric and electronic perturbations. **3.1** showed a bimodal dimerization behavior; that is, **3.1** was isolated as σ-dimer *RR*/*SS* form and π-dimer in crystalline form, which was undoubtedly confirmed by X-ray crystallographic analyses.[1] Moreover, three diamagnetic dimers (**3.1**$_2$ σ-dimer *RR*/*SS* form, **3.1**$_2$ σ-dimer *RS* form, and **3.1**$_2$ π-dimer) were unambiguously observed and characterized in solution state, giving a first quantitative insight into the preference of dimerization mode. Surprisingly, **3.1**$_2$ σ-dimer *RR*/*SS* form demonstrated unusual reactions in solution states due to its σ-bond fluxionality; 1) the facile dissociation into monomeric **3.1**s, and 2) the random σ-bond shift resulting in the rapid isomerization between **3.1**$_2$ σ-dimer *RR*/*SS* forms. The intriguing fluxional σ-bond was fairly accounted for by the presence of a dynamic equilibrium between **3.1**$_2$ σ-dimer *RR*/*SS* form and **3.1**$_2$ π-dimer, which was undoubtedly observed by 2D-EXSY measurements.

3.2 Synthesis of TMPLY

The synthetic method for the hydro-precursor **3.11** was reported by Leitch *et al.* in 1974,[3] whereas a new synthetic route was developed to avoid using some toxic reagents, such as hydrogen fluoride and Raney-Nickel alloy. The optimized synthetic procedure for **3.1** was displayed in Scheme 3.2.1. 2,7-Dimethylnaphthalene **3.2** was prepared from 2,7-dibromonaphthalene **2.2** by the Kumada-Tamao coupling reaction. Introduction of bromine to **3.2** as a directing group enabled to obtain naphthaldehyde derivative **3.4** as a single isomer in next formylation reaction. After the Horner-Emmons reaction, the unsaturated ester **3.5** obtained was reduced to the saturated ester **3.6** under hydrogen atmosphere. In this step, the bromine on naphthalene ring was removed in the same reaction condition. Hydrolysis and subsequent Friedel-Crafts reaction gave dimethylphenalanone **3.8**, then the treatment of the enolate, which was prepared from **3.8** and lithium diisopropylamide (LDA), with methyl iodide afforded trimethylphenalanone **3.9**. Hydro-precursor phenalene **3.11** was obtained by reduction followed by dehydration in excellent yield. Treatment of **3.11** with *p*-chloranil in degassed solvent gave a wine red solution of **3.1**, and pure **3.1** was obtained by recrystallization in a degassed sealed tube. **3.1** was persistent in oxygen-free solvents, however, facile decomposition occurred in air to afford an insoluble peroxide compound.

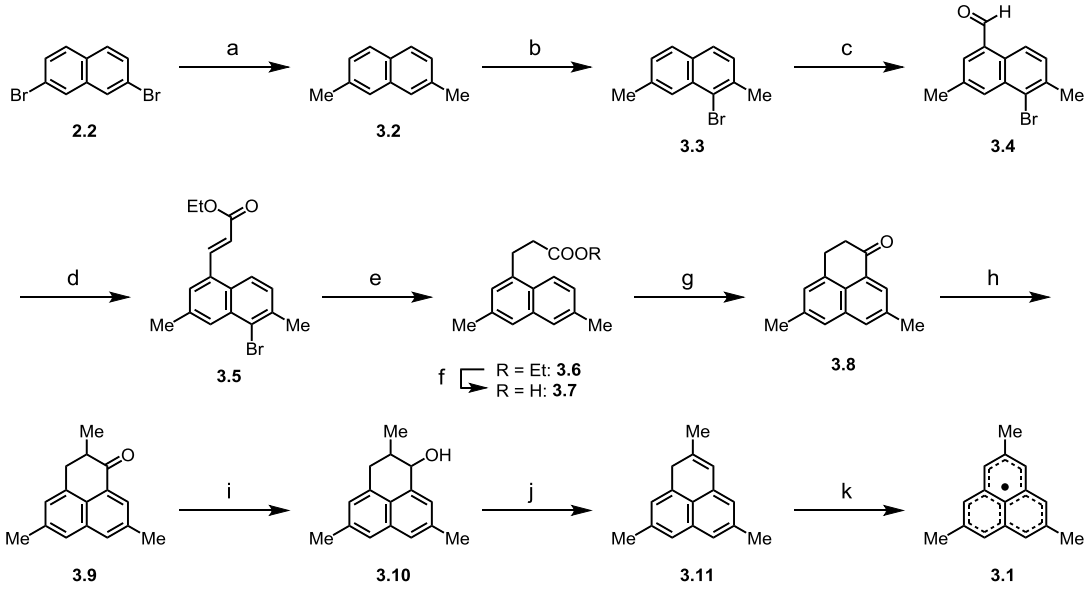

Scheme 3.2.1. Synthetic procedure for **3.1**. Reagent and condition: a) Ni(II)(dppp)Cl_2 DCM adduct, MeMgI, THF/ether (1/1), 45 °C, 87% yield; b) NBS, DMF, 0 °C to RT, quantitative yield; c) dichloromethyl methyl ether, $TiCl_4$, DCM, −78 °C, 85% yield; d) NaH, triethyl phosphonoacetate, THF, RT, quantitative yield; e) H_2 (1 atm), 10% Pd-C, DCM/EtOH (1/10), RT, quantitative yield; f) 10% NaOHaq., EtOH, 90 °C, quantitative yield; g) (i) $(COCl)_2$, 60 °C, (ii) $TiCl_4$, DCM, −78 to −40 °C, 54% yield; h) (i) LDA, THF, −78 °C, (ii) MeI, THF, −78 °C to RT, 64% yield; i) $NaBH_4$, DCM/EtOH (1/1), RT, j) *p*-TsOH·H_2O, toluene, 120 °C, 87% yield (2 steps); k) *p*-chloranil, pentane, RT, 33% yield. Ni(II)(dppp)Cl_2 = [1,3-bis(diphenylphosphino)propane]dichloronickel(II), LDA = lithium diisopropylamide, *p*-chloranil = 2,3,5,6-tetrachloro-1,4-benzoquinone.

3.3 X-ray crystallography

3.3.1 Molecular geometry of TMPLY σ-dimer

Recrystallization of **3.1** from degassed hexane or dichloromethane/hexane mixed solvent gave colorless platelet crystals suitable for X-ray crystallographic analysis. Molecular geometry of **3.1** in crystalline state was shown in Figure 3.3.1. In the colorless crystals, **3.1** adopted a σ-dimer with a chiral configuration (an enantiomer mixture of *RR* and *SS* form) arising from two asymmetric sp^3 carbon atoms. The bond lengths of the central $C(sp^3)$–$C(sp^3)$ single bonds connecting two phenalenyl sites were 1.616(3) Å and 1.612(3) Å for two crystallographically-independent two **3.1₂** σ-dimers, which are significantly longer than that of the general $C(sp^3)$–$C(sp^3)$ single bond (1.54 Å) but slightly shorter than that of TPFPPLY **2.1b₂** σ-dimer (1.636(6) Å).[2] In **2.1b₂** σ-dimer, the $C(sp^3)$–$C(sp^3)$ single bond is considered to be elongated by the larger steric repulsion between **2.1b** units. With focused on the bond lengths in phenalenyl moieties, **3.1₂** σ-dimer *RR*/*SS* form is expected to have a similar electronic structure to phenalene derivative as observed in **2.1b₂** σ-dimer. **3.1₂** σ-dimer *RR*/*SS* form adopted a "close" conformation with the π–π overlap between two phenalenyl planes in contrast to the "open" conformation of **2.1b₂** σ-dimer, which is well consistent with the optimized geometry predicted by a computational calculation at M05-2X/6-31G** level.[1] The conformation of **3.1₂** σ-dimer *RR*/*SS* form would be dominated by the van der Waals interaction between phenalenyl moieties, leading to the close conformation. It should be noted that the red crystalline powder was obtained, together with the colorless crystals of **3.1₂** σ-dimer *RR*/*SS* form. Unfortunately, the low quality of the crystal prevented the detailed characterization using X-ray crystallographic analysis, whereas the red color of the crystal infers the other association mode was formed in solution state.

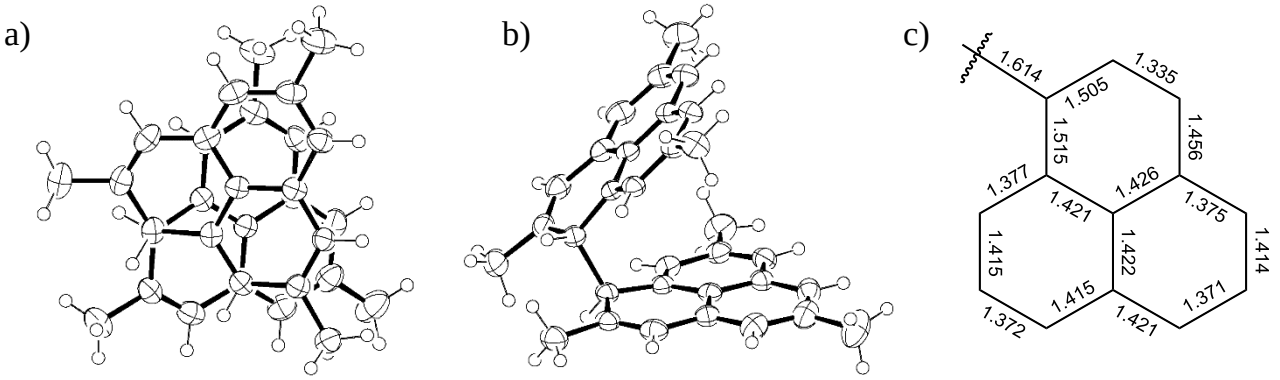

Figure 3.3.1. Ortep drawing of **3.1₂** σ-dimer *RR*/*SS* form at the 50% probability level. a) Top view and b) side view. c) Averaged bond lengths of a phenalenyl moiety in **3.1₂** σ-dimer *RR*/*SS* form.
Crystal System = triclinic, a = 10.4471(4) Å, b = 11.2032(3) Å, c = 19.9952(6) Å, α = 93.7663(10)°, β = 99.8235(10)°, γ = 90.3569(10)°, V = 2300.60(13) Å^3, Space Group = $P\bar{1}$ (#2), Z = 8, μ(MoKα) = 0.67 cm^{-1}, T = 200 K, $R1$ [F^2>2σ(F^2)] = 0.0478, $wR2$(all data) = 0.1773, S = 1.146, Refl./param. = 10426/589.

3.3.2 Molecular geometry of TMPLY π-dimer

According to the computational prediction,[1] the energy difference between **3.1** dimers is considerably small; thus, another dimerization modes can be isolable in crystalline state. Heating the powdered sample of $\mathbf{3.1}_2$ σ-dimer *RR*/*SS* form at 573 K in a degassed sealed tube resulted in melting, accompanied by a noticeable color change from white to violet, and subsequent cooling to room temperature gave violet platelet crystals, together with colorless crystals of $\mathbf{3.1}_2$ σ-dimer *RR*/*SS* form. The crystal structure of **3.1** in the unidentified violet crystals were undoubtedly confirmed by X-ray crystallographic analysis (shown in Figure 3.3.2). **3.1** in the violet crystals adopted a π-dimerization mode, which indicates that **3.1** is a first derivative demonstrating both σ- and π-dimerization. The π–π separation distance between α carbon atoms of phenalenyl units was estimated to be 3.054 Å on average at 100 K, which is substantially shorter than that of $\mathbf{1.4}_2$ π-dimer (3.295 Å at 300 K)[4] but slightly longer than that of $\mathbf{2.1a}_2$ (3.017 Å at 100 K).[1] In $\mathbf{2.1a}_2$ π-dimer, CH–π interactions between side phenyl groups lead to the shorter separation distance than $\mathbf{3.1}_2$ π-dimer. On the other hand, the distance between central carbon atoms was 3.145 Å at 100 K, resulting in a concave-concave packing motif of $\mathbf{3.1}_2$ π-dimer as observed in $\mathbf{2.1a}_2$ π-dimer. Notably, the steric and electronic effects of methyl groups on the geometry of π-dimer are negligible; therefore, the geometry of $\mathbf{3.1}_2$ π-dimer confirmed by X-ray crystallographic analysis reflects the essential structure of phenalenyl π-dimer.

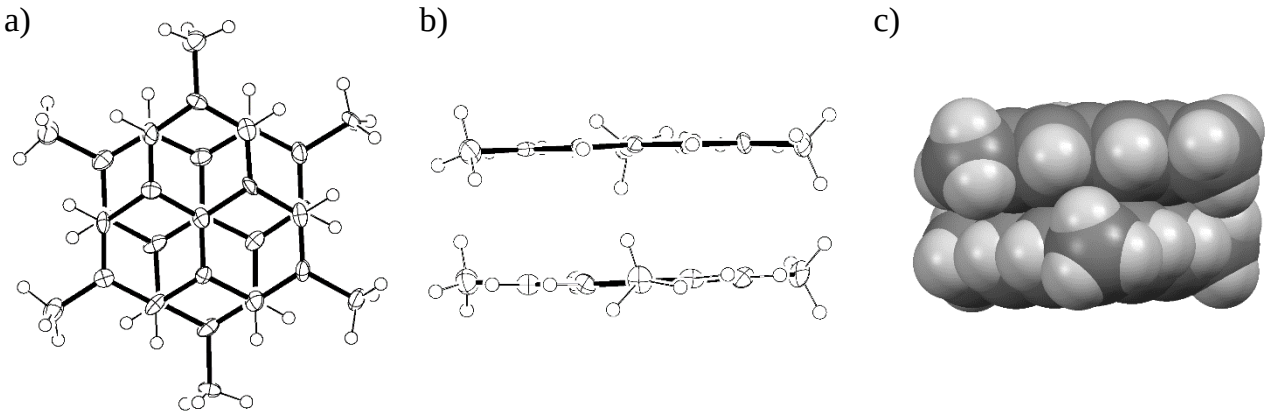

Figure 3.3.2. Ortep drawing of $\mathbf{3.1}_2$ π-dimer at the 50% probability level. a) Top view and b) c) side views Figure 3.3.2c was described in Ortep style and space fill model, respectively

Crystal System = triclinic, a = 8.1570(13) Å, b = 8.8163(13) Å, c = 9.1728(15) Å, α = 61.817(4)°, β = 75.861(4)°, γ = 78.188(4)°, V = 560.75(15) Å^3, Space Group = P1 (#1), Z = 2, μ(MoKα) = 0.69 cm^{-1}, T = 100 K, R1 [F^2>2σ(F^2)] = 0.0606, wR2(all data) = 0.2669, S = 0.930, Refl./param. = 4128/295.

3.4 Dimerization behavior of TMPLY in solution state

3.4.1 Electron spin resonance spectrum

Although **3.1** was isolated as diamagnetic dimers (**3.1**$_2$) in the crystalline state, **3.1**$_2$ demonstrated a facile dissociation into two monomeric radicals in the solution state at room temperature to show a well-resolved multiline electron spin resonance (ESR) signal (g = 2.003). Experimentally obtained ESR spectrum of **3.1** measured in degassed toluene was shown in Figure 3.4.1, together with the simulated spectrum. The paramagnetic species giving the ESR signal was undoubtedly assigned to monomeric **3.1**. Hyperfine coupling constants (HFCCs) corresponding to protons of phenalenyl unit and methyl groups are fully consistent with the values expected by theoretical calculations with a UBLYP/6-31G**//UB3LYP/6-31G** method. HFCCs of α protons on the phenalenyl moiety (a(H$_\alpha$) = 0.620 mT) are almost identical to that of parent phenalenyl (a(H$_\alpha$) = 0.630 mT)[5,6] and other derivatives (**1.4**: a(H$_\alpha$) = 0.620 mT, **2.1a**: a(H$_\alpha$) = 0.620 mT, **2.1b**: a(H$_\alpha$) = 0.620 mT),[1,2,4] supporting the idea that introduction of methyl group at the β carbon atoms bearing little spin densities does not affect the spin nature of phenalenyl.

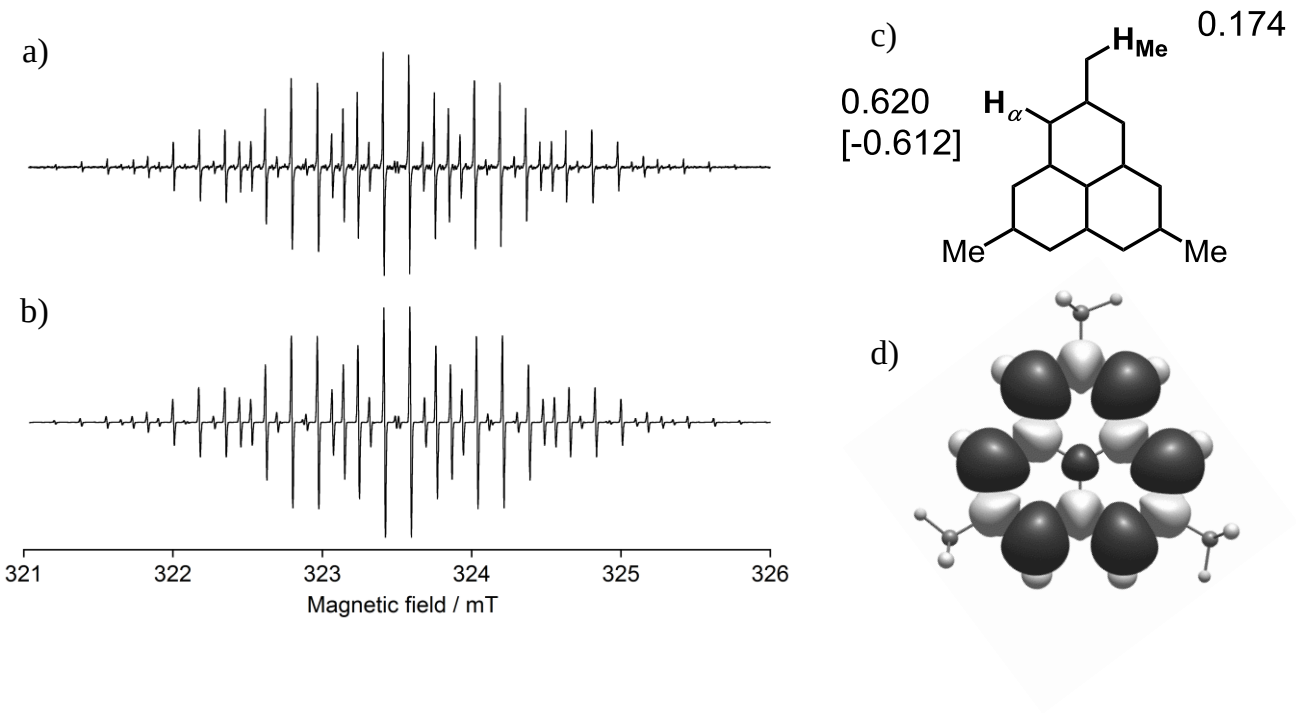

Figure 3.4.1. a) Observed (5×10^{-5} M, g = 2.003) and b) simulated ESR spectra of **3.1** in toluene at 250 K. c) Experimentally determined HFCCs (in mT) of **3.1**. In parentheses, HFCCs estimated by a UBLYP/6-31G**//UB3LYP/6-31G** method and the McConnell model (Q = −2.4 mT). c) Spin density map calculated with a UBLYP/6-31G**//UB3LYP/6-31G** method. Black and gray surfaces represent α and β spin densities drawn at 0.0005 e/au^3 level, respectively. Reprinted with permission from ref. 1. Copyright 2014, American Chemical Society.

The ESR signal decreased in intensity with decreasing temperature and almost disappeared at 170 K. This result suggests that **3.1** forms diamagnetic dimers $\mathbf{3.1_2}$ at lower temperature as observed in other phenalenyl derivatives. The temperature-dependence of an intensity change observed by ESR measurements can be expressed quantitatively along the thermodynamic equilibrium, and thermodynamic parameters ΔH and ΔS, can be determined by using the van't Hoff equation to be −9.7 kcal mol^{-1} and –22 cal K^{-1} mol^{-1}, respectively. The value of enthalpy change is almost identical to that of parent phenalenyl (ΔH = −10 kcal mol^{-1})[7,8] and **2.1a** (ΔH = −9.6 kcal mol^{-1}),[1] which indicates that methyl groups do not suppress the formation of diamagnetic dimers $\mathbf{3.1_2}$. It should be noted that **3.1** demonstrated a quite similar dimerization behavior in THF. Thermodynamic parameters for dimerization determined in THF (ΔH = −9.4 kcal mol^{-1} and ΔS = –22 cal K^{-1} mol^{-1}) were almost identical to that estimated in toluene, suggesting the dimerization modes is independent of the solvent polarity as observed in radical ions of **1.7** and **1.9**.[9,10]

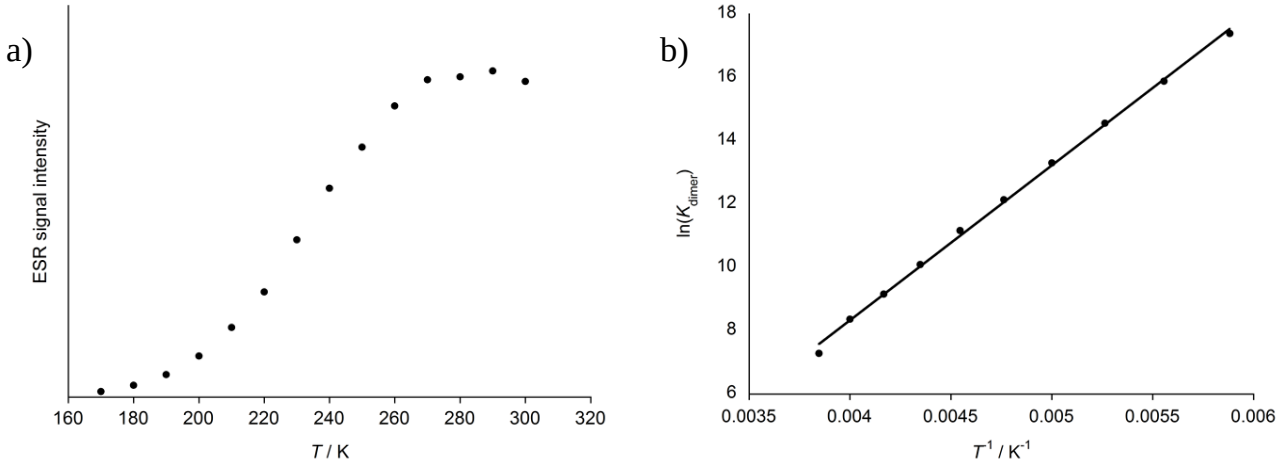

Figure 3.4.2. a) Temperature dependence of the ESR signal intensity in toluene (4.6×10^{-5} M). b) Van't Hoff plot. Reprinted with permission from ref. 1. Copyright 2014, American Chemical Society.

3.4.2 ^{1}H NMR spectroscopy of TMPLY

The dimerization mode of **3.1** adopted in solution state was confirmed by ^{1}H NMR spectroscopy. ^{1}H NMR spectrum of **3.1** recorded in degassed THF-d_8 at 173 K was shown in Figure 3.4.3. **3.1** formed three diamagnetic dimers (shown with ●, ■, and ▲) that are fully identified to σ-dimer *RR*/*SS* (chiral) form (●), σ-dimer *RS* (*meso*) form (■), and π-dimer (▲) on the basis of 2D-NMR techniques as well as theoretical predictions of NMR chemical shifts with a GIAO-(U)B3LYP/6-31+G** method. $\mathbf{3.1_2}$ σ-dimer *RR*/*SS* form with the C_2 configuration demonstrated prominent six singlets in 8–4 ppm region and three singlets in 3–1 ppm region. In contrast to the spectral simplicity of $\mathbf{3.1_2}$ σ-dimer *RR*/*SS* form with C_2 symmetry, $\mathbf{3.1_2}$ σ-dimer *RS* form having a C_1 geometry showed twelve singlet peaks corresponding to two independent phenalenyl moieties in 8–4 ppm region. It should be noted that an aromatic proton (H_b in Figure 3.4.4) shifted upfield to 5.46 ppm due to the strong shielding effect arising from the ring current of a neighboring phenalenyl ring. This result supports strongly the computational prediction that the H_b proton lies on the other phenalenyl plane.[1] Moreover, characteristic broaden singlets at 6.5 ppm and 2.2 ppm are assignable to $\mathbf{3.1_2}$ π-dimer. The chemical shift of a peak corresponding to α protons on phenalenyl moiety is almost identical to

that of **2.1a**$_2$ π-dimer (6.8 ppm)[1] and **1.4**$_2$ π-dimer (6.5 ppm).[9]

^{1}H NMR spectroscopy gave a substantial insight into the energetic preference between three **3.1**$_2$ dimers; that is, the energy difference between three **3.1**$_2$ dimers was estimated quantitatively from the integration ratio of ^{1}H NMR signals. **3.1**$_2$ σ-dimer *RR*/*SS* form showing distinctive NMR signals with the largest intensity is energetically the most favorable isomer. Although **3.1**$_2$ σ-dimer *RS* form is less stable in energy than **3.1**$_2$ σ-dimer *RR*/*SS* form, the energy difference of 0.08 kcal mol^{-1} is extraordinarily small. In comparison with **3.1**$_2$ σ-dimer *RR*/*SS* form, **3.1**$_2$ π-dimer giving weak NMR signals is 0.68 kcal mol^{-1} less favorable in energy. The energetic preference is fairly consistent with the computational prediction that **3.1**$_2$ σ-dimer *RS* form and **3.1**$_2$ π-dimer are 1.21 kcal mol^{-1} and 3.64 kcal mol^{-1} less stable, respectively.[1] Thus, the extraordinarily small energy difference between three **3.1**$_2$ dimers was corroborated experimentally.

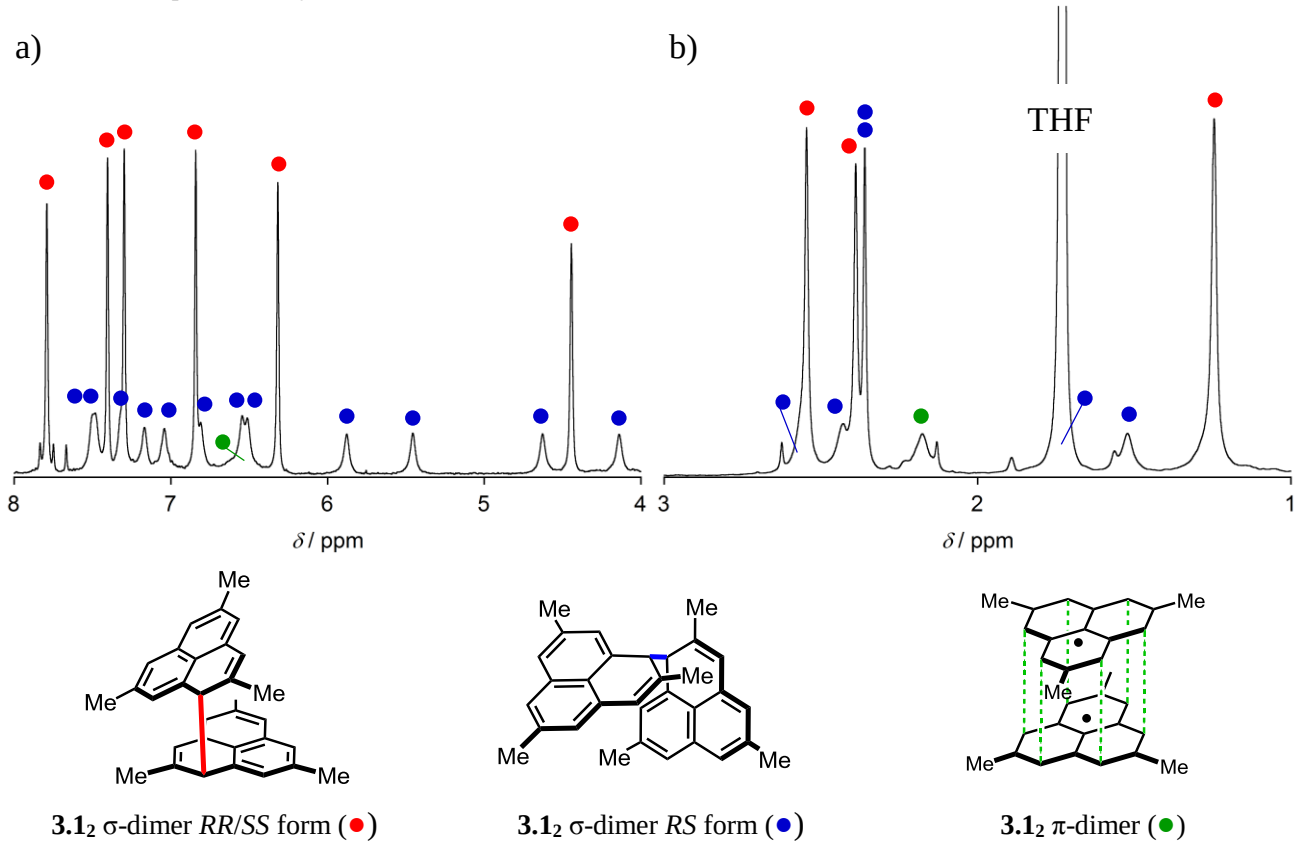

Figure 3.4.3. ^{1}H NMR spectrum of **3.1**$_2$ dimers in degassed THF-d_8 measured at 173 K. 8–4 ppm region (a) was magnified three times with respect to 3–1 ppm region for clarity.

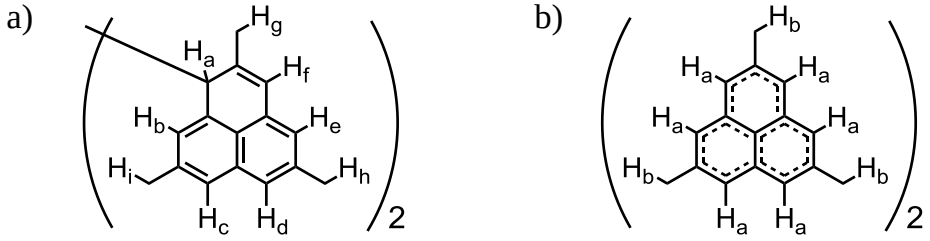

Figure 3.4.4. Numbering of protons of a) **3.1**$_2$ σ-dimers and b) **3.1**$_2$ π-dimer for NMR assignments.

Table. 3.4.4. Experimentally determined chemical shifts together with the computationally predicted chemical shifts with a GIAO-(U)B3LYP/6-31+G** method.

	3.1$_2$ σ-dimer *RR*/*SS* form								
	H_a	H_b	H_c	H_d	H_e	H_f	H_g	H_h	H_i
Experimental	4.45	7.79	7.41	7.30	6.84	6.32	1.25	2.55	2.39
Theoretical	3.80	7.25	6.48	6.71	6.73	6.70	2.17	2.02	2.11
	3.1$_2$ σ-dimer *RS* form								
	H_a	H_b	H_c	H_d	H_e	H_f	H_g	H_h	H_i
Experimental	4.14	5.46	7.04	7.17	6.55	5.87	ca. 1.7	1.52	2.36
	4.63	7.50	7.48	7.32	6.81	6.51	2.43	ca. 2.6	2.36
Theoretical	3.82	5.63	6.95	7.10	6.56	5.80	1.53	1.38	2.13
	4.28	7.39	7.58	7.38	6.81	6.57	2.30	2.48	2.35
	3.1$_2$ π-dimer								
	H_a						H_b		
Experimental	ca. 6.5						2.18		
Theoretical	6.56						1.91		

3.4.3 Electronic absorption spectrum of TMPLY

Dimerization behavior of **3.1** in solution state was estimated by a variable temperature (VT) electronic absorption measurements within the temperature range from 295 K to 173 K. Dilute solution of **3.1** showed a weak and sharp absorption band (550 nm, $\varepsilon = 320$ cm^{-1} M^{-1}) at room temperature arising from a forbidden transition of monomeric **3.1** (Figure 3.4.5). The gradual cooling of **3.1** solution in THF resulted in the appearance of a broad absorption band at ~500 nm. Whereas the σ-dimer of phenalenyl derivatives shows no characteristic absorption band in visible region, the π-dimer is known to show a broad and intense absorption band around 500-600 nm arising from its HOMO–LUMO transition.[7,8,12] Thus, the successive increasing in intensity of the broad absorption band in visible region can be ascribed to the increase of the concentration of π-dimer upon cooling. A similar spectral change was reported in **1.4** by Kochi *et al*. With decreasing temperature, an intense absorption band centered at 595 nm appeared, accompanied by the increase of the concentration of **1.4**$_2$ π-dimer.[12] Moreover, unlike the spectral change demonstrated by **1.4**, **3.1** showed a unique temperature dependence of the absorption spectrum upon decreasing temperature from 233 K to 173 K. Subsequent cooling from 233 K to 173 K resulted in the decrease in intensity of the absorption band at ~500 nm. To understand this characteristic behavior, the concentrations of monomeric **3.1** and **3.1**$_2$ dimers (**3.1**$_2$ σ-dimer *RR*/*SS* form, **3.1**$_2$ σ-dimer *RS* form, and **3.1**$_2$ π-dimer) were elucidated by using the thermodynamic parameters determined by VT-ESR measurements and energy difference between **3.1**$_2$ dimers obtained by ^{1}H NMR spectroscopy (see Figure 3.4.6). Upon decreasing temperature, **3.1** forms **3.1**$_2$ dimers, resulting in the increase of the concentrations of **3.1**$_2$ dimers. Notably, the concentration ratio between **3.1**$_2$ dimers follows the Boltzmann distribution; that is, the population of metastable **3.1**$_2$ σ-dimer *RS* form and **3.1**$_2$ π-dimer decreases with

decreasing temperature. With focused on the concentration change of **3.1**$_2$ π-dimer shown in Figure 3.4.6d, the concentration of **3.1**$_2$ π-dimer would be maximized at 213–223 K. Indeed, the absorption band corresponding to **3.1**$_2$ π-dimer showed the largest absorbance at 233 K, which is well accordance with the concentration simulation. Thus, the unique behavior observed in VT electronic absorption measurements strongly corroborates the fact that **3.1**$_2$ π-dimer is a metastable dimerization mode.

A broad absorption band centered at 536 nm remained even at 173 K. The concentration of monomeric **3.1** is estimated to be 3×10^{-6} M in the conditions, indicating that the absorption of **3.1** is negligible. Thus, the absorption band observed at 173 K is assignable to the HOMO–LUMO transition of **3.1**$_2$ π-dimer. The HOMO and LUMO of π-dimer is formed from the bonding and antibonding combinations of SOMOs of phenalenyl, therefore, the HOMO–LUMO transition of π-dimer reflects significantly the nature of multicenter 2e/12c bonding. The absorption band of **3.1**$_2$ π-dimer showed a blue shift with respect to that of **1.4**$_2$ π-dimer (λ_{max} = 595 nm),[12] which suggests that a covalent bonding interaction works more effectively between two phenalenyl units in **3.1**$_2$ π-dimer than that in **1.4**$_2$ π-dimer. This spectroscopic consideration is fully supported by the molecular geometry of **3.1**$_2$ π-dimer determined by the X-ray crystallographic analysis. As mentioned in chapter 3.3.2, **3.1**$_2$ π-dimer has a shorter π–π separation distance than **1.4**$_2$ π-dimer,[4] giving a stronger covalent bonding interaction.

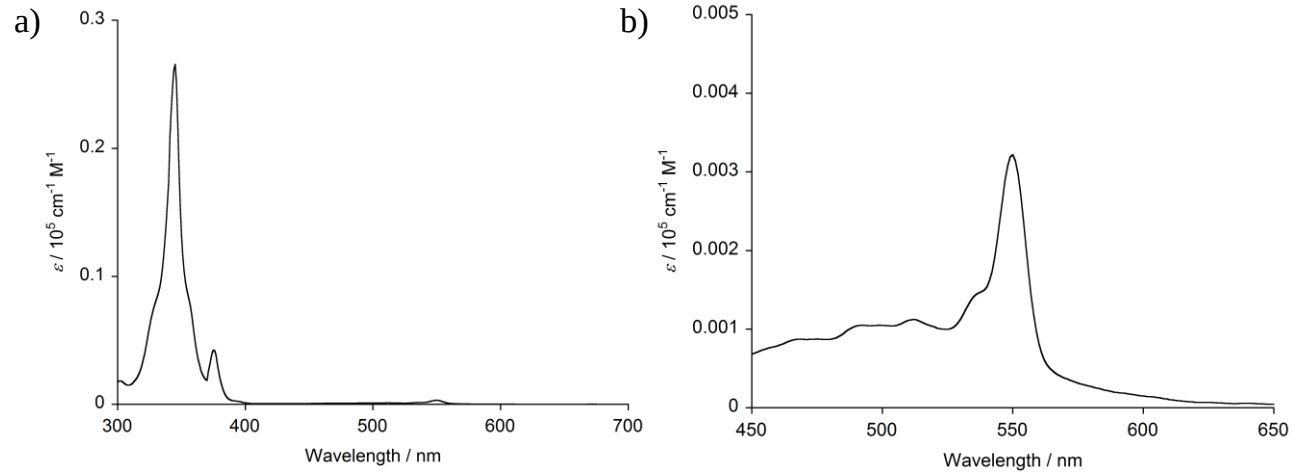

Figure 3.4.5. a) Electronic absorption spectrum of **3.1** solution (1×10^{-4} M) in degassed dichloromethane at room temperature. b) Magnified view of visible region.

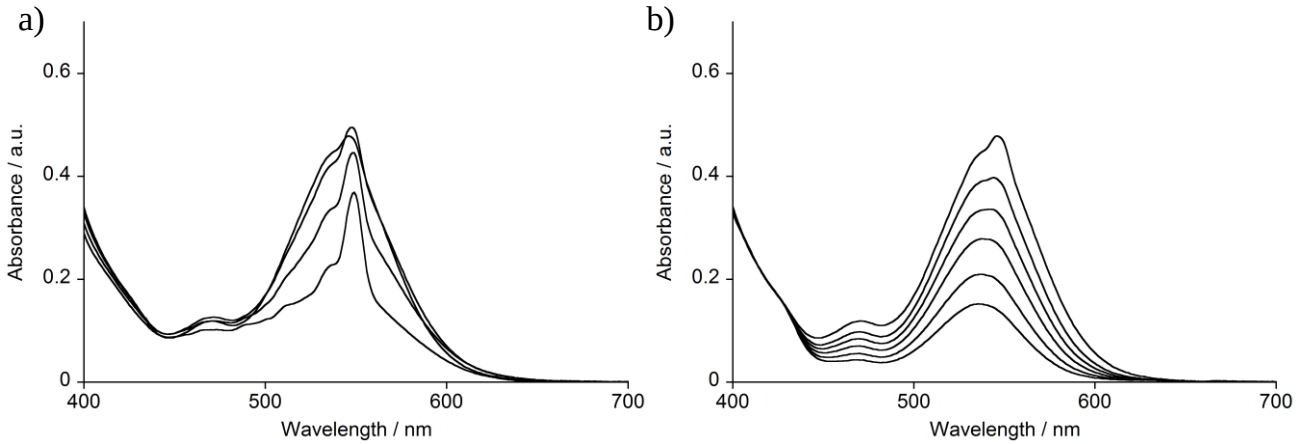

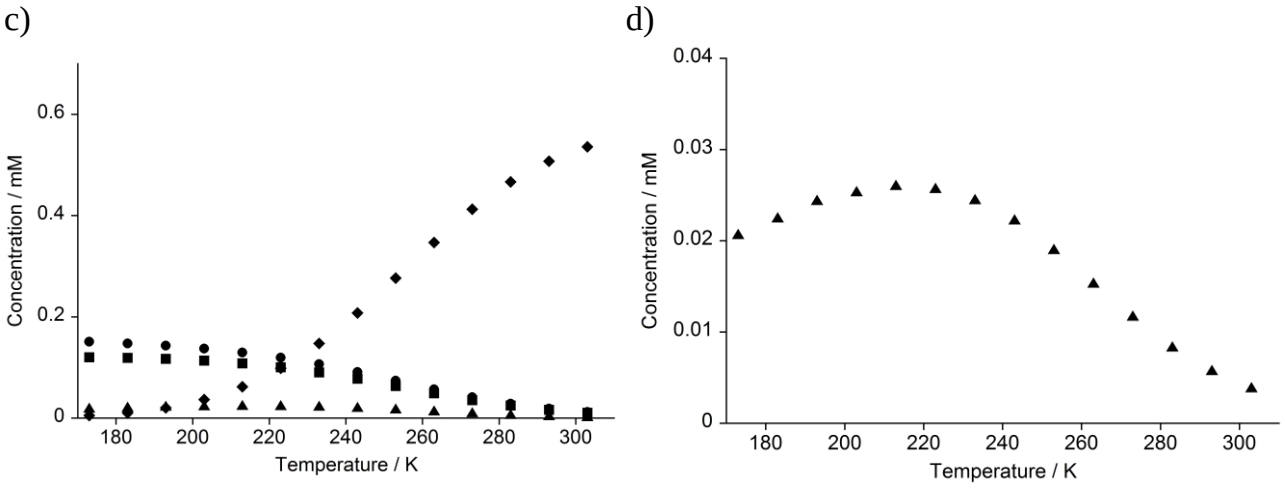

Figure 3.4.6. VT electronic absorption spectra of **3.1** solution (5.9×10^{-4} M) in degassed THF measured within the temperature range a) from 295 K to 233 K and b) from 233 K to 173 K. c) Calculated concentrations of monomeric **3.1** and $\mathbf{3.1_2}$ dimers in THF solution (5.9×10^{-4} M) at each temperature. The concentration of monomeric **3.1**, $\mathbf{3.1_2}$ σ-dimer *RR*/*SS* form, $\mathbf{3.1_2}$ σ-dimer *RS* form, and $\mathbf{3.1_2}$ π-dimer were shown with ♦, ●, ■, and ▲, respectively. d) Magnified view of the concentration change of $\mathbf{3.1_2}$ π-dimer (▲).

3.5 Solution state dynamics of TMPLY dimers

3.5.1 Dynamic ^{1}H NMR spectroscopy

To shed light on the dynamics of **3.1** dimers (**3.1**$_2$) in the solution state, variable temperature (VT) ^{1}H NMR measurements were performed within the temperature range from 173 K to 293 K (Figure 3.5.1).

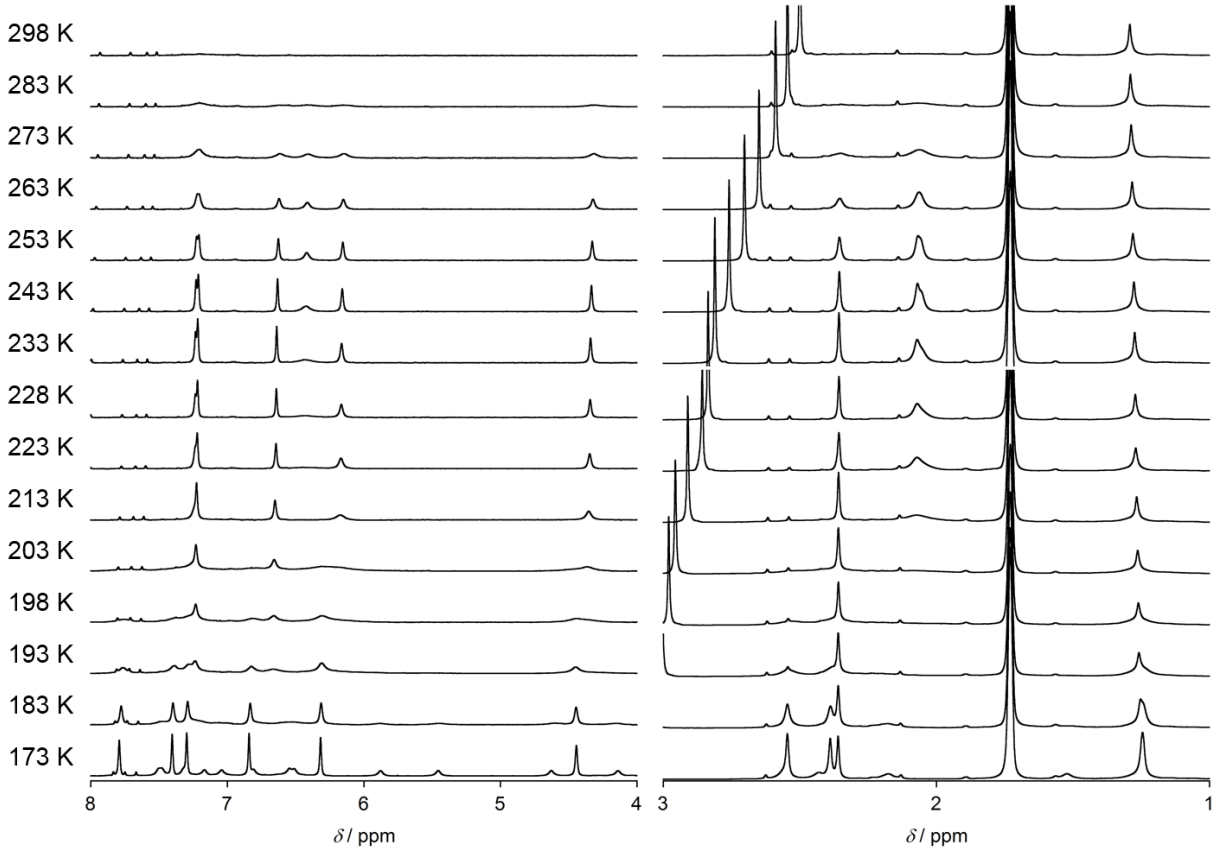

Figure 3.5.1. VT NMR spectra of **3.1** measured in degassed THF-d_8. 8–4 ppm region was three times magnified compared to 3–1 ppm region for clarity.

Regarding the signals of **3.1**$_2$ σ-dimer *RS* form, the complicated signals arising from non-equivalent phenalenyl sites showed a coalescence to give an averaged spectra showing six broad singlets of protons on phenalenyl moieties and three singlet peaks of methyl protons due to the rapid conformational change between two rotamers (*RS*1 and *RS*2 shown in Scheme 3.5.1) within the NMR time scale. The combinations of peaks giving a coalesced peak were fully assigned by VT NMR spectra and EXSY measurements (shown later). The activation barrier of the conformational change can be estimated from an exchange rate, k, and a coalescence temperature, T_c, of a representative pair of signals. With focused on the signals corresponding to benzyl protons at 4.14 ppm and 4.63 ppm as the representative, the exchange rate k at coalescence temperature 191 K is determined to be 435 s^{-1} by using the equation $k = \pi\Delta\nu/\sqrt{2}$, where $\Delta\nu$ is the frequency separation of the two corresponding peaks ($\Delta\nu$ = 196 Hz for H_a).

Therefore, the activation free energy, $\Delta G^{\ddagger}$, for the conformational change between *RS*1 and *RS*2 was determined from the Eyring equation to be 8.7 kcal mol^{-1}. This experimental result is fairly consistent with the computational prediction that the activation battier of the conformational change is estimated to be 7.34 kcal mol^{-1}.

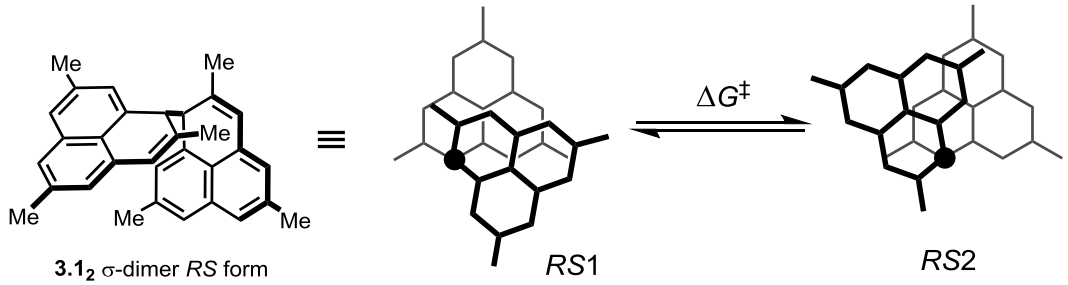

Scheme 3.5.1. Conformational change of **3.1**$_2$ σ-dimer *RS* form between two stable conformations, *RS*1 and *RS*2. C(sp^3) atoms were shown with black dots.

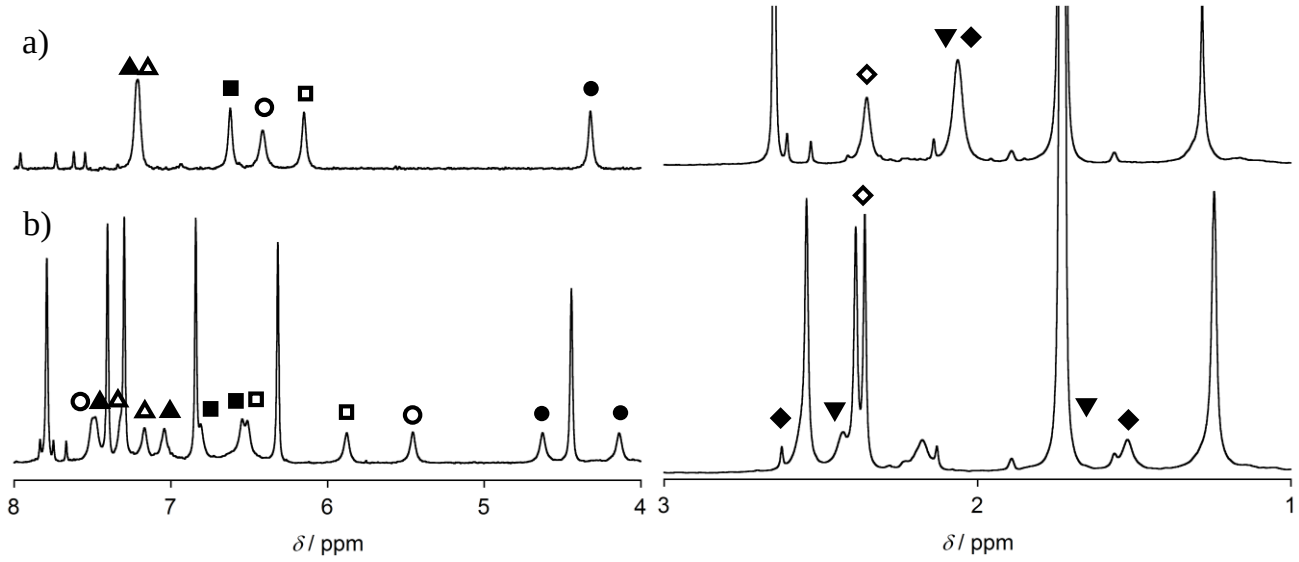

Figure 3.5.2. ^{1}H NMR spectra of **3.1** measured in degassed THF-d_8 at a) 263 K and b) 173 K. 8–4 ppm region was magnified three times with respect to 3–1 ppm region for clarity.

^{1}H NMR signals of **3.1**$_2$ π-dimer disappeared upon increasing temperature (Figure 3.5.3). The signal broadening of **3.1**$_2$ π-dimer evokes two possibility: 1) the singlet biradical nature of **3.1**$_2$ π-dimer, 2) a facile dissociation of **3.1**$_2$ π-dimer into two monomeric **3.1**. The singlet biradical compounds with small energy gaps (ΔE_{S-T}) between the singlet ground state and the excited triplet state are known to show a signal broadening in NMR spectra due to the presence of thermally excited triplet species. Actually, the singlet biradical ground state of **1.4**$_2$ π-dimer was expected by computational studies.[13] However, ΔE_{S-T} of **3.1**$_2$ π-dimer estimated with a UB3LYP/6-31G** method is extremely large (9075 K, 18.04 kcal mol^{-1}), which indicates that the NMR signal broadening is not due to the presence of a thermally excited triplet species. On the other hand, the activation barrier of the dissociation of **3.1**$_2$ π-dimer is expected to be smaller than ΔE_{S-T}. The structural change induced by the dissociation of π-dimer requires little, if any,

activation energy, which indicates that the activation barrier for the dissociation is almost comparable with the association energy, ΔG. The association energy at 173 K, ΔG_{173}, can be expected by using thermodynamic parameters of dimerization obtained by VT ESR measurements (ΔH = −9.4 kcal mol^{-1}, ΔS = −22 cal K^{-1} mol^{-1} in THF) and energy difference between **3.1**$_2$ σ-dimer and **3.1**$_2$ π-dimer. As shown in Figure 3.4.6c, the dimerization of **3.1** in solution state is dominated by the formation of **3.1**$_2$ σ-dimers involving *RR*/*SS* form and *RS* form, which indicates that the association energy of **3.1**$_2$ σ-dimers at 173 K is estimated to be −5.9 kcal mol^{-1}. In contrast, **3.1**$_2$ π-dimer is approximately 0.6 kcal mol^{-1} less stable than **3.1**$_2$ σ-dimers; thus, the association energy of **3.1**$_2$ π-dimer, which should be almost equivalent to the activation energy of the dissociation, is estimated to be ~5 kcal mol^{-1}. This activation barrier elucidated is significantly small enough to induce a facile dissociation into monomeric **3.1**.

Despite of the structural similarity with the **3.1**$_2$ σ-dimer *RS* form showing its NMR signals even at 273 K, **3.1**$_2$ σ-dimer *RR*/*SS* form also demonstrated a noticeable signal broadening in ^{1}H NMR spectra and the signals disappeared above 203 K. This result strongly suggests that **3.1**$_2$ σ-dimer *RR*/*SS* form dissociates into monomeric **3.1** through a unique pathway with a low activation barrier mentioned later.

.

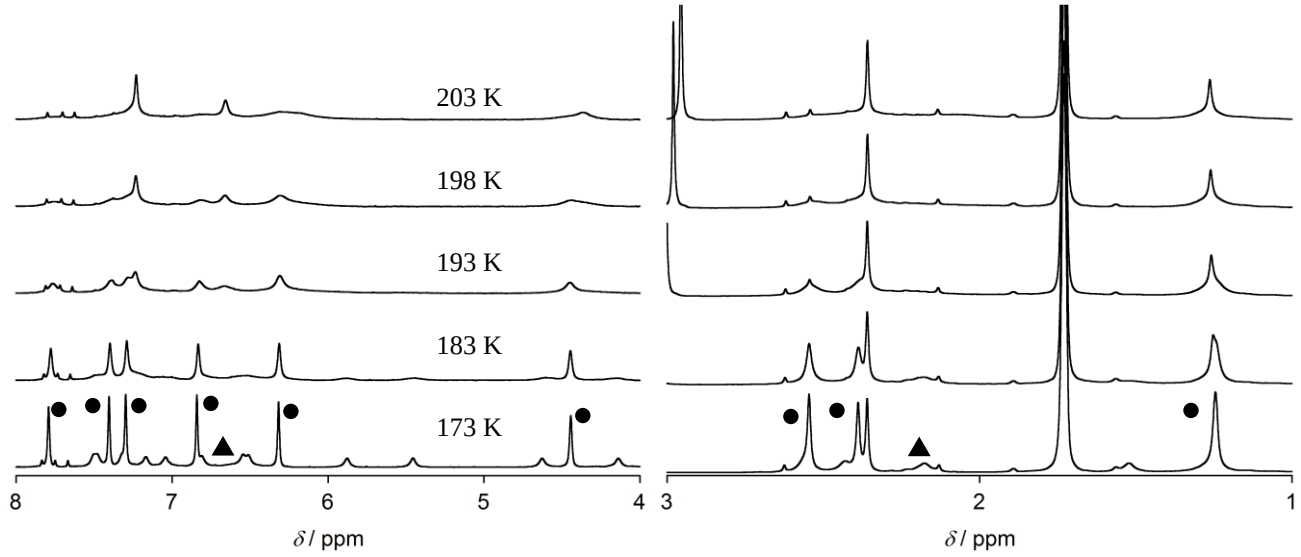

Figure 3.5.3. VT NMR spectra of **3.1** within the temperature range from 173 K to 203 K.

3.5.2 ^{1}H–^{1}H EXSY measurements of TMPLY dimers

Solution state dynamics of **3.1** dimers were also monitored by ^{1}H–^{1}H exchange spectroscopy (EXSY) measurements at 173 K (Figure 3.5.4). **3.1**$_2$ σ-dimer *RS* form showed one-to-one correlations in the same sign with the diagonal peaks due to the dynamic exchange between six sets of α protons peaks. A benzylic proton (H_a in Figure 3.4.4) on the one phenalenyl unit showed a cross peak with the other benzylic proton on the other phenalenyl unit (H_a'), and other protons gave cross peaks in the same manner; thus, a cross peaks was observed between H_x and H_x'. This indicates the cross peaks are due to the conformational change between two rotamers (*RS*1 and *RS*2 shown in Scheme 3.5.1) as observed in VT ^{1}H NMR spectroscopy (chapter 3.5.1).

In contrast to the simplicity of EXSY cross peaks demonstrated by **3.1**$_2$ σ-dimer *RS* form, the structural isomer, **3.1**$_2$ σ-dimer *RR*/*SS* form, showed a fascinating phenomenon in EXSY spectra; that is, the protons on phenalenyl moieties showed cross peaks with all the other phenalenyl protons due to the chemical exchange and the methyl protons showed cross peaks with all the other methyl protons. This fascinating result can be ascribed to the six-fold σ-bond shift within the time scale of the EXSY measurement as illustrated in Scheme 3.5.2, which is the first evidence for the σ-bond fluxionality of phenalenyl dimers. To elucidate the mechanism of the six-fold σ-bond shift, the exchange rates of the reaction, k_{ex}, were estimated from the mixing time dependence of intensity ratios of cross peaks (I_b–I_f/I_a).[14] Exchange rates between H_b–H_f and H_a, $k_{ex}(H_x–H_a)$ in Figure 3.5.5, were estimated and shown in Figure 3.5.5. Protons H_c–H_f gave similar exchange rates of 0.7–0.8 s^{-1} at 173 K, whereas the exchange rate between protons H_a and H_b gave a larger value of 2 s^{-1}. Cross peaks observed between H_a and H_b, which are in close proximity to each other, should include a non-negligible contribution of dipole–dipole interactions; thus, the exchange rate $k_{ex}(H_b–H_a)$ estimated from EXSY measurements would not be an essential value of the σ-bond shift.

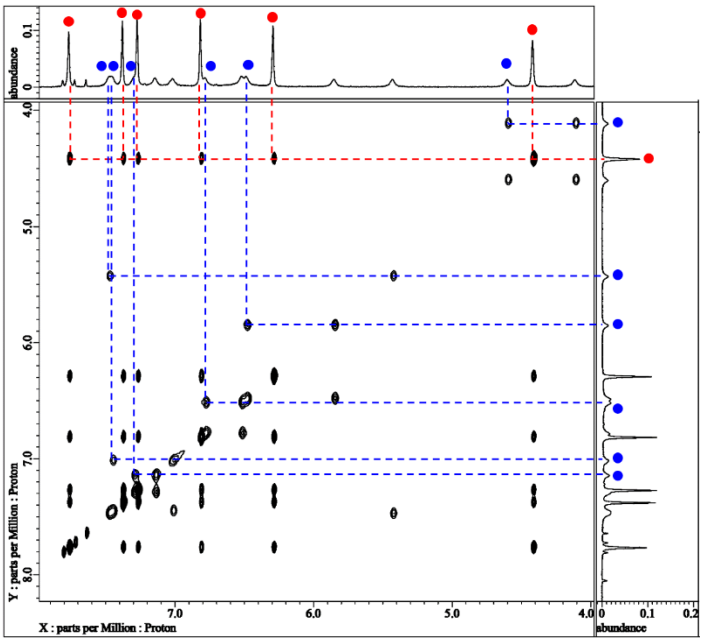

Figure 3.5.4. ^{1}H–^{1}H EXSY spectrum of **3.1** in THF-d_8 at 173 K (mixing time: 500 ms). 8–4 ppm region was magnified for clarity, and cross peaks of **3.1**$_2$ σ-dimer *RR*/*SS* form and **3.1**$_2$ σ-dimer *RS* form were shown with red and blue lines, respectively.

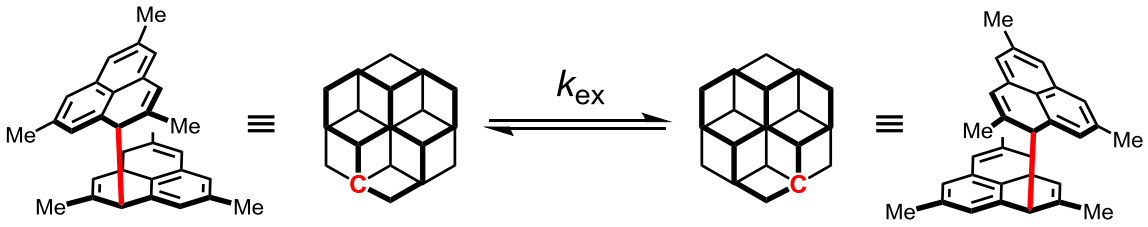

Scheme 3.5.2. σ-Bond shift of **3.1**$_2$ σ-dimer *RR*/*SS* form.

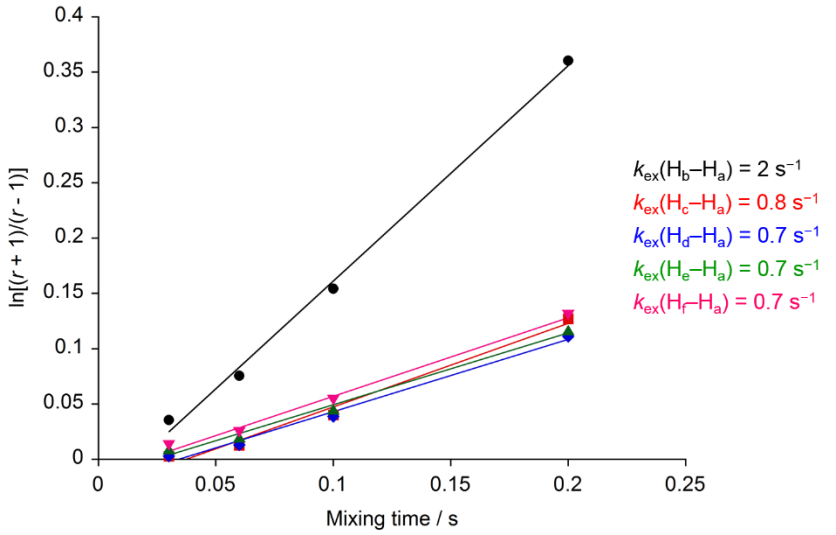

Figure 3.5.5. ln[(r + 1)/(r − 1)] plots as a function of mixing time to determine the exchange rates, where r = (I_{xx}+I_{aa})/(I_{xa}+I_{ax}). I_{xx}, I_{aa}: intensity of diagonal peaks. I_{xa}, I_{ax}: intensity of cross peaks.[14]

With focused on the aliphatic region of the ^{1}H–^{1}H EXSY spectrum, the unambiguous cross peaks due to the chemical exchange were found between the methyl protons of **3.1**$_2$ σ-dimer *RR*/*SS* form and that of **3.1**$_2$ π-dimer. This is a crucial evidence for the presence of the dynamic equilibrium between **3.1**$_2$ σ-dimer *RR*/*SS* form and **3.1**$_2$ π-dimer. It should be noted that the cross peaks were not observed between **3.1**$_2$ σ-dimer *RS* form and **3.1**$_2$ π-dimer. This result rules out the possibility that the dynamic exchange between **3.1**$_2$ σ-dimer *RR*/*SS* form and **3.1**$_2$ π-dimer proceeds via monomeric **3.1** generated by the dissociation of these dimers. The activation barrier for the direct conversion of **3.1**$_2$ σ-dimer *RR*/*SS* form to **3.1**$_2$ π-dimer was estimated by theoretical calculations to be 7.14, which would be a reliable value for the reaction.

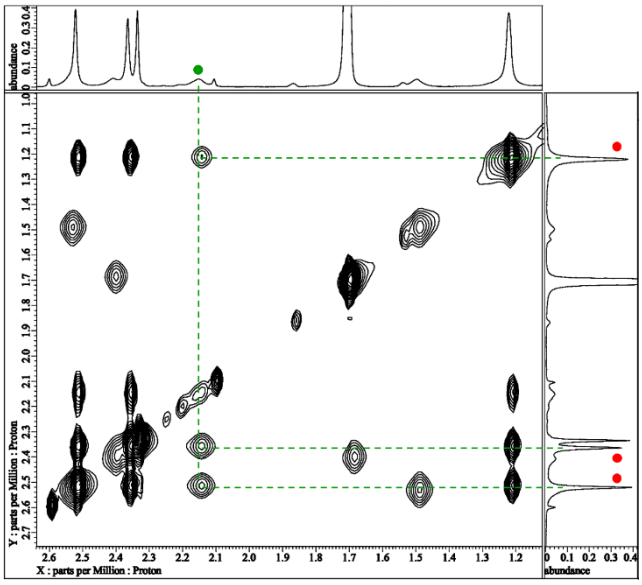

Figure 3.5.6. $^{1}H-^{1}H$ EXSY spectrum of **3.1** in THF-d_8 at 173 K (mixing time: 500 ms). 3–1 ppm region was magnified and cross peaks between **3.1**$_2$ σ-dimer *RR*/*SS* form and **3.1**$_2$ π-dimer were shown with dashed lines.

On the basis of the experimental results obtained by EXSY measurements, following reaction mechanisms are considerable; 1) a concerted [*m*,*m*]-sigmatropic rearrangements (*m* = 3, 5, 7) as shown in Scheme 3.5.3a, and 2) a stepwise interconversion via **3.1**$_2$ π-dimer as an intermediate (Scheme 3.5.3b).

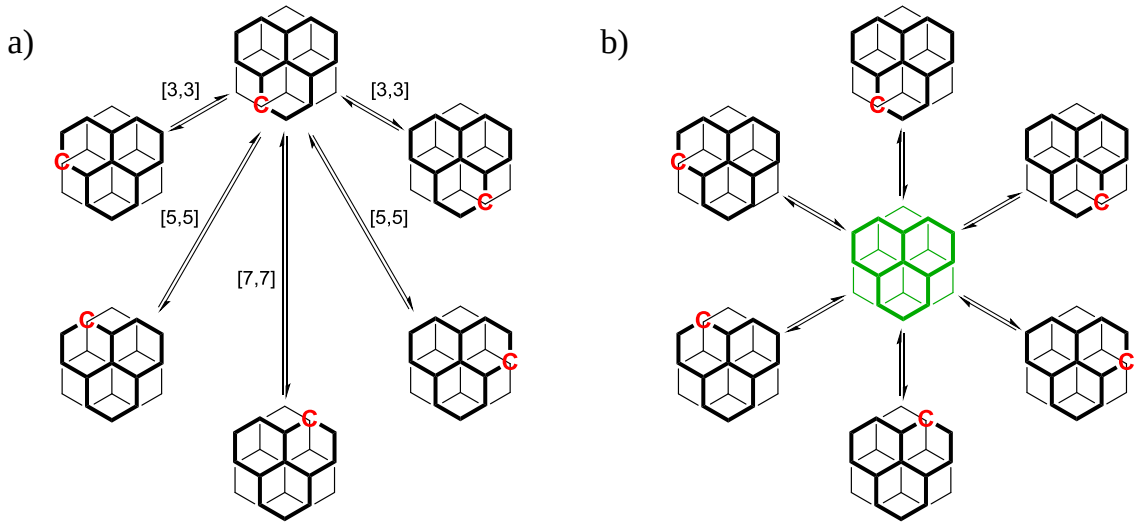

Scheme 3.5.3. a) Concerted [*m*,*m*]-sigmatropic rearrangements (*m* = 3, 5, 7). b) Stepwise interconversion via **3.1**$_2$ π-dimer.

For deeper understanding of the mechanism of the σ-bond rearrangement, molecular geometry of **3.1**$_2$ σ-dimer *RR*/*SS* form determined by X-ray crystallographic analysis was focused on. Generally, the exchange rates of the σ-bond rearrangement strongly depends on the molecular structure. Indeed, C(sp^3)–B σ-bond shift demonstrated by 1-phenalenyl(diisopropyl)borane, which was investigated using EXSY spectra, takes place selectively between α carbon pairs in close proximity.[15] Distances between corresponding α carbon pairs involving the six-fold σ-bond shift were summarized in Figure 3.5.7.[1] The distance between C_{d1} and C_{d2} was determined to be 6.298 Å, which is considerably larger than that between C_{b1}–C_{f2} (3.355 Å). On the assumption of a concerted [*m*,*m*]-sigmatropic rearrangement mechanism shown in Scheme 3.5.3a, the presence of a significant difference in the exchange rates is expected due to the large structural difference. However, the difference in the exchange rates is negligible, inferring the σ-bond shift takes place in equal probabilities between six sets of α carbon pairs. The experimental observation strictly rules out the concerted mechanism and strongly supports the stepwise σ-bond shift via **3.1**$_2$ π-dimer. The σ-bond reformation step in **3.1**$_2$ π-dimer having a D_{3d} geometry should take place in equal probabilities in six sets of α carbon pairs as observed in the exchange rates estimated experimentally.

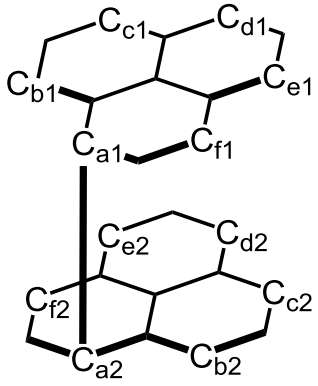

C_α–C_α	distance / Å
C_{a1}–C_{a2}	1.614
C_{b1}–C_{f2}	3.355
C_{c1}–C_{e2}	5.132
C_{d1}–C_{d2}	6.298
C_{e1}–C_{c2}	5.591
C_{f1}–C_{b2}	3.582

Figure 3.5.7. Averaged distances between corresponding α carbon pairs that involves the six-fold σ-bond shift. Methyl groups on the phenalenyl moieties were omitted for clarity.

3.6 Conclusion

On the basis of the experimental findings mentioned above, a plausible potential energy surface involving the dimerization of TMPLY **3.1** was exhibited in Figure 3.6.1. **3.1** adopts three dimerization modes; that is, **3.1**$_2$ σ-dimer *RR*/*SS* form, **3.1**$_2$ σ-dimer *RS* form, and **3.1**$_2$ π-dimer. The preference of the dimerization modes was undoubtedly determined and the extraordinarily small energy difference was confirmed experimentally. In contrast to the energetic similarity, noticeable differences of the activation barriers for the dissociation were observed. Whereas **3.1**$_2$ σ-dimer *RS* form was observed in ^{1}H NMR spectra even at higher temperature due to the large activation energy in TS1, **3.1**$_2$ σ-dimer *RR*/*SS* form and **3.1**$_2$ π-dimer demonstrated a facile dissociation into **3.1**s. Although a substantially low activation barrier in TS2 is well expected, the facility of a dissociation of **3.1**$_2$ σ-dimer *RR*/*SS* form requires a comment. This substantial difference in the dissociation behavior can be accounted for by the presence of a direct interconversion path between **3.1**$_2$ σ-dimer *RR*/*SS* form and **3.1**$_2$ π-dimer through TS3, which was doubtlessly

confirmed by EXSY measurements as well as computational studies. **3.1**$_2$ σ-dimer *RR*/*SS* form is expected to undergo a facile dissociation in a stepwise pathway through TS2 and TS3 with lower activation barrier than TS1. Moreover, the six-fold σ-bond shift observed by EXSY measurements also proceeds through TS3 via **3.1**$_2$ π-dimer as an intermediate. Stepwise process via **3.1**$_2$ π-dimer having D_{3d} symmetry leads to the random σ-bond migration in six sets of α carbon pairs.

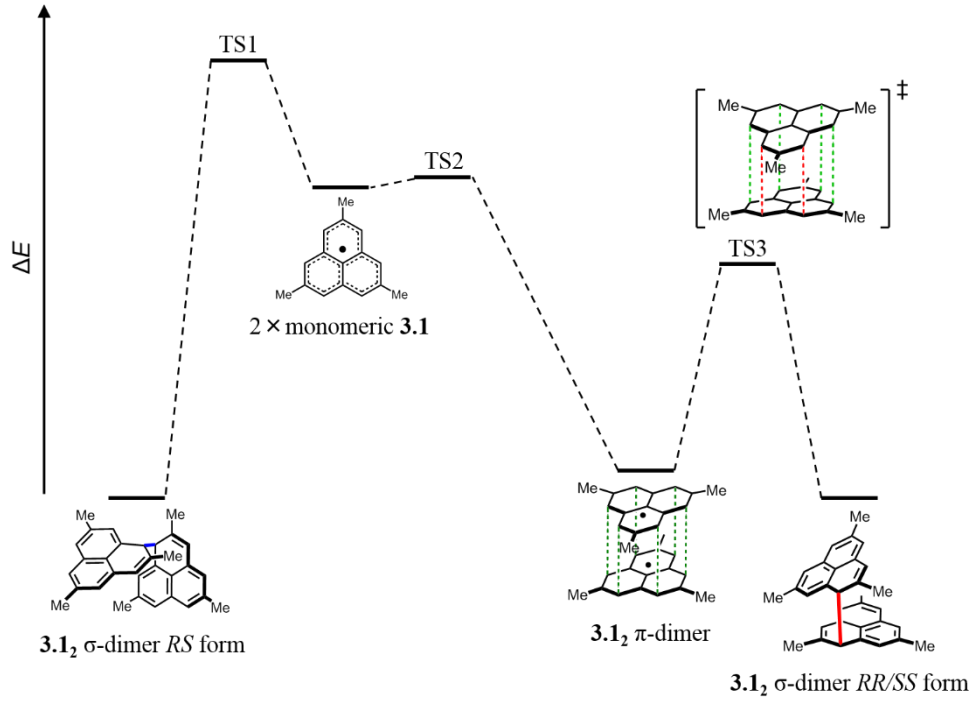

Figure 3.6.1. Plausible potential energy surface.

3.7 Experimental

General: All experiments with moisture- or air-sensitive compounds were performed in anhydrous solvents under nitrogen atmosphere in well-dried glassware. Dried solvents were prepared by distillation under nitrogen. Anhydrous dichloromethane and THF were purchased from Kanto Chemical Co., Inc. and were used without further purifications. Toluene was dried and distilled over calcium hydride. THF-d_8 was dried over Na-K alloy and distilled under reduced pressure. Column chromatography was performed with silica gel [Silica gel 60 (MERCK)]. Melting points were taken on a Yanako MP 500D apparatus. ^{1}H and ^{13}C NMR spectra were obtained on JEOL ECS400 and ECA500 spectrometers. The chemical shift was recorded by using tetramethylsilane (0.00 ppm) as an internal standard for ^{1}H NMR and $CHCl_3$ (77.00 ppm) for ^{13}C NMR spectra. Positive EI mass spectra were taken by using Shimadzu QP-5050. High resolution mass spectra were analyzed by using Applied Biosystems Japan Ltd. Analyst QS 2.0. Infrared spectra were recorded on a JASCO FT/IR-660M spectrometer. ESR spectra were measured in a toluene solution on a JEOL JES-RE1X. Data collection for X-ray crystal analysis was performed on Rigaku/Varimax diffractometer (Mo-Kα, λ = 0.71069 Å). The structure was solved with direct methods and refined with full-matrix least squares (teXsan).

^{1}H–^{1}H EXSY measurements were performed on a JEOL ECS400 spectrometer. The electronic absorption spectra were recorded on a JASCO V-570 spectrometer and a Shimadzu UV-3100PC spectrometer.

2,7-Dimethylnaphthalene (3.2)

To a solution of [1,3-bis(diphenylphosphino)propane]dichloronickel(II) (95 mg, 0.17 mmol) and 2,7-dibromonaphthalene **2.2** (1.0 g, 3.5 mmol) in THF (25 mL) was added methyl magnesium iodide (14 mmol) in ether (25 mL), and then the reaction mixture was heated at 45 ºC for 24 hours under nitrogen atmosphere. After cooled to room temperature, the reaction mixture was poured into ice-cold water, and 1 M hydrochloric acid was added, and then the organic layer was separated. The aqueous layer was extracted with ether. The combined organic layer was washed with brine and dried over anhydrous sodium sulfate. After filtration, the filtrate was evaporated and the residue was purified by column chromatography on silica gel (hexane) to give **2** as a white powder (0.48 g, 87%). R_f = 0.43 (hexane); ^{1}H NMR (500 MHz, $CDCl_3$) δ 7.69 (d, J = 8.0 Hz, 2H), 7.51 (s, 2H), 7.24 (dd, J = 8.5 Hz, 1.5 Hz, 2H), 2.49 (s, 6H).

1-Bromo-2,7-dimethylnaphthalene (3.3)

2,7-Dimethylnaphthalene **3.2** (0.48 g, 3.0 mmol) was dissolved in DMF (15 mL), and the solution was cooled to 0 ºC with an ice-bath. To the solution *N*-bromosuccinimide (0.60 g, 3.3 mmol) was added, and the solution was stirred at room temperature for 16 hours. The reaction mixture was stirred for more 11 hours after addition of *N*-bromosuccinimide (0.29 g, 1.6 mmol). To the solution was added water and dichloromethane, and the organic layer was separated and washed with aqueous sodium sulfite and brine, dried over anhydrous sodium sulfate. After filtration, the filtrate was evaporated and the residue was purified by column chromatography on silica gel (hexane) to give **3.3** as a colorless oil (0.71 g, 99%). R_f = 0.52 (hexane); ^{1}H NMR (400 MHz, $CDCl_3$) δ 8.06 (s, 1H), 7.68 (d, J = 8.4 Hz, 1H), 7.65 (d, J = 8.4 Hz, 1H), 7.31-7.27 (m, 2H), 2.61 (s, 3H), 2.56 (s, 3H); ^{13}C NMR (126 MHz, $CDCl_3$) δ 137.16, 135.91, 132.59, 131.25, 127.87, 127.83, 127.76, 126.95, 125.89, 123.36, 24.16, 22.02.

5-Bromo-3,6-dimethyl-1-naphthaldehyde (3.4)

To a solution of 1-bromo-2,7-dimethylnaphthalene **3.3** (0.70 g, 3.0 mmol) in dichloromethane (25 mL) was added dichloromethyl methyl ether (0.29 mL, 3.3 mmol) at −78 ºC under nitrogen atmosphere. To the solution titanium(IV) chloride (0.65 mL, 6.0 mmol) was added and stirred for 1.5 hours. After quenched with 1 M hydrochloric acid, the organic layer was separated and washed with brine, dried over anhydrous sodium sulfate. After filtration, the filtrate was evaporated and the residue was purified by column chromatography on silica gel (dichloromethane/hexane 40%) to give **3.4** as a white solid (0.67 g, 85%). mp 102-103 ºC; R_f = 0.50 (dichloromethane/hexane 50%); ^{1}H NMR (500 MHz, $CDCl_3$) δ 10.34 (s, 1H), 9.10 (d, J = 9.0 Hz, 1H), 8.19 (s, 1H), 7.76 (s, 1H), 7.51 (dd, J = 8.5 Hz, 1.5 Hz, 1H), 2.70 (s, 3H), 2.59 (s, 3H); ^{13}C NMR (126 MHz, $CDCl_3$) δ 192.81, 138.29, 137.55, 135.51, 132.96, 131.79, 130.72, 130.04, 127.96, 126.57, 124.57, 24.12, 21.92; IR (KBr) ν = 2948 (w), 2919 (w), 2831 (w), 2725 (w), 1694 (s), 1683 (s), 1548 (m), 1514 (s), 1447 (w), 1391 (w), 1334 (w), 1226 (m), 1176 (m), 1073 (m), 1038 (m), 976 (m), 957 (m), 818 (s) cm^{-1}; EI-MS *m/z* 264 (M^{+}+ 1), 262 (M^{+}− 1); Anal. Calcd for $C_{13}H_{11}BrO$: C, 59.34; H, 4.21. Found: C, 59.16; H, 4.16.

Ethyl (*E*)-3-(5-bromo-3,6-dimethylnaphthalen-1-yl)acrylate (3.5)

To a suspension of 60% sodium hydride (0.12 g, 3.0 mmol) in THF (10 mL) was added triethyl phosphonoacetate (0.61 mL, 3.0 mmol) under nitrogen atmosphere and the reaction mixture was stirred at room temperature for 10 min. 5-Bromo-3,6-dimethyl-1-naphthaldehyde **3.4** (0.67 g, 2.5 mmol) in THF (20 mL) was added and stirred for 1 hour. After quenched with aqueous ammonium chloride, the reaction mixture was extracted with ether. The organic layer was separated and washed with brine, dried over anhydrous sodium sulfate. After filtration, the filtrate was evaporated and the residue was purified by column chromatography on silica gel (dichloromethane/hexane 40%) to give **3.5** as a white solid (0.84 g, 99%). mp 72-73 ºC; R_f = 0.60 (dichloromethane/hexane 50%); ^{1}H NMR (500 MHz, $CDCl_3$) δ 8.40 (d, *J* = 15.5 Hz, 1H), 8.11 (s, 1H), 8.01 (d, *J* = 8.5 Hz, 1H), 7.52 (s, 1H), 7.37 (dd, *J* = 8.5 Hz, 1.5 Hz, 1H), 6.50 (d, *J* = 16.0 Hz, 1H), 4.31 (q, *J* = 7.5 Hz, 2H), 2.61 (s, 3H), 2.56 (s, 3H), 1.37 (t, *J* = 7.5 Hz, 3H); ^{13}C NMR (126 MHz, $CDCl_3$) δ 166.76, 141.11, 137.57, 135.71, 132.73, 130.88, 129.07, 128.68, 126.71, 126.60, 126.08, 123.49, 121.13, 60.64, 24.27, 21.84, 14.34; IR (KBr) ν = 3037 (w), 2982 (w), 2920 (m), 1714 (s), 1633 (s), 1552 (w), 1511 (w), 1447 (w), 1433 (m), 1364 (m), 1339 (m), 1302 (s), 1227 (m), 1174 (s), 1064 (m), 1036 (s), 991 (s), 975 (m), 857 (s), 814 (m) cm^{-1}; EI-MS *m/z* 334 (M^++ 1), 332 (M^+− 1); Anal. Calcd for $C_{17}H_{17}BrO_2$: C, 61.28; H, 5.14. Found: C, 61.23; H, 5.18.

Ethyl 3-(3,6-dimethylnaphthalen-1-yl)propanoate (3.6)

To a solution of ethyl (*E*)-3-(5-bromo-3,6-dimethylnaphthalen-1-yl)acrylate **3.5** (0.84 g, 2.5 mmol) in dichloromethane (3 mL) and ethanol (18 mL) was added 10% Pd-C (90 mg, 10wt%), and the suspension was stirred under hydrogen atmosphere for 3 hours. After removal of Pd-C by filtration, filtrate was evaporated. The residue was purified by column chromatography on silica gel (dichloromethane/hexane 40%) to give **3.6** as a colorless oil (0.56 g, 87%). R_f = 0.60 (dichloromethane/hexane 50%); ^{1}H NMR (500 MHz, $CDCl_3$) δ 7.86 (d, *J* = 8.0 Hz, 1H), 7.53 (s, 1H), 7.41 (s, 1H), 7.28 (dd, *J* = 8.5 Hz, 1.5 Hz, 1H), 7.12 (d, *J* = 1.0 Hz, 1H), 4.16 (q, *J* = 7.0 Hz, 2H), 3.35 (t, *J* = 8.0 Hz, 2H), 2.72 (t, *J* = 8.0 Hz, 2H), 2.49 (s, 3H), 2.45 (s, 3H), 1.25 (t, *J* = 7.0 Hz, 3H); ^{13}C NMR (126 MHz, $CDCl_3$) δ 173.11, 136.19, 135.17, 135.06, 134.43, 128.06, 127.42, 127.35, 127.18, 125.38, 123.08, 60.43, 35.37, 28.08, 21.61, 21.49, 14.21; IR (KBr) ν = 2979 (m), 2922 (s), 2859 (m), 1735 (s), 1633 (m), 1614 (m), 1513 (m), 1462 (m), 1442 (m), 1372 (s), 1297 (m), 1258 (m), 1179 (s), 1039 (m), 944 (w), 877 (m), 817 (m) cm^{-1}; HRMS (ESI, positive): m/z Calcd for $C_{17}H_{20}O_2Na$: 279.1356 $[M+Na]^+$; found: 279.1359.

3-(3,6-Dimethylnaphthalen-1-yl)propanoic acid (3.7)

Ethyl 3-(3,6-dimethylnaphthalen-1-yl)propanoate **3.6** (0.56 g, 2.2 mmol) was dissolved in ethanol (16 mL), and 10% aqueous sodium hydroxide (8 mL) was added. The reaction mixture was heated at 90 ºC for 16 hours. After cooled to room temperature, 6 M hydrochloric acid and ether was added. The organic layer was separated and washed with brine, dried over anhydrous sodium sulfate. After filtration, filtrate was evaporated, and the residual white solid was collected and washed with ether/hexane to give **3.7** as white solid (0.50 g, 100%). mp 167-169 ºC; R_f = 0.30 (ethyl acetate/hexane 50%); ^{1}H NMR (500 MHz, Acetone-d_6) δ 7.95 (d, *J* = 9.0 Hz, 1H), 7.58 (s, 1H), 7.45 (s, 1H), 7.32 (dd, *J* = 8.5 Hz, 1.5 Hz, 1H), 7.20 (d, *J* = 1.0 Hz, 1H), 3.34 (t, *J* = 7.5 Hz, 2H), 2.72 (t, *J* = 8.0 Hz, 2H), 2.47 (s, 3H), 2.43 (s, 3H); ^{13}C NMR (126 MHz, DMSO-d_6) δ 173.79, 136.44, 134.75, 134.59, 133.93, 127.77, 127.31, 127.08,

126.82, 124.88, 123.14, 34.69, 27.34, 21.25, 21.07; IR (KBr) ν = 3020 (m), 2919 (m), 2856 (m), 2632 (m), 2550 (m), 1710 (s), 1692 (s), 1631 (w), 1513 (w), 1437 (m), 1411 (m), 1339 (w), 1304 (m), 1267 (w), 1219 (m), 1204 (m), 952 (w), 928 (w), 903 (w), 846 (m) cm^{-1}; HRMS (ESI, positive): m/z Calcd for $C_{15}H_{16}O_2Na$: 251.1043 $[M+Na]^+$; found: 251.1046.

5,8-Dimethyl-2,3-dihydro-1*H*-phenalen-1-one (3.8)

3-(3,6-Dimethylnaphthalen-1-yl)propanoic acid **3.7** (0.50 g, 2.2 mmol) was dissolved in oxalyl chloride (20 mL) and heated at 60 ºC for 16 hours. After removal of excess oxalyl chloride under reduced pressure, the residue was dissolved in dichloromethane (30 mL) and cooled to −78 ºC under nitrogen atmosphere. To the solution was added titanium(IV) chloride (0.51 mL, 4.6 mmol). The reaction mixture was stirred at −78 ºC for 2 hours, and then warmed gradually to −30 ºC. The reaction was quenched with 1 M hydrochloric acid and extracted with dichloromethane. The organic layer was separated and washed with aqueous sodium carbonate, dried over anhydrous sodium sulfate. After filtration, the filtrate was evaporated and the residue was purified by column chromatography on silica gel (dichloromethane/hexane 60%) to give **3.8** as a colorless solid (0.26 g, 57%). mp 93-95 °C; R_f = 0.36 (dichloromethane/hexane 75%); ^{1}H NMR (500 MHz, $CDCl_3$) δ 7.96 (s, 1H), 7.77 (s, 1H), 7.48 (s, 1H), 7.23 (s, 1H), 3.38 (t, *J* = 7.0 Hz, 2H), 2.95 (t, *J* = 7.0 Hz, 2H), 2.55 (s, 3H), 2.51 (s, 3H); ^{13}C NMR (126 MHz, $CDCl_3$) δ 199.00, 136.05, 135.52, 134.00, 132.78, 132.47, 129.38, 128.30, 126.86, 125.90, 124.48, 38.60, 28.35, 21.65, 21.54; IR (KBr) ν = 3022 (w), 2962 (m), 2917 (m), 2897 (m), 2853 (w), 1678 (s), 1622 (m), 1577 (m), 1503 (m), 1424 (m), 1388 (m), 1366 (m), 1334 (m), 1283 (m), 1221 (m), 1167 (w), 1153 (w), 1130 (m), 1041 (w), 1014 (w), 877 (w), 786 (w), 739 (w) cm^{-1}; HRMS (ESI, positive): m/z Calcd for $C_{15}H_{14}ONa$: 233.0937 $[M+Na]^+$; found: 233.0940.

2,5,8-Trimethyl-2,3-dihydro-1*H*-phenalen-1-one (3.9)

To a solution of diisopropylamine (0.21 mL, 1.5 mmol) in THF (10 mL) was added 1.6 M ^{n}BuLi in hexane (0.8 mL, 1.3 mmol) at −78 ºC under nitrogen atmosphere. After 1 hour, 5,8-dimethyl-2,3-dihydro-1*H*-phenalen-1-one **3.8** (0.26 g, 1.3 mmol) in THF (15 mL) and hexamethylphosphoramide (0.66 mL, 3.8 mmol) were added, and the reaction mixture was stirred for 1 hour. After addition of methyl iodide (0.78 mL, 13 mmol), the solution was warmed gradually to room temperature and stirred for 13 hours. The reaction was quenched with 1 M hydrochloric acid, and the mixture was extracted with dichloromethane. The organic layer was separated and washed with brine, dried over anhydrous sodium sulfate. After filtration, the filtrate was evaporated and the residue was purified by column chromatography on silica gel (dichloromethane/hexane 60%) to give **3.9** as a white solid (0.21 g, 75%). R_f = 0.42 (dichloromethane/hexane 75%); ^{1}H NMR (500 MHz, $CDCl_3$) δ 7.93 (d, *J* = 1.5 Hz, 1H), 7.75 (s, 1H), 7.47 (s, 1H), 7,21 (s, 1H), 3.38 (dd, *J* = 15.5 Hz, 6.0 Hz, 1H), 3.12 (dd, *J* = 15.0 Hz, 11.0 Hz, 1H), 3.04-2.97 (m, 1H), 2.54 (s, 3H), 2.51 (s, 3H), 1.33 (d, *J* = 6.5 Hz, 3H).

2,5,8-Trimethyl-1*H*-phenalene (3.11)

To a solution of 2,5,8-Trimethyl-2,3-dihydro-1*H*-phenalen-1-one **3.9** (0.21 g, 0.94 mmol) in THF (10 mL) was added lithium aluminum hydride (43 mg, 1.1 mmol) under nitrogen atmosphere. After 1 hour stirring, the reaction was quenched with ethyl acetate, and aqueous ammonium chloride and dichloromethane were added. The organic

layer was separated and washed with brine and dried over anhydrous sodium sulfate. After filtration, the filtrate was evaporated and the residue was purified by column chromatography on hydrous (6%) silica gel (dichloromethane/hexane 80%) to give 2,5,8-trimethyl-2,3-dihydro-1*H*-phenalen-1-ol **3.10** as a diastereomer mixture (0.19 g, 92%).

The diastereomer mixture (32 mg, 0.14 mmol) was dissolved in toluene (7 mL) under nitrogen atmosphere. To the solution was added a catalytic amount of *p*-toluenesulfonic acid monohydrate, and the solution was heated at 120 ºC for 5 min. The reaction mixture was cooled at 0 ºC and then the solution diluted with hexane (21 mL) was filtered rapidly on hydrous (6%) silica gel to give **3.11** as a colorless powder (29 mg, 99%). R_f = 0.65 (dichloromethane/hexane 25%); ^{1}H NMR (500 MHz, $CDCl_3$) δ 7.23 (s, 1H), 7.16 (s, 1H), 7.02 (d, J = 1.5 Hz, 1H), 6.70 (s, 1H), 6.30 (q, J = 1.5 Hz, 1H), 3.87 (s, 2H), 2.41 (s, 3H), 2.38 (s, 3H), 1.91 (d, J = 1.0 Hz, 3H); ^{13}C NMR (126 MHz, $CDCl_3$) δ 136.48, 135.92, 135.58, 134.36, 133.93, 132.94, 125.66, 124.97, 124.05, 123.59, 123.11, 122.65, 36.60, 23.19, 21.65 (2C).

2,5,8-Trimethylphenalenyl (3.1)

2,5,8-Trimethyl-1*H*-phenalene **3.11** (29 mg, 0.14 mmol) and *p*-chloranil (17 mg, 0.070 mmol) were dissolved in degassed dichloromethane (2 mL) and hexane (12 mL), and stirred for 3 hours. White precipitate generated was filtered out in degassed sealed tube. Slow evaporation at room temperature gave colorless crystals of **3.1**$_2$ σ-dimer *RR*/*SS* form (13 mg, 45%).

A glass tube was charged with powdered sample of **3.1**$_2$ σ-dimer *RR*/*SS* form and sealed under reduced pressure (about 10^{-3} Pa). The glass tube was heated by a heat gun until the sample had been melted. Gradual cooling gave violet crystals of **3.1**$_2$ π-dimer, together with the colorless crystals of **3.1**$_2$ σ-dimer *RR*/*SS* form.

3.8 References

(1) Mou, Z.; Uchida, K.; Kubo, T.; Kertesz, M. *J. Am. Chem. Soc.* **2014**, *136* (52), 18009.

(2) Uchida, K.; Hirao, Y.; Kurata, H.; Kubo, T.; Hatano, S.; Inoue, K. *Chem. - An Asian J.* **2014**, *9* (7), 1823.

(3) Wolinska-Mocydlarz, J.; Canonne, P.; Leitch, L. C. *Synthesis* **1974**, *1974* (8), 566.

(4) Goto, K.; Kubo, T.; Yamamoto, K.; Nakasuji, K.; Sato, K.; Shiomi, D.; Takui, T.; Kubota, M.; Kobayashi, T.; Yakusi, K.; Ouyang, J. *J. Am. Chem. Soc.* **1999**, *121* (7), 1619.

(5) Bennett, J. E. *Nature* **1960**, *188* (4749), 485.

(6) Gerson, F. *Helv. Chim. Acta* **1966**, *49* (5), 1463.

(7) Small, D.; Rosokha, S. V; Kochi, J. K.; Head-Gordon, M. *J. Phys. Chem. A* **2005**, *109* (49), 11261.

(8) Zaitsev, V.; Rosokha, S. V; Head-Gordon, M.; Kochi, J. K. *J. Org. Chem.* **2006**, *71* (2), 520.

(9) Lü, J.-M.; Rosokha, S. V; Kochi, J. K. *J. Am. Chem. Soc.* **2003**, *125* (40), 12161.

(10) Rosokha, S. V.; Kochi, J. K. *J. Am. Chem. Soc.* **2007**, *129* (4), 828.

(11) Suzuki, S.; Morita, Y.; Fukui, K.; Sato, K.; Shiomi, D.; Takui, T.; Nakasuji, K. *J. Am. Chem. Soc.* **2006**, *128* (8), 2530.

(12) Small, D.; Zaitsev, V.; Jung, Y.; Rosokha, S. V.; Head-Gordon, M.; Kochi, J. K. *J. Am. Chem. Soc.* **2004**, *126* (42), 13850.

(13) Takano, Y.; Taniguchi, T.; Isobe, H.; Kubo, T.; Morita, Y.; Yamamoto, K.; Nakasuji, K.; Takui, T.; Yamaguchi, K. *J. Am. Chem. Soc.* **2002**, *124* (37), 11122.

(14) Perrin, C. L.; Dwyer, T. J. *Chem. Rev.* **1990**, *90* (6), 935.

(15) Tok, O. L.; Gridnev, I. D.; Korobach, E. M.; Bubnov, Y. N. *Chem. Commun.* **2000**, No. 4, 311.

-Chapter 4-
Biphenalenylidene:
Direct Observation of Reactive Intermediates on the Decomposition Pathway of Phenalenyl

4.1 Introduction

Numerous experimental attempts to prepare parent phenalenyl **1.3** were reported in 1950s.[1–3] Successful generation of **1.3** was confirmed, whereas the product contained hydrocarbon impurities, such as peropyrene **4.3**, which were generated by the dehydrogenation of $\mathbf{1.3}_2$ σ-dimer. In 2003, Agranat *et al.* predicted that *E*- and *Z*-biphenalenylidene (*E*, *Z*-**4.1**) and dihydroperopyrene **4.2** should exist as the reactive intermediates, and the mechanism was supported by theoretical calculations.[4] In contrast, an experimental attempt to detect the intermediates directly was unsuccessful.[4] Desulfurization followed by dimerization of phenalenethione derived from phenalenone afforded a green product which showed an absorption band at 647 nm. Unfortunately, the rapid decomposition into **4.3** prevented the detailed characterization and isolation of the colored species. In order to detect and characterize the intermediates, a moderate synthetic approach is required.

This chapter describes the first isolation of *E*, *Z*-**4.1** in solution state, which was reported in previous literature.[5] *E*, *Z*-**4.1** were prepared from **4.2** by means of photoinduced electrocyclic ring-opening reaction, and the structural characterizations were performed by spectroscopic analyses. Kinetic studies performed with transition absorption measurements and VT electronic absorption measurements gave significant insights into the unusual reactivities of *E*, *Z*-**4.1**; that is *E*, *Z*-**4.1** demonstrated a rapid *E*-*Z* isomerization and a facile conrotatory ring-closure, which involve in the decomposition mechanism of **1.3**. The unique reactivities can be rationalized by the singlet biradical ground states of *E*, *Z*-**4.1**, and the experimental findings were fully supported by the detailed investigations with theoretical calculations.

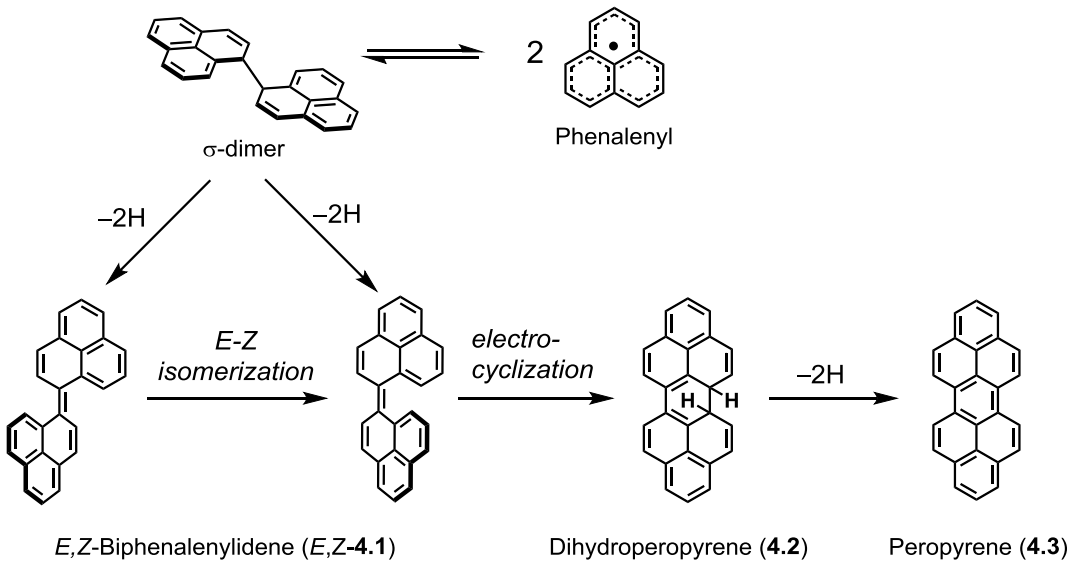

Scheme 4.1.1. The proposed mechanism of the decomposition pathway of parent phenalenyl.[4] Reprinted with permission from ref. 5. Copyright 2016, American Chemical Society.

4.2 Elucidation of the ground state of biphenalenylidenes

In order to estimate the electronic structures of *E, Z*-**4.1**, theoretical calculations were conducted. The singlet biradical ground states of *E, Z*-**4.1** were suggested by Agranat *et al.*[4]; thus, the structural optimization was performed with a broken-symmetry (BS) UB3LYP/6-31G** method. The optimized structures of *E, Z*-**4.1** were shown in Figure 4.2.1. *E, Z*-**4.1** represented twisted geometries due to the steric repulsion between the protons on phenalenyl sites, resulting in the decrease of covalent bonding interaction between two phenalenyl sites and the enhancement of the biradical character.[4] The twisted angles of *E*- and *Z*-**4.1** calculated are 45° and 58°, respectively, which suggests that *Z*-**4.1** with larger twisted angle is less stable in energy than *E*-**4.1**. The total and relative energies of *E, Z*-**4.1** estimated with a UB3LYP(BS)/6-31G** calculation were summarized in Table 4.2.1. As expected, *E*-**4.1** is 1.4 kcal mol^{-1} more stable than *Z*-**4.1** after the zero point energy correction. Moreover, triplet states of *E, Z*-**4.1** were higher in energy than each singlet states, suggesting *E, Z*-**4.1** have the singlet ground states.

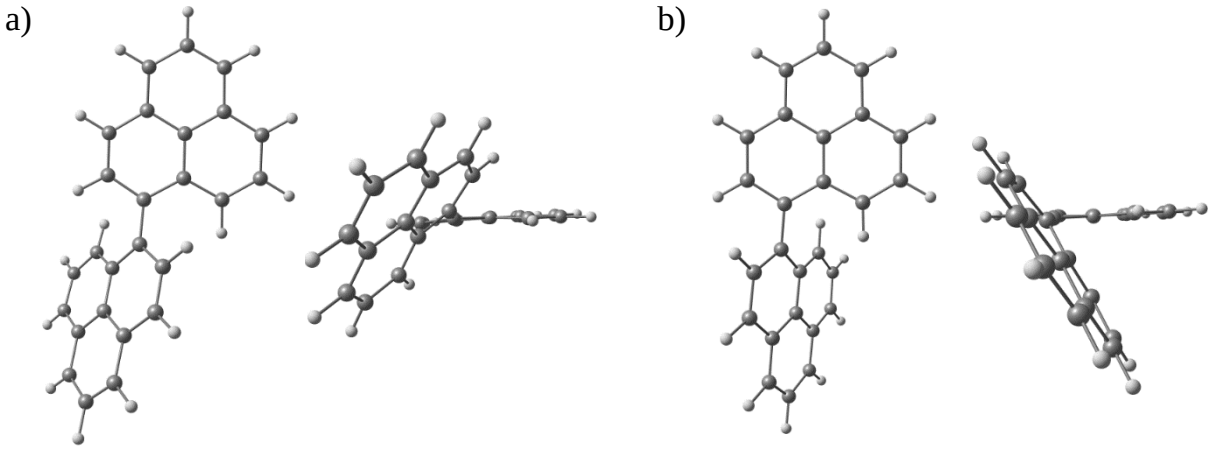

Figure 4.2.1. Optimized geometries of a) *E*-**4.1** and b) *Z*-**4.1** calculated with a UB3LYP(BS)/6-31G** method.

Table 4.2.1. Hartree-Fock energies (hartree), spin-squared expectation values $<S^2>$, and relative energies (K) of *E,Z*-**4.1** calculated by a UB3LYP(BS)/6-31G** method.

.

	Singlet/UB3LYP(BS)/6-31G**		Triplet/UB3LYP(BS)/6-31G**	
	Energy	$<S^2>$	Energy	$<S^2>$
E-**4.1**	−1000.4540156	0.639	−1000.4432821	2.083
Relative Energy / K	0	–	4888	–
Z-**4.1**	−1000.4510391	0.983	−1000.4475451	2.089
Relative Energy / K	0	–	2084	–

Spin density distribution maps calculated with a UB3LYP(BS)/6-31G** method were described in Figure 4.2.2. Large spin densities are localized on α carbon atoms of two phenalenyl sites with antiparallel spins. The singlet biradical characters y_0 of *E*, *Z*-**4.1** were estimated with CASSCF(2,2)/6-31G**//UB3LYP/6-31G** and UB3LYP(BS)/6-31G** methods. A CASSCF(2,2)/6-31G**//UB3LYP/6-31G** calculation gave an admixture of 14% of the doubly excited configuration into the ground state of *E*-**4.1**; thus, the biradical character of *E*-**4.1** was estimated to be 28%. A broken-symmetry UB3LYP/6-31G** calculation gave a similar value; the natural orbital occupancy number (NOON) of LUMO of *E*-**4.1** is 0.36, indicating the biradical character is 36%. The biradical character of *Z*-**4.1** was also determined with the same calculation methods to be 67% and 94%, respectively, which suggests that the biradical character of *Z*-**4.1** having a larger twisted angle is considerably larger than that of *E*-**4.1**.

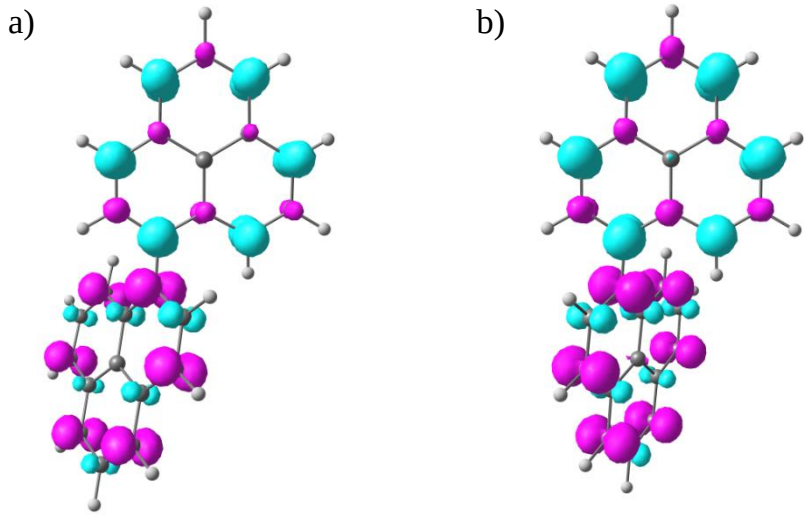

Figure 4.2.2. Spin density distribution maps of a) *E*-**4.1**, and b) *Z*-**4.1** calculated at UB3LYP(BS)/6-31G** level.

4.3 Synthesis and characterization of dihydroperopyrene

The key precursor, dihydroperopyrene **4.2**, was obtained according to the synthetic scheme displayed in Scheme 4.3.1. Dibromobinaphthyl **4.5** prepared from binaphthyl **4.4** was converted into the unsaturated ester **4.6** by the Heck reaction. Reduction of C–C double bonds under hydrogen atmosphere and subsequent hydrolysis in basic condition gave the carboxylic acid **4.8** then Friedel-Crafts cyclization of the acyl chloride derived from **4.8** afforded biphenalanone **4.9** in high yield. Reduction followed by dehydration gave biphenalene **4.11**. Treatment of **4.11** with an equimolar *p*-chloranil under nitrogen atmosphere gave a deep blue solution in the early stage of the reaction, and stirring in the dark resulted in a gradual color change from deep blue to greenish yellow.

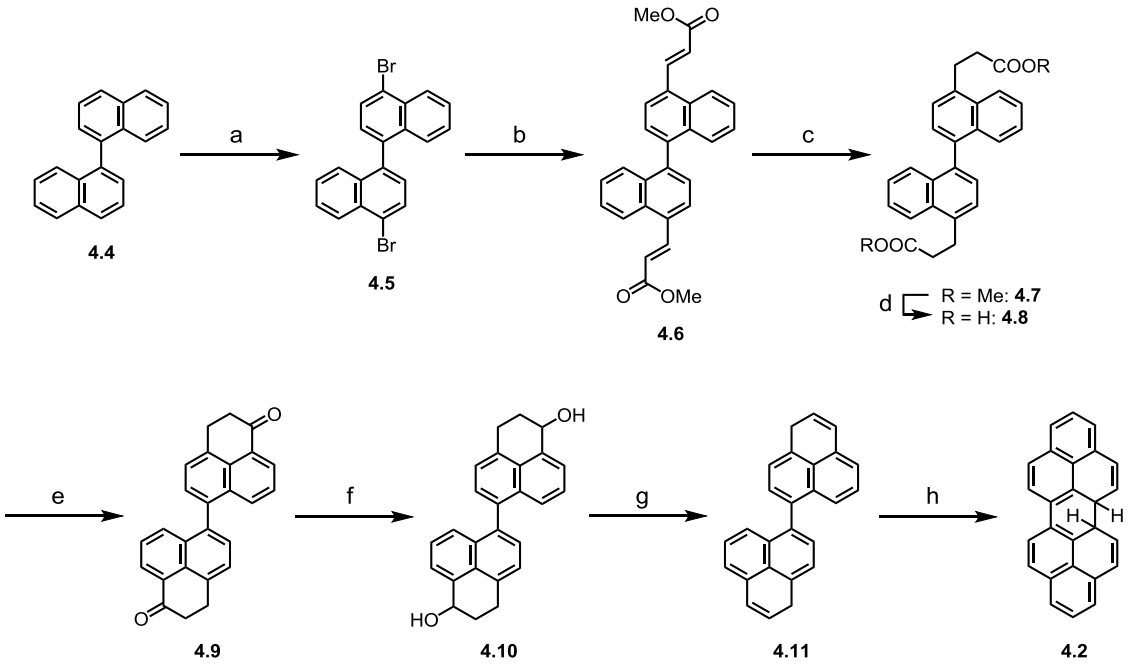

Scheme 4.3.1. Synthetic procedure for dihydroperopyrene (**4.2**). Reagent and condition: a) bromine, $CHCl_3$, 0 °C, 64% yield; b) methyl acrylate, $Pd(OAc)_2$, PPh_3, K_2CO_3, $^nBu_4NBr$, DMF, 80 °C, 93% yield; c) H_2 (1 atm), 10% Pd-C, DCM/AcOEt (1/9), RT, 88% yield; d) 10% NaOHaq., EtOH, 90 °C, 94 yield; e) (i) $(COCl)_2$, 60 °C, (ii) $AlCl_3$, DCM, −78 to −30 °C, 88% yield; f) $NaBH_4$, DCM/EtOH (1/1), RT; (g) *p*-$TsOH{\cdot}H_2O$, toluene, 120 °C, 92% yield (2 steps); h) *p*-chloranil, toluene, RT, 24% yield. *p*-chloranil = 2,3,5,6-tetrachloro-1,4-benzoquinone.

The product obtained after the purification by silica gel column chromatography represented a well-resolved ^{1}H NMR spectrum as depicted in Figure 4.3.1. A characteristic singlet peak observed at 4.4 ppm was assignable to a benzyl proton on the phenalene scaffold, and the product was unambiguously characterized to **4.2** on the basis of 2D-NMR techniques as well as computational calculations.

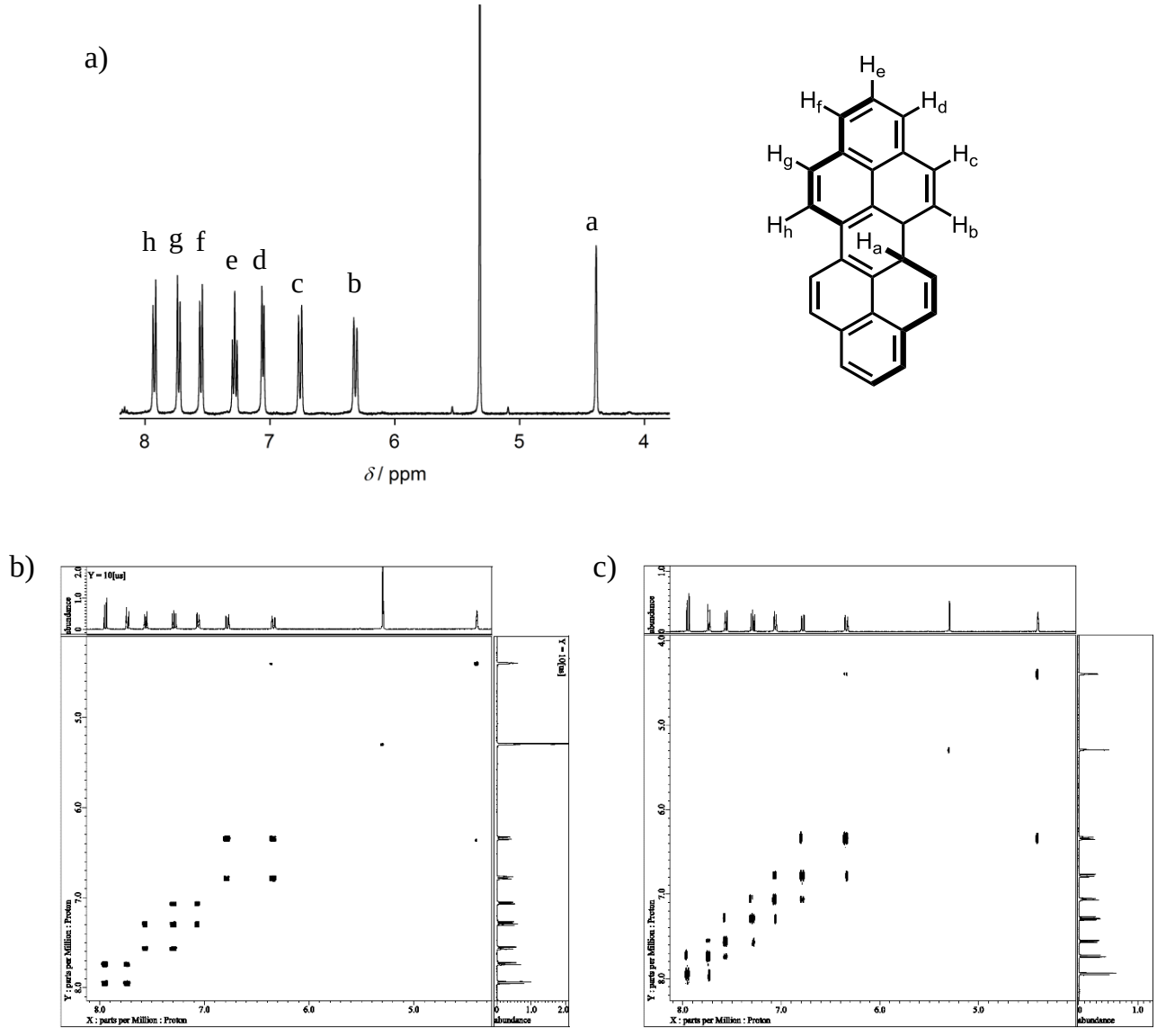

Figure 4.3.1. a) ^{1}H NMR spectrum of **4.2** measured in dichloromethane-d_2. b) ^{1}H–^{1}H COSY and c) NOESY of **4.2** measured in dichloromethane-d_2. Reprinted with permission from ref. 5. Copyright 2016, American Chemical Society.

Table 4.3.1. Chemical shifts of the protons of *anti*-**4.2** predicted with a GIAO-B3LYP/6-31G** method, together with the experimental values.

	H_a	H_b	H_c	H_d	H_e	H_f	H_g	H_h
Experimental	4.42	6.37	6.81	7.09	7.32	7.59	7.76	7.97
Theoretical	4.82	6.34	6.65	6.97	7.39	7.51	7.74	8.01

4.4 Molecular geometry of dihydroperopyrene

4.4.1. Optimized geometry of dihydroperopyrene

Dihydroperopyrene **4.2** has two stereoisomers, a diastereomer pair of **4.2** *RR*/*SS* form (*anti*-**4.2**) and **4.1** *RS* form (*syn*-**4.2**), originating from two asymmetric carbon atoms at the central six-membered ring. The optimized geometries of *anti*- and *syn*-**4.2** estimated with a UB3LYP(BS)/6-31G** method were displayed in Figure 4.4.1. *Anti*-**4.2** adopted almost planar structure with C_2 symmetry, and the twisted angle between two phenalenyl planes was estimated to be 21°. In contrast, *syn*-**4.2** demonstrated a highly distorted conformation with C_1 symmetry. The energy difference between *anti*- and *syn*-**4.2** can be determined at UB3LYP(BS)/6-31G** level to be 11.7 kcal mol^{-1} after the zero point energy (ZPE) correction, which is almost identical to the reported value.[4] Thus, *anti*-**4.2** is energetically more favorable than *syn*-**4.2**, and **4.2** obtained experimentally would adopt an *anti*-configuration.

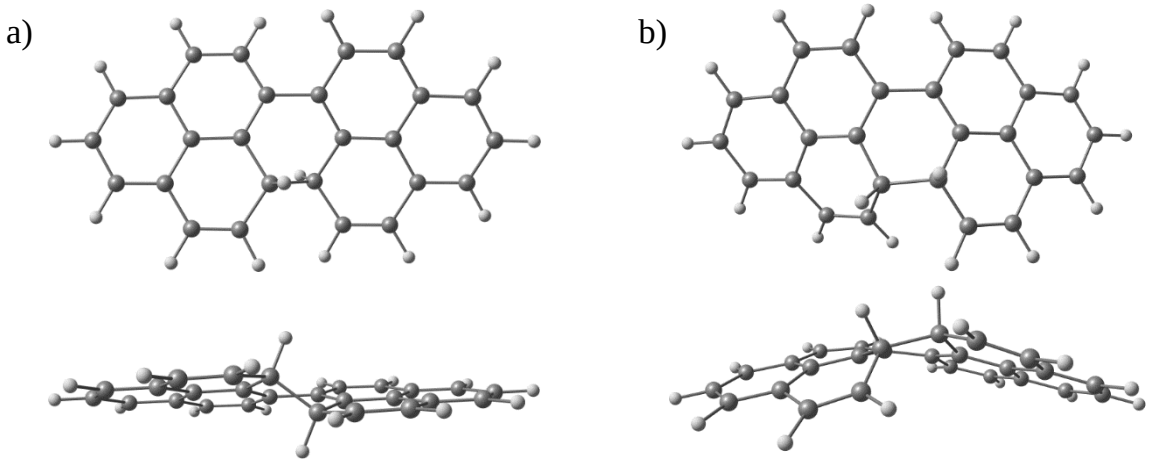

Figure 4.4.1. Optimized geometries of a) *anti*-**4.2** and b) *syn*-**4.2** determined by a UB3LYP(BS)/6-31G** method. Reprinted with permission from ref. 5. Copyright 2016, American Chemical Society.

4.4.2 Variable temperature ^{1}H NMR spectroscopy of dihydroperopyrene

In order to assign the configuration of dihydroperopyrene **4.2**, ^{1}H NMR spectrum of **4.2** was focused again. As observed in a spectrum shown in Figure 4.3.1a, **4.2** obtained experimentally showed a simple spectrum arising from a single diastereomer having magnetically-equivalent two phenalenyl moieties. The simplicity of ^{1}H NMR spectrum evokes two possibilities: 1) **4.2** obtained adopts the *anti*-configuration with C_2 symmetry, 2) **4.2** adopting the *syn*-configuration gives an averaged spectrum due to the dynamic equilibrium between stable conformations with C_1 symmetry. To exclude the possibility of the dynamic equilibrium, variable temperature (VT) ^{1}H NMR was conducted within the temperature range from 298 K to 183 K. **4.2** demonstrated no signal splitting even at 183 K, inferring that **4.2** adopts the *anti*-configuration having C_2 symmetry. The result is consistent with the computational prediction that **4.2** adopts the energetically favorable *anti*-configuration. However, it should be noted that the possibility of the

dynamic equilibrium was not strictly ruled out. The activation barrier for the conformational change of *syn*-**4.2**, which was estimated with a UB3LYP(BS)/6-31G** method, was extremely small (2.3 kcal mol^{-1}), thus, an averaged spectrum might be observed even at 183 K.

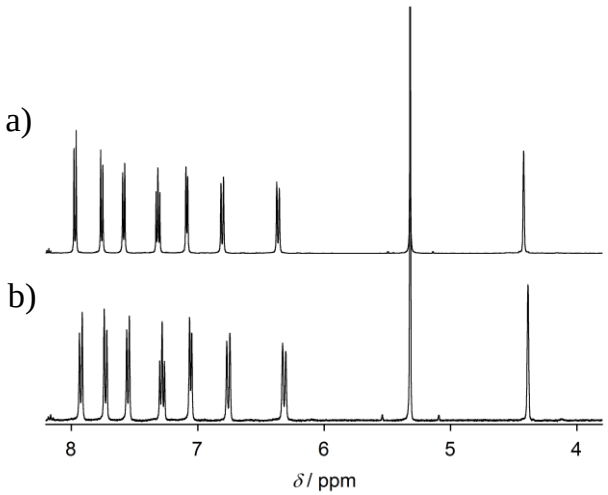

Figure 4.4.2. VT ^{1}H NMR of **4.2** measured in dichloromethane-d_2 at a) 298 K and b) 183 K.

4.4.3 X-ray crystallographic analysis

Recrystallization of dihydroperopyrene **4.2** from chloroform/hexane mixed solvents under argon flow gave a pale yellow platelet crystals suitable for X-ray crystallographic analysis. Molecular geometry of **4.2** was displayed in Figure 4.4.3. The geometry obtained remains a structural ambiguity around the sp^3 carbon atoms due to the disordered alignment of **4.2** *RR* and *SS* isomers in crystalline state, whereas the planar molecular back bone indicates strongly that **4.2** obtained adopts the *anti*-configuration as expected by computational studies and VT ^{1}H NMR spectroscopy.

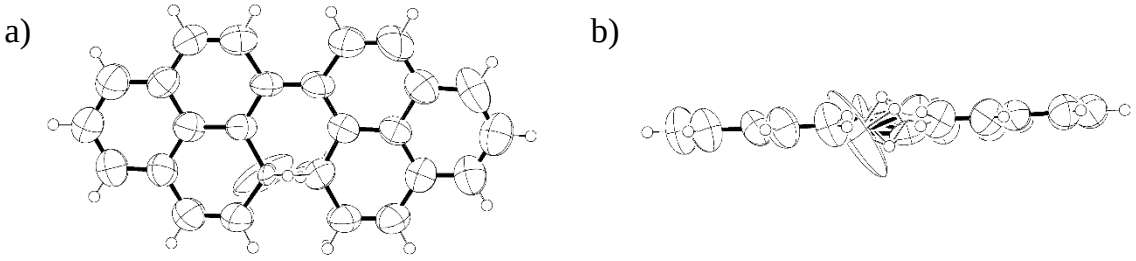

Figure 4.4.3. Ortep drawing of **4.2** at the 50% probability level. a) Top view and b) side view.
Crystal System = monoclinic, a = 11.958(2) Å, b = 9.5891(16) Å, c = 14.538(3) Å, β = 92.944(5)°, V = 1664.8(5) $Å^3$, Space Group = $P2_1$ (#4), Z = 4, μ(MoKα) = 0.74 cm^{-1}, T = 200 K, $R1$ [$F^2>2\sigma(F^2)$] = 0.0535, $wR2$(all data) = 0.2083, S = 0.887, Refl./param. = 6715/513.

4.5 Direct observation of biphenalenylidenes

4.5.1 Characterization of *E*-biphenalenylidene by ^{1}H NMR spectroscopy

With focused on the electronic structure of *anti*-dihydroperopyrene (*anti*-**4.2**), the central six-membered ring can be regarded as 1,3-cyclohexadiene, which is a well-known scaffold that demonstrates the electrocyclic ring-opening reaction to afford *cis*-1,3,5-hexatriene structure. As predicted by the Woodward-Hoffmann rule based on the orbital symmetry consideration, 1,3-cyclohexadiene scaffold undergoes a photochemically allowed ring-opening reaction in conrotatory mode; thus, *anti*-**4.2** would be converted into *Z*-biphenalenylidene (*Z*-**4.1**) by photochemical reaction.

Irradiation of UV light (365 nm) to *anti*-**4.2** in degassed dichloromethane-d_2 at 195 K resulted in the unambiguous change in ^{1}H NMR spectrum, accompanied by a noticeable color change from yellow to deep blue. ^{1}H NMR spectrum recorded after irradiation was shown in Figure 4.5.1, together with the spectrum of *anti*-**4.2** measured before irradiation. Upon irradiation for 30 seconds, *anti*-**4.2** disappeared completely and a new species was generated. The species was fully identified to biphenalenylidene **4.1** by 2D-NMR spectroscopies (Figure 4.5.2a) as well as the computational prediction of the chemical shifts at GIAO-UB3LYP(BS)/6-31G** level. In order to determine the stereochemistry of **4.1** observed in ^{1}H NMR spectrum, a ROESY measurement was conducted at 223 K. **4.1** showed cross peaks between H_a and H_h in opposite sign with respect to diagonal peaks, which indicates that H_a and H_h are in close proximity to each other. Hence, **4.1** observed in ^{1}H NMR adopts *E*-configuration. The product of the electrocyclic ring-opening reaction is expected to be *Z*-**4.1**, therefore, a rapid thermal isomerization from *Z*-**4.1** to *E*-**4.1** would take place (see chapter 4.5.2).

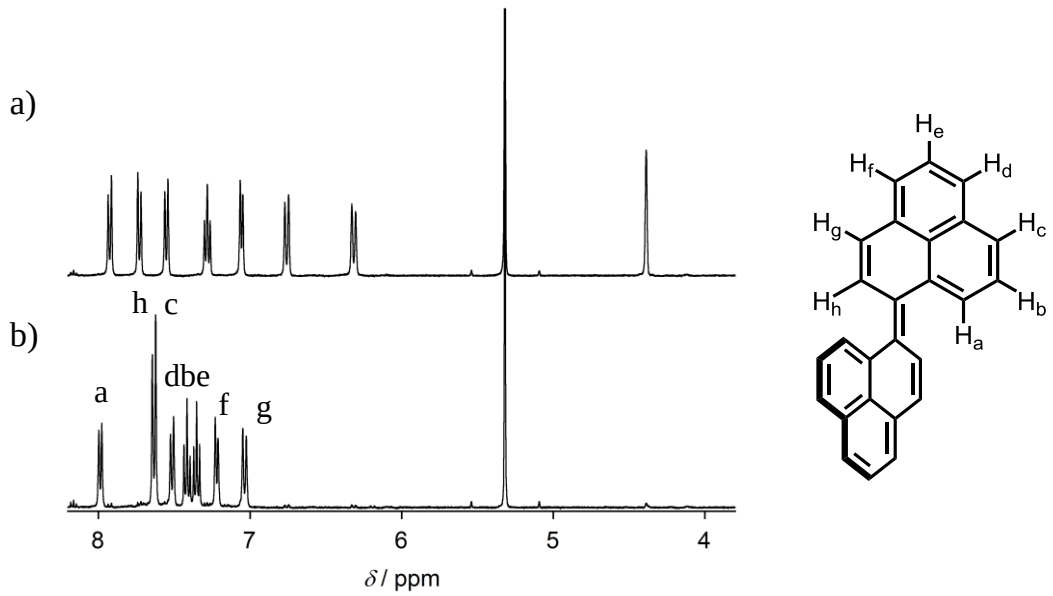

Figure 4.5.1. ^{1}H NMR spectra recorded in degassed dichloromethane-d_2 at 183 K, a) before irradiation and b) after irradiation of UV light (365 nm) for 30 sec. Reprinted with permission from ref. 5. Copyright 2016, American Chemical Society.

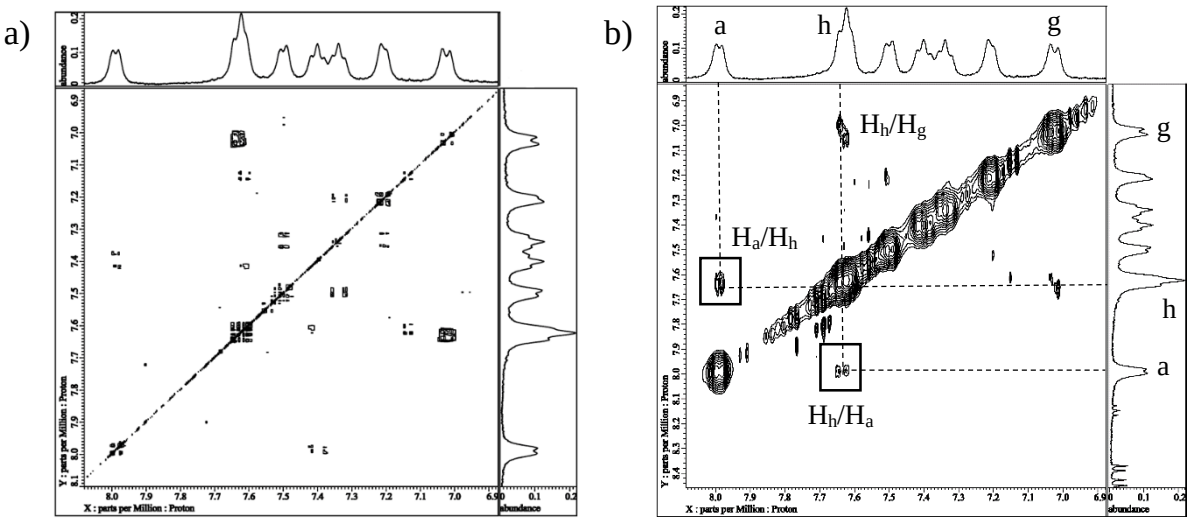

Figure 4.5.2. a) ^{1}H–^{1}H COSY and b) ROESY of **4.1** measured in dichloromethane-d_2 at 223 K.

Table 4.5.1. Chemical shifts of the protons of *E*-**4.1** expected by computational studies at GIAO-UB3LYP(BS)/6-31G** level, together with the experimental values determined at 183 K.

	H_a	H_b	H_c	H_d	H_e	H_f	H_g	H_h
Experimental	7.99	7.42	7.63	7.51	7.35	7.22	7.04	7.63
Theoretical	8.02	7.50	7.49	7.41	7.48	7.23	7.12	7.59

Variable temperature (VT) ^{1}H NMR gave a significant insight into the biradical character of *E*-biphenalenylidene (*E*-**4.1**). A progressive signal broadening was observed in ^{1}H NMR spectrum of *E*-**4.1** upon increasing the temperature, and the signals almost disappeared at 253 K. The characteristic behavior is undoubtedly due to the singlet biradical ground state of *E*-**4.1**. Singlet biradical compounds having small energy gaps (ΔE_{S-T}) between the singlet ground state and the excited triplet state shows the signal broadening in NMR spectroscopy due to the effect of thermally accessible triplet species.[6–9] Actually, the small ΔE_{S-T} value of 4888 K (9.7 kcal mol^{-1}) was expected by computational calculations, thus, the signal broadening can be ascribed to the singlet biradical character of *E*-**4.1**.

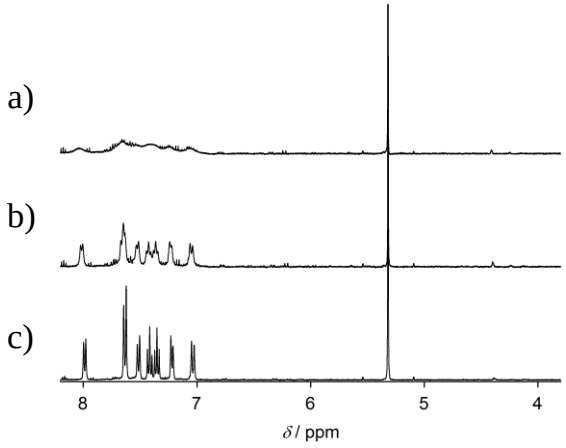

Figure 4.5.3. VT ^{1}H NMR spectra of *E*-**4.1** measured in dichloromethane-d_2 at a) 253 K, b) 223 K, and c) 183 K.

4.5.2 Electronic absorption spectrum of biphenalenylidene and dihydroperopyrene

The electrocyclic ring-opening reaction of *anti*-dihydroperopyrene (*anti*-**4.2**) was also monitored by the electronic absorption spectrum. *Anti*-**4.2** showed no characteristic absorption band in visible region, whereas, *E*-biphenalenylidene (*E*-**4.1**) generated by UV irradiation showed an intense absorption band centered at 619 nm. This result is fully consistent with the computational prediction by TDDFT calculation that the HOMO–LUMO transition of *E*-**4.1** is located at 720 nm (f = 0.384). In contrast, *Z*-**4.1** is expected to show its HOMO–LUMO transition at 859 nm (f = 0.106), however, the absorption band corresponded to *Z*-**4.1** was not observed experimentally by the steady-state electronic absorption spectrum because of the rapid thermal isomerization to *E*-**4.1**.

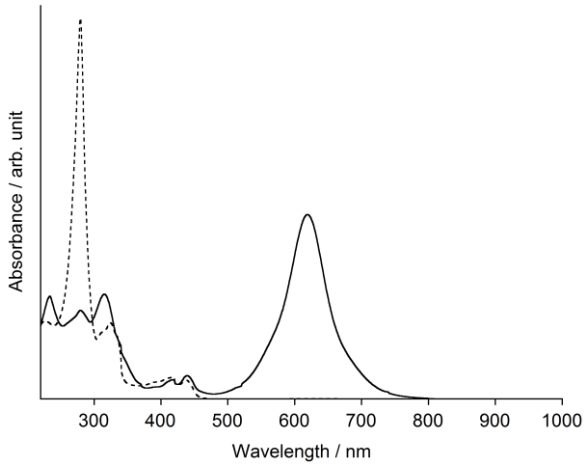

Figure 4.5.4. Electronic absorption spectra of *E*-**4.1** (solid) and *anti*-**4.2** (dashed) measured in dichloromethane (1×10^{-5} M). *E*-**4.1** was generated by UV irradiation (365 nm) for 30 sec. at 195 K.

Suppressing the rotation about the central double bond enabled to observe *Z*-**4.1** directly by spectroscopic analyses. The electronic absorption spectrum was monitored in a glassy 2-methyltetrahydrofuran (MTHF) matrix at 98 K. Irradiation of UV light (355 nm) to *anti*-**4.2** in a rigid matrix of MTHF resulted in the appearance of a broad absorption band centered at 700 nm (Figure 4.5.5a), which is ascribed to the HOMO–LUMO transition of *Z*-**4.1** as predicted by a TDDFT calculation at UB3LYP(BS)/6-31G** level. The absorption band remained unchanged in a MTHF matrix for long time, indicating *Z*-**4.1** is persistent in a condition that the rotation about the central double bond is suppressed kinetically. A substantial change was observed in the electronic absorption spectrum with raising temperature from 98 K to 120 K (Figure 4.5.5b), where a viscosity of MTHF matrix dramatically changes from 10^7 to 10^3 P.[10] The differential spectra were dominated by the bleaching of an absorption band at 700 nm and by growing with maximum at 630 nm, suggesting the relaxation of MTHF matrix leads to the thermal isomerization of *Z*-**4.1** to *E*-**4.1** through the rotation about the central double bond.

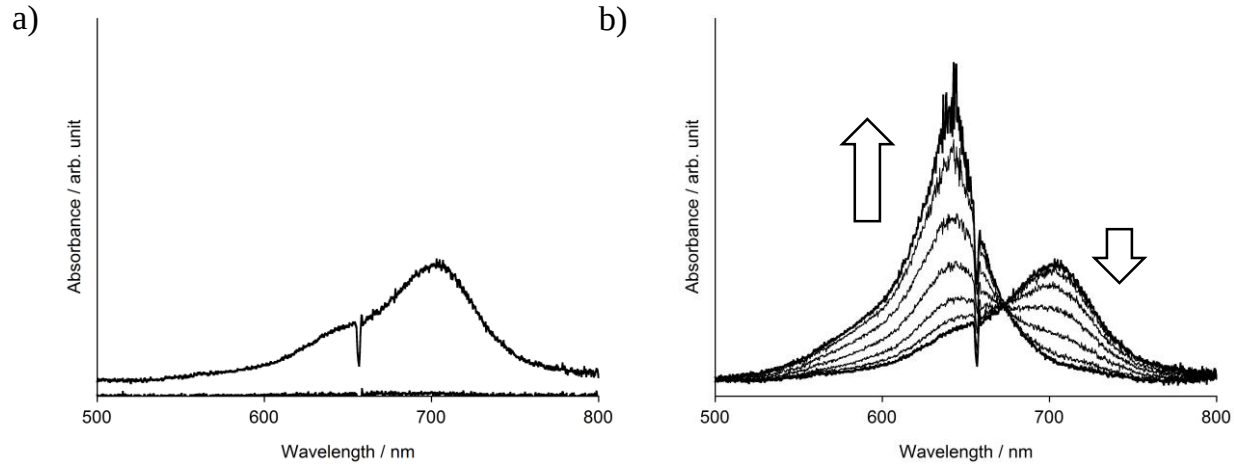

Figure 4.5.5. a) Differential electronic absorption spectra of *Z*-**4.1** generated by UV irradiation (355 nm) in MTHF matrix (1×10^{-4} M) at 98 K. b) Differential absorption spectra measured periodically at 120 K. Reprinted with permission from ref. 5. Copyright 2016, American Chemical Society.

The kinetics of the rapid thermal isomerization was investigated by the transient absorption spectrum measured in dichloromethane within the temperature range from 183 K to 203 K. The absorption band corresponding to *Z*-**4.1** decayed with a clean first-order kinetics, and the absorption of *E*-**4.1** grew with the same rate constant as the decay rate constant of *Z*-**4.1**, which indicates *Z*-**4.1** is quantitatively converted into *E*-**4.1** through thermal isomerization. From the temperature dependence of a decay rate constant, the activation barrier of the thermal isomerization from *Z*-**4.1** to *E*-**4.1** can be estimated by using Arrhenius equation to be 4.3 ± 0.3 kcal mol^{-1} (log *A* = 12).

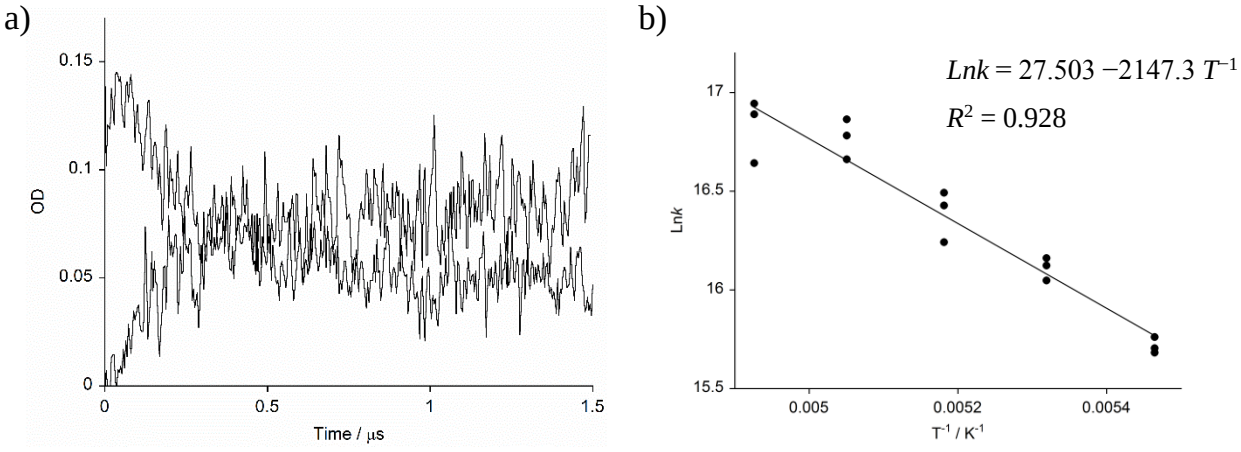

Figure 4.5.6. a) Transient absorption spectra measured in MTHF (1×10^{-4} M) at 175 K. The decay rate of *Z*-**4.1** and the glow rate constant of *E*-**4.1** were monitored at 705 nm and 630 nm, respectively. b) Arrhenius plot to determine the activation barrier of thermal isomerization from *Z*-**4.1** to *E*-**4.1**. Reprinted with permission from ref. 5. Copyright 2016, American Chemical Society.

The activation barrier is extraordinarily lower than that of *E*-*Z* isomerization for general alkenes. The isomerization of alkene is considered to proceed through a biradical transition structure as illustrated in Scheme 4.5.1. In the case of **4.1**, the biradical transition state can be stabilized thermodynamically by the delocalization of unpaired electrons over phenalenyl sites. Moreover, the destabilized ground states of singlet biradical *E*, *Z*-**4.1** also enhance the facility of the isomerization. Small HOMO–LUMO gaps of the singlet biradical species lead to an admixture of the doubly excited configuration into the ground state description, resulting in the decrease of covalent bonding interactions and destabilization of the ground state. Actually, the contribution of the doubly excited configuration to the ground state of *E*,*Z*-**4.1** was corroborated by CASSCF(2,2)/6-31G**//UB3LYP(BS)/6-31G** calculations (see chapter 4.2). Thus, the combination of destabilized ground states and stabilized transition state leads to the facile isomerization.

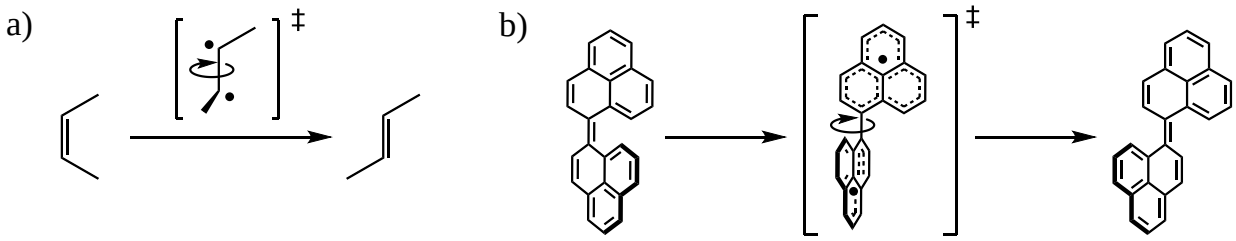

Scheme 4.5.1. Thermal isomerization of a) alkenes and b) **4.1** through biradical transition structures. Reprinted with permission from ref. 5. Copyright 2016, American Chemical Society.

4.6 Electrocyclic ring-closure reaction of biphenalenylidene

According to the Woodward-Hoffmann rule, the interconversion between *anti*-dihydroperopyrene (*anti*-**4.2**) and *Z*-biphenalenylidene (*Z*-**4.1**) can take place through photochemically allowed conrotatory mode. Indeed, *anti*-**4.2** was converted into *Z*-**4.1** by photoinduced electrocyclic ring-opening reaction. Notably, the ring-opening reaction did not proceed thermally by heating up to 393 K in degassed toluene. On the other hand, despite the reconversion of *Z*-**4.1** to *anti*-**4.2** is also expected as a photochemically allowed process, irradiation (700 nm) of *Z*-**4.1** in a MTHF matrix resulted in no perceptible change in the electronic absorption spectrum. In contrast, **4.1** demonstrated the thermal ring-closure reaction in conrotatory mode, which is not conforming to the Woodward-Hoffmann rule, being investigated by spectroscopic analyses.

4.6.1 Observation of the electrocyclic ring-closure reaction by ^{1}H NMR spectroscopy

Thermal ring-closure reaction of biphenalenylidene *E*-**4.1** was monitored by ^{1}H NMR spectroscopy. The signals of *E*-**4.1** generated in degassed dichloromethane-d_2 almost disappeared after storing in the dark for one hour, and the peaks of *anti*-dihydroperopyrene (*anti*-**4.2**) was observed again (Figure 4.6.1). This result suggests that *E*-**4.1** underwent thermal ring-closure in conrotatory fashion even at 298 K. It should be noted that *syn*-**4.2**, which is a product of the kinetically favorable disrotatory process, was not found in the ^{1}H NMR spectrum.

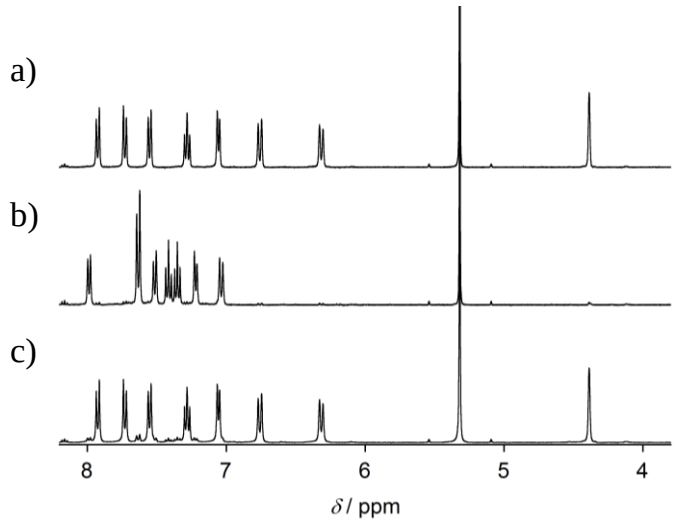

Figure 4.6.1. ^{1}H NMR spectra measured in dichloromethane-d_2 at 183 K a) before irradiation, b) just after irradiation of UV light (365 nm), c) after kept in the dark for 1 hour. Reprinted with permission from ref. 5. Copyright 2016, American Chemical Society.

4.6.2 Kinetics of the electrocyclic ring-closure reaction

Thermal ring-closure reaction was observed by the electronic absorption spectrum. The absorption band of *E*-biphenalenylidene (*E*-**4.1**) at 619 nm decayed with a clean first-order kinetics, and an intense absorption band attributed to *anti*-dihydroperopyrene (*anti*-**4.2**) at shorter wavelength region was recovered. *E*-**4.1** is expected to undergo the ring-closure reaction through a stepwise pathway via *Z*-**4.1** as an intermediate. The experimental and computational results suggest that the activation energy of *E*-*Z* isomerization is substantially small; thus, the ring-closing step from *Z*-**4.1** to *anti*-**4.2** should be the rate determining step. The activation barrier for the rate determining step was estimated from the temperature dependence of a decay rate constant to be 15.7 ± 1.0 kcal mol^{-1} (log *A* = 7.9).

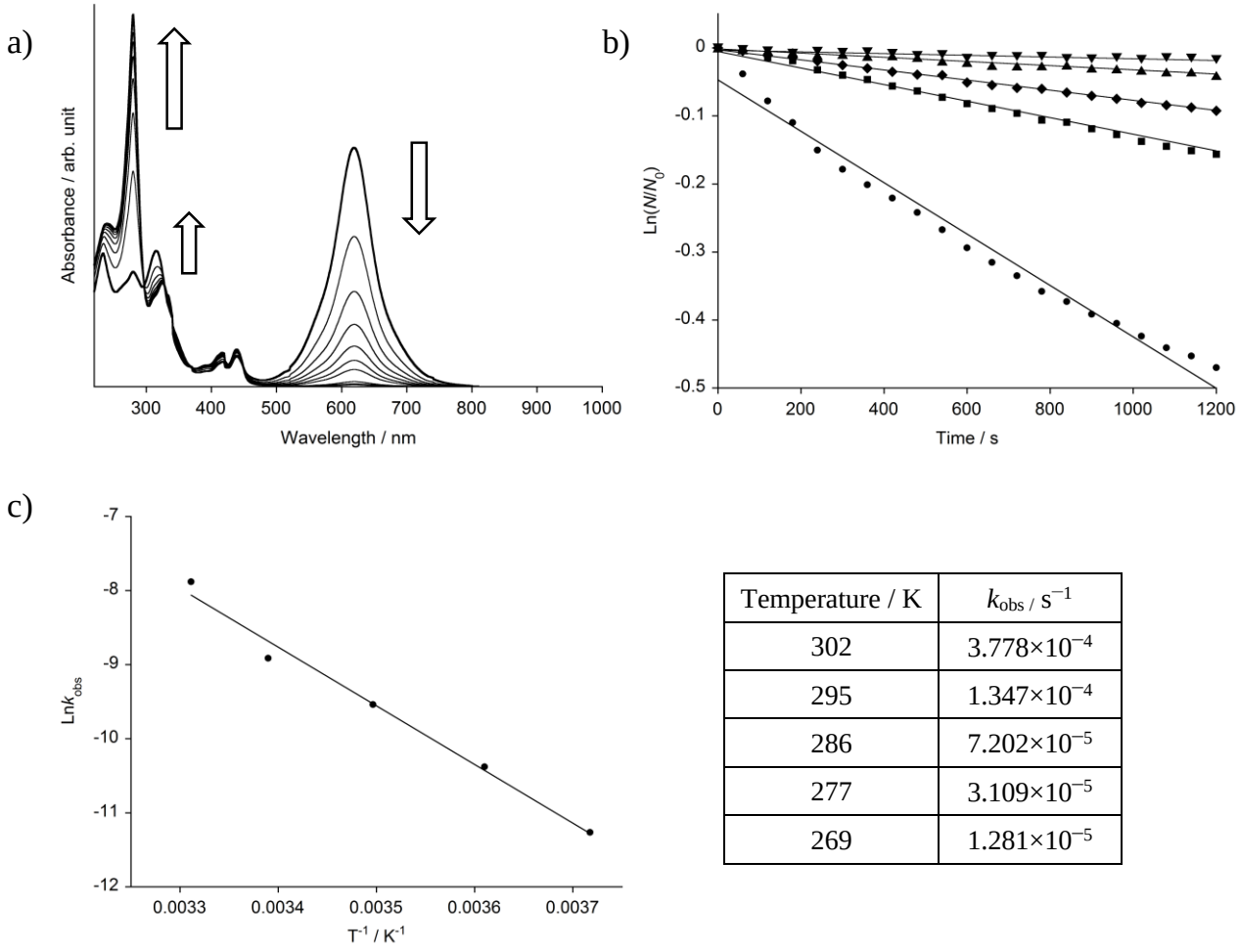

Temperature / K	k_{obs} / s^{-1}
302	3.778×10^{-4}
295	1.347×10^{-4}
286	7.202×10^{-5}
277	3.109×10^{-5}
269	1.281×10^{-5}

Figure 4.6.2. a) Time dependence of the electronic absorption spectra of *E*-**4.1** measured in dichloromethane (1×10^{-5} M) at room temperature. b) Decay of the normalized absorbance monitored at 619 nm (●: 302 K, ■: 295 K, ♦: 286 K, ▲: 277 K, ▼: 269 K). c) Arrhenius plot to determine the activation barrier for the electrocyclic ring-closure reaction. Reprinted with permission from ref. 5. Copyright 2016, American Chemical Society.

1,3-Cyclohexadiene and *cis*-1,3,5-hexatriene derivatives which demonstrate an unusual electrocyclization were shown in Scheme 4.6.1. 4a,4b-Dihydrophenanthrene (**4.12a**), which is analogous to 1,3-cyclohexadiene, is well-known to demonstrate a facile ring-opening in conrotatory process, which is not conforming to the Woodward-Hoffmann rule, to afford *cis*-stilbene (**4.12b**).[11] Loss of aromatic stabilization energy destabilizes **4.12a** with respect to **4.12b**, resulting in the decrease of a relative activation barrier to induce a conrotatory ring-opening. On the other hand, **4.13a** undergoes a ring-closure in conrotatory mode to the corresponding 1,3-cycrohexadiene analogue (**4.13b**).[12,13] In this case, the structural strain of **4.13a** leads to the ring-closure reaction in the kinetically unfavorable mode.

The orbital symmetry forbidden reaction of a singlet biradical was reported by Michl *et al.*[14,15] Pleiadene (**4.14a**), which is analogous to *o*-quionodimethane, represents a facile dimerization owing to its singlet biradical ground state,[14,16] whereas a dimethyl derivative (**4.15a**) undergoes the disrotatory ring-closure in kinetically unfavorable process to form a corresponding cyclobutene derivative (**4.15b**).[15] The facile ring-closure was accounted for by the destabilized ground state of pleiadene by the singlet biradical character. The unusual ring-closure reaction of *Z*-**4.1** can be also rationalized by the singlet biradical ground state of *Z*-**4.1**. As mentioned in chapter 4.5.2, an admixture of the doubly excited configuration into the ground state description destabilizes the ground state, resulting in the decrease of relative activation barrier for the kinetically unfavorable conrotatory ring-closure process.

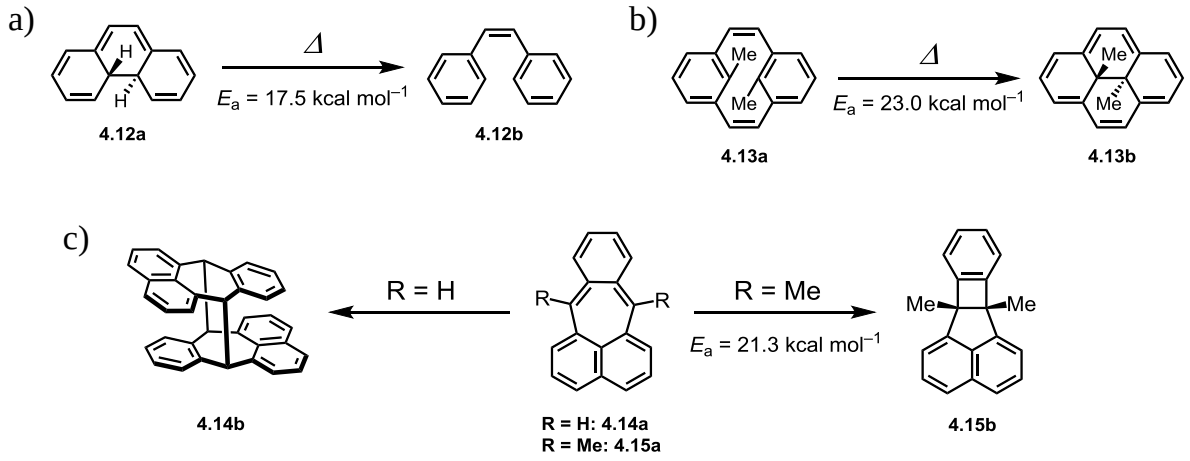

Scheme 4.6.1. a), b) Thermal conversion in conrotatory process between 1,3-cyclohexadiene and *cis*-1,3,5-hexatriene analogues. c) Thermal reactions demonstrated by pleiadene derivatives.

4.7 Computational studies on the reactions mechanism

Computational calculations were conducted to support the experimental results. As shown in Figure 4.7.1, molecular orbitals of *Z*-biphenalenylidene (*Z*-**4.1**) and *anti*-dihydroperopyrene (*anti*-**4.2**) reflect the electronic structures of *cis*-1,3,5-hexatriene and 1,3-cyclohexadiene, respectively. Thus, the thermal ring-closure in conrotatory fashion should be a kinetically unfavorable pathway. To gain an energetic insight into the ring-closure process, the transition states in conrotatory (TS1) and disrotatory (TS2) modes were estimated with a UB3LYP(BS)/6-31G**

method (Figure 4.7.2). The activation barrier for conrotatory ring-closure process was 22.6 kcal mol^{-1}, which is comparable with that determined experimentally (15.7 ± 1.0 kcal mol^{-1}) and the reported value.[4] This computational elucidation supports the idea that the destabilized ground state of *Z*-**4.1** results in the decrease of relative activation barrier for the conrotatory process not conforming to the Woodward-Hoffmann prediction. In contrast to the facility of the conrotatory process, larger activation energy (30.8 kcal mol^{-1}) is required for the disrotatory process. As shown in Figure 4.7.2, transition structure of disrotatory ring-closure reaction is highly contorted, leading to the large activation barrier. Therefore, the ring-closure in conrotatory process is the kinetically and thermodynamically favorable pathway, which is in line with the experimental finding that the thermal ring-closure solely gave *anti*-**4.2**.

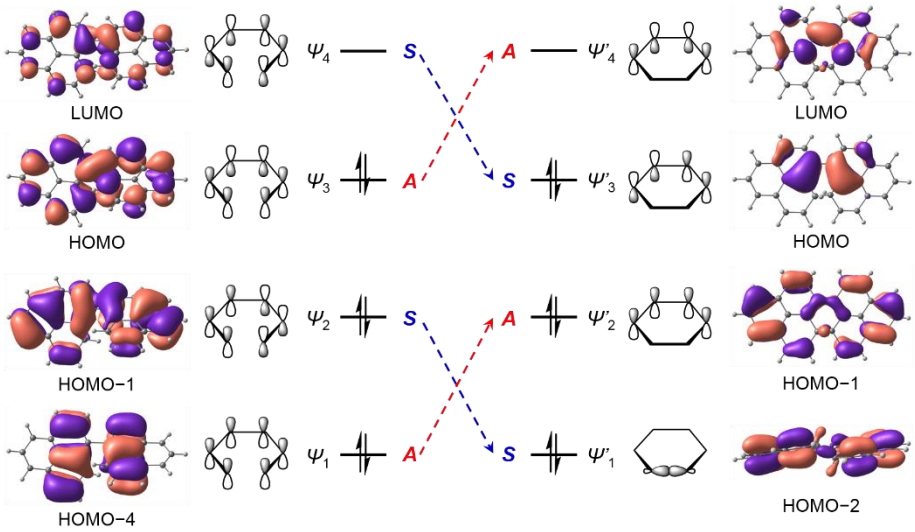

Figure 4.7.1. Molecular orbitals of *Z*-**4.1** (left) and *anti*-**4.2** (right) described with a CASSCF(2,2)/6-31G**//UB3LYP(BS)/6-31G** method.

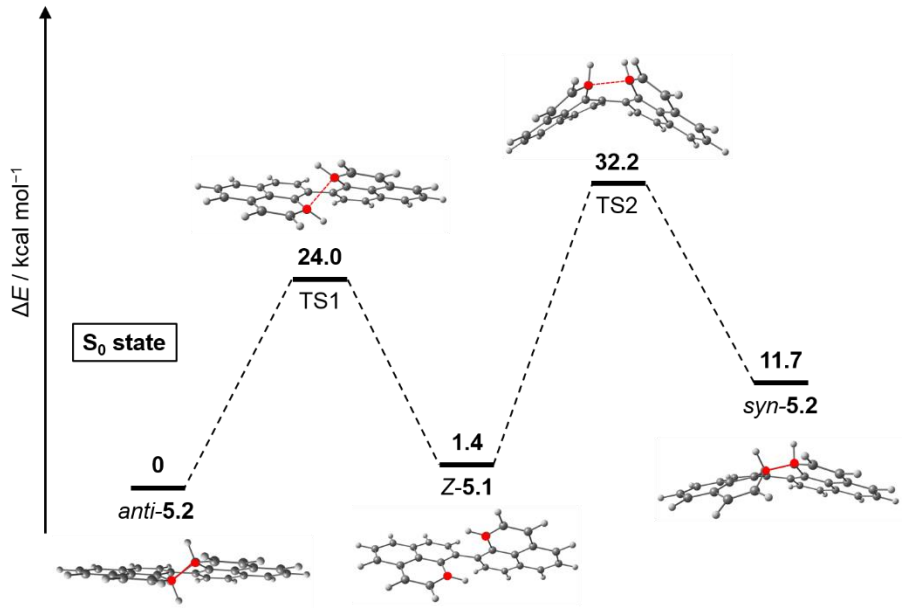

Figure 4.7.2. Energy diagram of the electrocyclic reaction in conrotatory and disrotatory processes. Transition states were identified by one imaginary frequency at the saddle point. The relative energies were estimated after ZPE correction. Reprinted with permission from ref. 5. Copyright 2016, American Chemical Society.

The overall energy diagram was displayed in Figure 4.7.3. The activation barrier for *E*-*Z* isomerization of *Z*-**4.1** was estimated to be 0.8 kcal mol^{-1}, which is considerably lower compared to that of general alkenes, as estimated by transient absorption spectra (4.3 ± 0.3 kcal mol^{-1}). As mentioned, the stabilization of transition state (TS3) as well as the destabilization of ground state contributes to the extraordinarily small activation energy. The computational results suggest the *E, Z*-**4.1** exist as an equilibrium mixture; thus, the ring-closure step should be a rate determining step.

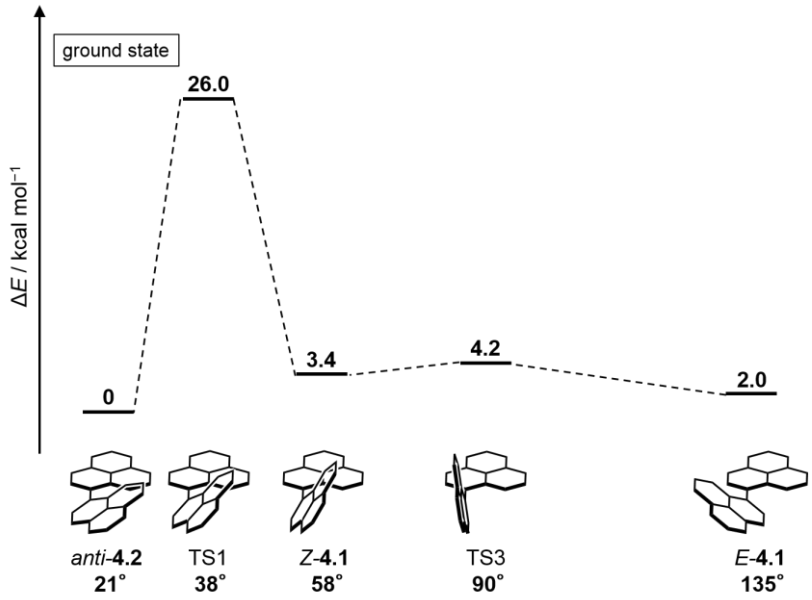

Figure 4.7.3. Energy diagram calculated with a UB3LYP(BS)/6-31G** method. Transition states were identified by one imaginary frequency at the saddle point. The relative energies in the S_0 state were estimated after ZPE collection. Reprinted with permission from ref. 5. Copyright 2016, American Chemical Society.

Furthermore, the S_1 energies were calculated with a spin flip TD-DFT method at BHHLYP/6-311G* level to elucidate the reaction mechanism of the photochemical reaction demonstrated by *anti*-**4.2**. Spin flip TDDFT calculation is a remarkable method to estimate the S_1 energies of the singlet biradical species. For a deeper understanding of the reaction mechanism, the detailed assignments of the S_1 states of **4.1**s are required. The singlet biradicals are known to have a low-lying doubly excited state (HOMO, HOMO → LUMO, LUMO),[17] whereas the singly excited states (HOMO → LUMO) of *E, Z*-**4.1** and *anti*-**4.2** are always lower in energy than the doubly excited states; thus, the S_1 states dominating the photochemical reaction of *E, Z*-**4.1** and *anti*-**4.2** are their singly excited states. As shown in Figure 4.7.4, the photoinduced ring-opening reaction of *anti*-**4.2** to *Z*-**4.1** is the exothermic process; in contrast, the ring-closure of *Z*-**4.1**, which would be a photochemically allowed reaction according to the Woodward-Hoffmann rule, is energetically uphill. Hence, the photoinduced ring-closure reaction was not observed experimentally, at least in the experimental conditions. In addition, the structural optimizations in the S_1 state gave two local minima between *Z*-**4.1** and TS3, and TS3 and *E*-**4.1** by using the molecular geometries of *Z*-**4.1** and *E*-**4.1** as the initial structures. On the basis of the S_1 potential energy surface, the ring-opening reaction should proceed as the following mechanism: *anti*-**4.2** (S_0) → *anti*-**4.2** (S_1) → *Z*-**4.1′** (S_1) → *Z*-**4.1′** (S_0) → *Z*-**4.1** (S_0). This computational

considerations were fully supported by the experimental findings that the photochemical reaction of *anti*-**4.2** gave solely *Z*-**4.1**.

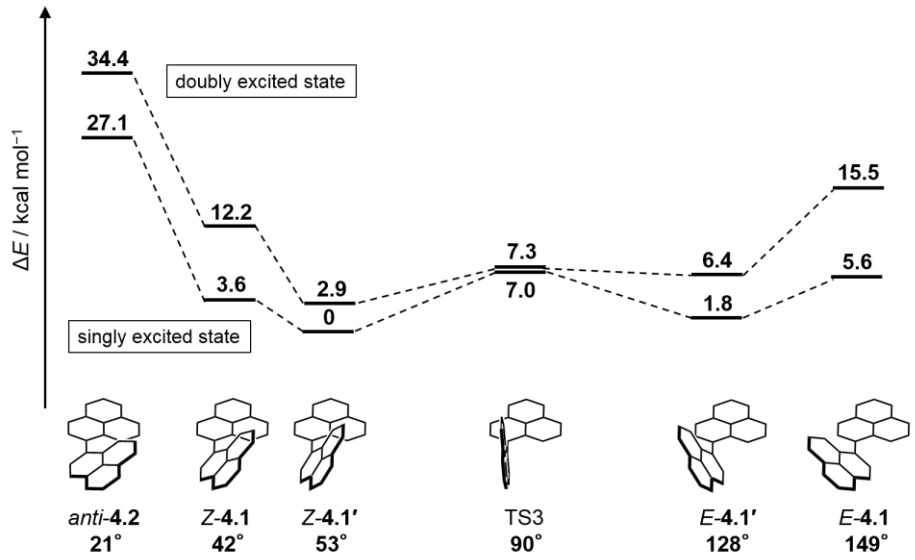

Figure 4.7.4. Energy diagram calculated with a spin flip TDDFT calculation at BHHLYP/6-31G* level. Reprinted with permission from ref. 5. Copyright 2016, American Chemical Society.

4.8 Reactivity of dihydroperopyrene

Dihydroperopyrene (*anti*-**4.2**) demonstrated a gradual decomposition to give peropyrene **4.3**. Storing the solution of *anti*-**4.2** in air resulted in the substantial change in ^{1}H NMR spectrum. Approximately 50% of *anti*-**4.2** decomposed after 2 weeks, and **4.3** was solely formed. A half-life was estimated from the integral value of ^{1}H NMR spectrum to be 11 days. The decomposition reaction took place even in degassed condition by heating and accelerated by the addition of polar solvents, such as ethyl acetate and DMF.

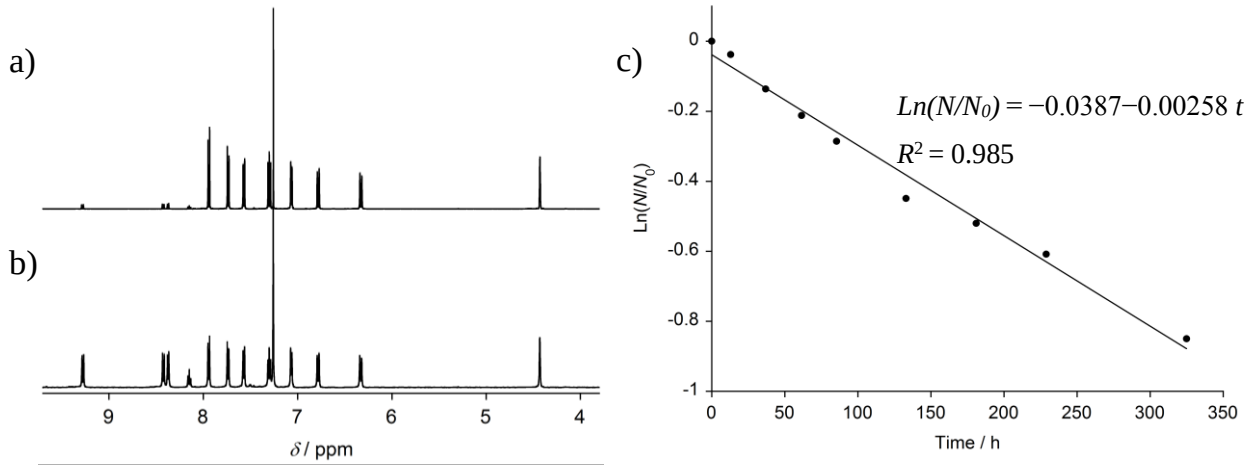

Figure 4.8.1. ^{1}H NMR spectra of *anti*-**4.2** recorded in air-saturated $CDCl_3$ a) just after preparation, and b) after 2 weeks. Hexamethylbenzene was used as an internal standard to normalize the intensity of *anti*-**4.2** signals. c) Half-life determination at room temperature from the time dependence of a ^{1}H NMR intensity. Reprinted with permission from ref. 5. Copyright 2016, American Chemical Society.

The electron accepters, such as TCNE, F_4-TCNQ, and 2,4,7-trinitrofluoren-9-one, induced the decomposition of *anti*-**4.2** into **4.3**. Octafluoronaphthalene, which is a weak electron accepter, also facilitated the decomposition and formed cocrystals with **4.3** generated (Figure 4.8.2). Octafluoronaphthalene and **4.3** constructed the alternate stacking 1D-chain with the intermolecular distance of 3.326–3.376 Å, and the 1D-chains were tied together with the CH–F hydrogen bonds.

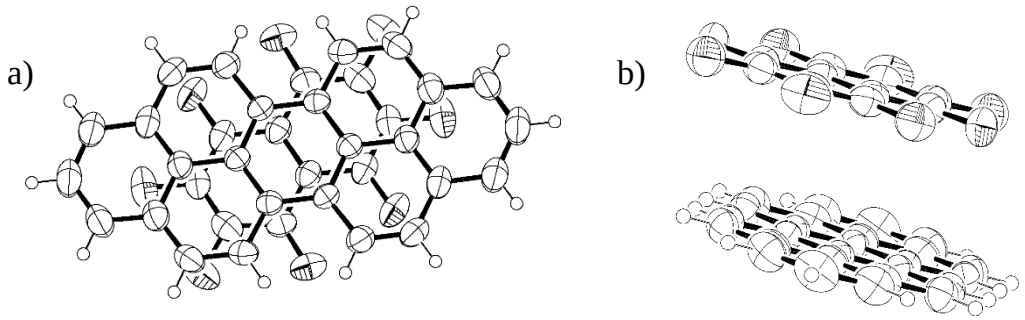

Figure 4.8.2. Ortep drawing of the cocrystal of **4.3** and octafluoronaphthalene at the 50% probability level. Views perpendicular to a) the (0 1 0) plane and b) (0 0 1) plane. Crystal System = monoclinic, a = 8.0597(11) Å, b =

7.0002(8) Å, c = 21.678(3) Å, β = 96.846(3)°, V = 1214.3(3) Å^3, Space Group = $P2_1/n$ (#14), Z = 2, μ(MoKα) = 1.38 cm^{-1}, T = 230 K, $R1$ [$F^2>2\sigma(F^2)$] = 0.0573, $wR2$(all data) = 0.2545, S = 1.308, Refl./param. = 2765/199.

4.9 Direct observation of the reactive intermediates

Finally, the reactive intermediate on the decomposition pathway of phenalenyl **1.3** was directly observed by the electronic absorption spectrum. In early attempts to synthesize **1.3**, green or blue products showing an absorption band at 613 nm were found, whereas the products were not identified.[3] To an excess amount of hydro-precursor phenalene was added *p*-chloranil in degassed dichloromethane, and the electronic absorption spectra were recorded periodically. A characteristic absorption band centered 620 nm was observed in the early stage of the reaction, then the band gradually decreased in intensity and disappeared within 1 hour. The spectral feature are fully identical to that of *E*-**4.1**, suggesting strongly that *E*-**4.1** should exist as an intermediate on the decomposition pathway of parent phenalenyl. With the decay of an absorption band of *E*-**4.1**, an intense peak at 441 nm, which is assignable to peropyrene **4.3**, grew up to 7 hours. Notably, a weak band observed at 565 nm remained unchanged over a couple of days after disappearing *E*-**4.1**. The absorption band would be ascribed to a forbidden transition of parent phenalenyl, thus, phenalenyl is considered to be persistent in a condition without any oxidants.

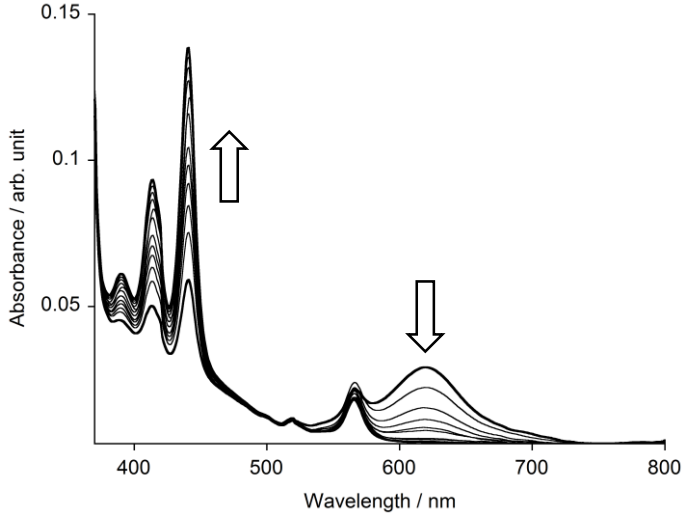

Figure 4.9.1. Electronic absorption spectra of phenalenyl recorded periodically in dichloromethane (2×10^{-5} M). Reprinted with permission from ref. 5. Copyright 2016, American Chemical Society.

4.10 Conclusion

First isolation of *E*, *Z*-biphenalenylidene (*E*, *Z*-**4.1**) in solution state was accomplished by mean of the photoinduced electrocyclic ring-opening reaction of *anti*-dihydroperopyrene (*anti*-**4.2**). The structural characterizations of *E*, *Z*-**4.1** and *anti*-**4.2** were performed by spectroscopic analyses (^{1}H NMR spectroscopy and the electronic absorption spectra) as well as computational studies. *Z*-**4.1**, which was trapped in a rigid matrix of a solvent, demonstrated the rapid *E*-*Z* isomerization to *E*-**4.1**, and the kinetic investigation indicated that the activation barrier of 4.3 ± 0.3 kcal mol^{-1} is extraordinarily smaller than that of general alkenes. Furthermore, *Z*-**4.1** represented the unusual ring-closure reaction in conrotatory process to afford *anti*-**4.2**, which is not conforming to the Woodward-Hoffmann prediction. The activation barrier was also determined by spectroscopic techniques to be 15.7 ± 1.0 kcal mol^{-1}. These fascinating reactions can be rationalized by the singlet biradical ground state of *E*, *Z*-**4.1**. Admixture of the doubly excitation configuration into the ground state description resulted in the decrease of the intramolecular covalent bonding interaction and destabilized the ground state. In addition, the biradical transition state (TS3 in Figure 4.7.1) of *E*-*Z* isomerization was stabilized by the delocalization of unpaired electrons over phenalenyl planes. Thus, the unusual reaction demonstrated by **4.1** is ascribed to the singlet biradical ground state.

The presence of *E*-**4.1** in the decomposition pathway of parent phenalenyl was confirmed by generating phenalenyl in a degassed solvent. Indeed, *E*-**4.1** was detected experimentally in the early stage of the reaction, and the appearance of peropyrene **4.3** was also observed. Thus, the decomposition mechanism of parent phenalenyl was unambiguously clarified experimentally.

4.11 Experimental

All experiments were conducted according to the literature reported previously.[5]

4.12 References

(1) Boekelheide, V.; Larrabee, C. E. *J. Am. Chem. Soc.* **1950**, *72* (3), 1245.

(2) Reid, D. H. *Tetrahedron* **1958**, *3* (3), 339.

(3) Reid, D. H. *Q. Rev. Chem. Soc.* **1965**, *19* (3), 274.

(4) Pogodin, S.; Agranat, I. *J. Am. Chem. Soc.* **2003**, *125* (42), 12829.

(5) Uchida, K.; Ito, S.; Nakano, M.; Abe, M.; Kubo, T. *J. Am. Chem. Soc.* **2016**, DOI: 10.1021/jacs.5b13033.

(6) Ohashi, K.; Kubo, T.; Masui, T.; Yamamoto, K.; Nakasuji, K.; Takui, T.; Kai, Y.; Murata, I. *J. Am. Chem. Soc.* **1998**, *120* (9), 2018.

(7) Kubo, T.; Shimizu, A.; Sakamoto, M.; Uruichi, M.; Yakushi, K.; Nakano, M.; Shiomi, D.; Sato, K.; Takui, T.; Morita, Y.; Nakasuji, K. *Angew. Chemie Int. Ed.* **2005**, *44* (40), 6564.

(8) Konishi, A.; Hirao, Y.; Nakano, M.; Shimizu, A.; Botek, E.; Champagne, B.; Shiomi, D.; Sato, K.; Takui,

T.; Matsumoto, K.; Kurata, H.; Kubo, T. *J. Am. Chem. Soc.* **2010**, *132* (32), 11021.

(9) Li, Y.; Heng, W.-K.; Lee, B. S.; Aratani, N.; Zafra, J. L.; Bao, N.; Lee, R.; Sung, Y. M.; Sun, Z.; Huang, K.-W.; Webster, R. D.; López Navarrete, J. T.; Kim, D.; Osuka, A.; Casado, J.; Ding, J.; Wu, J. *J. Am. Chem. Soc.* **2012**, *134* (36), 14913.

(10) Tomioka, *Advances in Stained and Interesting Organic Molecules*, Vol. *8*. (Ed.: Halton, B). JAI Press, Greenwich CT, **2000**, 83.

(11) Muszkat, K. A.; Fischer, E. *J. Chem. Soc. B* **1967**, 662.

(12) Boekelheide, V.; Phillips, J. B. *J. Am. Chem. Soc.* **1966**, *5991* (4), 1695.

(13) Blattmann, H.-R.; Schmidt, W. *Tetrahedron* **1970**, *26* (24), 5885.

(14) Kolc, J.; Michl, J. *J. Am. Chem. Soc.* **1970**, *92* (13), 4147.

(15) Steiner, R. P.; Michl, J. *J. Am. Chem. Soc.* **1978**, *100* (20), 6413.

(16) Cava, M. P.; Schlessinger, R. H. *Tetrahedron* **1965**, *21* (11), 3073.

(17) Di Motta, S.; Negri, F.; Fazzi, D.; Castiglioni, C.; Canesi, E. V. *J. Phys. Chem. Lett.* **2010**, *1* (23), 3334.

-Chapter 5-
Synthesis and Properties of Novel Peropyrene Derivatives

5.1 Introduction

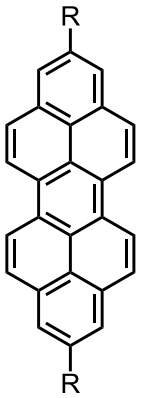

R = H: **4.3**
R = ^{n}Bu: **5.1a**
R = ^{t}Bu: **5.1b**
R = Ph: **5.1c**

Peropyrene **4.3** is a fascinating molecule to the application for organic materials owing to its wide π-electron surface and highly planar geometry. Especially, **4.3** is a promising candidate for the organic solar cells based on the singlet fission mechanism.[1–7] Singlet fission is a photochemical process, in which two triplet excitons (T_1) are generated from a singlet exciton (S_1) sharing its excitation energy with a neighboring molecule in the ground state (S_0).[8] The mechanism of singlet fission evokes an energetic requirements; that is, twice the energy of the T_1 state should be less than that of the S_1 state ($2E(T_1) \leq E(S_1)$). Most organic compounds do not satisfy the demanding; in contrast, **4.3** demonstrates a suitable energy matching owing to its π-electronic structure ($E(S_1)$ = 2.79 eV, $E(T_1)$ = 1.36 eV),[9] suggesting **4.3** is a remarkable candidate for singlet fission. Photophysical properties of parent **4.3** in solution and solid state were reported by Bardeen *et al.*[10] Although **4.3** satisfied the energetic requirement at the single-molecule level, the excimer formation in crystalline state stabilizes the S_1 state, preventing the singlet fission process. As mentioned in the literature, tuning the crystal structure by chemical substitution is required to improve the performance.

First synthesis of parent **4.3** was reported by Clar *et al.*[11,12] **4.3** was prepared by a reductive coupling of phenalenone (perinaphthenone) or reduction of peropyrene quionone with zinc dust. Spectroscopic studies have been well conducted and its electronic structure has been reported;[9] in contrast, effective ways to synthesize peropyrene scaffold have not yet been developed. In 2003, Agranat and his coworkers reported the synthesis of **4.3** by dimerization followed by dehydrogenation of phenalenethione in moderate yield,[13] whereas the method is not suitable for a selective synthesis of peropyrene derivatives with various substituted groups.

In chapter 4, the decomposition mechanism of parent phenalenyl was investigated and **4.3** was obtained as a final product by the dehydrogenation of biphenalene **4.11**. Therefore, the biphenalene derivatives can be regarded as suitable precursor for peropyrene derivatives. This chapter describes a novel synthetic procedure and properties of 2,9-disubstituted peropyrene derivatives (**5.1a–c**). Crystal structures were determined by X-ray crystallographic analyses, and photophysical properties in both solution and crystalline state were studied by spectroscopic measurements, such as the electronic absorption spectrum and fluorescence spectrum. In addition, the electronic structure of **5.1a** radical cation was also investigated by spectroscopic techniques.

5.2 Elucidation of the electronic structure of peropyrene

Theoretical calculation is an efficient tool to explore the feasible compounds on the singlet fission. A clear relationship between the excited states contributing to the singlet fission mechanism and the open-shell characters was reported by Nakano *et al.*[14] The energetic aspect of the feasibility on singlet fission can be assessed by the multiple diradical indicator y_i (defined by the occupation number of LUMO+i (i = 0, 1, …)) calculated with a PUHF/6-31G* method. This computational approach suggests that the molecules with low/intermediate biradical characters y_0 should satisfy the energetic requirements of singlet fission.

To estimate the electronic structure including the singlet biradical character of peropyrene **4.3**, theoretical calculations were conducted. In Figure 5.2.1, frontier orbitals of **4.3** calculated with a B3LYP/6-31G** under D_{2h} symmetry were displayed. Molecular orbitals widely distributes over the molecule, and the HOMO–LUMO gap is estimated to be 2.82 eV. Theoretical calculation performed with a broken-symmetry (BS) UB3LYP/6-31G** method suggested the close-shell ground state of **4.3**, whereas meaningful multi-radical indices (y_0 = 0.26, y_1 = 0.05) were shown with a PUHF/6-31G* method. Hence, the theoretical calculation supports the idea that **4.3** is a feasible compound to singlet fission at the single-molecule level.

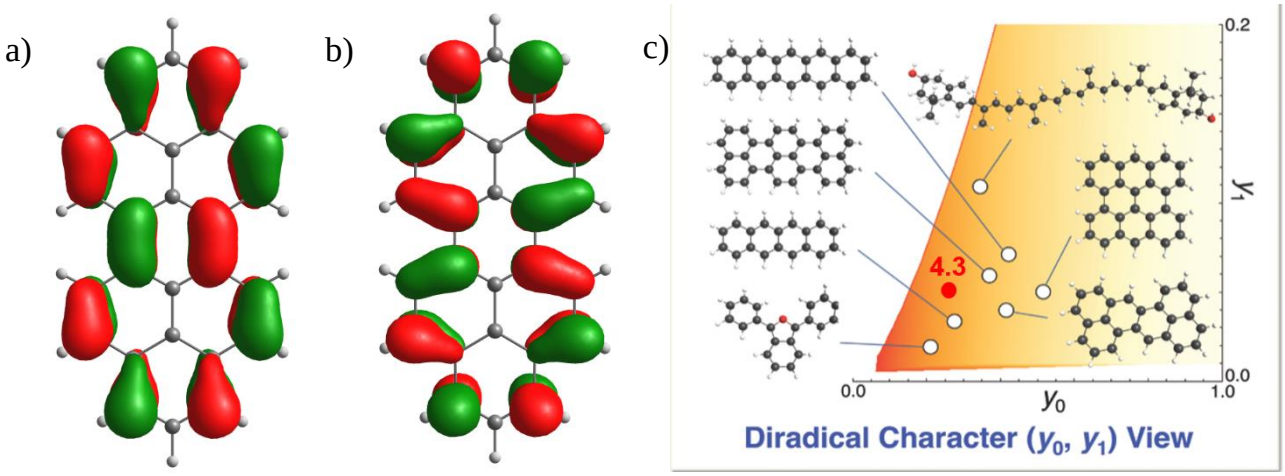

Figure 5.2.1. a) Highest occupied molecular orbital (HOMO) and b) lowest unoccupied molecular orbital (LUMO) of **4.3** calculated with a B3LYP/6-31G** method under D_{2h} symmetry. c) Nakano map for the feasibility of singlet fission. Figure 5.2.1c was reprinted with permission from ref. 14. Copyright 2012, American Chemical Society.

With focused on the bond lengths estimated at B3LYP/6-31G** level (shown in Figure 5.2.2a), the bond ***a*** is noticeably short (1.361 Å) compared to the others, indicating the considerable double bond character in the bond ***a***. The bond alternation is reflected on the NICS values calculated with a GIAO-HF/6-311G**//B3LYP/6-31G** method. NICS(1)$_{zz}$ values were summarized in Figure 5.2.2b. Although the ring ***A*** and ***C*** showed large negative values (ring ***A***: −38.07, ring ***C***: −40.68, *cf.* benzene: −31.93) due to the prominent aromatic ring current, the NICS(1)$_{zz}$ value of the ring ***B*** is considerably smaller (−16.08), suggesting that the bond alternation resulted in the decrease of the aromaticity of ring ***B*** including the bond ***a***.

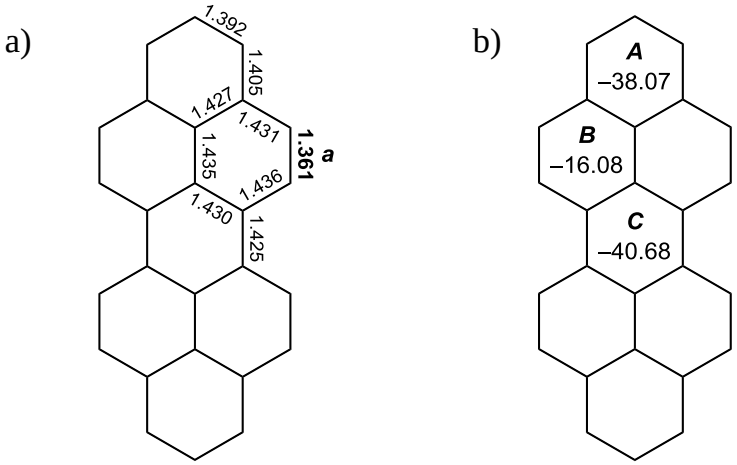

Figure 5.2.2. a) Bond lengths of **4.3** estimated with B3LYP/6-31G** method. b) NICS(1)$_{zz}$ values of **4.3** estimated at GIAO-HF/6-311G**//B3LYP/6-31G** level.

5.3 Synthesis of peropyrene derivatives

As mentioned above, biphenalene is the key precursor for peropyrene; thus, biphenalene derivatives with corresponding substituents (**5.9a–c**) were prepared according to the procedure displayed in Scheme 5.3.1.

2,9-Dibutylperopyrene (**5.1a**) was prepared from the benzyl bromide **5.2** in 8 steps. Treatment of **5.2** with the enolate of methy hexanolate gave the corresponding saturated ester **5.3a** and subsequent hydrolysis in basic condition led to a carboxylic acid **5.4a**. Intramolecular Friedel-Crafts cyclization of the acyl chloride derived from **5.4a** afforded phenalanone derivative **5.5a** in high yield. The phenalanone **5.5a** was converted into the corresponding boronic ester **5.6a** by the Miyaura borylation. The Suzuki-Miyaura coupling of **5.5a** with **5.6a** gave biphenalanone **5.7a** as a diastereomer mixture. Reduction followed by dehydration led to biphenalene **5.9a**. Treatment of **5.9a** with *p*-chloranil afforded a crude **5.1a** then the crude product was purified by column chromatography and recrystallization.

2,9-Di-*tert*-butylperopyrene (**5.1b**) was synthesized along the similar procedure to that of **5.1a**. It should be noted that the steric hindrance of *tert*-butyl groups prevented the hydrolysis of **5.3b** and reduction of **5.7b**; thus, optimization of the reaction conditions was required. Heating of **5.3b** in the presence of lithium iodide gave the carboxylic acid **5.4b** cleanly. Reduction of **5.7b** was accomplished by using lithium aluminium hydride instead of sodium borohydride. **5.1b** obtained was purified by column chromatography and recrystallization.

2,9-Diphenylperopyrene (**5.1c**) was also prepared along Scheme 5.3.1. Introduction of phenyl groups resulted in the decrease of the solubility of biphenalanone **5.7c** and biphenalene **5.9c**. **5.1c** also has low solubility, leading to the difficulty of purification. Therefore, the purification of **5.1c** was performed by sublimation under reduced pressure and recrystallization.

^{1}H NMR spectra of peropyrene derivatives **5.1a–c** were displayed in Figure 5.4.1, together with that of parent peropyrene **4.3**. **5.1a–c** exhibited two sets of doublets and a singlet peak in aromatic region, suggesting the highly symmetric geometries of **5.1a–c**.

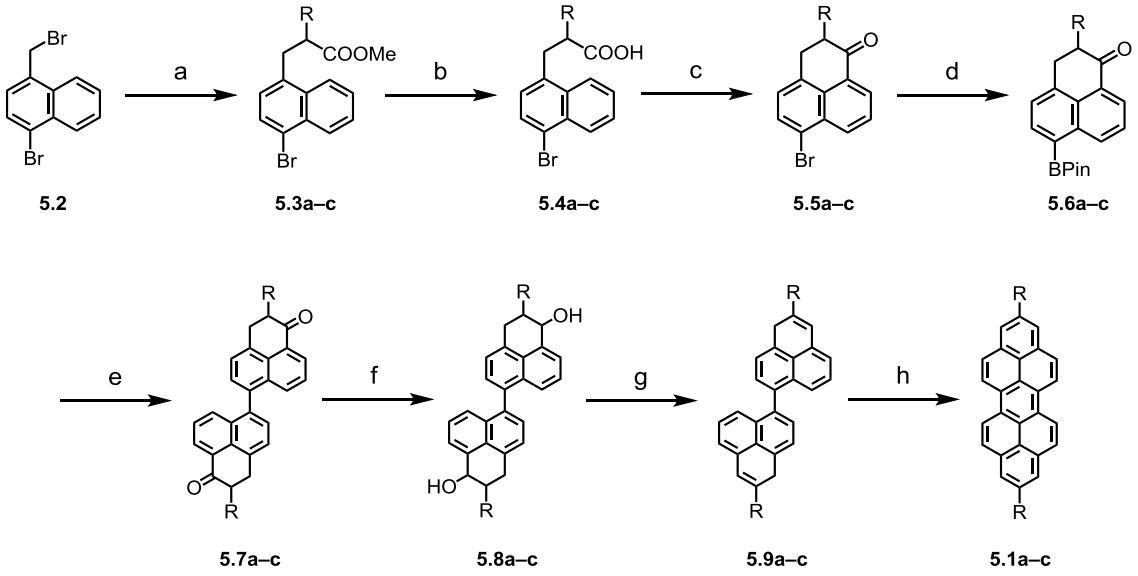

Scheme 5.3.1. Synthetic procedure for **5.1a–c**. Reagent and condition: a) LDA, RCH_2COOMe, THF, −78 °C to RT; b) method A: 10% NaOHaq., EtOH, 90 °C; method B: LiI, 2,4,6-trimethylpyridine, 185 °C; c) (i) $(COCl)_2$, 60 °C, (ii) $AlCl_3$, DCM, −78 to −30 °C; d) Pd(dppf)Cl_2 DCM adduct, bis(pinacolato)diboron, KOAc, 1,4-dioxane, 80 °C; e) **5.5a–c**, $Pd(PPh_3)_4$, K_2CO_3, toluene/EtOH/H_2O (4/1/1), 70 °C, f) method A: $NaBH_4$, DCM/EtOH (1/1), RT; method B: $LiAlH_4$, THF, RT; g) *p*-TsOH·H_2O, toluene, 120 °C, h) *p*-chloranil, DCM, RT. LDA = lithium diisopropylamide, dppf = diphenylphosphinoferrocene, *p*-chloranil = 2,3,5,6-tetrachloro-1,4-benzoquinone.

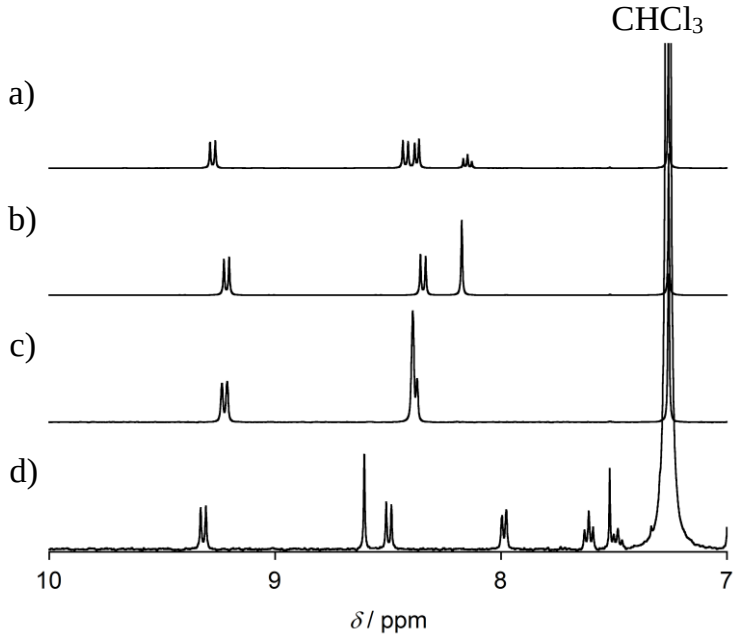

Figure 5.3.1. ^{1}H NMR spectra of a) **4.3**, b) **5.1a**, c) **5.1b**, and d) **5.1c** recorded in $CDCl_3$.

5.4 Photophysical properties in solution state

To elucidate the electronic structure of peropyrene derivatives (**5.1a–c**), the electronic absorption spectra and the fluorescence spectra were measured in chlorobenzene (see Figure 5.4.1 and Table 5.4.1). Parent peropyrene **4.3** showed an intense absorption band at 444 nm with distinctive vibrational structures and a fluorescence peak with maximum at 450 nm. The small Stokes shift (300 cm^{-1}) reflects the rigid molecular backbone. On the other hand, **5.1a–c** represented similar absorption and fluorescence spectra to those of **4.3**. The resemblance of the optical properties suggests the 2,9-substitution hardly affected the electronic structure of **4.3**. With focused on the molecular orbitals shown in Figure 5.2.1, 2,9-carbon atoms with substituted groups are nodes in HOMO and LUMO; therefore, the introduction of substituents on 2,9-positions has little, if any, influence on the S_0 and S_1 states of **4.3**. The S_1 energy levels of **5.1a–c** estimated from the fluorescence spectra are approximately 2.7 eV, satisfying the requirement of the energy matching for the singlet fission process ($2E(T_1) \leq E(S_1)$).

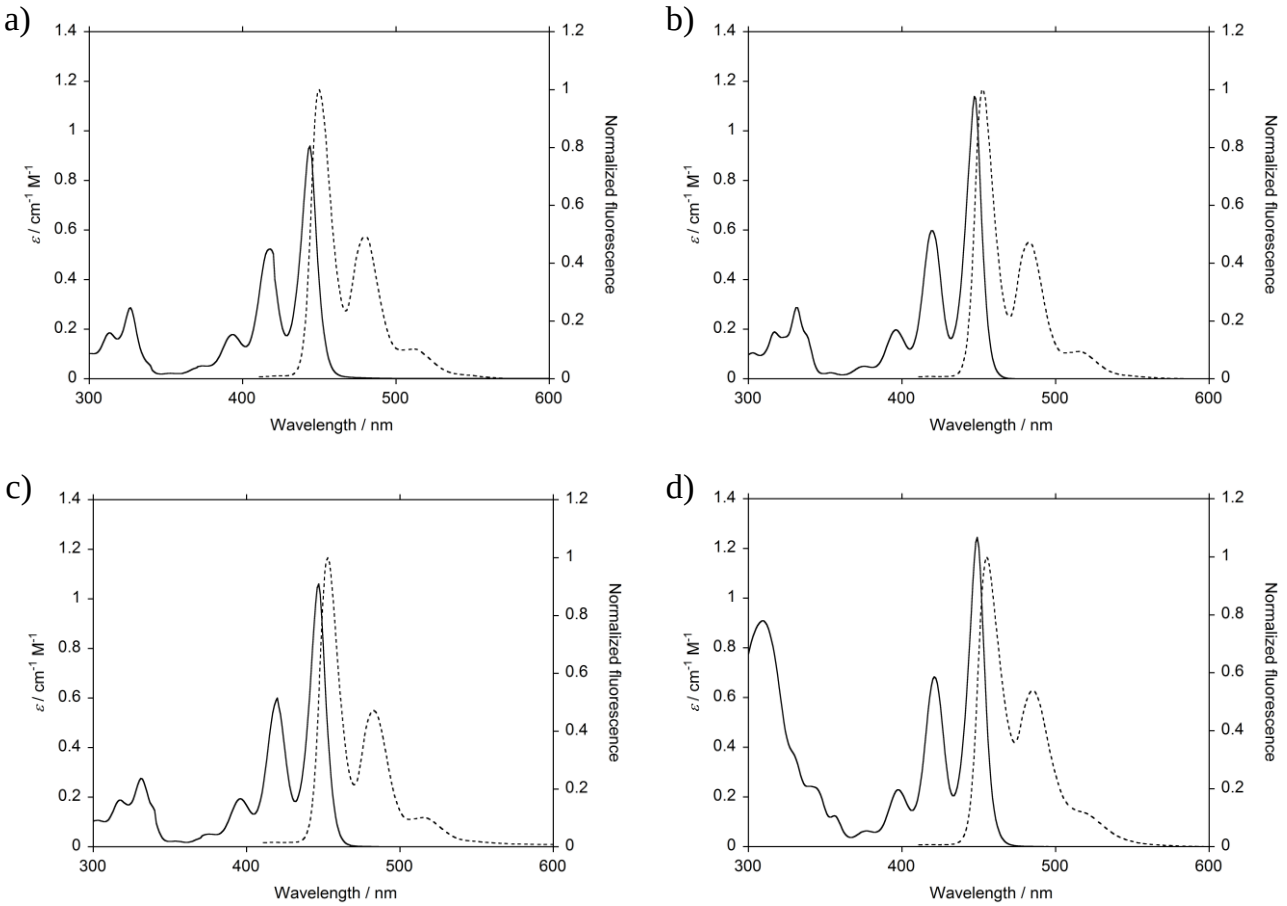

Figure 5.4.1. a) Electronic absorption spectra (1×10^{-5} M, solid line) and fluorescence spectra (1×10^{-7} M, dashed line, excitation at 400 nm) of a) **4.3**, b) **5.1a**, c) **5.1b**, and d) **5.1c** recorded in chlorobenzene.

Table 5.4.1. Photophysical data of **4.3** and **5.1a–c**.

	λ_{abs} / nm	ε_{max} / cm^{-1} M^{-1}	λ_{em} / nm	Stokes shift / cm^{-1}
4.3	444	0.94×10^5	450	300
5.1a	447	1.1×10^5	453	296
5.1b	447	1.1×10^5	453	296
5.1c	449	1.3×10^5	455	294

5.5 Molecular geometry

5.5.1 Crystal structure of 2,9-dibutylperopyrene

Slow evaporation of 2,9-dibutylperopyrene (**5.1a**) solution in chloroform/hexane grew yellow needle crystals suitable for X-ray crystallographic analysis. The molecular geometry of **5.1a** was unambiguously determined (Figure 5.5.1). The π-plane of **5.1a** was completely frat and the two butyl groups were directed perpendicular to the π-plane. The bond length reflects prominently the electronic structure of peropyrene. With focused on the bond ***a*** and ***a'***, the bond lengths are considerably shorter (1.350(2) Å and 1.353(2) Å) than that in general aromatic rings. The bond alternation is significantly reflected on the HOMA (harmonic oscillator model of aromaticity) values of the six-membered ring ***B*** and ***B'*** including bond ***a***, ***a'***. HOMA value, which is a geometry-based aromaticity index,[15,16] was estimated from the bond lengths determined by X-ray crystallographic analysis (shown in Figure 5.5.1d). Whereas the ring ***A*** showed a larger HOMA value (0.875), the HOMA values of ring ***B*** and ***B'*** were considerably smaller (0.553 and 0.572, respectively), indicating the decrease of the aromaticity due to the bond alternation. This result is fully consistent with the elucidation by NICS calculations.

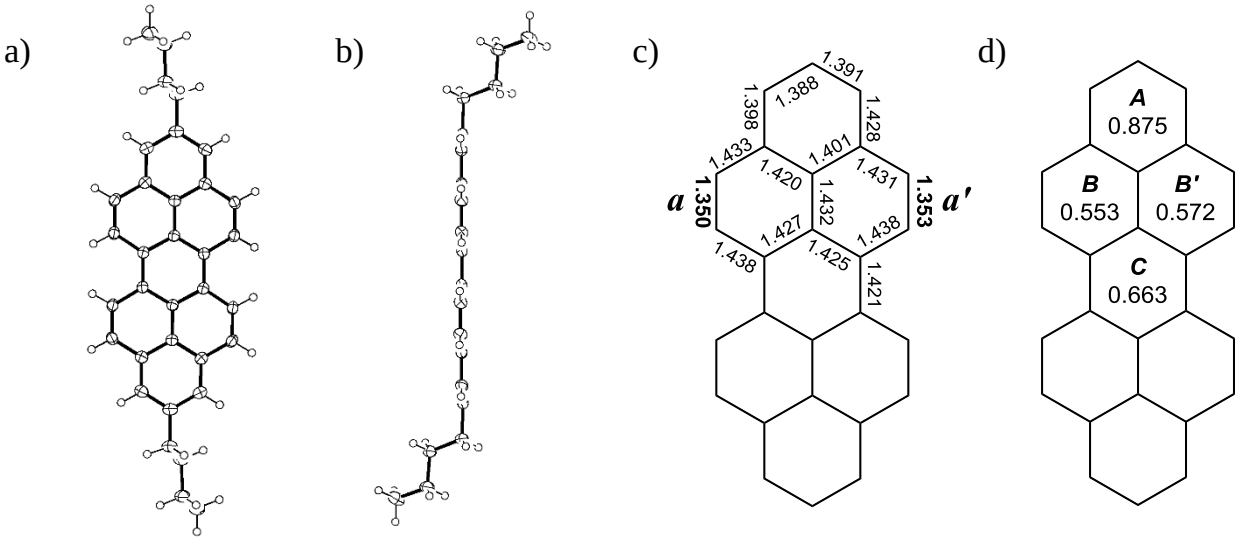

Figure 5.5.1. Ortep drawing of **5.1a** in the 1D-chain at the 50% probability level. a) Top view and b) side view. c) Bond lengths of peropyrene moiety. d) HOMA values.

Crystal System = triclinic, a = 4.5716(6) Å, b = 8.5913(12) Å, c = 15.400(2) Å, α = 75.911(5)°, β = 85.390(6)°, γ = 75.141(5)°, V = 567.12(13) Å^3, Space Group = $P\bar{1}$ (#2), Z = 1, μ(MoKα) = 0.72 cm^{-1}, T = 200 K, $R1$ [F^2>2σ(F^2)] = 0.0475, $wR2$(all data) = 0.1526, S = 1.111, Refl./param. = 2573/155.

Packing diagrams of **5.1a** were displayed in Figure 5.5.2. **5.1a** constructed the slipped stacking 1D-chain dominated by the van der Waals interactions between the π-planes. The π–π separation distance between **5.1a** in a 1D-chain was estimated to be 3.475 Å on average, which is almost comparable with the sum of the van der Waals radius of carbon atom (3.4 Å). On the other hand, the van der Waals interactions between hexyl chains at 2,9-positions contributed to tie together with the neighboring 1D-chains.

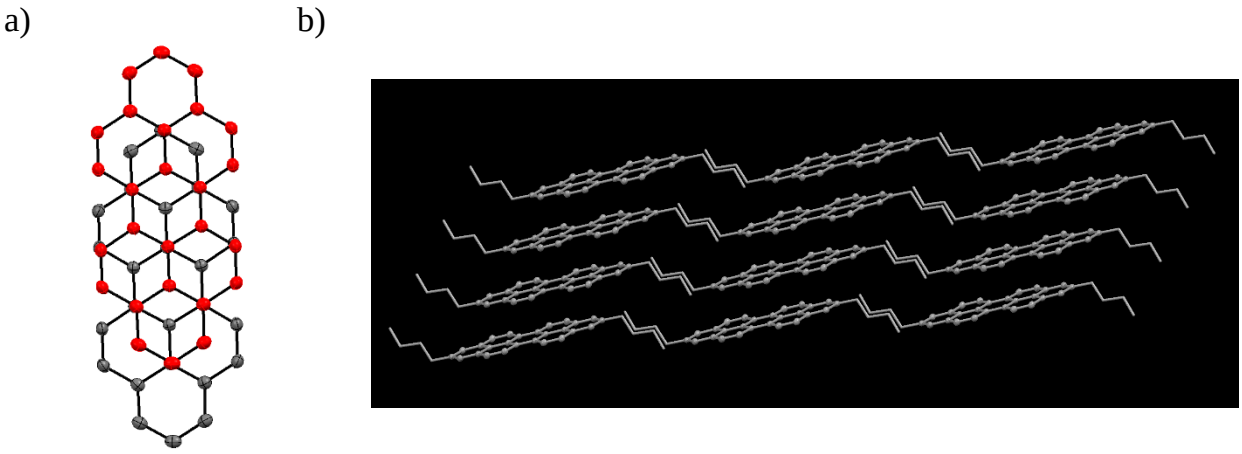

Figure 5.5.2. Packing diagrams of **5.1a** in the slopped stacking 1D-chain. a) Packing motif. Hydrogen atoms and butyl groups were omitted for clarity. b) View along b axis. Hydrogen atoms are omitted for clarity and butyl groups were shown as capped sticks.

Recrystallization of **5.1a** from hot DMF gave yellow platelet crystals together with the yellow needles of **5.1a** 1D-chain. Crystal structure of yellow plates determined by X-ray crystallographic analysis was depicted in Figure 5.5.3 and Figure 5.5.4. **5.1a** formed a face-to-face dimer in the platelet crystal as observed in the crystal structure of **4.3**.[10] The π–π separation distance in the dimer was estimated to be 3.340–3.529 Å (3.405 Å on average), which is considerably shorter than that in the face-to-face dimer of **4.3** (3.636–3.705 Å, 3.667 Å on average). On the other hand, the face-to-face dimers were tied together with the CH–π interactions, leading to the face-to-edge alignment of **5.1a**. The molecular structure of **5.1a** forming the face-to-face dimer is almost identical to that in a 1D-chain; thus, HOMA values estimated from the bond lengths are approximately identical (summarized in Figure 5.5.3).

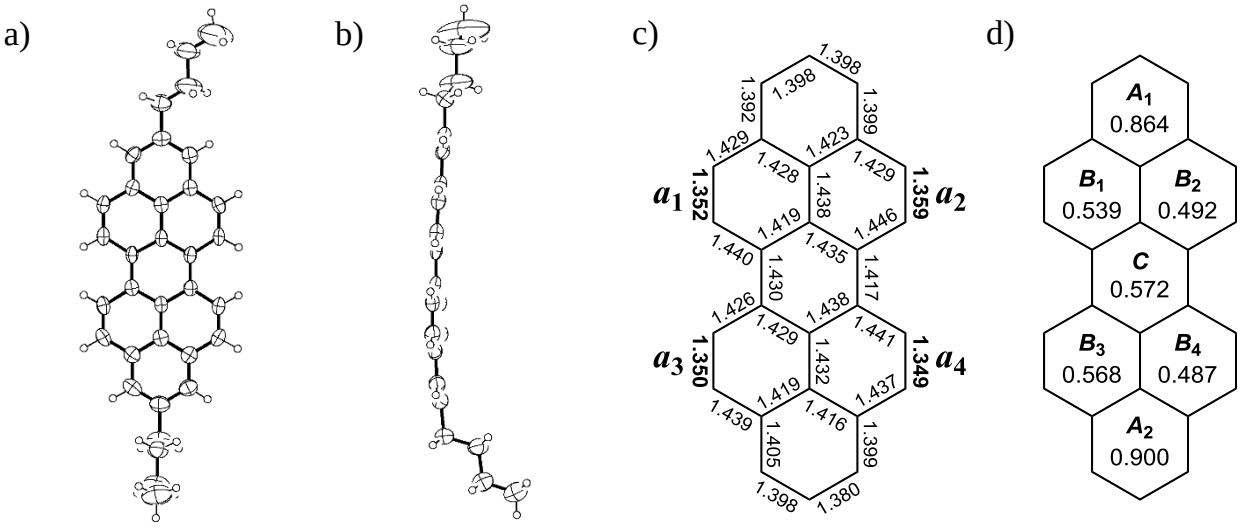

Figure 5.5.3. Ortep drawing of **5.1a** in the platelet crystal at the 50% probability level. a) Top view and b) side view. c) Bond lengths of peropyrene moiety. d) HOMA values.

Crystal System = monoclinic, a = 13.3501(12) Å, b = 9.0947(9) Å, c = 20.6140(18) Å, β = 103.245(7)°, V = 2436.3(4) Å^3, Space Group = $P2_1/a$ (#14), Z = 4, μ(MoKα) = 0.67 cm^{-1}, T = 200 K, $R1$ [$F^2>2\sigma(F^2)$] = 0.0841, $wR2$(all data) = 0.2424, S = 1.017, Refl./param. = 5538/307.

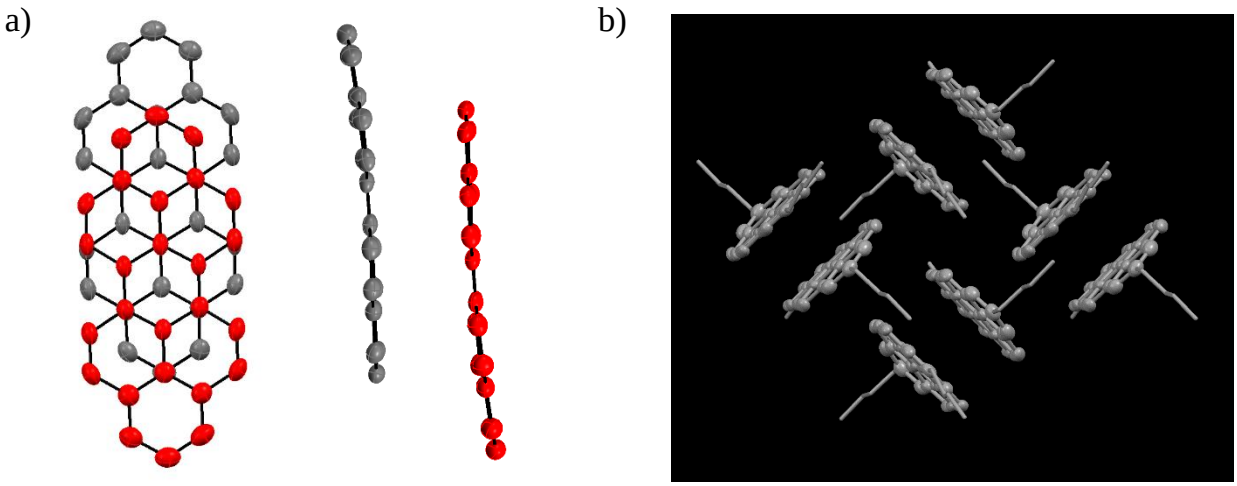

Figure 5.5.4. Packing diagrams of **5.1a** in the 2D-network constructed by the face-to-face dimers. a) Packing motif (top view and side view). Hydrogen atoms and butyl groups were omitted for clarity. b) View along c axis. Hydrogen atoms were omitted for clarity and butyl groups were shown as capped sticks.

5.5.2 Crystal structure of 2,9-di-*tert*-butylperopyrene

Recrystallization of 2,9-di-*tert*-butylperopyrene **5.1b** from chloroform/hexane gave yellow platelet crystals suitable for X-ray crystallographic analysis. Molecular geometry of **5.1b** was shown in Figure 5.5.5. Planar backbone of **5.1b** was confirmed as observed in **4.3** and **5.1a**. The bond lengths and HOMA values of **5.1b** were also summarized in Figure 5.5.5. As observed in **5.1a**, bond ***a*** and ***a'*** were significantly shorter (1.345(2)–1.353(2) Å) with respect to that in general aromatic rings, resulting in the decrease of HOMA values of ring ***B*** and ***B'*** (0.610 and 0.562 on average).

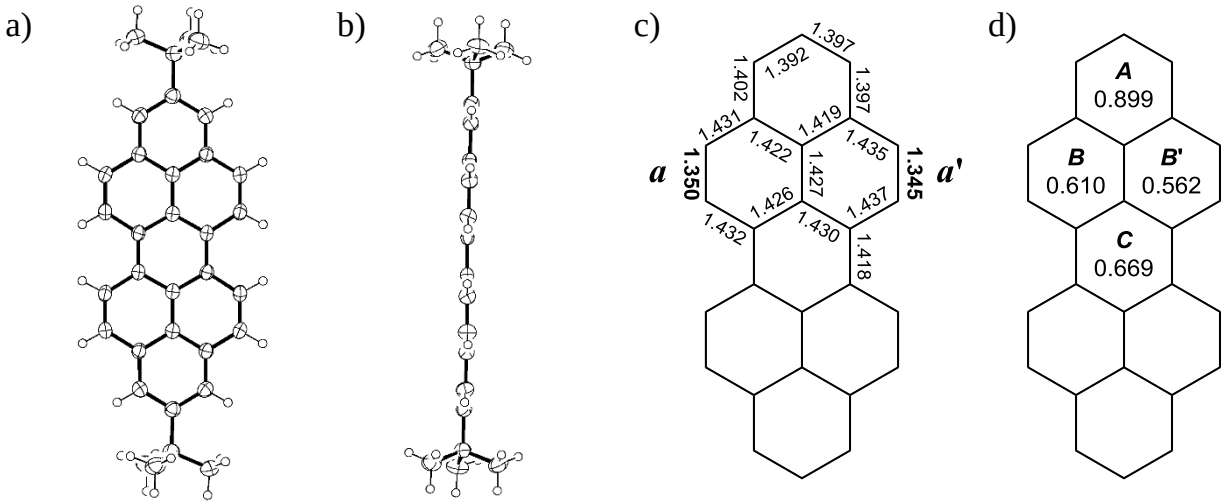

Figure 5.5.5. Ortep drawing of **5.1b** at the 50% probability level. a) Top view and b) side view. c) Bond lengths of peropyrene moiety. d) HOMA values.

Crystal System = triclinic, a = 6.3207(5) Å, b = 10.3801(8) Å, c = 18.1328(14) Å, α = 98.522(2)°, β = 90.597(2)°, γ = 93.252(2)°, V = 1174.44(16) Å^3, Space Group = $P\bar{1}$ (#2), Z = 2, μ(MoKα) = 0.70 cm^{-1}, T = 200 K, $R1$ [F^2>2σ(F^2)] = 0.0463, $wR2$(all data) = 0.1413, S = 1.008, Refl./param. = 5339/313.

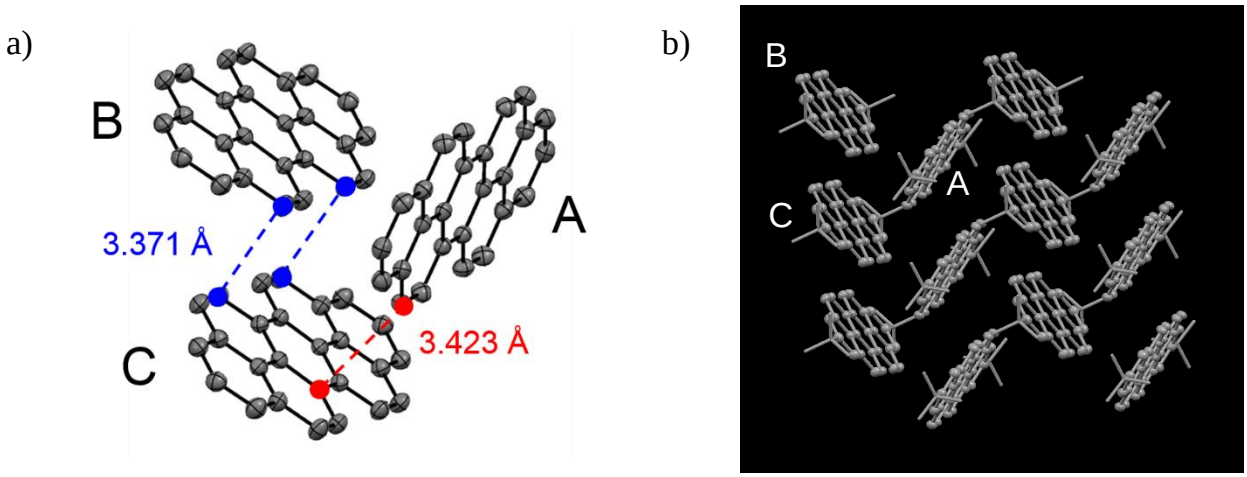

Figure 5.5.6. Packing diagrams of **5.1b**. In Figure 5.5.6a, hydrogen atoms and *tert*-butyl groups were omitted for clarity. In Figure 5.5.6b, hydrogen atoms were omitted and *tert*-butyl groups were shown as capped sticks.

Packing diagrams of **5.1b** were shown in Figure 5.5.6. **5.1b** constructed two-dimensional networks based on the van der Waals interactions between peropyrene moieties as well as CH–π interactions. Shortest intermolecular distance between the molecule ***B*** and the molecule ***C*** (***B***–***C***, as illustrated in Figure 5.5.6) was determined to be 3.371 Å, which is slightly shorter than the sum of the van der Waals radius. In contrast, the intermolecular distances between ***A***–***B*** and ***A***–***C*** were considerably longer than 3.4 Å. It should be noted that the 2D-sheets of **5.1b** were well-separated by the *tert*-butyl groups.

5.5.3 Crystal structure of 2,9-diphenylperopyrene

Recrystallization of 2,9-diphenylperopyrene **5.1c** from hot DMAc (N,N-dimethylacetamide) gave yellow platelet crystals suitable for X-ray crystallographic analysis. Molecular geometry of **5.1c** was shown in Figure 5.5.7. The peropyrene backbone was perfectly flat as observed in **5.1a** and **5.1b**, and twisted angle between phenyl groups at 2,9-positions and peropyrene unit was estimated to be 33.56° on average. With focused on the bond ***a*** and ***a'***, the bond lengths were 1.354(3) Å and 1.361(3) Å, which are comparable with those of **5.1a** and **5.1b**. The HOMA values determined from the bond lengths were represented in Figure 5.5.7d. The HOMA values of ring ***B*** and ***B'*** including bond ***a*** and ***a'*** were determined to be 0.615 and 0.585, respectively.

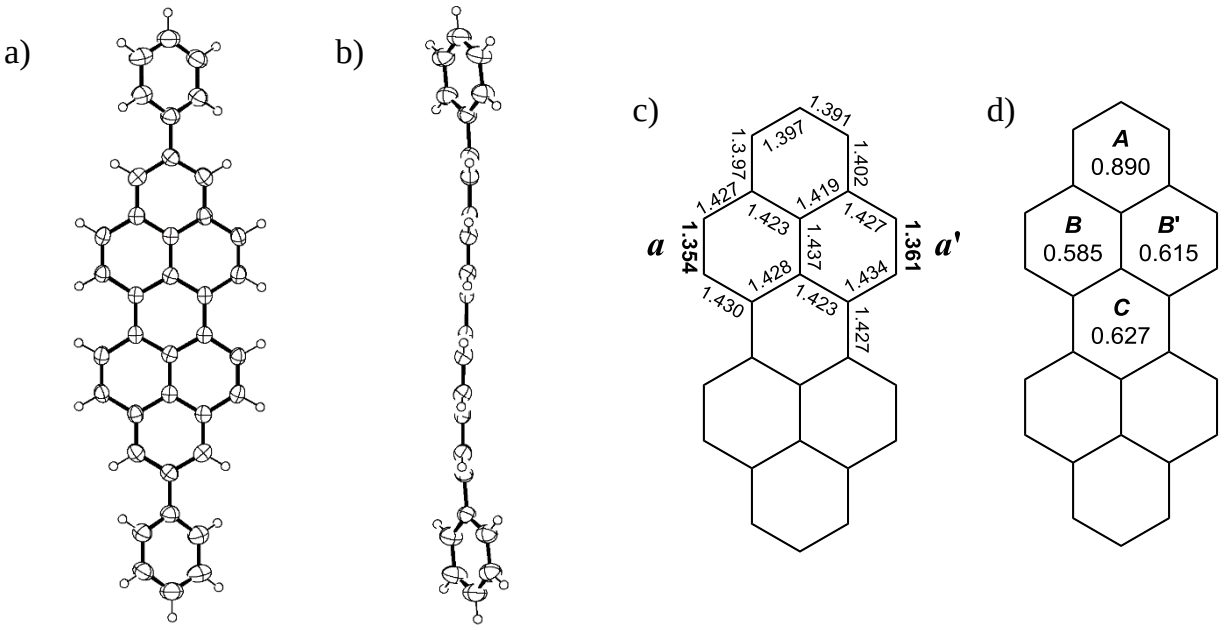

Figure 5.5.7. Ortep drawing of **5.1c** at the 50% probability level. a) Top view and b) side view. c) Bond lengths of peropyrene moiety. d) HOMA values.

Crystal System = orthorhombic, a = 7.1966(9) Å, b = 8.4849(9) Å, c = 39.817(4) Å, V = 2431.3(5) Å^3, Space Group = *Pcab* (#61), Z = 4, μ(MoKα) = 0.74 cm^{-1}, T = 200 K, $R1$ [F^2>2σ(F^2)] = 0.0772, $wR2$(all data) = 0.1571, S = 1.002, Refl./param. = 2765/172.

Packing diagrams of **5.1c** were displayed in Figure 5.5.8. **5.1c** adopted a herringbone packing structure to build two-dimensional networks dominated by the van der Waals interactions and CH–π interactions. Intermolecular distances (3.165–3.379 Å) between molecule ***A*** and molecule ***A'*** (***A***–***A'***, illustrated in Figure 5.5.8) were significantly shorter than the sum of the van der Waals radius (3.4 Å). On the other hand, distances between ***A***(***A'***)–***B*** were considerably shorter (3.294–3.491 Å), suggesting the presence of effective van der Waals interactions between ***A***(***A'***)–***B***. Intermolecular distances observed in the crystal of **5.1c** were noticeably shorter than those in the crystal of **5.1b**, which can be ascribed to the difference of the steric repulsion between phenyl groups and *tert*-butyl groups. Sterically-hindered *tert*-butyl groups prevented shorter contacts of peropyrene moieties. Notably, phenyl groups of **5.1c** adopted face-to-edge configurations due to the CH–π interactions, contributing to the dense packing of **5.1c**.

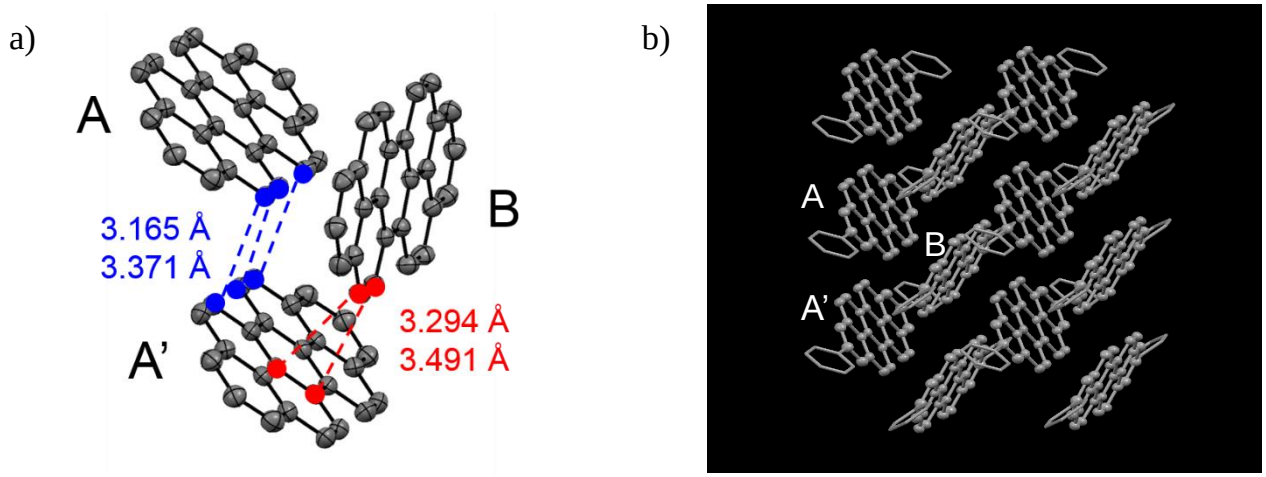

Figure 5.5.8. Packing diagrams of **5.1c**. In Figure 5.5.8a, hydrogen atoms and phenyl groups were omitted for clarity. In Figure 5.5.8b, hydrogen atoms were omitted and phenyl groups were shown as capped sticks.

5.6 Photophysical properties in solid state

Optical properties of novel peropyrene derivatives (**5.1a–c**) in solution state suggested that **5.1a–c** should be promising candidates for investigating the singlet fission. Although parent peropyrene **4.3** showed a suitable energy matching for the singlet fission at the single-molecule level, the formation of face-to-face dimers in crystalline state resulted in the excimer generation in the S_1 state, which prevented the singlet fission process.[10] In contrast, **5.1a–c** gave another crystal structures; that is, the slipped stacking 1D-chain of **5.1a** and the herringbone structures of **5.1b–c**. Thus, the electronic absorption spectra and the fluorescence spectra were measured with single crystals of **5.1a** and **5.1c** as representatives of each crystal structure in order to estimate the crystal structure dependence of photophysical properties.

5.6.1 Photophysical properties of the sipped stacking 1D-chain of 2,9-dibutylperopyrene

The electronic absorption spectra of **5.1a** slipped stacking 1D-chain measured with a single crystal was shown in Figure 5.6.1a, together with the spectrum in solution state. **5.1a** showed an intense absorption band at 447 nm with distinctive vibrational structures in solution state, and the slipped stacking 1D-chain of **5.1a** showed a broad absorption band centered at 451 nm. The spectral resemblance suggests the interactions between neighboring **5.1a** did not affect the electronic structure of **5.1a** in the S_0 state. In contrast, the noticeable difference was observed in the fluorescence spectra. The fluorescence spectrum of **5.1a** recorded with a single crystal of the slipped stacking 1D-chain was exhibited in Figure 5.6.1b, together with that measured in a chlorobenzene solution. **5.1a** showed an intense fluorescence peaks with maximum at 453 nm in solution state, whereas the single crystal of **5.1a** 1D-chain showed a fluorescence peak at 549 nm. The Stokes shift observed in crystalline state was estimated to be 3958 cm^{-1}, which is extraordinarily larger than that in solution state (296 cm^{-1}). The large Stokes shift in crystalline state can be ascribed to the excimer formation between neighboring molecules in the slipped stacking 1D-chain. Parent peropyrene **4.3** also demonstrated a large Stokes shift (4494 cm^{-1}) in crystalline state due to the formation of excimer in the face-to-face dimer.[10] The value of Stokes shift observed in **5.1a** 1D-chain are approximately the same as that of **4.3** dimer, suggesting the exciton in **5.1a** 1D-chain is delocalized over two molecules through the overlap of molecular orbitals. The excimer formation in **5.1a** 1D-chain resulted in the decrease of the S_1 energy from 2.74 eV to 2.26 eV, which indicates that **5.1a** in the slipped stacking 1D-chain no longer satisfies the energetic requirement for the singlet fission ($2E(T_1) \leq E(S_1)$).

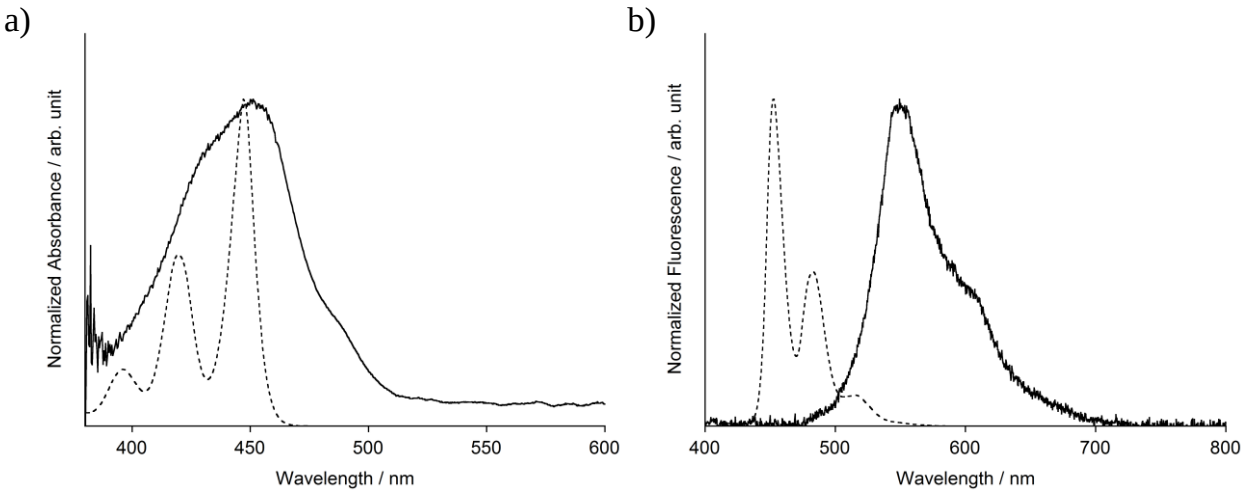

Figure 5.6.1. a) Electronic absorption spectra of **5.1a** recorded in the crystalline state (solid) and the solution state (dashed). b) Fluorescence spectra of **5.1a** recorded in the crystalline state (solid) and the solution state (dashed).

5.6.2 Photophysical properties of the herringbone 2D-network of 2,9-diphenylperopyrene

The electronic absorption spectrum of **5.1c** in the herringbone structure was displayed in Figure 5.6.2a, together with that measured in the solution state. The electronic absorption spectrum of **5.1c** includes the ambiguity in the shorter wavelength region due to the saturation of the absorption band. Fluorescence spectra of the single crystal of **5.1c** constructing herringbone structure was shown in Figure 5.6.2b. The fluorescence spectra of **5.1c** measured in the solution state exhibited an intense peak with distinctive vibrational structures at 455 nm, whereas the single crystal of **5.1c** showed a broad and weak fluorescence peak with maximum at 570 nm. The large Stokes shift (3203 cm^{-1}) observed in the crystalline state would be attributed to the formation of an excimer, inferring the stabilization of the S_1 state in the crystalline form. However, the fluorescence of **5.1c** in the crystalline state was extraordinarily weaker than that of **5.1a** 1D-chain, suggesting another photochemical processes and/or non-radiative decay exist.

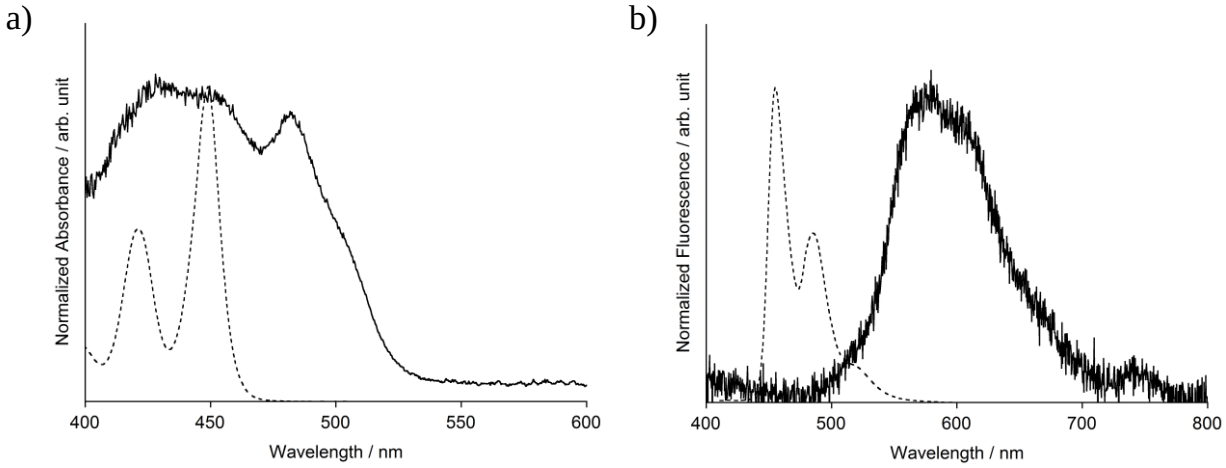

Figure 5.6.2. a) Electronic absorption spectra of **5.1c** recorded in the crystalline state (solid) and the solution state (dashed). b) Fluorescence spectra of **5.1c** recorded in the crystalline state (solid) and the solution state (dashed).

5.7 Electrochemical behavior of peropyrene derivatives

5.7.1 Cyclic voltammetry of peropyrene derivatives

The cyclic voltammogram of 2,9-dibutylperopyrene **5.1a** measured in dichloromethane showed a reversible oxidation wave and an irreversible oxidation wave: ${}^{ox}E_1$ = 0.41 V, ${}^{ox}E_2$ (peak potential) = 0.84 V (all values in V vs Fc/Fc^+; Figure 5.7.1a). First oxidation wave at 0.41 V is attributed to the formation of radical cation of **5.1a** (**5.1a**$^{\bullet+}$). The reversibility suggests that **5.1a**$^{\bullet+}$ is stable in the experimental condition. On the other hand, the oxidation wave observed at 0.84 V would be ascribed to the generation of dication of **5.1a** (**5.1a**$^{2+}$), and the irreversible oxidation wave inferred the instability of **5.1a**$^{2+}$. It should be noted that a characteristic oxidation wave appeared at 0.21 V with recording the cyclic voltammogram at higher scan rate (100 mV s^{-1}). Although the species observed has been

uncertain, the aggregates of **5.1a** would be generated by the oxidation of **5.1a**.

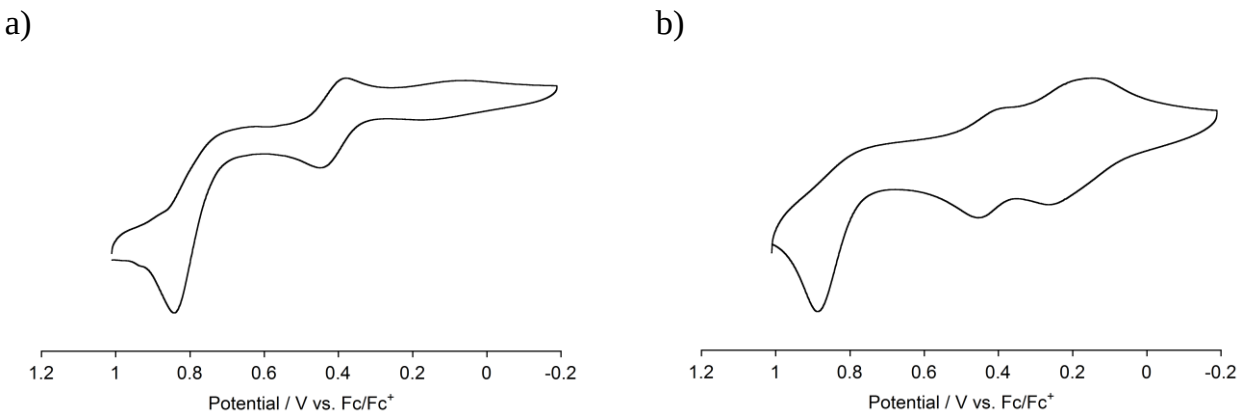

Figure 5.7.1. Cyclic voltammograms of **5.1a** (0.1 mM) measured in 0.1 M $^{n}Bu_4NClO_4$/dichloromethane (V vs. Fc/Fc^+). Scan rate: a) 10 mV s^{-1}, and b) 100 mV s^{-1}.

2,9-Di-*tert*-butylperopyrene **5.1b** gave quite similar voltammograms to those of **5.1a**; that is, a reversible oxidation wave and an irreversible oxidation wave were observed at 0.41 V and 0.88 V respectively. The first wave observed at 0.41 V is ascribed to the oxidation to radical cation of **5.1b** (**5.1b**$^{\bullet+}$), and the next wave at 0.88 V would be attributed to the formation of dication **5.1b**$^{2+}$. These oxidation potentials are almost identical to those of **5.1a**, indicating the effect of substituted groups on the electronic structure of peropyrene is negligible. The cyclic voltammogram recorded at higher scan rate (100 mV s^{-1}) showed a new oxidation wave at 0.17 eV as observed in **5.1a**, which would be ascribed to the molecular aggregates of charged **5.1b**.

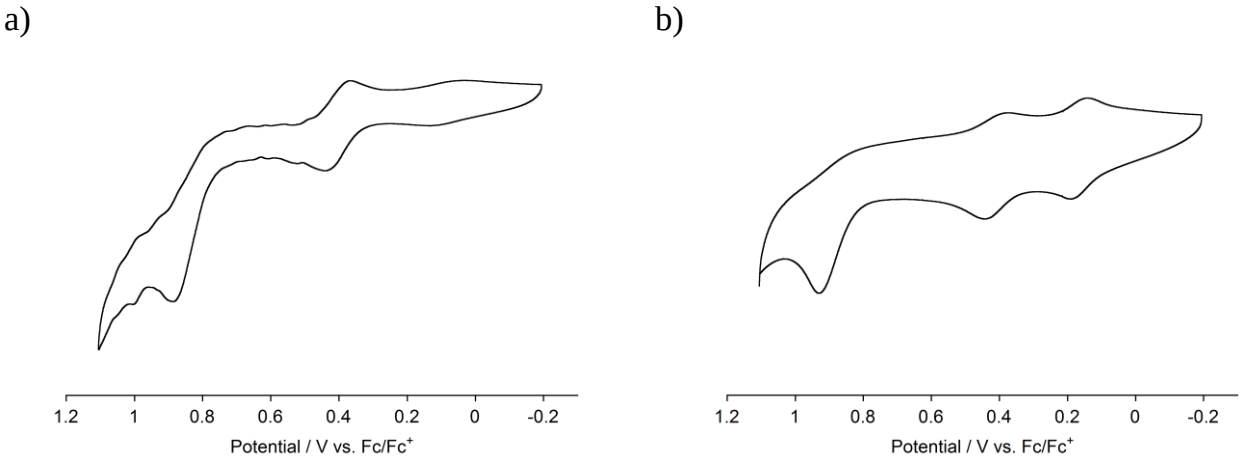

Figure 5.7.2. Cyclic voltammograms of **5.1b** (0.1 mM) measured in 0.1 M $^{n}Bu_4NClO_4$/dichloromethane (V vs. Fc/Fc^+). Scan rate: a) 10 mV s^{-1}, and b) 100 mV s^{-1}.

5.7.2 Electronic absorption spectrum of the radical cation of the peropyrene derivative

The electronic absorption spectrum of the radical cation of parent peropyrene **4.3** (**4.3**$^{\bullet+}$) was reported by Löhmannsröben *et al*.[9] In the literature, **4.3**$^{\bullet+}$ was prepared by using the secondary electron transfer technique with 9,10-dicyanoanthracene (DCA)–biphenyl (BP) system. Laser excitation of DCA resulted in the appearance of an intense absorption band at ~600 nm, together with a broad and weak absorption band in longer wavelength region (~700 nm), indicating the generation of **4.3**$^{\bullet+}$ as a transient species. On the other hand, the cyclic voltammetry measurements of peropyrene derivatives suggests the essential stability of radical cation of peropyrene derivatives. Therefore, chemical oxidation of **5.1a** was conducted with antimony pentachloride ($SbCl_5$) as an oxidant to elucidate the electronic structure of peropyrene derivatives. It should be noted that one electron can be removed from a substrate by adding 1.5 equivalent $SbCl_5$.

A successive addition of $SbCl_5$ to the solution of **5.1a** in dichloromethane resulted in a dramatic change in the electronic absorption spectrum, accompanied by a noticeable color change from yellow to deep blue. As shown in Figure 5.7.3a, an intense peak centered at 616 nm and weak absorption bands at 806 nm and 882 nm were appeared after the addition of 1.5 equivalent $SbCl_5$. An intense band at 444 nm with distinctive vibrational bands, which is ascribed to the neutral **5.1a**, disappeared completely after adding 6 equivalent $SbCl_5$. To assign the species observed in the electronic absorption spectrum, a time-dependent (TD) DFT calculation was conducted with a UB3LYP/6-31G** method by addopting **4.3**$^{\bullet+}$ as a simplified model of peropyrene derivatives. TDDFT calculation predicts that **4.3**$^{\bullet+}$ shows a weak absorption band at 814 nm (f = 0.0078) and an intense absorption peak at 542 nm (f = 0.6457), which is fully consistent with the experimental results of the oxidation titration of **5.1a**. Subsequent addition of excess amount of $SbCl_5$ (225 eq.) resulted in a spectral change (displayed in Figure 5.7.3b); that is, characteristic peaks of **4.3**$^{\bullet+}$ disappeared and new absorption band centered at 650 nm was observed. The spectral feature is partially in line with that of **5.1a**$^{2+}$ predicted by TDDFT calculation, however, the instability of **5.1a**$^{2+}$ prevented the detailed characterization.

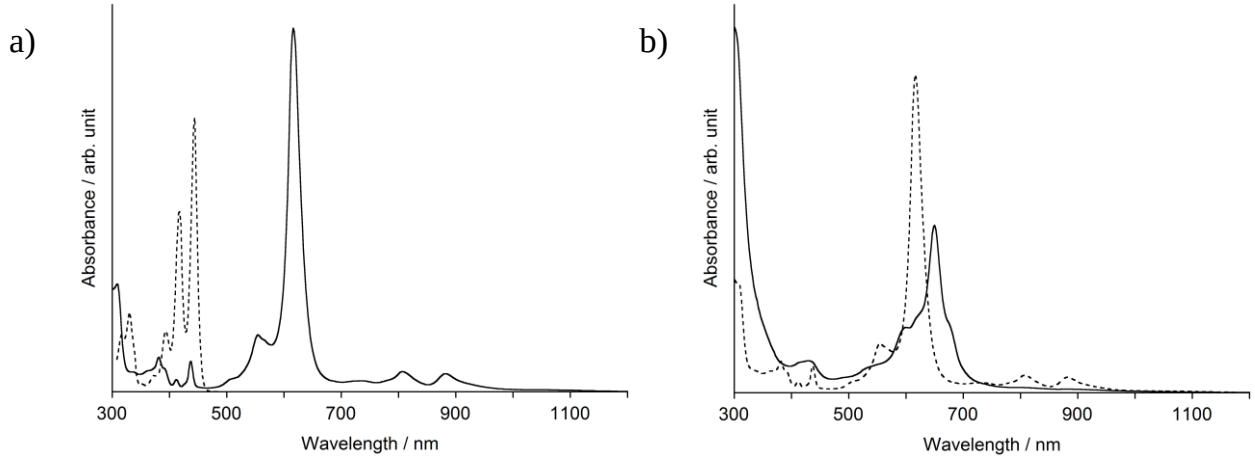

Figure 5.7.3. Electronic absorption spectra of oxidized **5.1a** recorded after the addition of a) 0 eq. (dashed) and 6 eq. (solid) of $SbCl_5$, b) 10 eq. (dashed) and 150 eq. (solid) of $SbCl_5$.

5.8 Conclusion

New peropyrene derivatives (**5.1a–c**) with various substituted groups (R = ^{n}Bu, ^{t}Bu, and Ph) at 2,9-positions were prepared according to a novel synthetic route. The oxidation of dihydroperopyrene derivatives, which were generated from corresponding biphenalenes **5.9a–c** in the presence of *p*-chloranil, gave **5.1a–c** in pure form. The substituted groups at 2,9-positions did not affected the electronic structure and molecular geometry of peropyrene in the single-molecule level, which were fully investigated by spectroscopic analyses with the electronic absorption and fluorescence spectra as well as X-ray crystallographic analyses. Whereas, introduction of substituted groups enabled a successful tuning of the packing diagrams. **5.1a** having *n*-butyl groups gave two crystalline phases; that is, the 2D-network based on the CH–π interactions between face-to-face dimers and the slipped stacking 1D-chain dominated by the van der Waals interactions between π-planes. Furthermore, **5.1b** and **5.1c** gave 2D-structures constructed by the herringbone alignment of peropyrene units. The photophysical properties in solid state depended significantly on the difference of molecular alignment, which were studied by the electronic absorption and fluorescence spectra of single crystals. The 1D-structure composed of **5.1a** showed a noticeable change in the fluorescence spectrum due to the excimer formation, resulting in the undesired S_1 energy shift for the feasibility of the singlet fission. The 2D-network of **5.1b** also showed a significant shift of a fluorescence spectra, whereas the fluorescence quantum yield would be extremely small; thus, the photochemical process should take place in the crystalline state. For deeper understanding of the photochemical process, further investigations with transient absorption measurements are required.

5.9 Experimental

General: All experiments with moisture- or air-sensitive compounds were performed in anhydrous solvents under nitrogen atmosphere in well-dried glassware. Dried solvents were prepared by distillation under nitrogen. Toluene and 1,4-dioxane were dried and distilled over calcium hydride. Anhydrous dichloromethane and THF were purchased from Kanto Chemical Co., Inc. and used without further purification. Commercially available 2,4,6-corydine was used without any further purifications. Column chromatography was performed with silica gel [Silica gel 60N (Kanto Chemical Co., Inc.)]. Melting points were taken on a Yanako MP 500D apparatus. ^{1}H NMR and ^{13}C NMR spectra were obtained on JEOL ECS400 and ECA500 spectrometers. The chemical shifts were recorded by using tetramethylsilane (0.00 ppm) as an internal standard for ^{1}H NMR and $CHCl_3$ (77.00 ppm) for ^{13}C NMR spectra. Positive EI mass spectra were taken by using Shimadzu QP-5050. Data collection for X-ray crystal analysis was performed on Rigaku/Varimax diffractometer (Mo-Kα, λ = 0.71069 Å). The structure was solved with direct methods and refined with full-matrix least squares (teXsan). Electronic absorption spectra and fluorescence spectra were measured in anhydrous chlorobenzene with a JASCO V-570 spectrometer and a JASCO FP-6300 spectrofluorometer, respectively. Cyclic voltammetry measurements were conducted with a BAS CV-50W electrochemical analyzer in a 0.1 M $^{n}Bu_4NClO_4$ dichloromethane solution at room temperature.

General procedure for preparing methyl 3-(4-bromonaphthalen-1-yl)propanoate derivatives (**5.3a–c**)

To a solution of diisopropylamine (1.2 eq.) in THF was added *n*-butyllithium (1.6 M, 1.2 eq.) at −78 °C under nitrogen atmosphere. After stirring for 1 hour, the corresponding methyl acetate derivative (1.2 eq.) was added dropwise over 10 min., and then the reaction mixture was stirred for an additional 1 hour at −78 °C. To the solution was added 1-bromo-4-(bromomethyl)naphthalene **5.2** (1.0 eq.) then the solution was warmed gradually to r.t. After stirred for 4 hours, hydrochloric acid was added for quenching. The organic layer was separated and extracted with ether, washed with brine, dried over anhydrous sodium sulfate. After filtration, the filtrate was evaporated and the residue was purified by column chromatography on silica gel (dichloromethane/hexane 20%) to give **5.3a–c**.

Methyl 2-((4-bromonaphthalen-1-yl)methyl)hexanoate (5.3a)

Colorless oil (72% yield); R_f = 0.38 (dichloromethane/hexane 33%); ^{1}H NMR (400 MHz, $CDCl_3$) δ 8.31-8.27 (m, 1H), 8.02-7.98 (m, 1H), 7.68 (d, *J* = 7.6 Hz, 1H), 7.62-7.56 (m, 2H), 7.15 (d, *J* = 7.6 Hz, 1H), 3.57 (s, 3H), 3.36 (dd, *J* = 14.4 Hz, 8.4 Hz, 1H), 3.17 (dd, *J* = 14.0 Hz, 6.4 Hz, 1H), 2.86-2.78 (m, 1H), 1.79-1.71 (m, 1H), 1.61-1.51 (m, 1H), 1.35-1.22 (m, 4H), 0.87 (t, *J* = 7.2 Hz, 3H); ^{13}C NMR (126 MHz, $CDCl_3$) δ 176.02, 135.63, 133.04, 132.15, 129.42, 128.06, 127.37, 126.92, 126.78, 123.98, 121.70, 51.46, 46.63, 35.53, 32.27, 29.52, 22.59, 13.89.

Methyl 2-((4-bromonaphthalen-1-yl)methyl)-3,3-dimethylbutanoate (5.3b)

White solid (97% yield); mp 96-97 ºC; R_f = 0.46 (dichloromethane/hexane 33%); ^{1}H NMR (400 MHz, $CDCl_3$) δ 8.28 (dd, *J* = 7.6 Hz, 1.2 Hz, 1H), 7.96 (dd, *J* = 7.6 Hz, 2.0 Hz, 1H), 7.65 (d, *J* = 7.6 Hz, 1H), 7.60-7.55 (m, 2H), 7.13 (d, *J* = 7.6 Hz, 1H), 3.42 (s, 3H), 3.39 (dd, *J* = 14.0 Hz, 2.8 Hz, 1H), 3.22 (dd, *J* = 13.6 Hz, 12.4 Hz, 1H), 2.65 (dd, *J* = 12.0 Hz, 2.4 Hz, 1H), 1.15 (s, 9H); ^{13}C NMR (126 MHz, $CDCl_3$) δ 174.79, 136.24, 133.01, 132.17, 129.50, 128.10, 127.25, 126.84, 126.70, 123.79, 121.58, 57.19, 50.84, 33.58, 30.88, 27.78; EI-MS *m/z* 350 ($[M+1]^+$), 348 ($[M-1]^+$); Anal. Calcd for $C_{18}H_{21}BrO_2$: C, 61.90; H, 6.06. Found: C, 61.84; H, 5.92.

Methyl 3-(4-bromonaphthalen-1-yl)-2-phenylpropanoate (5.3c)

Colorless oil (95% yield); R_f = 0.32 (dichloromethane/hexane 33%); ^{1}H NMR (400 MHz, $CDCl_3$) δ 8.29 (dd, *J* = 7.2 Hz, 2.4 Hz, 1H), 8.01 (dd, *J* = 7.2 Hz, 2.0 Hz, 1H), 7.61-7.55 (m, 3H), 7.34-7.27 (m, 5H), 7.05 (d, *J* = 7.6 Hz, 1H), 4.01 (dd, *J* = 8.4 Hz, 6.4 Hz, 1H), 3.87 (dd, *J* = 13.6 Hz, 8.4 Hz, 1H), 3.60 (s, 3H), 3.43 (dd, *J* = 14.0 Hz, 6.4 Hz, 1H); ^{13}C NMR (126 MHz, $CDCl_3$) δ 173.69, 138.58, 135.00, 132.92, 132.15, 129.42, 128.78, 128.15, 127.80, 127.59, 127.55, 126.92, 126.90, 123.82, 121.82, 52.21, 52.09, 36.71.

Synthetic procedures for synthesizing 3-(4-bromonaphthalen-1-yl)propanoic acid derivatives (**5.4a–c**)

Method A: To a solution of the corresponding ester (**5.3a** and **5.3c**, 1.0 eq.) in ethanol was added 10% aqueous sodium hydroxide (20 eq.) and heated at 90 ºC for 14 hours. After cooled to room temperature, the reaction mixture was poured into 6 M hydrochloric acid and the product was extracted with ether. The organic layer was separated and washed with brine, dried over anhydrous sodium sulfate. After filtration, the filtrate was evaporated, then the residue was collected by filtration and washed with dichloromethane-hexane to give **5.4a** and **5.4c**.

2-((4-Bromonaphthalen-1-yl)methyl)hexanoic acid (5.4a)

White solid (98% yield); mp 108-110 ºC; R_f = 0.69 (ethyl acetate/hexane 50%); ^{1}H NMR (400 MHz, Acetone-d_6) δ 10.63 (broad s, 1H), 8.28-8.24 (m, 1H), 8.22-8.18 (m, 1H), 7.77 (d, *J* = 8.0 Hz, 1H), 7.71-7.65 (m, 2H), 7.33 (d, *J* = 7.6 Hz, 1H), 3.39 (dd, *J* = 14.0 Hz, 8.8 Hz, 1H), 3.27 (dd, *J* = 14.0 Hz, 6.0 Hz, 1H), 2.87-2.80 (m, 1H), 1.81-1.71 (m, 1H), 1.69-1.61 (m, 1H), 1.46-1.25 (m, 4H), 0.87 (t, *J* = 7.2 Hz, 3H); ^{13}C NMR (126 MHz, Acetone-d_6) δ 176.64, 137.55, 134.27, 133.00, 130.58, 128.69, 128.53, 128.25, 128.02, 125.52, 121.91, 47.34, 36.25, 33.20, 30.40, 23.45, 14.34; EI-MS *m/z* 336 ([M+1]$^+$), 334 ([M-1]$^+$); Anal. Calcd for $C_{17}H_{19}BrO_2$: C, 60.91; H, 5.71. Found: C, 60.87; H, 5.58.

3-(4-Bromonaphthalen-1-yl)-2-phenylpropanoic acid (5.4c)

White solid (61% yield); mp 200-201 ºC; R_f = 0.31 (ethyl acetate/hexane 50%); ^{1}H NMR (400 MHz, Acetone-d_6) δ 10.89 (broad s, 1H), 8.28-8.21 (m, 2H), 7.71-7.68 (m, 3H), 7.40 (d, *J* = 7.2 Hz, 2H), 7.33 (t, *J* = 7.2 Hz, 2H), 7.27 (t, *J* = 7.2 Hz, 1H), 7.22 (d, *J* = 7.6 Hz, 1H), 4.11 (dd, *J* = 8.4 Hz, 6.8 Hz, 1H), 3.91 (dd, *J* = 14.4 Hz, 8.4 Hz, 1H), 3.49 (dd, *J* = 14.8 Hz, 6.8 Hz, 1H); ^{13}C NMR (126 MHz, Acetone-d_6) δ 174.52, 140.28, 136.97, 134.23, 132.97, 130.50, 129.61, 129.00, 128.84, 128.56, 128.32, 128.26, 128.15, 125.47, 121.99, 52.93, 37.28; EI-MS *m/z* 356 ([M+1]$^+$), 354 ([M-1]$^+$); Anal. Calcd for $C_{19}H_{15}BrO_2$: C, 64.24; H, 4.26. Found: C, 64.07; H, 4.27.

Method B: A mixture of methyl 2-((4-bromonaphthalen-1-yl)methyl)-3,3-dimethylbutanoate **5.3b** (1.0 eq.) and lithium iodide (10 eq.) in 2,4,6-corydine was heated at 185 °C for 3 hours under nitrogen atmosphere. After distillation under reduced pressure, the residue was poured into hydrochloric acid and the product was extracted with ether. The organic layer was washed with brine and dried over anhydrous sodium sulfate. After filtration, the filtrate was evaporated, and the residual solid was collected by filtration and washed with hexane to give **5.4b**.

2-((4-Bromonaphthalen-1-yl)methyl)-3,3-dimethylbutanoic acid (5.4b)

White solid (93% yield); mp 153-154 ºC; R_f = 0.73 (ethyl acetate/hexane 50%); ^{1}H NMR (400 MHz, Acetone-d_6) δ 10.45 (broad s, 1H), 8.25 (dd, *J* = 7.6 Hz, 2.0 Hz, 1H), 8.14 (dd, *J* = 7.6 Hz, 2.0 Hz, 1H), 7.74 (d, *J* = 7.6 Hz, 1H), 7.69-7.65 (m, 2H), 7.28 (d, *J* = 8.0 Hz, 1H), 3.49 (dd, *J* = 13.6 Hz, 2.4 Hz, 1H), 3.24 (dd, *J* = 13.2 Hz, 11.6 Hz, 1H), 2.67 (dd, *J* = 12.4 Hz, 2.4 Hz, 1H), 1.19 (s, 9H); ^{13}C NMR (126 MHz, Acetone-d_6) δ 175.54, 138.09, 134.25, 133.02, 130.63, 128.67, 128.57, 128.18, 127.97, 125.39, 121.83, 57.80, 33.95, 31.70, 28.29; EI-MS *m/z* 336 ([M+1]$^+$), 334 ([M-1]$^+$); Anal. Calcd for $C_{17}H_{19}BrO_2$: C, 60.91; H, 5.71. Found: C, 60.72; H, 5.63.

General procedure for Friedel-Crafts cyclization to synthesize 6-bromo-2,3-dihydro-1*H*-phenalen-1-one derivatives **(5.5a–c)**

A solution of the corresponding propanoic acid derivatives **5.4a–c** (1 eq.) in oxalyl chloride was heated at 55 ºC for 14 hours. The reaction mixture was concentrated *in vacuo* and the residue was dissolved in dichloromethane under nitrogen atmosphere. To the solution was added aluminum chloride (2 eq.) at −78 ºC then the reaction mixture was warmed gradually to −30 ºC. After stirring for 3 hours, the reaction was quenched by pouring into 1 M hydrochloric

acid and the product was extracted with dichloromethane. The organic layer was separated and washed with aqueous sodium carbonate, dried over anhydrous sodium sulfate. After filtration, the filtrate was evaporated and the residue was purified by column chromatography on silica gel (dichloromethane/hexane 70% for **5.5a** and **5.5c**, ethyl acetate/hexane 5% for **5.5b**) to give **5.5a-c**.

6-Bromo-2-butyl-2,3-dihydro-1*H*-phenalen-1-one (5.5a)

White solid (82% yield); mp 52-53 ºC; R_f = 0.54 (dichloromethane/hexane 67%); ^{1}H NMR (400 MHz, $CDCl_3$) δ 8.47 (dd, *J* = 8.4 Hz, 1.2 Hz, 1H), 8.23 (dd, *J* = 7.2 Hz, 1.2 Hz, 1H), 7.77 (d, *J* = 7.2 Hz, 1H), 7.71 (dd, *J* = 8.4 Hz, 7.2 Hz, 1H), 7.30 (dt, *J* = 7.6 Hz, 1.2 Hz, 1H), 3.46 (ddd, *J* = 16.0 Hz, 6.0 Hz, 1.2 Hz, 1H), 3.14 (ddd, *J* = 16.0 Hz, 9.2 Hz, 1.2 Hz, 1H), 2.93-2.86 (m, 1H), 1.93-1.84 (m, 1H), 1.55-1.29 (m, 5H), 0.90 (t, *J* = 7.2 Hz, 3H); ^{13}C NMR (126 MHz, $CDCl_3$) δ 200.18, 132.95, 132.85, 132.38, 131.61, 130.13, 129.99, 127.13, 126.28, 126.19, 120.85, 47.16, 33.95, 29.66, 29.24, 22.67, 13.95; EI-MS *m/z* 318 ($[M+1]^+$), 316 ($[M-1]^+$); Anal. Calcd for $C_{17}H_{17}BrO$: C, 64.37; H, 5.40. Found: C, 64.37; H, 5.31.

6-Bromo-2-(*tert*-butyl)-2,3-dihydro-1*H*-phenalen-1-one (5.5b)

White solid (51% yield); mp 102-103 ºC; R_f = 0.38 (ethyl acetate/hexane 5%); ^{1}H NMR (400 MHz, $CDCl_3$) δ 8.44 (d, *J* = 8.4 Hz, 1H), 8.18 (d, *J* = 7.2 Hz, 1H), 7.75 (d, *J* = 7.6 Hz, 1H), 7.70 (t, *J* = 8.0 Hz, 1H), 7.28 (d, *J* = 7.6 Hz, 1H), 3.48 (dd, *J* = 16.8 Hz, 6.0 Hz, 1H), 3.36 (dd, *J* = 16.4 Hz, 6.8 Hz, 1H), 2.75 (t, *J* = 6.8 Hz, 1H), 0.99 (s, 9H); ^{13}C NMR (126 MHz, $CDCl_3$) δ 199.70, 134.04, 132.55 (2C), 131.81, 131.47, 130.22, 127.18, 125.68, 125.58, 120.48, 56.43, 33.51, 30.56, 20.23; EI-MS *m/z* 318 ($[M+1]^+$), 316 ($[M-1]^+$); Anal. Calcd for $C_{17}H_{17}BrO$: C, 64.37; H, 5.40. Found: C, 64.22; H, 5.38.

6-Bromo-2-phenyl-2,3-dihydro-1*H*-phenalen-1-one (5.5c)

White solid (69% yield); mp 166-167 ºC; R_f = 0.45 (dichloromethane/hexane 67%); ^{1}H NMR (400 MHz, $CDCl_3$) δ 8.51 (d, *J* = 8.4 Hz, 1H), 8.28 (d, *J* = 7.2 Hz, 1H), 7.81 (d, *J* = 7.6 Hz, 1H), 7.73 (t, *J* = 8.0 Hz, 1H), 7.37-7.24 (m, 6H), 4.24 (dd, *J* = 9.2 Hz, 6.4 Hz, 1H), 3.77-3.64 (m, 2H); ^{13}C NMR (126 MHz, $CDCl_3$) δ 197.25, 138.03, 133.22, 132.72, 132.44, 131.71, 130.28, 130.00, 128.61, 128.23, 127.32, 127.24, 126.89, 126.19, 121.14, 53.08, 35.39; EI-MS *m/z* 338 ($[M+1]^+$), 336 ($[M-1]^+$); Anal. Calcd for $C_{19}H_{13}BrO$: C, 67.67; H, 3.89. Found: C, 67.47; H, 3.76.

General procedure for Miyaura borylation to prepare 6-(4,4,5,5-tetramethyl-1,3,2-dioxaborolan-2-yl)-2,3-dihydro-1*H*-phenalen-1-one derivatives (**5.6a–c**)

A mixture of corresponding 6-bromo-2,3-dihydro-1*H*-phenalen-1-one derivatives **5.6a–c** (1 eq.), bis(pinacolato)diboron (1.5 eq.), [1,1'-bis(diphenylphosphino)ferrocene]palladium(II) dichloride dichloromethane complex (0.1 eq.) and potassium acetate (3 eq.) was heated in 1,4-dioxane at 80 ºC under nitrogen atmosphere for 2 hours. After cooled down to room temperature, the reaction mixture was poured into water. The organic layer was separated and extracted with dichloromethane, washed with brine, dried over sodium sulfate. After filtration, the filtrate was evaporated and the residue was purified by column chromatography on silica gel

(dichloromethane/hexane 50%) to give **5.6a–c**.

2-Butyl-6-(4,4,5,5-tetramethyl-1,3,2-dioxaborolan-2-yl)-2,3-dihydro-1*H*-phenalen-1-one (5.6a)

Pale yellow oil (74% yield); R_f = 0.50 (dichloromethane/hexane 67%); ^{1}H NMR (400 MHz, $CDCl_3$) δ 9.03 (dd, *J* = 8.4 Hz, 1.2 Hz, 1H), 8.18 (dd, *J* = 7.2 Hz, 1.2 Hz, 1H), 8.08 (d, *J* = 6.8 Hz, 1H), 7.65 (dd, *J* = 8.0 Hz, 6.8 Hz, 1H), 7.45 (dt, *J* = 7.2 Hz, 1.2 Hz, 1H), 3.51 (ddd, *J* = 16.0 Hz, 5.6 Hz, 0.8 Hz, 1H), 3.19 (ddd, *J* = 16.0 Hz, 8.8 Hz, 1.2 Hz, 1H), 2.93-2.86 (m, 1H), 1.91-1.83 (m, 1H), 1.54-1.27 (m, 17H), 0.89 (t, *J* = 7.2 Hz, 3H); ^{13}C NMR (126 MHz, $CDCl_3$) δ 201.19, 136.60, 136.56, 136.05, 134.66, 131.07, 129.75, 126.27, 125.20, 125.14, 83.86, 47.23, 34.58, 29.83, 29.31, 24.95, 24.92, 22.70, 13.97.

2-(*Tert*-butyl)-6-(4,4,5,5-tetramethyl-1,3,2-dioxaborolan-2-yl)-2,3-dihydro-1*H*-phenalen-1-one (5.6b)

White solid (72% yield); mp < 45 ºC; R_f = 0.50 (dichloromethane/hexane 67%); ^{1}H NMR (400 MHz, $CDCl_3$) δ 9.00 (d, *J* = 7.6 Hz, 1H), 8.13 (d, *J* = 6.8 Hz, 1H), 8.07 (d, *J* = 6.8 Hz, 1H), 7.64 (t, *J* = 7.6 Hz, 1H), 7.44 (d, *J* = 7.2 Hz, 1H), 3.54 (dd, *J* = 16.8 Hz, 6.4 Hz, 1H), 3.42 (dd, *J* = 16.8 Hz, 6.4 Hz, 1H), 2.75 (t, *J* = 6.4 Hz, 1H), 1.43 (s, 12 H), 0.97 (s, 9H); ^{13}C NMR (126 MHz, $CDCl_3$) δ 200.71, 137.68, 136.48, 136.18, 134.37, 131.60, 131.35, 126.31, 124.61, 124.47, 83.85, 56.52, 33.60, 31.23, 28.30, 24.98, 24.94.

2-Phenyl-6-(4,4,5,5-tetramethyl-1,3,2-dioxaborolan-2-yl)-2,3-dihydro-1*H*-phenalen-1-one (5.6c)

Pale yellow solid (64% yield); mp < 45 ºC; R_f = 0.36 (dichloromethane/hexane 67%); ^{1}H NMR (400 MHz, $CDCl_3$) δ 9.07 (d, *J* = 7.6 Hz, 1H), 8.23 (d, *J* = 6.4 Hz, 1H), 8.12 (d, *J* = 7.2 Hz, 1H), 7.67 (t, *J* = 7.6 Hz, 1H), 7.50 (d, *J* = 6.8 Hz, 1H), 7.32-7.22 (m, 5H), 4.23 (dd, *J* = 8.8 Hz, 6.4 Hz, 1H), 3.81-3.68 (m, 2H), 1.44 (s, 12H).

Synthetic procedure for Suzuki coupling to prepare a diastereomer mixture of 4,4',5,5'-tetrahydro-6*H*,6'*H*-[1,1'-biphenalene]-6,6'-dione derivatives (**5.7a–c**)

Method A: A mixture of corresponding boronic ester derivatives (**5.6a** and **5.6b**, 1 eq.) and 6-bromo-2,3-dihydro-1*H*-phenalen-1-one derivatives (**5.5a** and **5.5b**, 1.1 eq.), tetrakis(triphenylphosphine)palladium(0) (5 mol%), potassium carbonate (2 eq.) in toluene/ethanol/water (4/1/1) was heated at 70 ºC under nitrogen atmosphere for 12 hours. After cooled down to room temperature, the reaction mixture was poured into water and the product was extracted with dichloromethane then the organic layer was separated, washed with brine, and dried over sodium sulfate. After filtration, the filtrate was evaporated and the residue was purified by column chromatography on silica gel (dichloromethane/hexane 80%) to give **5.7a** and **5.7c**.

5,5'-Dibutyl-4,4',5,5'-tetrahydro-6*H*,6'*H*-[1,1'-biphenalene]-6,6'-dione (5.7a)

White solid (74% yield); mp 163-164 ºC; R_f = 0.35 (dichloromethane/hexane 80%); ^{1}H NMR (400 MHz, $CDCl_3$) δ 8.18 (d, *J* = 7.2 Hz, 2H), 7.64-7.61 (m, 2H), 7.57 (d, *J* = 7.2 Hz, 2H), 7.50 (t, *J* = 7.2 Hz, 2H), 7.45-7.40 (m, 2H), 3.64-3.57 (m, 2H), 3.33-3.25 (m, 2H), 3.03-2.97 (m, 2H), 2.05-1.95 (m, 4H), 1.64-1.36 (m, 8H), 0.97-0.92 (m, 6H); EI-MS *m/z* 474 ($[M]^+$); Anal. Calcd for $C_{34}H_{34}O_2$: C, 86.04; H, 7.22. Found: C, 86.04; H, 7.21.

5,5'-Di-*tert*-butyl-4,4',5,5'-tetrahydro-6*H*,6'*H*-[1,1'-biphenalene]-6,6'-dione (5.7b)

White solid (78% yield); mp > 198 ºC (decomp.); R_f = 0.44 (dichloromethane/hexane 80%); ^{1}H NMR (400 MHz, $CDCl_3$) δ 8.13 (d, *J* = 5.6 Hz, 2H), 7.59-7.55 (m, 4H), 7.51-7.47 (m, 2H), 7.42-7.38 (m, 2H), 3.66-3.61 (m, 2H), 3.53-3.48 (m, 2H), 2.88-2.83 (m, 1H), 1.10 (s, 9H), 1.07 (s, 9H).

Method B: A mixture of corresponding boronic ester derivatives (**5.6c**, 1 eq.) and 6-bromo-2,3-dihydro-1*H*-phenalen-1-one derivatives (**5.5c**, 1.1 eq.), tetrakis(triphenylphosphine)palladium(0) (5 mol%), potassium carbonate (2 eq.) in toluene/ethanol/water (4/1/1) was heated at 70 ºC under nitrogen atmosphere for 12 hours. After cooled down to room temperature, the precipitate formed was collected by filtration and washed with water, ethanol and dichloromethane. The crude product **5.7c** was used in the next step without any further purifications.

5,5'-Diphenyl-4,4',5,5'-tetrahydro-6*H*,6'*H*-[1,1'-biphenalene]-6,6'-dione (5.7c)

Gray solid (crude quant); mp > 198 ºC (decomp.); R_f = 0.42 (dichloromethane/hexane 80%); ^{1}H NMR (400 MHz, $CDCl_3$) δ 8.25 (d, *J* = 6.8 Hz, 2H), 7.69-7.63 (m, 4H), 7.57-7.52 (m, 2H), 7.46 (t, *J* = 7.6 Hz, 2H), 7.42-7.30 (m, 10H), 4.38-4.32 (m, 2H), 3.94-3.77 (m, 4H).

Synthetic procedure for the reduction to yield a diastereomer mixture of 5,5',6,6'-tetrahydro-4*H*,4'*H*-[1,1'-biphenalene]-6,6'-diol derivatives (**5.8a–c**)

Method A: A mixture of 4,4',5,5'-tetrahydro-6*H*,6'*H*-[1,1'-biphenalene]-6,6'-dione derivatives (**5.7a** and **5.7c**, 1 eq.) and sodium borohydride (10 eq.) in dichloromethane/ethanol (2/1) was stirred for 4 hours under nitrogen atmosphere. The reaction mixture was quenched by pouring into aqueous ammonium chloride and the product was extracted with dichloromethane, then the organic layer was separated and washed with brine, dried over sodium sulfate. After filtration, filtrate was evaporated and the residue was purified by column chromatography on hydrous (6%) silica gel (dichloromethane) to give **5.8a** and **5.8c**.

Method B: To a solution of 5,5'-di-*tert*-butyl-4,4',5,5'-tetrahydro-6*H*,6'*H*-[1,1'-biphenalene]-6,6'-dione **5.7b** (1 eq.) in THF was added lithium aluminumhydride (3 eq.) under nitrogen atmosphere. After stirring for 1 hour, the reaction mixture was quenched with water and the product was extracted with dichloromethane. The organic layer was separated and washed with brine, dried over sodium sulfate. After filtration, filtrate was evaporated and the residue was purified by column chromatography on hydrous (6%) silica gel (dichloromethane) to give **5.8b**.

General procedure for synthesizing peropyrene derivatives (**5.1a–c**)

A mixture of corresponding 5,5',6,6'-tetrahydro-4*H*,4'*H*-[1,1'-biphenalene]-6,6'-diol derivatives **5.8a–c** (1 eq.) and *p*-toluenesulfonic acid monohydrate was heated in toluene at 120 ºC for 5 min. under nitrogen atmosphere. After cooled to 0 ºC, the reaction mixture was filtered rapidly on hydrous (6%) silica gel to give **5.9a–c**. The crude product was used in next step without any further purifications.

To a solution of crude **5.9a–c** in dichloromethane was added *p*-chloranil (2 eq.) under nitrogen atmosphere and the reaction mixture was stirred for 3 hours. The precipitate formed was collected by filtration then washed with acetone and dichloromethane to give **5.1a–c**. The crude product was purified by sublimation followed by recrystallization.

2,9-Dibutylperopyrene (5.1a)

Yellow solid (70% yield); mp. > 300 ºC; ^{1}H NMR (400 MHz, $CDCl_3$) δ 9.22 (d, J = 9.6 Hz, 4H), 8.35 (d, J = 9.6 Hz, 4H), 8.17 (s, 4H), 3.14 (t, J = 8.0 Hz, 4H), 1.91 (quin, J = 7.6 Hz, 4H), 1.52 (sex, J = 7.6 Hz, 4H), 1.02 (t, J = 7.2 Hz, 6H); EI-MS *m/z* 438 (M^+); Anal. Calcd for $C_{34}H_{30}$: C, 93.11; H, 6.89. Found: C, 93.12; H, 6.80.

2,9-Di-*tert*-butylperopyrene (5.1b)

Yellow solid (20% yield); mp. > 300 ºC; ^{1}H NMR (400 MHz, $CDCl_3$) δ 9.22 (d, J = 9.2 Hz, 4H), 8.39-8.37 (m, 8H), 1.65 (s, 18H).

2,9-Diphenylperopyrene (5.1c)

Yellow solid (90% yield); mp. > 300 ºC; ^{1}H NMR (400 MHz, $CDCl_3$) δ 9.32 (d, J = 9.2 Hz, 4H), 8.61 (s, 4H), 8.50 (d, J = 9.2 Hz, 4H), 7.99 (d, J = 7.6 Hz, 4H), 7.61 (t, J = 7.6 Hz, 4H), 7.48 (t, J = 7.6 Hz, 2H).

5.10 References

(1) Burdett, J. J.; Müller, A. M.; Gosztola, D.; Bardeen, C. J. *J. Chem. Phys.* **2010**, *133* (14), 144506.

(2) Wang, C.; Tauber, M. J. *J. Am. Chem. Soc.* **2010**, *132* (40), 13988.

(3) Johnson, J. C.; Nozik, A. J.; Michl, J. *J. Am. Chem. Soc.* **2010**, *132* (46), 16302.

(4) Eaton, S. W.; Shoer, L. E.; Karlen, S. D.; Dyar, S. M.; Margulies, E. A.; Veldkamp, B. S.; Ramanan, C.; Hartzler, D. A.; Savikhin, S.; Marks, T. J.; Wasielewski, M. R. *J. Am. Chem. Soc* **2013**, *135* (39), 14701.

(5) Yost, S. R.; Lee, J.; Wilson, M. W. B.; Wu, T.; McMahon, D. P.; Parkhurst, R. R.; Thompson, N. J.; Congreve, D. N.; Rao, A.; Johnson, K.; Sfeir, M. Y.; Bawendi, M. G.; Swager, T. M.; Friend, R. H.; Baldo, M. A.; Van Voorhis, T. *Nat. Chem.* **2014**, *6* (6), 492.

(6) Eaton, S. W.; Miller, S. A.; Margulies, E. A.; Shoer, L. E.; Schaller, R. D.; Wasielewski, M. R. *J. Phys. Chem. A* **2015**, *119* (18), 4151.

(7) Sanders, S. N.; Kumarasamy, E.; Pun, A. B.; Trinh, M. T.; Choi, B.; Xia, J.; Taffet, E. J.; Low, J. Z.; Miller, J. R.; Roy, X.; Zhu, X.-Y.; Steigerwald, M. L.; Sfeir, M. Y.; Campos, L. M. *J. Am. Chem. Soc.* **2015**, *137* (28), 8965.

(8) Smith, M. B.; Michl, J. *Chem. Rev.* **2010**, *110* (11), 6891.

(9) Wenzel, U.; Löhmannsröben, H.-G. *J. Photochem. Photobiol. A Chem.* **1996**, *96* (1-3), 13.

(10) Nichols, V. M.; Rodriguez, M. T.; Piland, G. B.; Tham, F.; Nesterov, V. N.; Youngblood, W. J.; Bardeen, C. J. *J. Phys. Chem. C* **2013**, *117* (33), 16802.

(11) Clar, E. *Ber. Dtsch. Chem. Ges.* **1943**, *75*, 458.

(12) Clar, E.; Fell, G. S.; Ironside, C. T.; Balsillie, A. *Tetrahedron* **1960**, *10* (1–2), 26.

(13) Pogodin, S.; Agranat, I. *J. Am. Chem. Soc.* **2003**, *125* (42), 12829.

(14) Minami, T.; Nakano, M. *J. Phys. Chem. Lett.* **2012**, *3* (2), 145.

(15) Kruszewski, J.; Krygowski, T. M. *Tetrahedron Lett.* **1972**, *13* (36), 3839.

(16) Krygowski, T. M. *J. Chem. Inf. Model.* **1993**, *33* (1), 70.

List of Publications

1. Original papers

3) "Biphenalenylidene: Isolation and Characterization of the Reactive Intermediate on the Decomposition Pathway of Phenalenyl Radical"
Kazuyuki Uchida, Soichi Ito, Masayoshi Nakano, Manabu Abe, and Takashi Kubo, *J. Am. Chem. Soc.* DOI: 10.1021/jacs.5b13033.

2) "Evidence of σ- and π-Dimerization in a Series of Phenalenyls"
Zhongyu Mou, Kazuyuki Uchida, Takashi Kubo, and Miklos Kertesz, *J. Am. Chem. Soc.* **2014**, *136*, 18009–18022.

1) "Dual Association Modes of the 2,5,8-Tris(pentafluorophenyl)phenalenyl Radical"
Kazuyuki Uchida, Yasukazu Hirao, Hiroyuki Kurata, Takashi Kubo, Sayaka Hatano, and Katsuya Inoue, *Chem. Asian. J.* **2014**, *9*, 1823–1829.

2. Related papers

2) "Design and Synthesis of New Stable Fluorenyl-Based Radicals"
Yi Tian, Kazuyuki Uchida, Hiroyuki Kurata, Yasukazu Hirao, Tomohiko Nishiuchi, and Takashi Kubo, *J. Am. Chem. Soc.* **2014**, *136*, 12784–12793.

1) "Direct Observation of Energy Band Development in a One-Dimensional Biradical Molecular Chain by Ultraviolet Photoemission Spectroscopy"
Harunobu Koike, Takashi Kubo, Kazuyuki Uchida, Masayuki Chikamatsu, Reiko Azumi, Kazuhiko Mase, and Kaname Kanai, *Appl. Phys. Lett.* **2013**, *102*, 134103-1–134103-4.

Acknowledgement

The studies described in this thesis have been performed under the direction of Professor Takashi Kubo at the Department of Chemistry, Graduate School of Science, Osaka University.

The author wishes to express his grateful gratitude to Professor Takashi Kubo for his continuous guidance, helpful suggestion and encouragement throughout the work. The author wishes to thank Dr. Tomohiko Nishiuchi, Dr. Yasukazu Hirao, Dr. Kouzou Matsumoto (he promoted to Senshu University), and Dr Hiroyuki Kurata (he promoted to Fukui University of Technology) for their kind advice and encouragement.

The author is grateful indebted to Professor Michael M. Haley in University of Oregon (United States) for offering him chance to study abroad for three months (2014.01 ~ 2014.03).

The author is deeply grateful to Professor Masayoshi Nakano (Department of Materials Engineering and Science, Graduate School of Engineering Science, Osaka University) and Professor Miklos Kertesz (Department of Chemistry, Georgetown University) for their valuable suggestions and guidance for quantum chemical calculations, and to Dr. Sachiko Tojo and Professor Tetsuro Majima (The Institute of Scientific and Industrial Research (SANKEN), Osaka University) for the variable temperature electronic absorption measurements, and to Professor Manabu Abe (Department of Chemistry, Graduate School of Science, Hiroshima University) for the nanosecond time-resolved difference absorption measurements, and to Dr. Kenji Kamada (Natural Institute of Advanced Industrial Science and Technology) for the electronic absorption and fluorescence measurements, and to Professor Akihito Hashidzume (Department of Macromolecular Science, Graduate School of Science, Osaka University) for helpful suggestions for the ^{1}H–^{1}H EXSY measurements, and to Professor Takuji Ogawa and Professor Yasuhiro Kajihara (Department of Chemistry, Graduate School of Science, Osaka University) for fruitful discussions on this thesis.

The author thanks all members of Kubo laboratory (2010.01 ~ 2016.03) for their kind encouragement. The author is grateful to the staffs of the Faculty of Science, Osaka University for elemental analysis, NMR, mass spectrum, X-ray measurement, and glass equipment.

The author express his special thanks for JSPS Fellowship for Young Scientists, for its financial support.

Finally, the author wishes to express his hearty thanks to his family.

Kazuyuki Uchida

March, 2016